Research and Development of Combustion Engines with Sustainable and Zero-Carbon Fuels.

The Thesis Submitted for the Degree of

Doctor of Philosophy

By

Mohamed Ali Saad Hussein Mohamed

College of Engineering, Design and Physical Sciences
Department of Mechanical and Aerospace Engineering
Brunel University London
2024

Abstract

As governments worldwide address the increasing levels of CO_2 emissions, the automotive industry faces a significant challenge in mitigating climate change. To this end, the industry is exploring various solutions, including electrification and battery electric vehicles, as well as the adoption of low-carbon and zero-carbon fuels in Internal Combustion (IC) engines.

While the electrification of vehicles has grown in popularity, it has challenges, such as the high cost of batteries, limited driving range, and the need for charging infrastructure. In light of this, there is also growing interest in using low-carbon and zero-carbon fuels, such as biofuels, hydrogen, and synthetic fuels, in IC engines.

These fuels represent a promising approach to achieving net zero-carbon transportation and reducing the industry's carbon footprint. Biofuels, for example, can be produced from renewable sources and significantly reduce greenhouse gas emissions compared to conventional fossil fuels. Hydrogen, meanwhile, can power internal combustion engines with zero emissions when produced using renewable energy sources. Synthetic fuels, produced with renewable energy, provide a more sustainable alternative to traditional fossil fuels.

Adopting low-carbon and zero-carbon fuels in IC engines offers an effective and accessible pathway towards a more sustainable future. While electrification gains momentum, using sustainable fuels in IC engines provides a promising approach to achieving net zero-carbon transportation and reducing the industry's carbon footprint.

The present study confidently investigates two key solutions for accomplishing net-zero targets. Firstly, it explores the feasibility of second-generation biofuels with varying ethanol and Research Octan numbers as immediate drop-in replacements for fossil fuels. The study meticulously examines injection strategies for mitigating particulate matter emissions associated with these fuels.

The study revealed that biogasoline fuel from 2nd generation feedstock could be used seamlessly in existing spark ignition engines without hardware modifications. This research emphasizes the significance of biofuels in attaining a zero-carbon future. Nevertheless, it is crucial to ensure sustainable biofuel production to offer low-carbon alternatives to conventional fossil fuels while considering land use, water consumption, and biodiversity conservation. The research findings provide strong evidence that biogasoline, due to its heavier components, is more likely to generate higher levels of PM emissions. However, it has been proven that deploying the right split injection methods can significantly minimise PM emissions.

Secondly, the study focuses on hydrogen as the primary power source for ICE platforms. Through a comprehensive analysis of various injection methods and proportions, the study showcases the full potential of hydrogen as a substitute for gasoline. Additionally, the study confidently addresses performance and emission concerns by investigating NO_x and CO_2/Hc emissions associated with lubricants, using a novel method to identify the potential of considering H2ICE as a zero-carbon solution. The findings of this study are expected to confidently contribute to achieving net-zero targets. Hydrogen fuel has many advantages, such as running engines efficiently in lean conditions and maintaining stable combustion while achieving up to lambda 3.8. This translates to higher thermal efficiency, lower cyclic variability, and zero NO_x emissions. Additionally, hydrogen combustion is an eco-friendly source of fuel, emitting no HC, CO, and CO_2. Even under low load, exhaust hydrogen slip remains below 1000 ppm, which drops below 500 ppm with increased load. These remarkable results

suggest that hydrogen would be an ideal fuel to replace gasoline and natural gas in a spark ignition engine with superior efficiency, zero emissions and greater engine performance. The study found that centrally-mounted (CDI) and side-mounted direct injection (SDI) direct injection systems had zero CO_2, CO, and HC emissions during the steady state operations. The CDI and SDI setups demonstrated stable engine operations over a broad range of air-to-fuel ratios, with CDI having a more extensive range of lean-burn operations. CDI also had notably higher thermal efficiencies than SDI. The study identified the optimal operational settings for each system. It showed that CDI and SDI had similar emissions characteristics at low and mid-load, with SDI producing higher NO_x and hydrogen emissions than CDI. After analysing NO_x and lubricant emissions, it has been determined that NO_x emissions are nearly non-existent within the lambda range of 2.75 to 3.7.

Furthermore, it has been discovered that hydrogen emits 13.8% less NO_x emissions than gasoline during stoichiometric operation. Lastly, the comprehensive NO_x time analysis indicates that hydrogen exhibits greater consistency in NO_x emissions than gasoline. The CO_2/HC averaged emissions are nearly zero, while the peak spikes are less than 18 ppm.

Statement of Originality

I certify that the work done in the thesis is my work under regular supervision. The thesis contains no materials accepted or examined for awarding any other degree or diploma in any university.

The thesis does not include materials previously published or written by another person except those referenced in the text.

I consent to the open access of the final version of my thesis worldwide when deposited in the University's Digital Repository, subject to the Copyright Act 1968 and any approved embargo.

Acknowledgement

Table Of Contents

List Of Figures

List Of Tables

List Of Publications

Title	Journal /Conference	Statues
Experimental Investigation of Combustion Characteristics, Performance, and Emissions of a Spark Ignition Engine with 2nd Generation Bio-Gasoline and Ethanol Fuels	SAE WCX 2023	Published
Impact of RON on a heavily downsized boosted SI engine using 2nd generation biofuel – A comprehensive experimental analysis.	Energy and management:X	Published
Effects of Dual Injection Operations on Combustion Performances and Particulate Matter Emissions in a Spark Ignition Engine Fueled with Second-Generation Biogasoline	International Journal of Engine Research	Accepted for Publication
Hydrogen Engine Insights: A Comprehensive Experimental Examination of Port Fuel Injection and Direct Injection	SAE WCX 2024	Published
Hydrogen Injection Position Impact: Experimental Analysis of Central Direct Injection and Side Direct Injection in Engines	SAE Engines	Published
Unveiling the Potential of Hydrogen in a Downsized Gasoline Direct Injection Engine- Performance and Emissions Experimental Study	SAE Fuel and Lube	Published
Experimental assessment of the carbon dioxide and hydrocarbon emissions on a downsized spark ignition engine using 100% hydrogen fuel	CWCX 2024	Published
A Comprehensive Experimental Investigation of NOx Emission Characteristics in Hydrogen Internal Combustion Engine	MDPI Energies	Peer Review

List Of Abbreviations

10%to90%BurnDuration	Burn Duration
50%MB	Combustion Phasing
AFR / λ	Relative Air-Fuel Ratio
ATDC	After Top Dead Centre
BEV	Battery Electric Vehicle
BTDC	Before Top Dead Centre
CAD	Crank Angle Degree
CCU	Carbo Capture utility
CO	Carbon Monoxide
CO_2	Carbon Dioxide
COV_{IMEP}	Coefficient of Variation of IMEP
COPD	chronic obstructive pulmonary disease
CLD	Chemiluminescence Detector
DAQ	Data Acquisition
DI	Direct Injection
ECU	Electronic Control Unit
EGT	Exhaust Gas Temperature
EV	Electric vehicles
FCEV	Fuel Cell Electric Vehicle
GHG	Greenhouse Gas
H_2	Hydrogen
H_2O	Water
HC	Hydrocarbons
ICE	Internal Combustion Engine
IMEP	Indicated Mean Effective Pressure
ITE	Indicated Thermal Efficiency
LIF	Laser-Induced Fluorescence
LNV	Lower Net Value
NH_3	Ammonia
NO_x	Nitrogen Oxides
O_2	Oxygen
PFI	Port Fuel Injection
PLC	Programmable Logic Controller
PID	Proportional–integral–derivative
PTG	Power to gas
PTL	Power to liquid
PM	Particulate Matter
PMEP	Peak Mean Effective Pressure
PN	Particulate number
R_{max}	Pressure Rise Rate
SI	Spark Ignition

Chapter 1. Introduction

1.1 The Internal Combustion Engines

Combustion engines have been the primary energy generators in the past two centuries, and they have been involved in many applications, such as transportation, electricity generation, powerplant facilities, and military services. Also, Combustion engines have been modified and optimised through the years to improve their efficiency to perform more reliably and benefit their application. Overall, Engines were the heart of the industry.

1.1.1 Historical Background About Internal Combustion Engines and Their Applications

In 1680, Huygens proposed gunpowder for providing motive power. In 1688, Papin introduced his engine to the Royal Society of London, and then in 1712, Newcomen constructed his first atmospheric steam engine. Lenoir introduced the first general-use engine in 1860, as shown in Figure 1.1 [1].
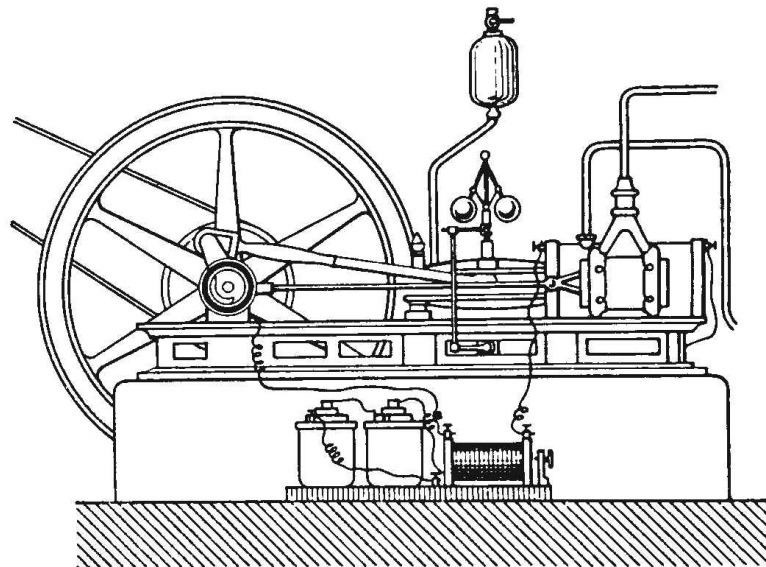
Figure 1.1: Steam Engine

In 1876, Otto produced the first four-stroke combustion engine, which was described as a silent engine compared to the free-piston engine, which Otto and Langen invented in 1866; then, twenty years later, the concept of compressing air to such an extent that fuel would spontaneously ignite, which known as diesel engine.

Due to its high expansion ratio and intrinsic lean burn, which allows heat to be dissipated by excess air, the diesel engine has the highest thermal efficiency (engine efficiency) of any practical internal or external combustion engine. Since unburned fuel is not present during valve overlap, no fuel goes directly from the intake/injection to the exhaust; a slight performance loss is avoided compared to non-direct-injection gasoline engines. Low-speed diesel engines (such as those used in ships and other applications where total engine weight is less concerned) can achieve up to 55 per cent effective efficiencies[2].

1.1.2 Engine Main Parameters and Classifications

Combustion engines are mainly divided into external combustion engines and internal combustion engines. External combustion engines, where the heat to drive the engine cycle is provided from outside the engine, can generate energy from various sources. The

main engine of this type for power generation use is the Stirling engine. Stirling engines have been widely used in solar power generation using heat collected using large solar dish reflectors. They have also been developed for domestic combined heat and power systems where natural gas generates heat that drives a Stirling heat engine with additional heat from the combustion process utilised for hot water and space heating. In principle, the engines can exploit heat energy from any source, but the applications where they offer a cost-effective solution are limited [3].

Internal combustion engines (ICE) are the most common form of heat engines, as they are used in vehicles, boats, ships, aeroplanes, and trains. They are named as such because the fuel is ignited to work inside the engine. The same fuel and air mixture is then emitted as exhaust. This can be done using a piston (reciprocating engine) or a turbine.

The main internal combustion engine structure, as shown in Figure 1.2, consists of the following:
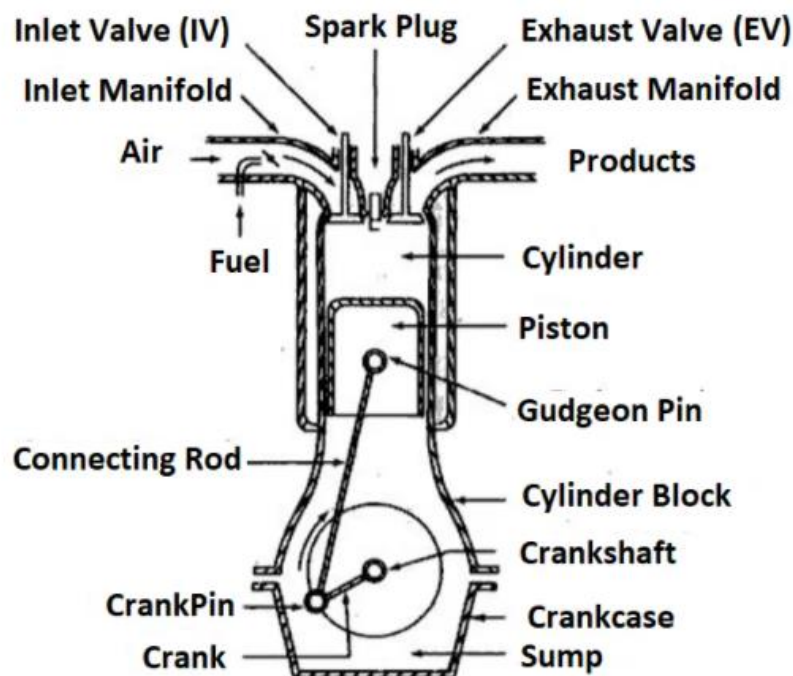
Figure 1.2: Engine components [4]

1- **The engine block** cast structure with cylindrical holes bored to guide and support the pistons and harness the working gases. It also provides a jacket to contains liquid coolant.[4]
2- **Cylinder head** casting encloses the combustion ends of the cylinder block and houses both the inlet and exhaust valves used to feed the cylinder with air and fuel mixture and allow exhaust gases to escape from the cylinder.
3- **Oil sump**-pressed steel or cast aluminium alloy container encloses the bottom of the crankcase and provides a reservoir for the engine lubricant.
4- **The piston is a pressure-tight cylindrical plunger subjected to** expanded gas pressure. Its function converts the gas pressure from combustion to a full driving thrust along the connecting rod, and it must, therefore, act as a guide to the small end of the connecting rod.

5- **Piston rings** circular rings seal the gaps between the piston and the cylinder. They aim to prevent gas from escaping and control the amount of lubricant allowed to reach the top of the cylinder.

6- **Piston pin:** this pin transfers the thrust from the piston to the connecting rod's small end.

7- The connecting rod acts as both a strut and tie link rod. It transmits the linear pressure impulses acting on the piston to the crankshaft prominent end journal, which converts them to turning effort.

8- **A valve spring** is a spring that is used to return the valve to its original position.

9- **The camshaft shaft is used to actuate the opening and closing** valves.

10- **Sparkplug (in gasoline engines)** is designed to be screwed into a hole formed in the cylinder head to ignite the mixture in the combustion chamber.

11- **An injector or carburettor pumps the fuel into the intake air to mix** the air with fuel to burn inside the cylinder.

There are many different types of internal combustion engines. They can be classified by:

1- Application. Automobiles, trucks, buses, locomotives, light aircraft, marine, portable power systems, and power generation.

2- Basic engine configuration. Reciprocating engines (in turn subdivided by the arrangement of cylinders: e.g., in-line, V, radial, opposed), rotary engines (Wankel and other geometries) as shown in figure 1.3.

Inline Vertical Engine   V-Type Engine   Horizontal Engine

Opposed Cylinder Engine   W-Type Engine   Radial Engine
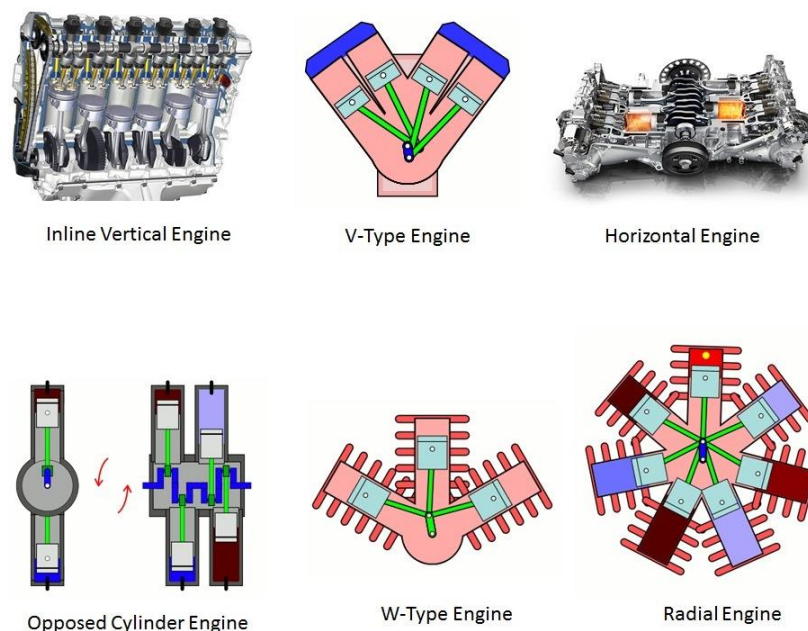
Figure1.3: Engine configurations

3- Working cycle. Four-stroke cycle: naturally aspirated (admitting atmospheric air), supercharged (admitting pre-compressed air), and turbocharged (admitting air compressed in a compressor driven by an exhaust turbine). Two-stroke cycle: crankcase scavenged, supercharged, and turbocharged, as shown in Figure 1.4.
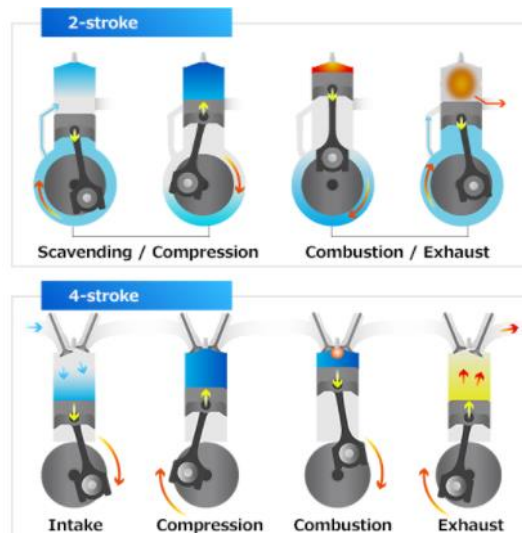
Figure 1.4: Engine working cycle

4- Valve or port design and location. Four-stroke cycle: Overhead (or I-head) valves, underheard (or L-head) valves, with two, three, or four valves per cylinder, and fixed or variable valve control (timing, opening and closing points, and lift), rotary valves. Two-stroke cycle: cross-scavenged porting (inlet and exhaust ports on opposite sides of the cylinder at one end), loop-scavenged porting (inlet and exhaust ports on the same side of the cylinder at one end), through- or uniflow-scavenged (inlet and exhaust ports or valves at different ends of cylinder).

5- Fuel. Gasoline (or petrol), fuel oil (or diesel fuel), natural gas, liquid petroleum gas (LPG), alcohols (Methanol, ethanol), hydrogen, and dual fuel.

6- Method of mixture preparation. Carburetion or single-point fuel injection upstream of the throttle, fuel injection into the intake ports, and fuel injection directly into the engine cylinder, as shown in Figure 1.5.
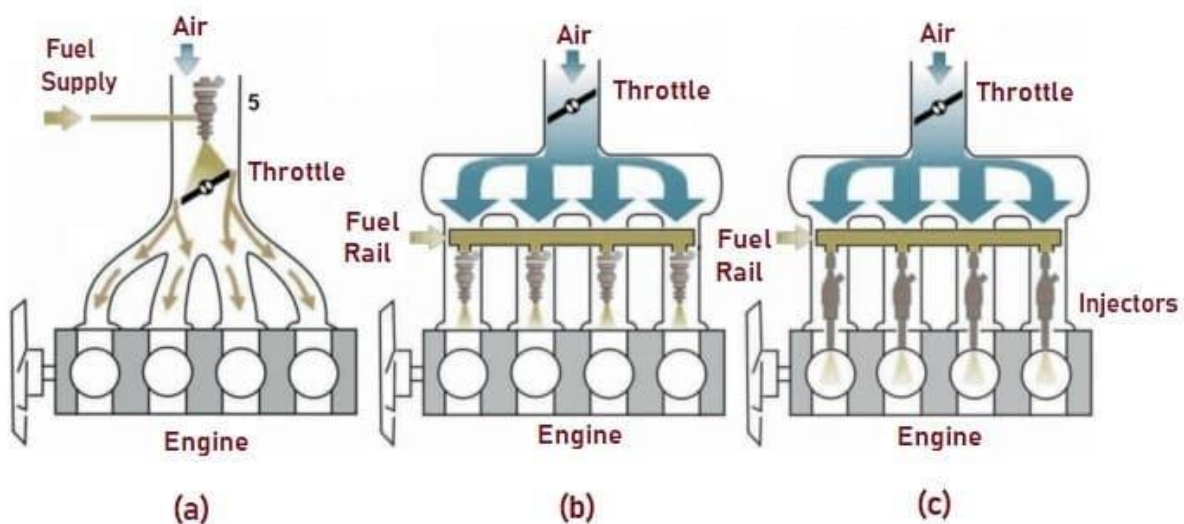
Figure 1.5: Methods of mixture preparations[5]

7- Method of ignition. In spark ignition engines, fuel is mixed with air and pulled into the cylinder during intake. Subsequently, the piston compresses the fuel-air mixture, and ignition is initiated by a spark, causing combustion. This combustion results in the expansion of gases, which drives the piston during the power stroke. On the other

hand, in diesel engines, only air is drawn into the engine and then compressed. The fuel is injected into the hot compressed air at a precisely controlled rate, leading to ignition.

8- Combustion chamber design. Open chamber (many designs: e.g., disc, wedge, hemisphere, pent-roof, bowl-in-piston), divided chamber (small and large auxiliary chambers; many designs: e.g., swirl chambers, pre chambers).

9- Method of load control. Varying fuel and airflow together, so mixture composition is essentially unchanged, controlling fuel flow alone, a combination of these.

10- Method of cooling. Water-cooled, air-cooled, and uncooled (other than by natural convection and radiation) [6].

1.1.3 Engine Operating Theory

The operating concept of both SI and CI engines is nearly identical, except for the fuel combustion process, which occurs in both engines. The spark generated by the spark plug positioned in the cylinder head ignites the fuel in SI engines. The fuel is compressed to extremely high pressures, and it burns at a consistent volume. In CI engines, the fuel is burned by compressing it at extremely high pressures, eliminating the need for a spark to start the combustion process. In this situation, the fuel is burned at a constant pressure.

The combustion engine operation can be described in thermodynamics as follows a constant cycle, and it is classified into many types. However, the most common two cycles are the Otto (constant volume) cycle for spark plug and the diesel (constant pressure) cycle for Diesel engines by drawing the pressure curve against the swept volume, as shown in Figure 1.6. Otto Cycle works on four processes, commencing with the intake stroke, where the air mass is pushed into the piston at unvarying pressure. The compression stroke is the next step, which involves isentropic compression. It is the time when the fuel and air mixture is compressed. The cylinder will now move from the bottom to the top dead centre. The piston rests at the top dead centre during the igniting phase. Heat is now injected into the system, which burns the existing mixture of air and fuel. It causes a rise in pressure while maintaining a constant volume. It then moves on to the expansion stroke, the heat rejection phase, and finally, the exhaust stroke. However, The diesel cycle comprises several processes, totalling four phases. It begins with adiabatic compression and then progresses to the next step of heat addition at constant pressure. Then, there is an adiabatic expansion and the process of rejecting heat at a constant volume.
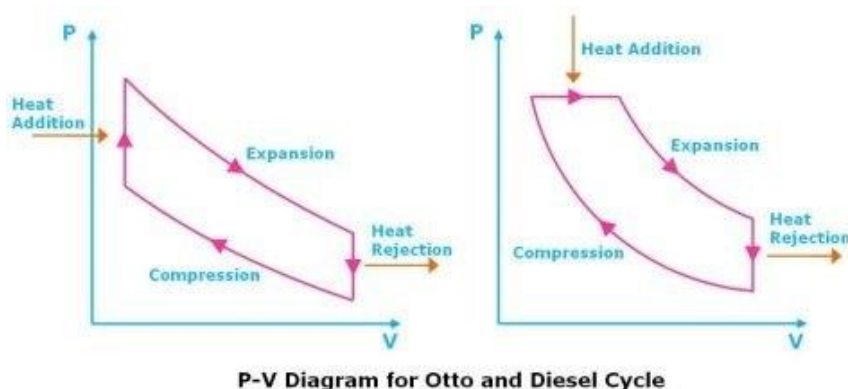
Figure 1.6: Engine cycles[7]

In a thermal engine, the combustion process depends on the air-fuel ratio inside the cylinder. The more air we can get inside the combustion chamber, the more fuel we can burn, and the higher the output engine torque and power, as shown in Figure 1.7.
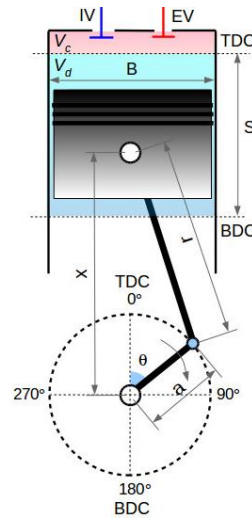
Figure 1. 7: Engine parameters [8]

Since air has mass, it has inertia. Also, the intake manifold, the valves and the throttle restrict the airflow into the cylinders. By volumetric efficiency, we measure the capacity of the engine to fill the available geometric volume of the engine with air. It can be seen as a ratio between the volume of air drawn by the cylinder (actual) and the geometric volume of the cylinder (theoretical).

Most of the internal combustion engines used in on-road vehicles nowadays have a fixed volumetric capacity (displacement), defined by the geometry of the cylinder and the crank mechanism. Strictly speaking, the total volume of an engine V_t [m3] is a calculated function of the total number of cylinders NC [-] and the volume of one cylinder V_{cyl} [m3].

The total volume of the cylinder is the sum between the displaced (swept) volume V_d [m3] and the clearance volume V_c [m3].

The clearance volume is minimal compared to the displacement volume (e.g. ratio 1:12), so it can be neglected when calculating the engine's volumetric efficiency.

The volumetric efficiency η_v [-] is defined as the ratio between the actual (measured) volume of intake air V_a [m3] drawn into the cylinder/engine and the theoretical volume of the engine/cylinder V_d [m3] during the intake engine cycle.

The Volumetric efficiency can also be regarded as the internal combustion engine's efficiency in filling the cylinders with intake air. The higher the volumetric efficiency, the higher the volume of intake air in the engine.

The intake air is mixed with fuel in indirect fuel injection engines (mainly gasoline). Since the amount of fuel is relatively tiny (ratio 1:14.7), we can neglect the fuel mass for volumetric efficiency calculation compared with air.

The volumetric efficiency is a maximum of 1.00 (or 100%). At this value, the engine is capable of drawing all of the theoretical volumes of air available into the engine. There are

exceptional cases in which the engine is specifically designed for one operating point, for which the volumetric efficiency can be slightly higher than 100 %.

Brake-specific fuel consumption (BSFC) measures the fuel efficiency of any prime mover that burns fuel and produces rotational or shaft power. It is typically used for comparing the efficiency of internal combustion engines with a shaft output.

The indicated mean adequate pressure of an engine is defined as the average (mean) pressure that would have to operate over the whole stroke (VS ¼ V1 V2) to give the same work output as the actual cycle, i.e.

It is the rate of fuel consumption divided by the power produced. It may also be thought of as power-specific fuel consumption for this reason. BSFC allows the fuel efficiency of different engines to be directly compared, as shown in Figure 1.8.
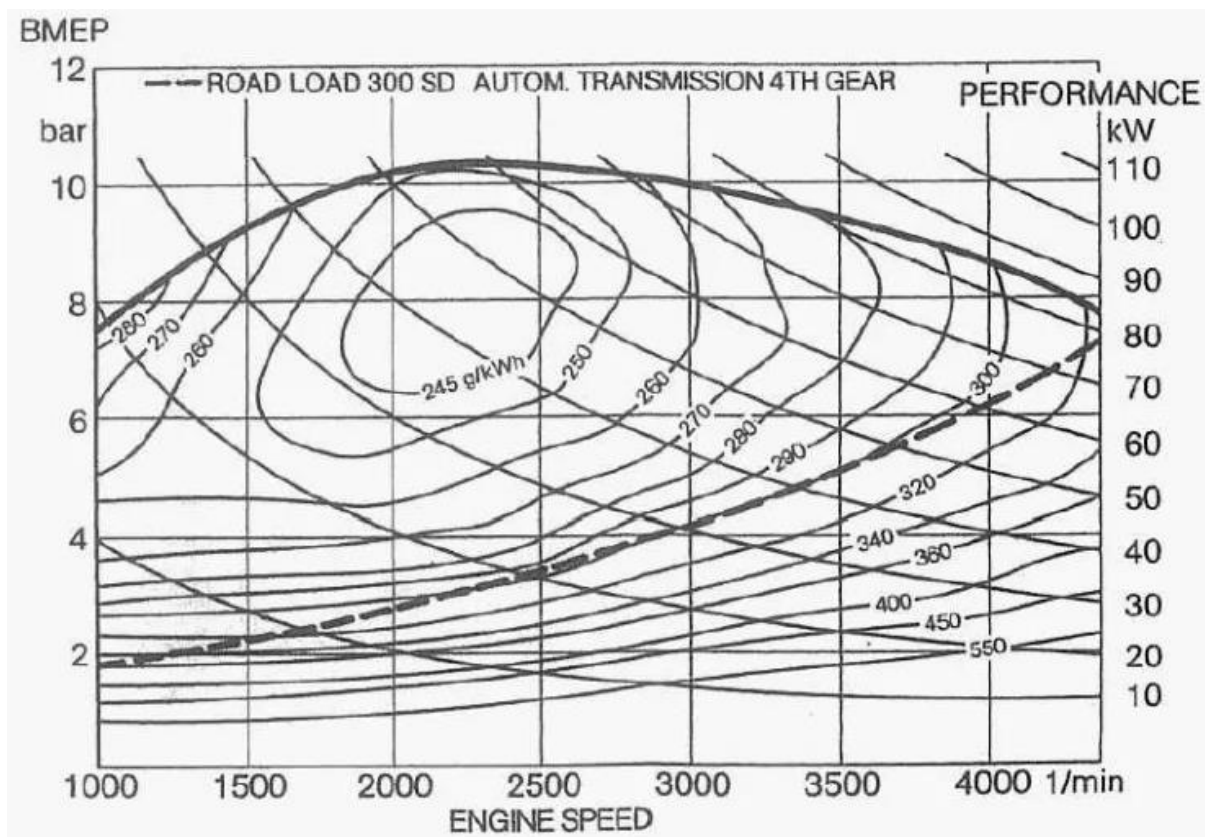
Figure 1.8: BSFC vs BMEP map[9]

Finally, the indicated power of an IC engine (briefly written as IP) is the power developed by the engine cylinder.

1.1.4 Engine Emission

Internal combustion is treated as the main guilty and the man responsible for climate change; however, it does not produce harmful gas but depends on the fuel source. According to the engine application, the types of fuels are various, such as the marine application for large ships uses diesel fuel with a large engine to produce high torque and low speed. On the other hand, the small two-stroke diesel engines are much more favourable to use for small yachts.

The heat release mechanism happens by burning the fuel with air inside the cylinder and then converting this energy into mechanical energy. Moreover, this process produces exhaust gases.

First, the internal combustion engine's fuel is a material that stores potential energy. Most fuels store potential energy in the bonds between their molecules, called chemical potential energy. Furthermore, it could be solid like wood or coal, liquid like petrol, diesel, ethanol, or gas like methanol and natural gas. Overall, the most common output gases from the combustion process can be simplified by analysing the fuel type. Complete combustion occurs when all the fuel is burned; no quantities of unburned fuel will be in the exhaust gas. As shown in the equation below, the relative air-fuel ratio (AFR) is the ratio between the mass of air ma and mass fuel mf used by the engine when running.

$$\lambda = \frac{AFR\ (actual)}{AFR(Ideal)} \qquad (1.1)$$

The ideal (theoretical) air-fuel ratio for complete combustion is the **stoichiometric** air-fuel ratio. The stoichiometric air-fuel ratio for a gasoline (petrol) engine is around 14.7:1. To burn 1 kg of fuel completely requires 14.7 kg of air. The combustion is possible even if the AFR is different from stoichiometric. For the combustion process to occur in a gasoline engine, the minimum AFR is around 6:1, and the maximum can go up to 20:1.

The air-fuel mixture is called lean when the air-fuel ratio is higher than the stoichiometric ratio. When the air-fuel ratio is lower than the stoichiometric ratio, the air-fuel mixture is called **rich**. For example, an AFR of 16.5:1 is lean for a gasoline engine, and 13.7:1 is rich. Table 1 shows the stoichiometric air-fuel ratio for several fuels.

Table 1. 1: Fuel comparison [10]*.*

Fuel	Chemical formula	AFR
Methanol	CH_3OH	6.47:1
Ethanol	C_2H_5OH	9:1
Butanol	C_4H_9OH	11.2:1
Diesel	$C_{12}H_{23}$	14.5:1
Gasoline	C_8H_{18}	14.7:1
Propane	C_3H_8	15.67:1
Methane	CH_4	17.19:1
Hydrogen	H_2	34.3:1

Air comprises oxygen, nitrogen, and small amounts of carbon dioxide, argon, and other trace species. Since the vast majority of the diluent in the air is nitrogen, for our purposes, it is perfectly reasonable to consider air as a mixture of 20.9% (mole basis) O_2 and 79.1 % (mole basis) N_2. Thus, for every mole of oxygen required for combustion, 3.78 mol of nitrogen must also be introduced. Although nitrogen may not significantly alter the oxygen balance, it significantly impacts the thermodynamics, chemical kinetics, and formation of pollutants in combustion systems. For this reason, carrying the "inert" species along in the combustion calculations is helpful. The stoichiometric relation for the complete oxidation of a hydrocarbon fuel, CnHm, becomes

$$C_nH_m + \left(n + \frac{m}{4}\right)(O_2 + 3.78N_2) \rightarrow nCO_2 + \frac{m}{2}H_2O + 3.78(n + \frac{m}{4})N_2 \qquad (1.2)$$
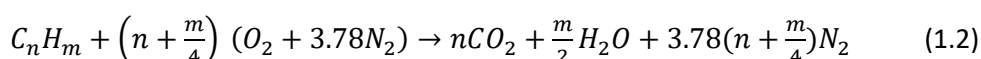
Thus, 4.78(n + m/4) mol of air is required for every mole of fuel burned, and 4. 78(n + m/4) + m/4 mol of combustion products are generated. The molar fuel/air ratio for stoichiometric combustion is 1/ [4. 78(n + m/4)] [11].

The products of the chemical combustion process are functions of lambda value; whether lean or rich, combustion could produce unburnt hydrocarbon, nitro monoxide, nitro dioxide, carbon monoxide, and carbon dioxide, as shown in Figure 1.9.
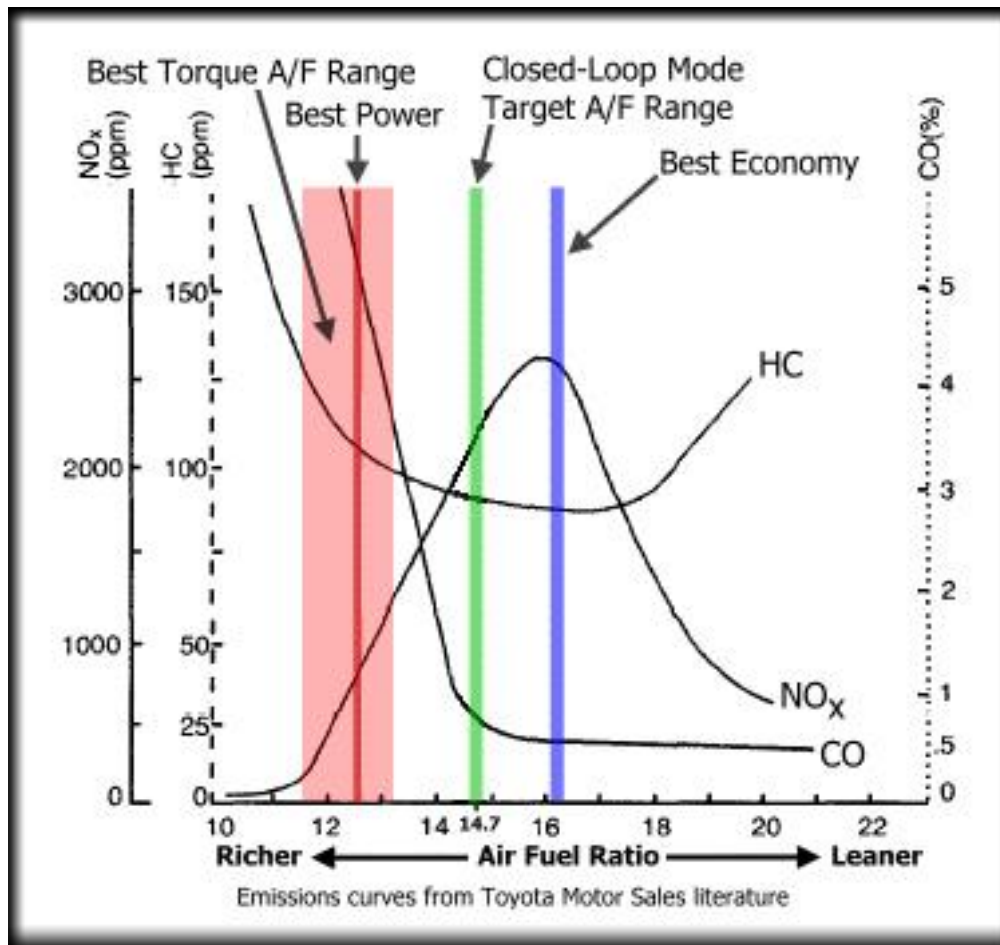
Figure 1.9: combustion products as functions of the lambda value[12]

The most important chemical reaction in a petrol engine –the one that provides the energy to drive the vehicle – is fuel combustion in the air. In an 'ideal system, combustion would be complete so that the only exhaust products would be carbon dioxide and steam. In practice, the complete oxidation of the fuel depends on several factors: first, there must be sufficient oxygen present; second, there must be adequate mixing of the petrol and air; and finally, there must be sufficient time for the mixture to react at high temperature before the gases are cooled. In internal combustion engines, the time available for combustion is limited by the engine's cycle to just a few milliseconds. There is incomplete combustion of the fuel, and this leads to emissions of the partial oxidation product, carbon monoxide (CO), and a wide range of volatile organic compounds (VOC), including hydrocarbons (HC) aromatics and oxygenated species. These emissions are exceptionally high during idling and deceleration when insufficient air is used for complete combustion.

Another significant result of the combustion process, particularly during acceleration, is the production of nitrogen oxides–nitric oxide (nitrogen monoxide, NO) and nitrogen dioxide (NO_2). Conventionally, these two nitrogen oxides are considered together and represented as NO_x. At high temperatures (excess of 1 500 °C), nitrogen and oxygen in the air drawn in with the fuel may combine to form NO. On leaving the engine, this monoxide

cools down and is oxidised by oxidants in the atmosphere to form the dioxide. Although the 'fixing' of nitrogen from the air is the primary source of NO_x, it may also arise from the oxidation of any nitrogenous components in the fuel.

Primary pollutants are those gases emitted directly from a vehicle's exhaust. None of these is a desirable addition to the atmosphere, but perhaps the most notorious consequence of exhaust emissions is their role in forming photochemical smog – a mixture of ozone, nitrogen dioxide, other secondary products and small particulates. These secondary pollutants can cause severe damage to human health.

The role of an emission control catalyst is to simultaneously remove the primary pollutants CO, VOCs and NO_x by catalysing their conversion to carbon dioxide (CO_2), steam (H_2O) and nitrogen (N_2), as shown in Figure 1.10 [13].
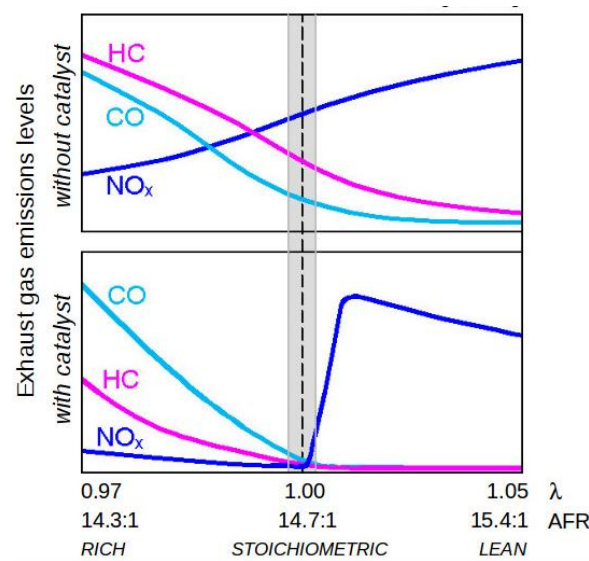
Figure 1.10: The effect of the catalyst[14]

1.1.5 Environmental Impact

The Internal combustion engine has been used in almost every industry with different fuel types in the last two centuries. As a result of uncontrolled emissions over the years, many scientists observed a change in the climate—also new environmental phenomena such as desertification, acid rain, and global warming.

Therefore, air pollution has a direct impact on human health. The most common diseases caused by air pollution include ischemic heart disease, stroke, chronic obstructive pulmonary disease (COPD), lung cancer and acute lower respiratory infections in children.

The Greenhouse effect is warming Earth's surface and troposphere (the lowest layer of the atmosphere) caused by water vapour, carbon dioxide, methane, and certain other gases in the air. Of those gases, known as greenhouse gases, water vapour has an enormous effect. The burning of all carbon-containing fuels inevitably produces vast quantities of carbon dioxide. With efficient combustion, all the carbon in the fuel is converted to carbon dioxide. Carbon dioxide is the desired product of fuel combustion. It is also a normal constituent of air at an average concentration of 0.0315% (315 parts per million). So it is

not usually considered a primary air pollutant, and it is better not because we drink it all the time in sodas. Figure 1.11 shows the GHE sources [15].
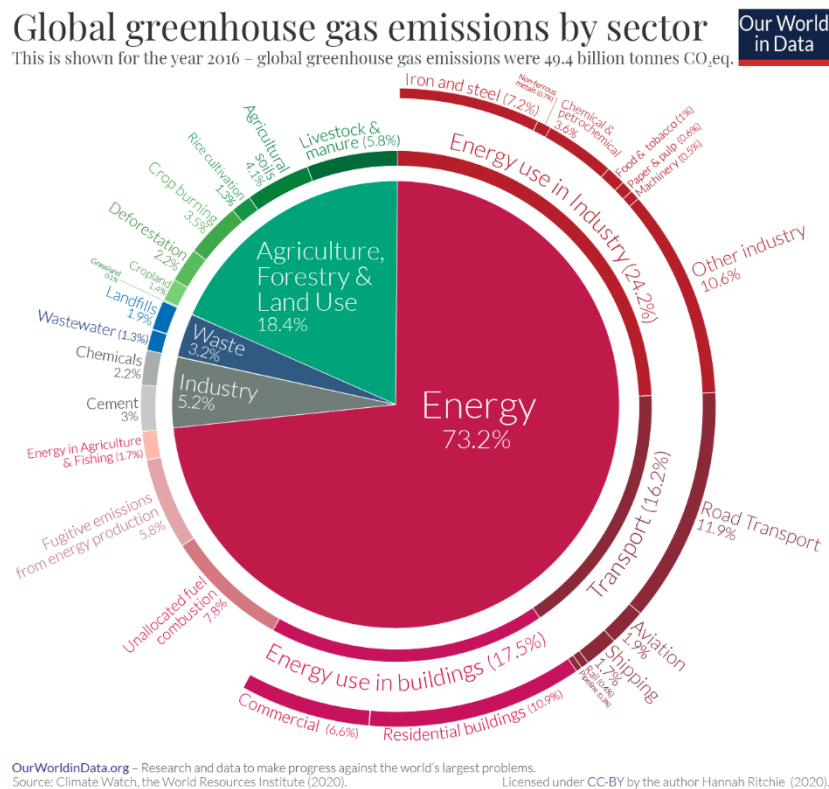
Figure 1.11: GHE sources[16]

1.2 Sustainable Fuels

The search for alternative fuels has garnered significant traction in pursuing a sustainable and environmentally favourable future. Sustainable fuels, also known as renewable or green, are gaining traction as viable alternatives to conventional fossil fuels. They have the potential to reduce greenhouse gas emissions, lessen reliance on finite resources, and advance a greener and more sustainable energy landscape. This article examines the concept of sustainable fuels and their types, advantages, and role in combating climate change.

1.2.1 Types of Sustainable Fuels

1. **Biofuels:** Biofuels are derived from biomass, which includes crops, crop residues, algae, and even municipal solid refuse. First-generation biofuels (such as ethanol from maise or sugarcane) and second-generation biofuels (such as cellulosic ethanol or biodiesel from non-food feedstocks) can be distinguished. Advanced biofuels, such as biofuels derived from phytoplankton, are the next iteration of sustainable fuels [9,10].

2. **Synthetic Fuels**: Synthetic fuels, also known as e-fuels or power-to-liquid fuels, combine carbon dioxide (CO_2) and hydrogen from renewable sources. These fuels have the potential to reduce CO_2 emissions substantially and can be used in existing combustion engines without significant modifications [11,12].

3. **Hydrogen**: Hydrogen is considered a promising sustainable fuel option because it can be produced from various renewable sources, such as water electrolysis using renewable electricity. Hydrogen produces electricity without emitting greenhouse gases when utilised in fuel cells, providing a clean and efficient energy solution [21].

1.2.2 The Advantages vs Challenges of Sustainable Fuels

Reduced greenhouse gas emissions: A benefit of sustainable fuels is that they have smaller carbon footprints than conventional fuels, significantly reducing greenhouse gas emissions. Thus, they are an indispensable instrument for combating climate change and attaining global emission reduction goals.

Energy security and independence: By diversifying energy sources and decreasing reliance on fossil fuels, sustainable fuels increase energy security and promote greater energy production independence for countries.

Sustainable fuels frequently use organic waste or agricultural residues as feedstocks, fostering the circular economy and reducing waste. This contributes to waste management and reduces the reliance on landfills and the environmental challenges associated with their use [22].

The transition to sustainable fuels necessitates the development of new technologies and infrastructure and creation of new jobs. This transition fosters innovation, research, and development, creating jobs and expanding economically. Challenges and Future Sustainable fuels face obstacles such as high production costs, limited scalability, and the need for robust regulatory frameworks despite their numerous advantages. However, ongoing technological advancements, combined with supportive policies and increased investments, are assisting in overcoming these obstacles [23].

Sustainable fuels are poised to play a pivotal role in the global energy transition as the world prioritises sustainability and decarbonisation. We can pave the way for a greener, more sustainable future by incorporating renewable energy sources and promoting pure and efficient fuel options [24].

1.2.3 Biofuels

Biofuels are an essential category of sustainable biomass derived from biomass, including organic materials such as plants, agricultural residues, algae, and municipal solid refuse. They offer a promising alternative to fossil fuels and have attracted great interest in the search for greener energy solutions. Consider the following essential factors when discussing biofuels:

First-Generation Biofuels: These are derived from edible commodities like maise, sugarcane, and vegetable oils. They include ethanol, frequently blended with petrol, and biodiesel, frequently used as an alternative to or blended with diesel fuel [25].

Second-Generation Biofuels: These biofuels are derived from non-food feedstocks such as agricultural residues (e.g., maise stover, wheat straw), dedicated energy crops (e.g., switchgrass, miscanthus), and wood residues. Second-generation biofuels benefit from using non-edible feedstocks, thereby minimising potential conflicts with food production [26].

Advanced Biofuels: This category includes biofuels produced from non-food feedstocks using advanced conversion technologies. It consists of cellulosic ethanol derived from the lignocellulosic fraction of biomass and biofuels derived from algae and other non-edible feedstocks [27].

A long-standing reliance on biomass marks the history of biofuels as a source of energy, and more recent advancements in biofuel technologies are motivated by concerns about energy security, climate change, and sustainability. The provided references offer more in-depth information on the historical context and development of biofuels and can be divided into four stages:

1- Early Development

The history of biofuels can be traced back to ancient times when humans used biomass such as wood and agricultural waste for cooking and heating. Biofuels such as vegetable oils and animal lipids were utilised in early internal combustion engines prior to the dominance of petroleum-based fuels in the 19th century [28].

2- Emergence of Ethanol

Henry Ford envisioned using ethanol as a fuel for his automobiles in the early 20th century, which led to the development of the Model T, which could operate on either ethanol or petrol. During World War II, biofuels acquired popularity as an alternative to petrol, especially in nations with fuel shortages. The energy crises of the 1970s increased interest in biofuels to decrease reliance on imported oil [29].

3- Commercialisation of Biodiesel

In the 1990s, biodiesel, a renewable fuel from vegetable oils or animal fats, acquired momentum in commercialisation. Countries such as Germany and Brazil have implemented policies and incentives to encourage the production and use of biodiesel, resulting in its increased adoption [30].

4- Advancements in Biofuel Technologies

Early in the 21st century, significant advancements were made in biofuel technologies, especially in producing cellulosic ethanol from non-edible feedstocks such as agricultural residues and energy crops [31].

Research and development efforts are focused on improving the efficiency and cost-effectiveness of biofuel production while addressing sustainability concerns. Biofuels offer environmental benefits such as reduced CO_2 emissions, renewable sourcing, and lower emissions of harmful pollutants, including sulphur dioxide, particulate matter, and nitrogen oxides.

Challenges and Research Efforts:

a. Availability and Competition of Biomass Feedstocks: The production of biofuels requires a sufficient supply of biomass feedstocks, and it remains challenging to balance the demand for biofuel feedstocks with other land uses, such as food production and conservation [32].

b. Technological advancements: Biochemical and thermochemical processes and other advanced conversion technologies are required to increase the efficacy and cost-effectiveness of biofuel production [33]

c. Environmental considerations: Ensure the sustainable production of biofuels by addressing issues such as land use change, water usage, and feedstock cultivation's effects on biodiversity.

In conclusion, Biofuels have emerged as a promising solution to energy security, climate change, and sustainability issues. They offer several benefits, including reduced greenhouse gas emissions, the availability of renewable feedstocks, and the potential for economic growth. However, successful biofuel implementation requires thoroughly considering technical, environmental, and socioeconomic factors.

1.2.4 Synthetic Fuels

Synthetic fuels, also known as carbon-neutral or carbon-neutral fuels, have attracted considerable interest as a potential solution for reducing greenhouse gas emissions and attaining a sustainable energy future. This section examines synthetic fuels, including their production processes, environmental benefits, and challenges. It investigates synthetic fuel technologies, including carbon capture and utilisation, power-to-gas, and power-to-liquid. In addition, the potential function of synthetic fuels in industries such as transportation, industry, and power generation is discussed.

Adopting synthetic fuels in the aviation industry could significantly reduce its environmental footprint. However, the transition to e-fuels would necessitate substantial financial and labour investments. In order to develop a road map and implement effective political measures, it is vital to conduct a comprehensive analysis of the associated benefits and obstacles. These measures would be indispensable for promoting the use of synthetic fuels and accomplishing a successful long-term transition, preferably by 2050. Regarding promoting Power-to-Liquid (PtL) fuels, our analysis indicates that various political measures would be advantageous. However, it is essential to recognise that the

international nature of the aviation industry presents obstacles that can impede the implementation of enhancements. Given this context, it is prudent to concentrate on national and European approaches while simultaneously engaging in international-level negotiations through organisations like the International Civil Aviation Organisation (ICAO). The aviation industry can make significant progress towards adopting synthetic fuels by adopting a multifaceted strategy and integrating national, regional, and international efforts. This strategy would entail implementing supportive policies, encouraging research and development, and establishing incentives for investment in infrastructure for synthetic fuel production. Ultimately, a collaborative and coordinated effort across all levels of government will be required for the aviation industry to transition to synthetic fuels successfully [34], [35].

Synthetic fuel technologies can be divided into four main applications:-

a. Carbon Capture and Utilization (CCU).

CCU technology can reduce CO_2 emissions and fight climate change. This high-level summary discusses CCU technology and its possible uses.

CCU captures CO_2 from industrial processes and power plants employing post-combustion, pre-combustion, and direct air capture. Pre-combustion capture involves gasification and reforming, while post-combustion capture uses chemical solvent absorption and adsorption. Direct air capture catches atmospheric CO_2.

Different pathways can use collected CO_2. Catalysts and optimised processes convert CO_2 into methanol, formic acid, and carbonates. Biofuels and bioplastics are made via microbial and enzymatic conversion. CO_2 is mineralised for carbon sequestration [36].

CCU reduces CO_2 and sequesters carbon. Energy, procedural, and economic issues must be addressed to promote CCU adoption.

Industry, transportation, and energy storage could use CCU. CCU technologies produce chemicals, fuels, and materials for a low-carbon economy. CCU deployment depends on market opportunity, regulatory backing, and technology.

CCU technologies can reduce CO_2 emissions and promote sustainable development. CCU implementation requires ongoing research, innovation, and supportive policies, as shown in Figure 1.12.
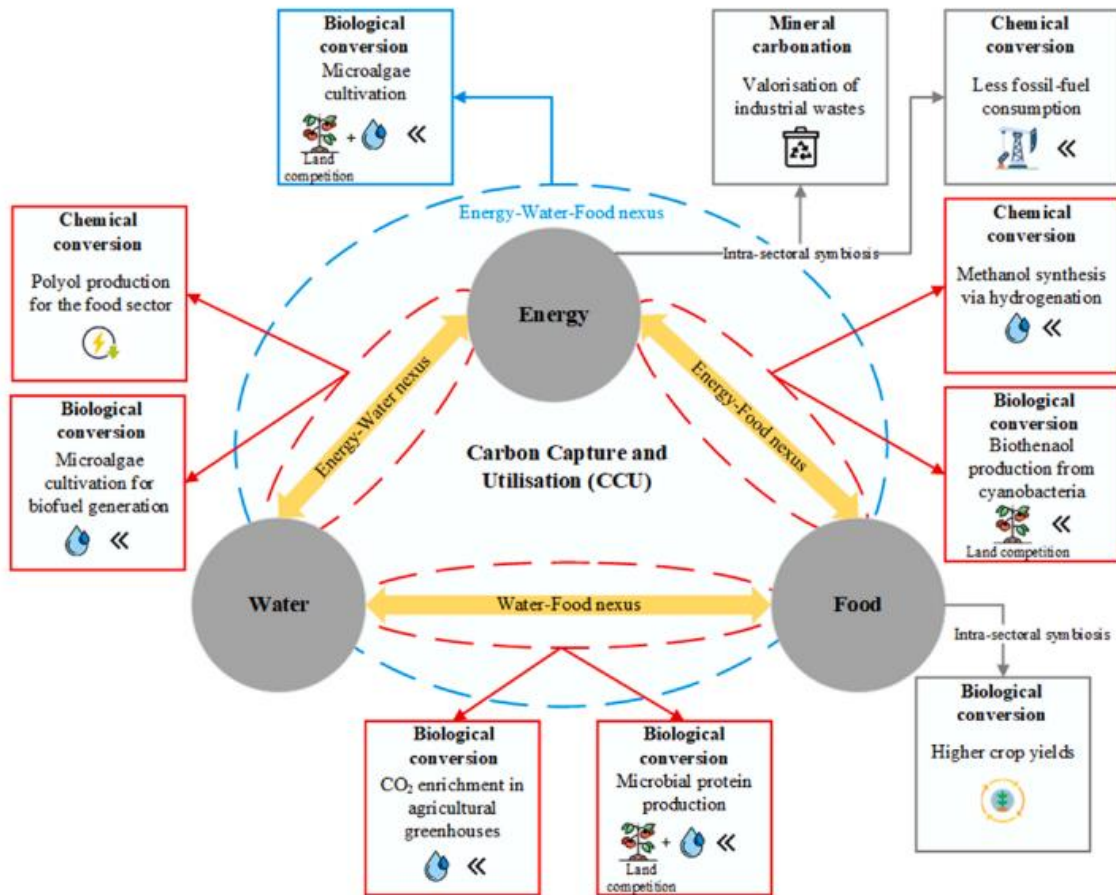
Figure 1.2: CCU opportunities within EWF systems [37].

b. Power-to-Gas (PtG)

Power-to-Gas (PtG) is a cutting-edge energy conversion technology that helps integrate renewable energy sources and create a sustainable energy system. This high-end brief covers PtG technology's features and applications. PtG technology turns surplus renewable electricity into hydrogen (H_2) and methane (CH_4). Electrolysis is followed by gas conversion, and electrolysis splits water molecules into hydrogen and oxygen. Hydrogen can be utilised as a clean energy carrier or methane with CO_2 to make methane. Synthetic or renewable methane is produced this way. PtG advantages:

It stores and uses excess renewable electricity, offering system flexibility and mitigating renewable energy intermittency [38].

Hydrogen and methane are adaptable energy carriers for industry, transportation, and power generation.

PtG helps integrate renewable energy across sectors by linking electricity and gas systems.

PtG has many uses. PtG-produced hydrogen can be used in chemical synthesis and fuel production. Hydrogen can power fuel cell vehicles, whereas methane can be a sustainable alternative to fossil natural gas. PtG stores excess electricity as gas. PtG has potential, but obstacles persist. Cost reduction, efficiency improvements,

infrastructure expansion, and sustainable carbon for methane generation are needed [39].

In conclusion, Power-to-Gas (PtG) technology may transform energy by transforming excess renewable electricity into gaseous fuels. It provides grid flexibility, energy storage, and sector coupling. With additional advances, PTG can help integrate renewable energy sources into a sustainable, decarbonised energy system, as shown in Figure 1.13, the whole PTG concept.
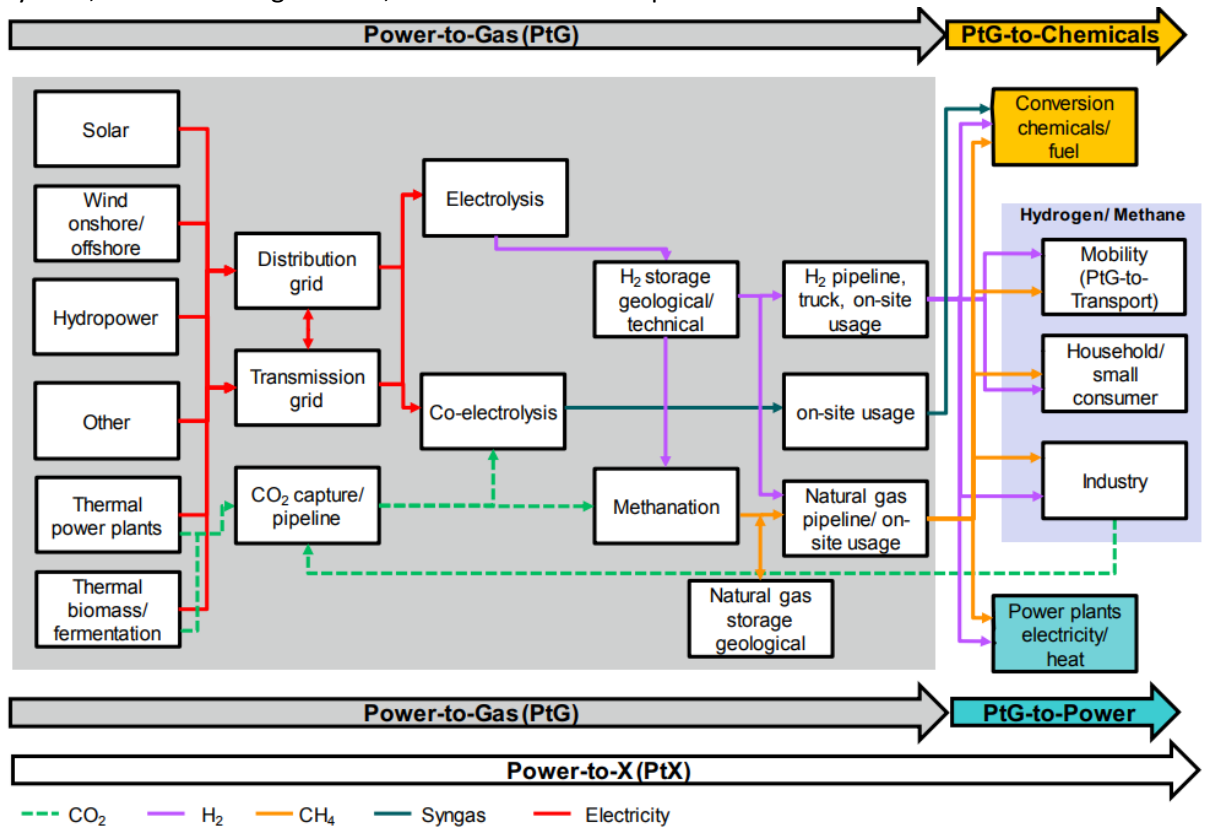
Figure 1.13: PTG concept[40]

c. Power-to-Liquid (PtL)

Power-to-Liquid (PtL) technology converts renewable electricity into liquid fuels, promising to decarbonise transportation and reduce greenhouse gas emissions. This high-level brief covers PtL technology, its significance, and prospective applications.

PtL converts renewable electricity like solar or wind power into energy-dense liquid fuels. Electrolysis, hydrogen generation, and liquid hydrocarbon synthesis comprise the process [41].

Electrolysis splits water into hydrogen and oxygen. Hydrogen can be utilised as a clean energy carrier or mixed with CO_2 from industrial operations or the atmosphere. Fischer-Tropsch synthesis converts hydrogen and CO_2 into liquid hydrocarbons like synthetic petrol, diesel, and jet fuel. These fuels can be combined with fossil fuels and used in internal combustion engines.

PtL has many advantages:

1- It allows surplus renewable electricity to be stored as energy-dense liquid fuels, addressing the intermittency of renewable energy sources, and permitting its use in liquid fuel-dependent sectors.
2- PtL fuels can reduce greenhouse gas emissions by using renewable electricity and recovering CO_2.
3- Without significant infrastructure upgrades, ptL fuels can be used in vehicles, aeroplanes, and ships.

PtL is versatile. PtL fuels can replace fossil fuels in transportation, providing a seamless transition to sustainable mobility. PtL fuels can decarbonise aviation, which relies on liquid fuels and struggles with electrification. PtL fuels reduce fossil fuel imports and provide energy security [42].

High energy requirements hinder ptL adoption, cost competitiveness with conventional fuels, sustainable CO_2 sources, and scaling up production to meet demand.

Power-to-Liquid (PtL) technology can transform transportation by transforming renewable electricity into energy-dense liquid fuels. It reduces greenhouse gas emissions, stores energy, and works with current infrastructure. PtL can decarbonise transport and accelerate the energy transition with continuous research, innovation, and supportive legislation.

1.2.5 Hydrogen

Hydrogen is a versatile energy carrier derived from various renewable and low-carbon sources, such as water electrolysis with renewable electricity, biomass gasification, and carbon capture and utilisation. Using hydrogen as a propellant has numerous advantages. First, it is a pure fuel with zero greenhouse gas emissions at the point of use, aiding in climate change mitigation. Second, hydrogen can be efficiently stored and transported, mitigating the intermittent nature of renewable energy sources. Thirdly, hydrogen can be utilised in various sectors, including transportation, industry, and power generation, making it an all-encompassing decarbonisation strategy. In transportation, hydrogen fuel cells provide a viable alternative to conventional internal combustion engines, facilitating zero-emission mobility. Hydrogen-powered fuel cell vehicles have longer ranges and faster refuelling periods than battery-powered electric vehicles, making them ideal for long-distance travel and heavy-duty applications. In addition, hydrogen can be used as a feedstock in industrial processes such as refining, ammonia production, and steel production, thereby reducing carbon emissions and facilitating the transition to a low-carbon economy. Several obstacles must be overcome to realise the maximum potential of hydrogen as a sustainable fuel. These include the establishment of a hydrogen infrastructure and the incorporation of hydrogen into existing energy systems. In addition, research and development efforts are ongoing to improve hydrogen storage and transportation technologies, increase the production efficacy of hydrogen, and lower costs. Numerous studies and reports emphasise hydrogen's potential as a sustainable fuel. The International Energy Agency (IEA) has published in-depth reports on the role of

hydrogen in decarbonisation initiatives, including the "Future of Hydrogen" report (2019). The Hydrogen Strategy (2020) of the European Commission emphasises the significance of hydrogen in attaining carbon neutrality. Zoulias et al. (2020) and Ogden et al. (2021) offer in-depth analyses of hydrogen's function in the energy transition and its potential as a sustainable fuel. Hydrogen holds great promise as a sustainable fuel, offering a variety of benefits and applications across various industries. Hydrogen has the potential to play a significant role in attaining a low-carbon and sustainable energy future, thanks to ongoing advancements in production, storage, and infrastructure [43], [44], [45], [46].

1.3 Carbon Reduction Strategy By The UK Government

The United Kingdom has achieved a significant milestone by reducing its emissions by 50% between 1990 and 2022 while growing its economy by 79%, making it the first major economy to do so. This surpasses the 23% reduction in France and no change in the USA during the same period. The country's use of renewables now constitutes over 40% of its electricity, a substantial increase from the 7% reported in 2010, demonstrating the UK's leadership in clean energy [47].

The UK has significantly reduced emissions by shifting from coal to renewables in energy generation. It has not only met but exceeded its targets for emissions reduction, surpassing all other G7 nations. Furthermore, companies are set to invest £30 billion in the energy sector to drive the development of green technologies. With ambitious targets to reduce emissions by 68% by 2030, the UK has demonstrated its commitment to environmental progress. Additionally, there has been a notable increase in renewable electricity generation, reaching nearly 50%.

1.4 Latest Powertrains Technologies to Mitigate CO_2 Emissions

At present, the energy density and refuelling time of fossil fuels make them the most convenient energy sources for vehicles. However, the rise in global temperatures and transportation of people and goods has led to strict regulations on pollutant and CO_2 emissions. While this challenges vehicle manufacturers, it also offers opportunities to develop new technologies and concepts. Hybrid powertrains with advanced internal combustion engine technologies and low electrification levels or high electrification levels combined with simpler internal combustion engines are being explored by automotive companies and researchers. While these hybridisation approaches can significantly improve efficiency and emissions, there is also a global push towards adopting zero-tailpipe-emitting vehicles at the consumer, manufacturing, and government levels. Reviews of the internal combustion engine, hybrid, and battery electric vehicle technologies have been conducted for the last few years [48].

1.4.1 Electrification

The first electric car was invented by Thomas Davenport in Scotland in 1834, preceding Benz and Daimler's cars with internal combustion engines. Electric cars had a significant market share in the early 1900s, especially for urban taxi applications. Cadillac's introduction of the "self-starter" in 1912 marginalised the electric car. Nonetheless, interest in the electric car persisted throughout the 20th century, particularly during World War II and the late 1960s and early 1970s, due to growing concerns about air pollution [49].

Despite the challenges, electric vehicles have the potential to revolutionise the global market and reduce carbon emissions. In order to achieve this, governments, corporations, and research and standards institutions must collaborate and push for strong regulations at national and international levels. The "3Cs"—costs, comfort, and climatic dependency—will be critical in enabling the widespread adoption of plug-in hybrid and fully electric vehicles. These vehicles are categorised into three types based on their energy source: BEVs (battery electric vehicles), PHEVs (plug-in hybrid electric vehicles), and HEVs (hybrid electric vehicles). We can accelerate the transition to a cleaner and more sustainable transportation system with concerted efforts and a focus on these key factors.

The main five types of electric vehicles, with technical details are listed below.

1. Battery Electric Vehicles (BEVs): BEVs use stored electricity and consist of a high-voltage battery, one or more electric motors, and a power electronics controller. Compared to traditional internal combustion engines (ICEs), BEVs deliver constant and high torque over a broad range of speeds, eliminating the need for a reduction gearbox or complex engine management systems [50].

2. Fuel Cell Electric Vehicles (FCEVs): FCEVs are powered by hydrogen and are more efficient than ICEs. They produce no tailpipe emissions and only emit water vapour and warm air. However, FCEVs and hydrogen infrastructure are still in the early stages of implementation.

3. Hybrid Electric Vehicles (HEVs): HEVs combine an internal combustion engine and an electric power system. They can function as electric vehicles and use regenerative brakes to convert kinetic energy into electric energy stored in a battery or supercapacitor. HEVs also use a start-stop mechanism to reduce idle emissions [51].

4. Plug-in Hybrid Electric Vehicles (PHEVs): PHEVs have an internal combustion engine and an electric motor, and an alternative or conventional fuel can power them. They also have a battery that can be charged by plugging into an electrical outlet or charging station. PHEVs have two configurations: series and parallel/blended

5. Extended-Range Electric Vehicles (EREVs): EREVs run on electricity only, but they have a generator onboard to recharge the battery when it is depleted. This eliminates range anxiety, and the petrol engine never directly powers the vehicle like other hybrids.

The future of internal combustion engines lies in optimising their powertrain and internal systems through a three-step approach: improving engine efficiency, utilising low-carbon or near-net-zero-carbon fuels, and electrification, including hybridisation. While the history of combustion engines has largely seen gradual improvements, the adoption of direct fuel injection coupled with turbocharging was a notable exception [52].

1.4.2 The Future ICE Technologies

To meet energy-saving and CO_2 emission reduction targets, the ICE must enhance thermal efficiency across the entire engine operating range. This requires gradually optimising ICE waste energy and adopting more radical technologies and combustion approaches. The primary goal is to increase the efficiency of gasoline engines to match that of diesel engines, with a long-term objective of achieving a brake thermal efficiency of up to 50%. [53].
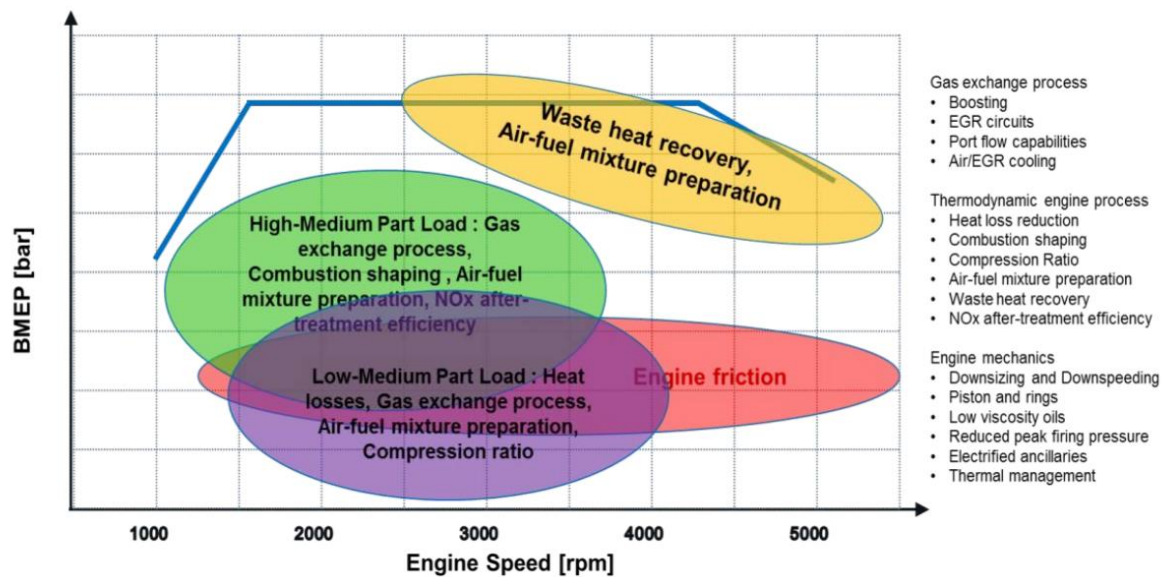
figure1. 14:ICE improvement areas towards higher energy efficiency [54]

Figure 1.14 highlights the key elements contributing to increased energy efficiency under different operating conditions. On the right side, there is a list of potential technological approaches. Our efforts to achieve these goals are supported concurrently with the development of electrification/hybridisation technologies. By utilising renewable, low-carbon fuel as a primary component of an electrified powertrain, we can pave the way for a sustainable and efficient future. Alternative fuels offer numerous advantages over fossil fuels, being renewable and biodegradable while addressing energy security, environmental concerns, and socio-economic issues. Consequently, renewable fuels can be widely used for transportation and power generation. Extensive experiments have been conducted on the use of producer gas for both spark ignition (SI) and compression ignition (CI) engine applications for both short and long-term trial runs. Biomass-derived producer gas is increasingly relied upon for rural power generation and shows promise in controlling NOx and soot emission levels. Research has shown that the brake thermal efficiency of producer gas-operated engines is considerably lower than diesel/biodiesel-operated engines. However, this can be improved by enhancing fuel properties, implementing good operating parameters, or modifying engine design. To address this, numerous researchers and scientists have proposed various solutions for enhancing the performance of producing gas-operated engines[55].

Dual fuel strategies in diesel engines, such as using methanol fumigation, have shown promise in reducing CO2 emissions. Methanol fumigation effectively reduces smoke and NOx emissions but may not enhance engine performance at low engine loads. Additionally, brake thermal efficiency (BTE) decreases with higher levels of methanol fumigation or methanol-diesel blends. Brake-specific fuel consumption (BSFC) also increases due to the lower calorific value of methanol than diesel.

While methanol fumigation and blending with diesel/biodiesel can increase unburned hydrocarbon and carbon monoxide emissions, this approach has effectively reduced NOx and smoke emissions simultaneously. Moreover, a marginal improvement in efficiency has been reported at higher engine loads [56].

An alternative method for optimizing combustion involves the use of a prechamber. Pre-chamber ignition is a crucial technology that can enhance the efficiency of spark-ignition engines. IAV's in-house development has demonstrated 2 to 9% fuel-saving potential in WLTC. While pre-chamber ignition technology has been previously introduced, significant challenges persist, such as cold operation at

low loads and the preparation of the mixture during active operation. IAV has introduced innovative solutions to address these challenges. This involves using both passive and active pre-chambers with a new low-pressure air/fuel injection system and incorporating complementary combustion technologies that leverage the specific benefits of pre-chamber ignition[57].

1.5 Thesis Outline and Structure

The present thesis is divided into **thirteen chapters** and aims to provide an in-depth analysis of alternative fuel solutions to mitigate CO_2 emissions. The first **two chapters** present a literature review of two main approaches: biofuels and hydrogen. Biofuels are analysed concerning their production, types, and the possibility of being adopted as a drop-in fuel and directly replacing fossil fuels. Hydrogen is discussed as a zero-carbon fuel that can be adopted in existing internal combustion engines (ICE).

The **third chapter** describes the testbed setup and measurement technique that will be used to analyse the second-generation prototype biofuels. This includes the equipment list and engine specifications. **Chapter four** discusses the effect of ethanol percentage on second-generation biofuels that have the same research octane numbers (RON). The aim is to study the impact of ethanol on performance and emissions compared to fossil fuels. **Chapter five** discusses the impact of higher RON on second-generation biofuels with similar ethanol ratios to assess the advantage gained by the higher octane numbers compared to standard fossil fuels.

Chapter six studies the main characteristics of second-generation biofuels, such as the higher particle numbers and different injection strategies to reduce the PM emissions and the PN numbers. **Chapter seven** discusses the main hydrogen properties and characteristics of hydrogen supply line design and analysis according to the standards. At the end of the chapter, there is an extensive analysis of the modification needed and the automated PLC shutdown with the new testbed layout.

Chapter eight comprehensively analyses hydrogen central direct injection vs gasoline direct injection over wider air-to-fuel ratios and different loads and injection matrices. The aim is to assess hydrogen's potential as a direct replacement for gasoline SI engines. **Chapter nine** discusses another challenge of adopting hydrogen as a main-supplied fuel by providing a full assessment of the hydrogen PFI vs. DI, the advantages of each system, and the limitations of the PFI.

Chapter ten takes a deep analysis based on hydrogen properties by discussing the impact of direct injection position on engine performance—the following two chapters of the thesis address two main concerns regarding H2ICE emissions. **Chapter eleven** provides a comprehensive analysis of the NO_x emissions and characteristics by measuring the NO_x in the crank and time domain and assessing the NO_x calculations over steady-state operations. **Chapter twelve** answers whether we can consider an H2ICE engine as a zero-carbon emission engine by analysing the CO_2 and Hc spikes due to lubricant oil, measuring per 0.25 crank degrees, and developing new methods to identify the severity of the HC spikes.

Chapter Thirteen presents the thesis summary and recommended future works. This chapter aims to comprehensively understand the research findings and their significance in the relevant field. Additionally, it outlines the scope for further research and development of hydrogen engines, emphasising the potential areas of improvement and the opportunities for innovation.

Chapter 2. Literature Review of Hydrogen and Biofuels Internal Combustion Technology

This chapter examines the advancements and difficulties of hydrogen internal combustion technology as a sustainable energy solution. Hydrogen internal combustion engines (HICE) have the potential to reduce carbon emissions and help the transportation industry meet its sustainability objectives. The research emphasises the advancements in engine design, combustion efficiency, and fuel injection systems to accommodate hydrogen's distinctive properties. In addition, various combustion strategies employed to improve engine performance and reduce emissions are discussed. The advantages of hydrogen internal combustion technology are discussed, including its compatibility with existing infrastructure, its high energy density for extended driving ranges, and its potential to facilitate a smooth transition in industries reliant on internal combustion engines [58].

Nonetheless, the article recognises the difficulties associated with hydrogen production, storage, distribution infrastructure, and engine efficacy. Safety concerns regarding the management of hydrogen are also addressed. In conclusion, the potential of hydrogen internal combustion technology for decarbonising transportation is highlighted. However, it emphasises the need for additional research, development, and infrastructure investments to overcome the obstacles. The sustainability of hydrogen production techniques and overall energy efficiency are crucial factors. By addressing these obstacles,

hydrogen internal combustion technology has the potential to play a significant role in the future of sustainable, low-carbon energy [59], [60].

2.1 Hydrogen Production

Hydrogen, the most abundant element in the universe, has enormous potential as a source of pure and sustainable energy. Transportation, industrial processes, electricity generation, and energy storage are just a few of its diverse applications. However, careful consideration is required to ensure that hydrogen production is environmentally benign and economically viable. There are diverse methods for producing hydrogen, including green, blue, brown, yellow, turquoise, and pink hydrogen. Depending on the feedstock and production process employed, each method has its environmental impact and characteristics. Figure 2.1 shows Hydrogen production routes, including renewables, fossil fuels and nuclear, with hydrogen being produced in power plants, pharmaceutical applications, synthetic fuels or their upgrades in transportation, ammonia synthesis, metal production or chemical industry applications [61], [62].
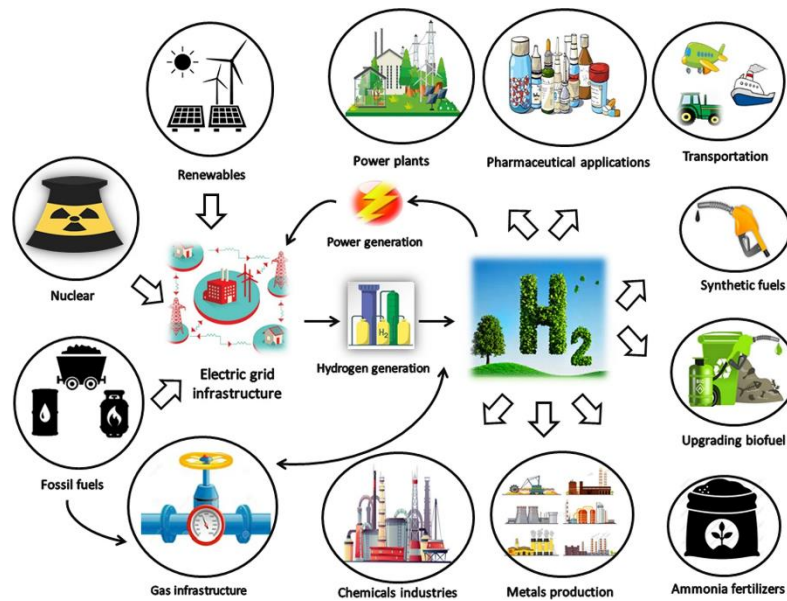
Figure 2. 1: CCU opportunities within EWF systems

There are many methods for producing hydrogen, including green, blue, brown, yellow, turquoise, and pink hydrogen. Depending on the feedstock and production process employed, each method has its environmental impact and characteristics, as per Figure 2.2 [63].
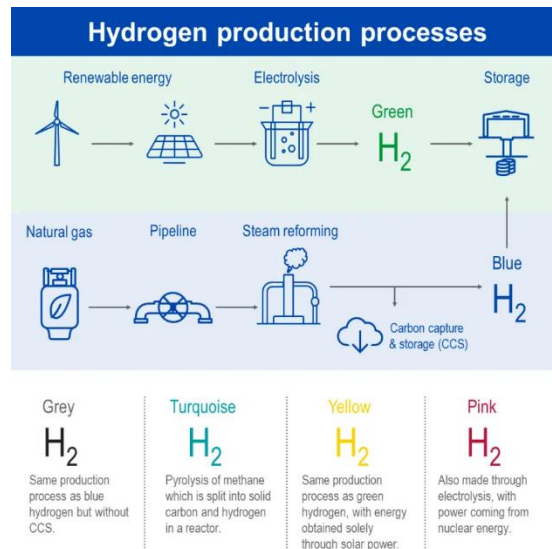
Figure 2. 2 Hydrogen production methodologies with different colour codes.

The main classifications of the hydrogen production methods are:-

1- Green Hydrogen:

Green hydrogen is produced through electrolysis using renewable energy sources such as solar, wind, or hydroelectric power. This method involves the separation of water molecules into hydrogen and oxygen using an electric current. It is considered the purest and most sustainable form of hydrogen production, with low greenhouse gas emissions, and provides a way to decarbonize sectors that are difficult to electrify directly [64].

2- Blue Hydrogen:

Blue hydrogen is primarily produced through steam methane reforming (SMR), a process that involves reacting natural gas (methane, CH4) with steam to generate hydrogen and carbon dioxide (CO2). Subsequently, carbon capture and storage (CCS) technologies are employed to capture and sequester CO2 emissions[65].

3- Brown Hydrogen:

Brown hydrogen is produced using coal in the same process as blue hydrogen, but it has high carbon emissions, significantly impacting the environment. As a result, there are more pure and sustainable options [66]

4- Yellow Hydrogen:

Yellow hydrogen is generated through the steam methane reforming process using natural gas, releasing carbon emissions into the atmosphere and leading to a substantial carbon footprint. This environmental impact is similar to conventional hydrogen production methods [67].

5- Turquoise Hydrogen:

Turquoise hydrogen is derived from natural gas through methane pyrolysis, which does not emit carbon dioxide. The resulting solid carbon byproduct can be stored or utilized, making it a potentially low-carbon emission option [68].

6- Pink Hydrogen:

Pink hydrogen is created through electrolysis, similar to green hydrogen, using electricity from nuclear power. By splitting water molecules into hydrogen and oxygen, it has the potential to serve as a low-carbon or emission-free option for hydrogen production. However, its feasibility hinges on the environmental implications of nuclear power, including the secure handling and disposal of nuclear waste [69].

2.2 Hydrogen Transportation and Storage

Hydrogen, a lightweight and highly reactive gas, necessitates specialized storage and transportation due to its low density and energy content. Efficient storage and safe transportation are crucial for utilising hydrogen as an energy carrier in various applications. Hydrogen can be stored in different forms, including compressed gas, liquid hydrogen, and solid-state materials. Compressed gas storage involves compressing hydrogen gas to high pressures and storing it in tanks, requiring robust tanks to withstand high pressures and relatively low energy density. Liquid hydrogen storage involves cooling hydrogen gas to shallow temperatures (-253°C) to convert it into a liquid state, offering higher energy density but requiring specialised cryogenic storage vessels and insulation. Solid-state hydrogen storage involves using metal hydrides, chemical hydrides, or carbon-based materials to absorb and release hydrogen at lower pressures and temperatures, offering potential advantages in terms of safety and practicality. However, further research and development are needed to enhance solid-state hydrogen storage materials' storage capacity and efficiency. The transportation of hydrogen can be challenging due to its low energy density, high flammability, and potential leakage risks. Currently, the most common method of hydrogen transportation is through pipelines, similar to natural gas distribution networks [70].

However, hydrogen pipelines require materials that can withstand hydrogen embrittlement, and dedicated infrastructure is needed to prevent hydrogen leakage and ensure safety. For long-distance transportation, hydrogen can be liquefied and transported in cryogenic tankers or delivered as ammonia, which has higher energy density and is easier to handle and store. Ammonia can be produced by combining hydrogen with nitrogen, and it can be liquefied at higher temperatures than hydrogen, making it more practical for large-scale transportation. In recent years, there has been increasing interest in hydrogen carriers such as liquid organic hydrogen carriers (LOHC) and hydrogenation-derived renewable fuels (HDRFs). These carriers enable hydrogen to be chemically bound and transported in a stable and safe form, quickly released and used as hydrogen when needed. Efforts are underway to develop advanced storage and transportation technologies to overcome hydrogen-related challenges. Research focuses on improving the energy density of hydrogen storage methods, developing cost-effective and scalable infrastructure, and ensuring safety measures are in place throughout the hydrogen value chain. As the demand for hydrogen grows in the transportation, industry, and power generation sectors, establishing a robust storage and transportation infrastructure is crucial to support hydrogen's widespread adoption as a clean and sustainable energy source [71].

One of the latest case studies was Ontario's low-carbon hydrogen strategy, which aims to pave the way for the private sector to expand the low-carbon hydrogen economy.

This work is essential for facilitating Ontario's transition to a low-carbon economy, rebuilding the province's manufacturing and industrial foundation, and supporting future well-paying employment.

By encouraging private sector innovation in this sustainable technology now, we can ensure that our energy system, environment, and economy will continue to flourish for future generations [72]

Ontario is prepared to do its part to attract more well-paying positions in science, technology, engineering, and skilled professions, jobs where individuals can take pride in contributing to a more sustainable and prosperous province, as shown in Figure 2.3.
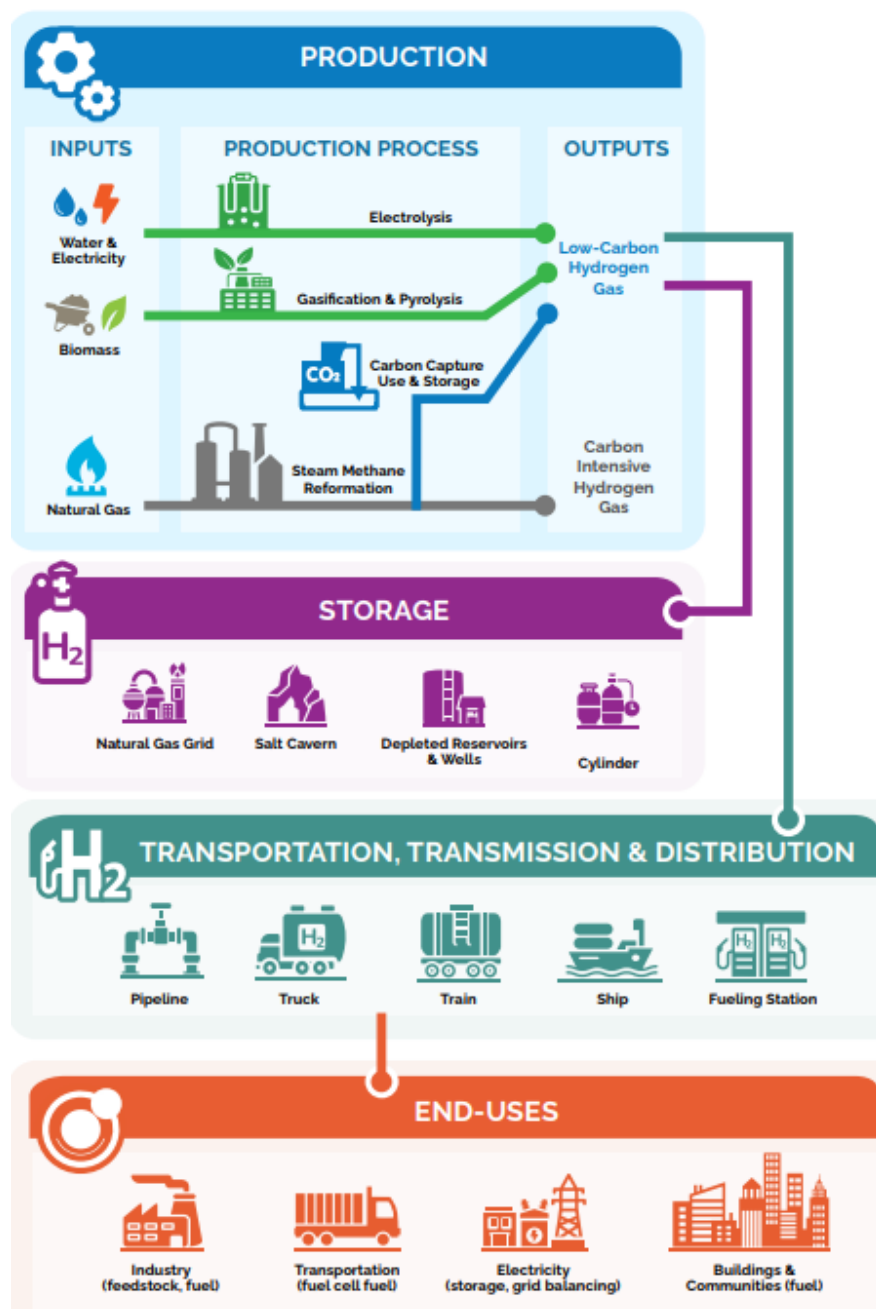
Figure 2. 3:Ontario's low-carbon hydrogen strategy [72]*.*

2.3 Hydrogen Internal Combustion Engines vs Fuel Cell

Hydrogen has emerged as a plausible energy carrier for decarbonising multiple sectors, including transportation. Hydrogen internal combustion engines (HICE) and fuel cells are two essential technologies for using hydrogen in vehicles—a thorough comparison of HICE and fuel cells highlights their merits, obstacles, and potential applications. The objective is to aid policymakers, researchers, and industry stakeholders in comprehending each technology's advantages and disadvantages and directing future developments in hydrogen-powered transportation. Hydrogen's potential as a pure energy source and the need for sustainable transportation solutions are examined.

2.3.1 Hydrogen Fuel Cell Technology

Hydrogen fuel cells are advanced energy conversion devices that produce electricity by combining hydrogen and oxygen in a chemical reaction, with the only byproducts being water vapour and heat. They are considered a promising alternative to traditional combustion engines and a vital technology in clean energy. Principal Hydrogen Fuel Cell Principles:

1- Electrochemical Process: Electrochemistry drives the operation of hydrogen fuel cells. The anode (negative electrode) of the fuel cell is supplied with hydrogen gas, which is divided into protons (H+) and electrons (e-). Electric current is generated when protons pass through an electrolyte membrane, and electrons are forced to travel through an external circuit.

2-Catalysts: With the assistance of a catalyst, usually platinum, electrons and protons recombine at the cathode (positive electrode). At the cathode, oxygen from the air reacts with the protons and electrons to produce only water (H_2O), as shown in Figure 2.4 [73].
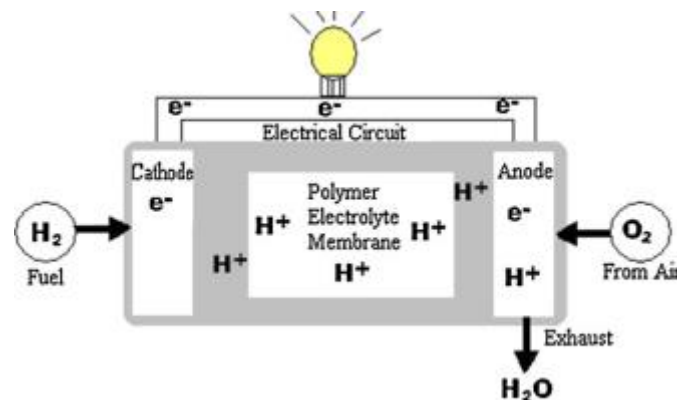
Figure 2. 4: The working principle of the Fuel cell.

Fuel cells differ according to operating temperature, efficiency, applications and costs. They are classified based on the choice of fuel and electrolyte into six main groups:

 - Alkaline fuel cell (AFC)

- Phosphoric acid fuel cell (PAFC)

 - Solid oxide fuel cell (SOFC)

- Molten carbonate fuel cell (MCFC)

- Proton exchange membrane fuel cell (PEMFC)

- Direct methanol fuel cell (DMFC)

Various fuel cell types are examined to determine the optimal application for each fuel cell. Although all varieties of fuel cells operate on a similar basis, Alkaline is the most efficient (60%) in terms of power efficiency, followed by Polymer electrolyte membrane (58%) and Molten carbonate (47%). Although AFCs are the most efficient, PEMFCs are ideally suited for transportation applications such as automobiles and buses. DMFC and PAFC are economically efficient, but their efficiency could be better. SOFC and MCFC have a high CHP performance. Comparing the estimated capital costs of ICEVs and FCEVs reveals that while FCEVs are more expensive due to the costs associated with hydrogen system modifications and distribution infrastructure, the operational costs over the vehicle's lifespan are more convincing. To be suitable for mass production, current innovative and modern fuel cell technologies must meet the economic characteristics and surpass the benefits of existing technologies. More R&D should be conducted by research institutes and businesses in order to increase the feasibility and effectiveness of FCEVs. Fuel cells offer numerous advantages over internal combustion engines (ICE) and other current power generators [74].

Advantages of Hydrogen Fuel Cells: Efficiency: Fuel cells are highly efficient at converting the chemical energy stored in hydrogen into electricity, typically surpassing the efficiencies of combustion-based power generation technologies. Hydrogen fuel cells produce zero greenhouse gas emissions and air contaminants, with only water vapour as a byproduct. This makes them an environmentally beneficial and clean energy source. Fuel cells can be used in a variety of applications, including transportation (e.g., automobiles, buses, railroads), stationary power generation (e.g., buildings, data centres), and portable devices (e.g., laptops, smartphones). Like conventional internal combustion engines, hydrogen fuel cells can be refuelled rapidly, providing shorter refuelling times compared to battery electric vehicles. Difficulties and Restrictions: The current difficulty resides in hydrogen production since most hydrogen is derived from fossil fuels, contributing to carbon emissions. However, sustainable hydrogen production methods, such as electrolysis powered by renewable energy sources, are the subject of ongoing research and development. Infrastructure: Developing a hydrogen infrastructure, including production, storage, and distribution facilities, is essential for the widespread adoption of hydrogen fuel cell technology. This necessitates a substantial financial commitment and coordination among stakeholders. Hydrogen fuel cell systems are presently more expensive than conventional power technologies. However, advancements in materials, manufacturing processes, and economies of scale are anticipated to lead to cost reductions in the future. Hydrogen's low energy density per unit volume necessitates efficient storage methods. To ensure the widespread acceptance of hydrogen as a fuel source, it is necessary to resolve safety concerns associated with hydrogen storage, transportation, and handling [75], [76].

While promising, the hydrogen fuel cell technology is not without its complexities. The main disadvantages of this technology can be summarized in the following points:

The requirement for ultra-high hydrogen purity is a significant challenge. This increases the cost of pure hydrogen rapidly and puts the entire equipment at a higher risk of toxicity.

The need for higher hydrogen pressure up to 400 bar , unlike the H2ICE technology, which can operate between 100 and 4 bar and with less hydrogen purity.

Another significant drawback is the need for higher heat dissipation and thermal management challenges. This is particularly problematic in moving applications like economic vehicles, where the higher aerodynamic air resistance and the need for costly additional heat exchangers further compound the issue.

The degradation rate of the equipment is significantly higher than that of ICE platforms. As it's a pioneer technology, the degradation rate and running cost of equipment are significantly higher than those of ICE platforms.

2.3.2 Hydrogen Internal Combustion Engine

Hydrogen's potential as a fuel source was recognised in the early 19th century when the first hydrogen internal combustion engines (H2ICE) were developed. Here is a concise summary of the significant milestones in the evolution of the hydrogen internal combustion engine: In the early 1800s, the Swiss inventor Francois Isaac de Rivaz created the first internal combustion engine that utilised a hydrogen-oxygen mixture as fuel. This engine signified the beginning of research into hydrogen as a possible alternative to conventional fuels. In the 1860s, Nikolaus Otto, the inventor of the four-stroke internal combustion engine, modified his engine to utilise hydrogen as a propellant. These investigations aimed to evaluate the performance and combustion properties of hydrogen. During the middle of the 20th century, hydrogen was investigated as a supplement fuel for internal combustion engines. Researchers investigated the possibility of combining hydrogen with fossil fuels such as petrol or diesel to enhance combustion efficiency and reduce emissions. Experimental Hydrogen Engines (1970s-1980s): In the 1970s and 1980s, dedicated hydrogen internal combustion engine research intensified. These engines were designed to use hydrogen as their principal fuel source. Various prototypes and experimental engines were developed to evaluate hydrogen combustion's efficacy and emissions characteristics. Hydrogen Engine Vehicles (1990s-Present): As part of their research into hydrogen-powered transportation, several automakers, including BMW and Mazda, developed hydrogen internal combustion engine vehicles in the 1990s. The objective of these vehicles was to demonstrate the viability of using hydrogen as a propellant in conventional internal combustion engines. Efficiency Enhancements in Hydrogen Combustion: Over time, engine design and combustion control improvements have led to efficiency enhancements in hydrogen combustion. This includes modifying the air-fuel mixture, ignition timing, and fuel injection systems to optimise performance. While hydrogen internal combustion engines have been investigated and developed, the focus has shifted in recent years to hydrogen fuel cell technology, which offers greater efficiency and fewer emissions than combustion engines [77], [78].

Moving towards zero-emission technology will require massive changes in the existing market. Hydrogen ICE engine technology can represent a potential for smooth energy transitioning as the modifications for adopting hydrogen will be minimised.

Several essential factors highlight the potential of hydrogen ICE:

Environmental Benefits: When burned in an internal combustion engine, hydrogen emits no pollutants. It contributes to enhanced air quality and lower greenhouse gas emissions by producing only water vapour as a byproduct. Hydrogen internal combustion engines (ICEs) have the potential to substantially reduce carbon dioxide (CO_2) emissions and mitigate the environmental impacts of conventional fossil fuel combustion [79].

Utilisation of Existing Infrastructure: One advantage of hydrogen ICEs is that they can utilise existing technology and infrastructure for internal combustion engines. Adapting internal combustion engines to operate on hydrogen facilitates a more seamless transition from conventional fuels to hydrogen because it requires fewer modifications than other propulsion systems.

Hydrogen is a lightweight and energy-dense fuel due to its high energy content per unit mass. This characteristic is advantageous for applications in the automotive and aviation industries, where weight and dimension are crucial factors. Hydrogen internal combustion engines (ICEs) can generate high power output and torque, making them suitable for various transportation applications.

Like conventional petrol or diesel vehicles, hydrogen internal combustion engine (ICE) vehicles can be rapidly refuelled. Long refuelling periods are one of the primary challenges of alternative fuel vehicles, as they limit their practicality. Additionally, hydrogen has the potential to provide comparable travelling ranges to conventional vehicles without sacrificing performance.

Hydrogen internal combustion engines offer flexibility in fuel options. They can be designed to operate as hydrogen-only engines or as dual-fuel systems, permitting them to function on hydrogen or a combination of hydrogen and conventional fuels. This adaptability can facilitate the transition to hydrogen by utilising existing fuel infrastructure and addressing potential fuel availability concerns [80], [81]

Economic Potential: As the demand for clean and sustainable transportation grows, hydrogen internal combustion engines (ICEs) can contribute to employment creation and economic growth in industries related to hydrogen production, storage, and distribution. The development of fueling infrastructure for hydrogen could also spur investment and innovation [82].

In spark-ignited (SI) engines, hydrogen utilisation has been documented as an alternative or in conjunction with other fuels. Hydrogen Por fuel injection challenges such as backfire and pre-ignition primarily stem from the interaction of the fresh mixture with hot residual gases, hotspots, and exhaust backflow. Hydrogen direct injection might reduce abnormal combustion and allow the engine to reach higher engine loads (above GDI operating conditions), higher engine efficiency at the same load and lambda, and higher combustion velocity due to the turbulence induced by the fuel injection. Direct injection of hydrogen also enables operation under stratified charge conditions, extending the lean limit of a spark ignition engine [83], [84], [85].

Recent studies suggested that the use of hydrogen in its pure form or as an additive can enable stable lean combustion with different fuels, including gasoline, compressed Natural Gas and Acetone-Butanol-Ethanol. Because of its low ignition energy and high adiabatic flame speed, the inclusion of hydrogen decreases cycle-to-cycle variability and expands the lean-burn limit. Consequently, in applications involving pure hydrogen, exceptionally

high dilution rates with air or exhaust gas recirculation (EGR) are possible, resulting in minimal NOx emissions with lean and ultra-lean mixtures, all while maintaining satisfactory combustion stability.

Kawamura et al. [86], showed that to allow a larger degree of fuel-air mixture stratification, Close-coupled injection and ignition strategies can be used, namely plume-head and plume-tail. The plume-head ignition is triggered soon after the SOI, whereas the plume-tail ignition strategy triggers the ignition of the jet just after the end of the injection. Karaya et al. [87]demonstrate a location-dependent interaction between GDI engine injector nozzle size and performance. Smaller nozzles optimised for the original location enhance mixture formation, IMEP, and HC emissions across all orientations. Conversely, the new location favours larger nozzles, achieving similar benefits as indicated by a stratification index closer to unity. Rouleau et al.[88] conducted a comprehensive investigation, employing both experimental and numerical techniques, to explore the application of hydrogen combustion in a spark ignition (SI) engine. A high-efficiency gasoline single-cylinder engine was modified for hydrogen combustion using direct injection and a platinum-free cold spark plug. The study demonstrated that the lean mixture, early hydrogen injection, and high tumble level produced maximum efficiency (near to 47%), minimal NOx (less than 10 ppm), and acceptable unburnt H2 emissions (1% input energy). The pre-ignition, one of the highest challenges in hydrogen combustion, is successfully limited by adjusting the injection timing and camshaft phasing [89], [90], [91], [92], [93].

The scarcity of fossil fuel reserves, geopolitical fears associated with fossil fuel depletion, issues of environmental pollution and climate change, and the need to ensure the independence of energy supply make the low-carbon economy with an essential hydrogen vector inevitable in the coming decades. Today first series of hydrogen-fuelled buses and cars are already on the road, and refuelling stations are operating in different countries around the world [94].

Hydrogen is an abundant fuel, burns cleanly, and has a high energy content. It features zero carbon dioxide emissions, a broad flammability range, and a rapid combustion rate. A design must be modified when internal combustion engines are modified to operate on hydrogen, fuel injection, ignition, and combustion chamber.

Compared to fossil fuels, hydrogen in internal combustion engines reduces greenhouse gas emissions and pollutants. However, hydrogen combustion in ICEs may be less efficient than fuel cell combustion. Dual-fuel systems permit using both hydrogen and conventional fuels, providing flexibility and maximising the utilisation of existing infrastructure.

Although hydrogen internal combustion engines offer advantages such as speedy refuelling and compatibility with existing infrastructure, emissions control and optimising efficiency remain obstacles. Additional research and development are required to enhance hydrogen internal combustion technology and realise its potential as a sustainable energy solution [95].

H2's broader flammability range allows for leaner operation without increased ignition energy, reducing the likelihood of abnormal combustion such as pre-ignition and backfire. These issues typically arise under stoichiometric conditions that limit engine load and power output. A leaner operation also significantly drops engine-out NO_x with relative air-

fuel ratio (λ) values exceeding 2. According to White et al., a boosted hydrogen ICE running at lean conditions can achieve very low NO_x levels without requiring an after-treatment system. This is critical because hydrogen combustion's high flame temperature produces NO_x, which can cause thermal dissociation and oxidation of nitrogen in atmospheric air during combustion[96], [97], [98].

Therefore, an effective H2 combustion strategy involves running the engine at an ultra-lean mixture while maintaining the desired power density and higher engine load. However, leaner combustion can result in lower combustion efficiency, leading to more unburned fuel and reducing thermal efficiency and exhaust gas temperature (EGT), negatively impacting the enthalpy available for driving turbochargers. It is, therefore, essential to consider these factors when designing an H_2 combustion system for ICEs to ensure optimal performance and emission reduction [99].

As speed increases, the issue of backfire becomes more pressing. However, DI can effectively prevent backfire in the intake manifold and minimize pre-ignition by reducing fuel residence time in the cylinder. The timing of injection is crucial, as injection pressure and time significantly impact volumetric efficiency. Late injection during the compression stroke can increase thermal efficiency and power output, providing a significant advantage compared to PFI systems. In a study comparing the effects of intake and compression stroke injections in a light-duty SI single-cylinder engine, Mohammadi et al. [94], found that direct hydrogen injection mitigates backfire. However, increasing the quantity of hydrogen injected can decrease volumetric efficiency and limit maximum power output. Injecting hydrogen during the compression stroke reduces knock and enhances both thermal efficiency and maximum output power. Late hydrogen injection can further improve thermal efficiency and greatly decrease NO_x emissions under high engine output conditions but requires injectors with high flow rates for thorough mixing with air prior to ignition timing [100], [101], [102].

Hydrogen has been recognised as a promising alternative or complementary fuel for spark-ignited (SI) engines. Nevertheless, a few challenges must be tackled when utilising hydrogen as a fuel in SI engines. These challenges include backfire and pre-ignition, which primarily arise due to the interaction of the fresh mixture with hot residual gases, hotspots, and exhaust backflow. [103].

One potential solution to overcome these challenges is the direct injection of hydrogen. Direct injection of hydrogen can mitigate abnormal combustion and enable the engine to achieve higher engine loads, which is impossible under conventional gasoline direct injection (GDI) operating conditions. Additionally, direct injection of hydrogen can improve engine efficiency and combustion velocity and allow for operation under stratified charge conditions, thereby extending the lean limit of a spark ignition engine[104], [105].

Overall, hydrogen direct injection holds immense potential for addressing some of the challenges associated with using hydrogen as a fuel in SI engines. Enhancing engine performance and efficiency can pave the way for a more sustainable and cleaner future[106].

Kawamura et al. [86]showed that to allow a larger degree of fuel-air mixture stratification, Close-coupled injection and ignition strategies can be used, namely plume-head and plume-tail. The plume-head ignition is triggered soon after the SOI, whereas the plume-tail

ignition strategy triggers the ignition of the jet just after the end of the injection. Karaya et al. Y. Karaya et al. [87] demonstrate a location-dependent interaction between GDI engine injector nozzle size and performance. Smaller nozzles optimised for the original location enhance mixture formation, IMEP, and HC emissions across all orientations. Conversely, the new location favours larger nozzles, achieving similar benefits as indicated by a stratification index closer to unity. Takagdi et al. [107]demonstrated that the injection angle plays a crucial role in engine performance, and its optimisation is essential to minimise wall heat loss by achieving the optimal separation of hydrogen jets from the chamber walls. L. zhi Bao et al.[108] emphasised the significance of high injection pressure in achieving elevated engine load at mid to high engine speeds while maintaining low NO_x emissions. They highlighted that early injection leading to improved fuel homogenisation is crucial for reducing NO_x emissions.

2.3.3   Hydrogen Potential and Opportunity

Advantages of Hydrogen Fuel Cells: Typically eclipsing 50%, the energy conversion efficiency of fuel cells exceeds that of internal combustion engines—this efficacy results in improved fuel economy and decreased energy waste. Hydrogen fuel cells emit only water vapour, resulting in zero exhaust emissions. They offer a clean and sustainable alternative to conventional combustion engines, thereby contributing to improved air quality and decreased greenhouse gas emissions. Since no combustion processes are involved, fuel cell-powered vehicles operate in silence. This feature can improve the driving experience overall and reduce noise pollution. More Extended Range: Hydrogen fuel cell vehicles typically have longer ranges than battery-electric vehicles. They provide a viable solution for applications requiring long-range capabilities, such as long-distance travel and commercial conveyance. Hydrogen fuel cell vehicles can be refuelled in minutes, similar to conventional vehicles, providing a more convenient refuelling experience than battery electric vehicles, which typically require lengthier charging times. Disadvantages of Hydrogen Fuel Cells: Infrastructure Restriction: The infrastructure for hydrogen fueling stations is presently restricted, making widespread adoption of hydrogen fuel cell vehicles difficult. The expense and complexity of establishing a comprehensive refuelling network are significant obstacles.

High Production and Distribution Costs: Due to the energy-intensive processes involved, the production and distribution of hydrogen fuel can be costly. This cost factor contributes to fuel cell vehicles' higher overall price than internal combustion engines. Storing hydrogen fuel safely and compactly remains a challenge. Hydrogen requires high-pressure containers or cryogenic storage systems, increasing vehicle design's complexity and weight. The benefits of hydrogen internal combustion engines (ICE) are as follows: Utilisation of Existing Infrastructure: Hydrogen ICEs can utilise existing technology and infrastructure for internal combustion engines, requiring fewer modifications than fuel cell vehicles. This benefit facilitates the transition to hydrogen as a fuel and reduces the requirement for extensive infrastructure development. Similar to conventional petrol or diesel vehicles, hydrogen-powered ICE vehicles can be rapidly refuelled. This addresses the problem of lengthy refuelling durations associated with other alternative fuel vehicles, enhancing their utility. Flexibility and Dual-Fuel Options: Hydrogen internal combustion

engines (ICEs) offer flexibility in fuel options, permitting the use of hydrogen or a combination of hydrogen and conventional fuels. This dual-fuel capability can facilitate the transition to hydrogen by utilising the existing fuel infrastructure and resolving fuel availability concerns.

Hydrogen Internal Combustion Engines (ICE) disadvantages:

Previous studies showed that Nitrogen oxides (NO_x) are still produced by hydrogen combustion in internal combustion engines despite the emissions being lower than those of fossil fuels. NO_x emissions contribute to air pollution and are restricted by regulations. Hydrogen internal combustion engines have a lower energy conversion efficiency than fuel cells. Due to combustion processes, the overall efficiency of converting hydrogen into usable mechanical energy is lower in ICEs, resulting in poorer fuel economy. it should be pointed out that most previous studies on hydrogen engines were conducted with near stoichiometric air fuel ratios, hence not insignificant NO_x emissions. In addition, the engine used was not optimised for Hydrogen fuel for better efficiency. hydrogen and the combustion process's overall efficacy can affect the vehicle's range and output.

In conclusion, the high potential of overcoming all H_2 ICE disadvantages with the easy adoption of internal combustion makes H_2 ICE have a higher potential to be represented and adopted in different applications.

As shown in Figure 2.5, which shows the hydrogen opportunities over different applications in Australia, it is clear that moving to zero-emission is not achieved with one solution.
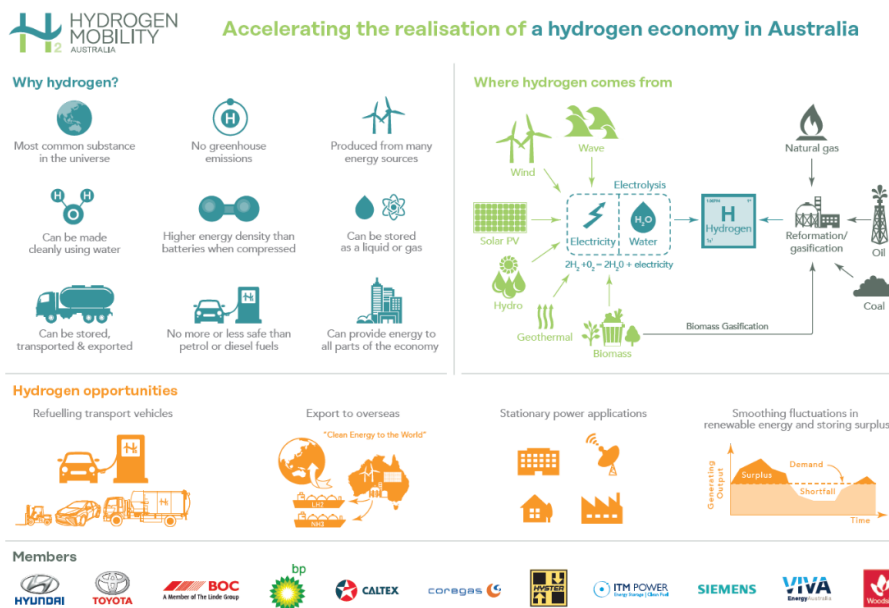
Figure 2. 5: hydrogen opportunities over different applications in Australia [109]*.*

2.4 Biofuels Production

Biofuel production converts biological materials, such as cereals, agricultural residues, or algae, into liquid or gaseous fuels that can replace fossil fuels. Biofuels are considered renewable energy sources because they are produced from replenishable organic matter.

Several varieties of biofuels are produced through various processes:

Ethanol: Ethanol is the most common biofuel produced primarily by fermenting sugars or starches from crops like maize, sugarcane, or wheat. It can be mixed with petrol and used as a fuel for vehicles.

Biodiesel: Biodiesel is produced from vegetable oils or animal lipids via transesterification. It can be used as an alternative to diesel fuel in vehicles and emits less particulate matter and sulphur than conventional diesel.

Biogas is produced by the anaerobic digestion of organic waste, such as agricultural residues, culinary waste, and sewage. It consists predominantly of methane and carbon dioxide and can be used to generate electricity or as a vehicle fuel.

Hydroprocessing Vegetable Oils (HVO): HVO is produced by hydroprocessing vegetable oils or animal lipids, yielding a fuel with diesel-like properties. It has superior cold flow properties and can be blended with regular diesel or used as a direct replacement [110].

Biofuel production presents numerous benefits:

a- Biofuels have the potential to reduce greenhouse gas emissions when compared to fossil fuels because the carbon dioxide emitted during their combustion is balanced by the carbon dioxide absorbed during plant growth.
b- Biofuels can reduce reliance on imported fossil fuels because they can be generated domestically from local biomass resources.
c- Biofuel production can stimulate rural economies by establishing new agricultural opportunities and jobs in the biomass supply chain.

However, the production of biofuels is not without obstacles:

a- Biofuel production competes with food crops for land, water, and other resources, which raises concerns about food security and deforestation [111].
b- Expanding biofuel crops may convert natural habitats and forests, leading to indirect greenhouse gas emissions.
c- The availability and sustainability of biomass feedstocks for biofuels can differ geographically and depend on crop yields, agricultural practices, and land management.

Technological and economic feasibility: The production of biofuels on a large scale and at a cost competitive with fossil fuels requires further technological development and favourable market conditions.

The production of biofuels has a substantial impact on the transition to a more sustainable and low-carbon energy system. Through continued research, development, and policy support, biofuel production processes must be more effective, sustainable, and economically viable [112].

2.5 Biofuels as a Drop-in Fuel.

Drop-in biofuels are renewable fuels that can directly replace or be merged with conventional fossil fuels without modifying existing engines or infrastructure. They are engineered to possess the same chemical properties and energy content as their fossil fuel counterparts, allowing for a seamless transition to renewable alternatives.

The concept of drop-in biofuels addresses the difficulty of integrating renewable fuels into existing transportation systems without requiring costly engine modifications or infrastructure alterations. By emulating the properties of fossil fuels, drop-in biofuels can be utilised in conventional vehicles, aircraft, and other combustion engines without requiring significant modifications or restrictions[113].

The following are examples of drop-in biofuels:

Renewable Diesel: Renewable diesel is a drop-in fuel derived from renewable feedstocks, such as vegetable oils, animal lipids, or waste oils, through a hydrotreating or hydrogenation process. It has the same chemical properties as petroleum diesel and can be used as a direct replacement or compounded in varying proportions.

Sustainable Aviation Fuel (SAF): Sustainable Aviation Fuel is a drop-in biofuel explicitly designed for aviation applications. Through hydroprocessing or Fischer-Tropsch synthesis, it is produced from renewable feedstocks such as vegetable oils, algae, and refuse oils. SAF can be utilised without modification in aircraft engines and has the potential to reduce greenhouse gas emissions in the aviation industry substantially.

Using advanced biofuel conversion technologies, renewable petrol is produced from biomass sources such as maise, sugarcane, or cellulosic materials. It can be used as a direct replacement for conventional petrol or infused with it.

Among the benefits of drop-in biofuels are the following:

a- Compatible: Drop-in biofuels can be used in existing engines and infrastructure without costly modifications or infrastructure enhancements, allowing for a more seamless transition to renewable fuels.
b- Reduced emissions: Typically, biofuels emit less carbon dioxide than fossil fuels, resulting in reduced greenhouse gas emissions and enhanced air quality.

Using locally available renewable feedstocks, drop-in biofuels can help reduce dependence on fossil fuel imports and improve energy security[114].

Nevertheless, drop-in biofuels present several obstacles:

The production of drop-in biofuels requires a sustainable and reliable supply of feedstocks, which can compete with food production and raise concerns regarding land use change, deforestation, and biodiversity loss.

Spending and scalability: Drop-in biofuels encounter economic challenges due to higher production costs than fossil fuels. Scaling up production and achieving cost parity with petroleum-based fuels remain key biofuel industry objectives.

Policy support and market demand are indispensable for drop-in biofuels' widespread adoption and commercial viability.

Drop-in biofuels offer a promising way to decarbonise the transportation industry while utilising existing infrastructure. Ongoing research and development efforts and supportive policies will be essential to advance further drop-in biofuel production, sustainability, and market penetration.

Compared to conventional fossil fuels, they offer the benefit of substantial well-to-wheel and vehicle lifecycle CO_2 reductions. This investigation focuses on using 100% bio-derived

fuel in spark-ignited internal combustion engines, such as those commonly found in automobiles. The biofuels evaluated in this study were meticulously designed to closely resemble the properties of petrol derived from fossil fuels despite being derived from second-generation feedstocks. Second-generation bio-feedstocks are non-food-based biomass, such as agricultural and forestry residues, that do not compete with food production and provide a more sustainable feedstock option. Comparing the performance characteristics of these bio-gasoline fuels to those of conventional fossil fuels, the research presents exhaustive combustion data to provide a detailed understanding of these characteristics. Exhaustive research is conducted on both engine-out and after-treated emissions. Engine-out emissions are those emitted directly from the engine, while after-treated emissions are those emitted after passing through exhaust treatment systems. This comprehensive analysis evaluates all current emissions regulations and analyses exhaust CO_2 emissions under steady-state and transient driving conditions. To ensure a comprehensive analysis, the study employed engine-dynamometer testing to examine the combustion behaviour under various operating conditions. Researchers can gain valuable insights regarding these biofuels' performance, emissions, and compatibility in internal combustion engines by conducting tests in controlled laboratories. This study contributes to our comprehension of the efficacy of biofuels as drop-in replacements for conventional fossil fuels throughout the entire vehicle lifecycle by examining their potential as direct replacements. The objective is to provide policymakers, automotive manufacturers, and researchers with valuable data and insights to aid their pursuit of sustainable transportation solutions. Chapter three will evaluate the viability and practicability of using bio-gasoline in spark-ignited internal combustion engines, paving the way for a greener and more sustainable future in transportation.

The use of alcohol fuels as an alternative to fossil fuels has been gaining popularity worldwide due to its immediate impact on reducing carbon emissions in the tailpipe and creating a CO_2 fuel life cycle. This contrasts with other alternative fuels that require extensive infrastructure and fleet upgrades. Ethanol and methanol, in particular, have been found to outperform gasoline engines in terms of thermal efficiency, especially at higher loads and power outputs. This is due to their strong knock resistance, which allows for more advanced combustion phasing and eliminates the need for over-fueling under full load and power operations [115], [116],[117]. However, higher ethanol concentrations, such as cold start issues, can pose challenges. Premixed alcohol/gasoline fuels have shown a significant drop in the total emission of vehicles with less particulate number. However, the response of some emission pollutants, such as NO_x, on SI engines depends on the powertrain setup[118], [119], [120].

Biofuels, derived from or created by recently lived creatures, offer an alternative to fossil fuels. First-generation biofuels derived from food crops have been problematic due to the necessity of choosing between fuel and food alternatives. Second-generation biofuels have been developed to overcome this disadvantage and are derived from non-food crops like grass, wood, and other organic waste[121], [122].

Bio-gasoline, a type of biofuel, has also been tested and found to be a drop-in substitute for typical gasoline fuel produced from fossil sources without requiring engine adjustments or changes in the fuelling system. A study investigated the performance and emission performance of a spark-ignited (SI) engine operated with bio-gasoline with three different concentrations of ethanol, E5, E10, and E20, all with a RON value of 95.

Alcoholic fuels such as ethanol and methanol have the potential to address complex issues associated with fossil fuel usage, paving the way for a low-carbon and sustainable energy future. These renewable fuels can be easily integrated into existing combustion technologies, making them significant contributors to global climate action and energy security. However, their full potential is yet to be unlocked due to challenges related to energy-efficient production, feedstock conflicts, and distribution efficiency. Researchers, governments, industry, and society must collaborate to overcome these challenges. Technological advancements and supportive regulations are essential for the industry's growth, and educating consumers on alternative fuels is crucial. Alcoholic fuels offer a promising pathway to a cleaner and greener future, providing a sustainable solution to reduce emissions, enhance energy security, and diversify energy sources. As technology advances and collaborations strengthen, alcoholic fuels could become mainstream, ensuring a sustainable energy future for generations to come [123], [124].

Biogasoline is a drop-in fuel critical in reducing greenhouse gas emissions and improving energy security in the transportation industry. Its ability to replace conventional gasoline without requiring modifications to cars or infrastructure makes it an ideal solution for sustainable mobility. However, some challenges must be addressed through a multifaceted approach. While biogasoline is environmentally friendly, concerns exist regarding feedstock availability and diversity. To overcome these limitations, research is needed to identify various biomass sources and improve feedstock production and conversion technology. Additionally, to ensure biogasoline's economic viability, production efficiency must be improved, costs must be lowered, and refining must be optimised [125], [126], [127]

Previous studies aim to investigate the impact of the research octane number on the combustion characteristics, performance, and emissions, and the main outcomes align with previous research on varying the research octane number for fossil fuels [128], [129].

Biofuels are fuels made from renewable resources, such as crops, agricultural waste, or other organic matter. These fuels have a higher concentration of heavier aromatics than fossil fuels, which makes them a significant contributor to increased particulate matter (PM) emissions. PM emissions are a major concern for air quality and public health, as they can cause respiratory problems and other health issues[130], [131].

There are two fuel injection systems used in engines: port fuel injection (PFI) and direct injection (DI). Studies have shown that DI produces higher PM emissions than PFI, so optimising fuel injection strategies between the two systems could significantly reduce PM emissions. However, this optimisation could also affect engine performance and increase other pollutant emissions[132], [133], [134], [135].

One promising solution to these issues is the use of various alcoholic fuels, such as ethanol. *Ethanol* is a renewable fuel source that burns cleaner than gasoline or diesel and can significantly reduce emissions. In addition, ethanol has a greater influence on engine performance, which means that it can help to improve overall engine efficiency and reduce greenhouse gas emissions. Overall, using biofuels and other cleaner fuels is an important step towards reducing emissions and protecting public health [136], [137].

2.6 Sustainable Fuels Research Gaps

The literature review indicates that synthetic and biofuels exhibit great potential as drop-in fuels, which could substantially reduce CO_2 emissions throughout their life cycle. Nonetheless, using food crops for the first generation of biofuels poses a significant challenge, raising concerns about food security. Therefore, the second generation of biofuels produced from non-food biomass may offer the best solution.

While recent scientific research on second-generation biofuels has yielded promising results, much remains to be explored to unlock their full potential, especially concerning the effect of ethanol blends with various octane ratings. Furthermore, studies must address particulate matter (PM) mitigation in second-generation biofuels.

Regarding alternative fuels, hydrogen is a zero-carbon fuel that could eliminate CO_2 emissions and substantially drop the tailpipe emissions near zero. However, the transition to hydrogen-based transportation will present significant challenges, such as the need for major infrastructure upgrades and modifications to existing vehicles. In addition, more research is required to explore a spark ignition engine that can run on pure hydrogen with ultra-low NOx emission and higher efficiency through ultra-lean-burn combustion.. A significant research gap specifically addresses the impact of injector location on engine performance and emissions (Side Direct injection vs Central Direct injection). To bridge this gap, a comprehensive study was conducted on a single-cylinder SI engine to assess the performance and emissions of hydrogen direct injection IC engines using both Side Direct Injection and Central Direct Injection systems. The study was conducted at varying engine speeds, engine loads, and relative air-fuel ratios through three experiments: fuel matrix, λ sweep, and engine load sweep. The findings of this study could have significant implications for the future design and development of hydrogen direct injection engines.

2.7 The Aim and Objectives of The PhD

Reducing CO_2 emissions is crucial for a positive environmental impact in light of the increasingly severe effects of climate change. This PhD aims to assess two approaches for reducing green house gas emissions in applications that rely on ICE as their primary platform. The first approach evaluates second-generation biofuels with varying ethanol and RON numbers to compare their visibility and CO_2 footprint in relation to traditional fuels. This comparison will provide valuable insights into how these fuels can reduce life cycle emissions.

The second approach explores using hydrogen, a zero-carbon fuel, as a direct replacement for gasoline in the SI engine. This involves addressing the challenges of establishing a hydrogen supply line and implementing safety measures to ensure proper isolation and ventilation. A comprehensive report will be provided, including extensive experimental analysis of injection techniques. Additionally, two key questions will be addressed: What are the emissions associated with hydrogen, and how can it be considered a zero-carbon fuel.

Chapter 3. Experimental Assessment of Combustion Characteristics, Performance, and Emissions of SI Engine with 2nd Generation Bio-Gasoline

The automotive industry is confronted with stringent regulations intended to reduce greenhouse gas emissions and transition to a more sustainable future. Achieving zero exhaust carbon dioxide (CO_2) emissions within the next decade is one of the primary objectives. Although electric vehicles have received considerable attention as a viable solution, they may only be suitable for some applications or capable of addressing emissions from the current fleet or manufacturing process. Biofuels and entirely synthetic fuels have emerged as potential solutions to these problems. These fuels can be derived from renewable resources like plant biomass, agricultural residues, and algae.

3.1 Introduction

This investigation focuses on second-generation biofuels, which utilise feedstocks that do not directly displace food crops but rather utilise the non-food portions of the crop. The feedstock is used to produce ethanol as a starting point for the fuel, which is then further processed to produce a gasoline-like fuel engineered to perform similarly to gasoline derived from fossil fuels and to meet the gasoline CEN standard. This procedure's specifics are discussed in detail in the following section. Due to the additional processes required, this method will use more energy during production than if ethanol were used directly as a fuel. It has been demonstrated that first-generation biofuels from crops offer negligible GHG benefits compared to fossil-derived fuels. These biofuels of the second generation offer considerably more advantages. Ethanol has been demonstrated to be a technically superior alternative to fossil fuel petroleum; however, internal combustion engines must be redesigned to achieve maximum engine efficiency, minimise emissions of pollutants, and ensure long-term dependability [138]. Therefore, it is not suitable as a drop-in replacement for decarbonising the extant fleet and would necessitate additional investment in powertrain engineering and fuel distribution for use in new internal combustion engine products. Synthetic fuels offer a potential route to zero-carbon internal combustion engine operation and can be engineered to function as drop-in replacements. It has been demonstrated that these fuels perform as well as, if not better than, those derived from fossil fuels, potentially with superior emissions performance. However, they are the most energy-intensive fuels to produce, requiring up to six times more renewable electricity than battery-electric vehicles to power a vehicle. This will incur

a hefty cost penalty, but it could provide a solution for applications that are difficult to decarbonise, such as aviation and transportation, and a way to continue using historic, classic, performance, and motorsport vehicles. Other synthetically produced e-fuels, such as hydrogen, ammonia, methanol, and methane, also offer zero-carbon solutions; however, as with ethanol, they require re-engineering of the internal combustion engine, and in these cases, the fuel storage and refuelling systems, so they are not suitable for the legacy fleet. Through testing, it will be demonstrated that the proposed bio-gasoline fuels achieve the same performance as fossil-derived fuels while emitting levels of pollutants that are typically well below legislative targets and, in the case of particulate emissions, orders of magnitude lower than other vehicle-based sources [139], [140], [141]

3.2 Fuel Properties

The second-generation bio-gasoline fuel utilised was produced via a two-step process designed to convert waste biomass or agricultural residues, such as straw, into a viable fuel source. In the first stage, lignocellulosic biomass was converted into bioethanol. The biomass was subjected to a pre-treatment procedure to increase enzyme accessibility and facilitate decomposition. Following pre-treatment, the biomass was subjected to enzymatic hydrolysis, which converts the complex carbohydrates into simple sugars. Bioethanol was then produced by fermenting these carbohydrates with a variety of microorganisms.

The bioethanol produced in the first stage was further refined to produce biogasoline. The bioethanol was dehydrated to produce ethylene, a building block for longer-chain hydrocarbons. This dehydration occurred between 300 and 400 degrees Celsius and utilised a zeolite catalyst. The ethylene molecules were catalytically "grown" into hydrocarbons with extended chain lengths, simulating the composition of conventional petrol [142], [143].

Figure 3.1 depicts the two-step procedure for producing bio-gasoline from lignocellulosic biomass, emphasising bioethanol conversion into longer-chain hydrocarbons.
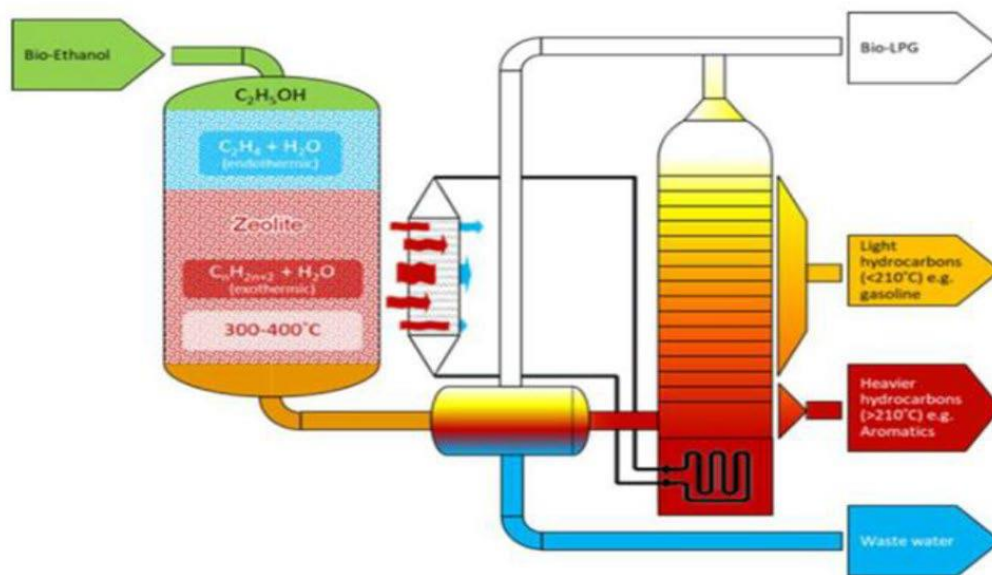
Figure 3. 1: Schematic of the ethanol-to-gasoline conversion [144].

To ensure uniformity and facilitate comparisons, the test fuels were prepared according to the specifications listed in Table 3.1. The petrol used in the investigation complies with the EN228 fuel standard, which imposes stringent performance requirements. This standard addresses many fuel properties, including combustion efficiency, emissions, and overall fuel quality. Using the EN228 standard as a benchmark, the efficacy and viability of bio-gasoline fuels as an alternative to conventional gasoline were evaluated using a stringent set of criteria [145].

Table 3.1's specifications guided the bio-gasoline fuels used in the study, ensuring that they met the requirements for testing and comparison. By employing such stringent standards and specifications, researchers could accurately evaluate the bio-gasoline fuel's performance and potential, allowing for meaningful comparisons with the standard petrol and providing valuable insights into its suitability for internal combustion engines.

This method allowed for a comprehensive analysis of the bio-gasoline fuel's composition, properties, and performance, which assisted in determining its viability as a direct replacement for conventional petrol. Bio-gasoline fuels have the potential to substantially reduce greenhouse gas emissions and contribute to a more sustainable transportation sector by utilising waste biomass and advanced conversion processes. This study provides valuable insights into developing and utilising bio-gasoline fuels, paving the way for future environmentally benign and greener fuel alternatives.

Table 3. 1: Biofuels Properties vs Fossil Fuel.

Parameter / Test	Units	Method	BIO - 95E10	BIO - 95E5	Bio-95RON_E20	Bio-99RON_E20	Fossil 95 E10
Bio-Content	% v/v	Blending	100	82.9	100	100	10.1
Honda Particulate Mass Index	ASTM D6730 mod	2.25	2.17	1.88	2.09	1.03
Simplified Particulate Mass Index		Calculation	2.49	2.15	-2.95	2.21	-
R.O.N.		ASTM D2699	95.90	95.20	96.20	99.00	95.50
M.O.N.		ASTM D2700	84.60	85.10	85.00	86.10	85.10
Carbon	% (m/m)	ASTM D6730 mod	83.10	84.77	79.02	79.43	83.06
Hydrogen	% (m/m)	ASTM D6730 mod	13.31	13.44	13.57	13.30	13.35
Density at 15°C	kg/L	ASTM D4052	0.763	0.752	0.761	0.766	0.753
Initial Boiling Point	°C	EN ISO 3405	30.1	30.1	34.9	28.5	34.9
Final Boiling Point	°C	EN ISO 3405	205.0	205.2	201.9	205.3	189.9
% vap evap at 70°C	% (v/v)	EN ISO 3405	40.4	37.0	33.0	34.4	41.5
% vap evap at 100°C	% (v/v)	EN ISO 3405	47.6	48.0	58.2	58.8	55.8
E130	% (v/v)	EN ISO 3405	58.0	64.7	65.7	63.3	72.7
% vap evap at 150°C	% (v/v)	EN ISO 3405	70.5	76.2	76.6	73.7	89.5
E170	% (v/v)	EN ISO 3405	85.8	87.8	89.7	87.5	93.4
% vap evap at 180°C	% (v/v)	EN ISO 3405	92.1	93.2	94.1	93.3	97.2
Recovery	% (v/v)	EN ISO 3405					-
Residue	% (v/v)	EN ISO 3405	1.10	1.10	1.10	1.10	1.1
Loss	% (v/v)	EN ISO 3405					-
Oxygen (subcontracted)	% (m/m)	Elemental Analysis*	3.59	1.79	7.41	7.28	3.59
H/C Ratio			1.908	1.889	2.046	1.995	1.915
O/C Ratio			0.03243	0.01585	0.07039	0.06880	.03244

AFR (Stoic)	assumes	unoxygenated fuel	14.65	14.63	14.85	14.78	14.66
AFR (Stoic)	assumes	oxygenated fuel	13.97	14.29	13.43	13.39	13.98
Percentage H+C+O	%		100.00	100.00	100.00	100.01	100
Ethanol & Higher Alcohols	% (v/v)	IP 466	10	4.9	20.4	20.2	9.8
Net Calorific value **(LHV)**	MJ/kg	ASTM D3338	40.98	41.91	39.36	39.23	41.33
Gross Calorific value	MJ/kg	ASTM D3338	43.8	44.76	42.23	42.05	44.17
Sulfur Content	mg/kg	EN ISO 20846	<1	<1	<1	<1	3.2

3.3 Experimental Setup

The engine being tested is a single-cylinder engine equipped with a cylinder block and a cylinder head sourced from Mahle Powertrains' 3-cylinder gasoline engine. This particular engine has undergone significant downsizing to improve its overall performance. The engine is mounted on an AC dynamometer testbed, fully equipped with various instruments, as illustrated in Figure 3.2. The testing approach for this single-cylinder engine provides great flexibility and adaptability, which helps to streamline engine development by minimising the time, cost, and complexity associated with the engine control unit. Overall, the engine is designed to offer a high level of performance while also being efficient and cost-effective.

The engine's cylinder head has two intake valves and two exhaust valves, along with double overhead camshafts that feature hydraulically adjustable cam phasers, capable of adjusting up to 40 degrees crank angle. The engine also has a centrally mounted direct injector, capable of precise fuel delivery at high pressures of up to 200 bar. An extra port fuel injection (PFI) injector is installed in the engine's intake manifold, which can inject fuel at up to 8 bar pressures. The ignition system incorporates a centrally positioned spark plug with a 100 mJ coil-on-plug configuration, which improves combustion. A MAHLE Flexible ECU (MFE) controls the engine's operation for more detailed specifications in Table 3.2.
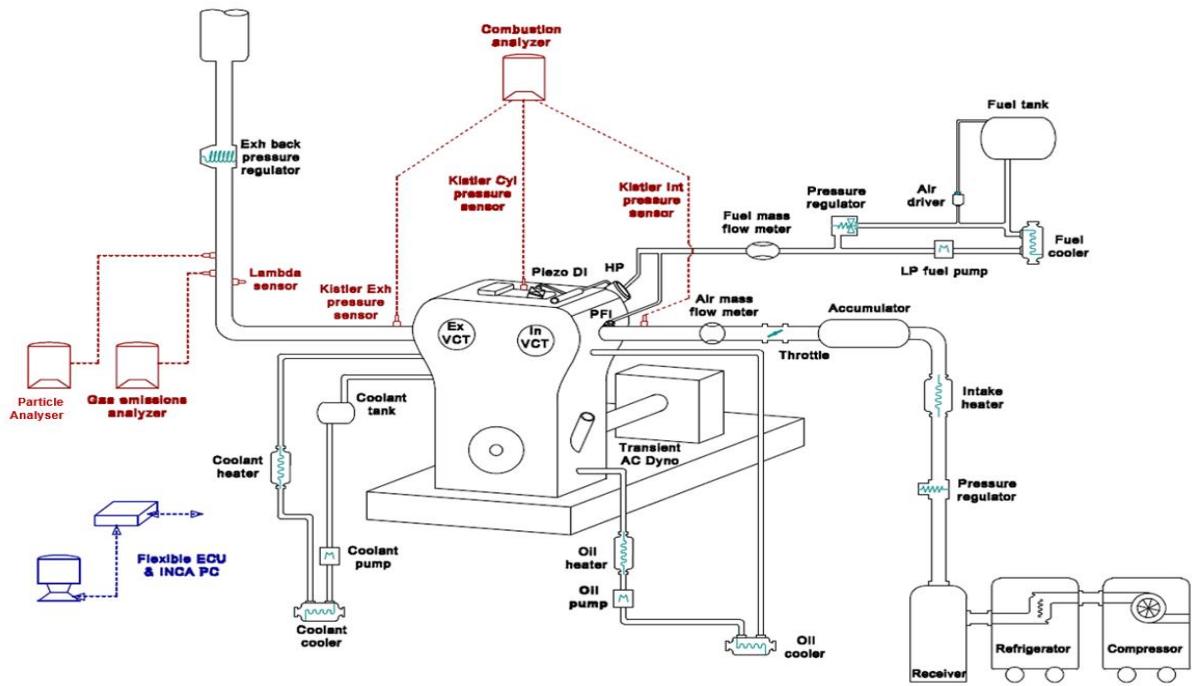
Figure 3. 2 Test cell schematic structure [146].

Table 3. 2: Specification of the Single-Cylinder Engine [147]

Configuration	Single Cylinder
Displaced volume	400 cc
Stroke/Bore	73.9 mm /83 mm
Geometric Compression Ratio	11.1: 1
Number of Valves	4
Exhaust Valve Timing	EMOP (Exhaust Maximum Opening Point at maximum valve lift) 100-140 °CA BTDCg, 11 mm Lift, 278 °CA Duration
Inlet Valve Timing	IMOP (Intake Maximum Opening Point at maximum valve lift) 80-120 °CA ATDC,g 11 mm Lift, 240°CA Duration
Injection System	Central Direct Injection with an injection pressure of 50 to 200 bar. PFI injector with an injection pressure of 4 to 10 bar
Injection Control	MAHLE Flexible ECU (MFE)

The testbed arrangement, as shown in Figure 3.2, includes an external boosting system operated separately. The two high-speed piezo-resistive pressure sensors were used to measure the pressure of the intake and exhaust gases. The coolant and oil temperatures were also controlled to ensure stable and consistent temperatures for the steady-state testing conducted under all engine operating conditions. The gaseous emissions were analysed using a HORIBA analyser (MEXA-554JE for CO/CO_2) and Signal analyser (Ambitech model 443 chemiluminescent NO/NO_x and Rotork Analysis model 523 flame ionisation

detection (FID) hydrocarbon (HC) analysers)[148]. Particle emissions were quantified using a Cambustion DMS500 particle analyser. The equipment uses a high-voltage discharge to charge each particle proportionally to its surface area. After charging, the particles are introduced into a solid radial electrical field classification section, which causes the particles to drift through a sheath flow toward the electrometer detectors. The particles are detected at different distances down the column, depending on their aerodynamic drag/charge ratio[149].

The particle analyser includes 22 electrometers whose outputs are processed in real-time at 10 Hz to provide spectral data and other metrics. The Cambustion DMS500 particle analyser can measure the particle size distribution, providing an accurate and detailed characterisation of the particles emitted by the engine. This data is particularly useful in determining the engine's overall emissions performance. Finally, in Table 3.3, there is a list of the measurement devices with their range and accuracy.

The test cell boasts a comprehensive data acquisition system designed for precise monitoring and analysis of engine performance. This advanced system has cutting-edge components, including the NI-USB 6353 fast card and the NI-USB 6210 card, which effectively handle data acquisition tasks. The NI-USB 6353 fast card can handle up to 32 analogue inputs at an impressive speed of 1.25 MS/s, allowing the system to capture data with exceptional accuracy and detail. The NI-USB 6210 card is an extra-time domain card, further enhancing the system's capabilities. This sophisticated setup allows the data acquisition system to record data in the crank and time domains effortlessly. Moreover, the system seamlessly integrates data from additional pressure and temperature sensors in the time domain. An in-house combustion analysis programme enables real-time monitoring and data recording, allowing for live monitoring of primary combustion parameters and recording in-cylinder pressure data for up to 300 cycles.

Table 3. 3 Test cell measurement devices

Measurement	Device	Manufacturer	Measurement range	Linearity/Accuracy
Engine speed	AC Dynamometers (Asynchronous)	Sierra Cp Engineering	0-6000 rpm	±1 rpm
Engine torque	AC Dynamometers (Asynchronous)	Sierra Cp Engineering	-50-500 nm	±0.25% of FS
Clock Signal	EB582	Encoder Technology	0-25000 rpm	0.2 CAD
Hydrogen flowrate	Coriolis flowmeter K000000453	Alicate Scientific	0-10000 g/h	±0.20% of reading
Intake air mass flow rate	F-106 AI	Bronkhust	4-200 kg/h	±0.2% of reading
In-cylinder pressure	Piezoelectric pressure sensor Type 6125C	Kistler	0-30 MPa	≤ ±0.4% of FS
Intake pressure	Piezoresistive pressure sensor Type 4049A	Kistler	0-1 MPa	≤ ±0.5% of FS
exhaust pressure	Piezoresistive pressure sensor Type 4049B	Kistler	0-1 MPa	≤ ±0.5% of FS
Oil pressure	PX309-10KGI	omega	0-0.8 MPa	< ±0.2% of FS
Temperature	Thermocouple K Type	RS	233-1473 K	≤ ±2.5 K
Fuel injector current signal	Current probe PR30	LEM	0-20 A	±2 mA
PM emissions	DMS 500	Cambustion	0-5000 PPS	-
CO emissions	MEXA-584L	Horiba	0-12 vol%	≤ ±1.0% of FS or ±2.0% of readings

CO$_2$ emissions	MEXA-584L	Horiba	0-20 vol%	$\leq \pm 1.0\%$ of FS or $\pm 2.0\%$ of readings
O$_2$	MEXA-584L	Horiba	0-25 vol%	$\leq \pm 1.0\%$ of FS or $\pm 2.0\%$ of readings
THC emissions	Rotork Analysis Model 523	Signal	0-5000 ppm	$\leq \pm 1.0\%$ of FS or $\pm 2.0\%$ of readings
NO/NO$_2$ emissions	CLD 150 (Heated Chemiluminescence Detector)	Cambustion	0-500 ppm or 0-10k ppm	$\leq \pm 1.0\%$ of FS or $\pm 2.0\%$ of readings
H2 slip emissions	Air sens500	V&F	0-5000 ppm or 0-100% vol	0.5% of fs or 1%vol

3.4 Aim and objectives of the second-generation Biofuels Analysis

The primary aim of the investigation is to evaluate the performance of second-generation biofuels. Coryton has provided four different fuels with varying research octane numbers and ethanol ratios, making it challenging to gauge the bi-fuels' performance. To overcome this, the study will be split into three parts, and their results will be presented and discussed in the subsequent chapters:

1- By comparing the fixed RON number with different ethanol ratios, we can assess the effect of the ethanol addition.
2- By comparing the 20% ethanol ratios and different RON numbers, we can determine the benefits of higher RON on the second-generation biofuels.
3- Optimise the injection strategies to mitigate emissions and balance the performance of the second-generation biofuels.

Chapter 4. Experimental Investigation of Combustion Characteristics, Performance, and Emissions of a Spark Ignition Engine With 2nd Generation Bio-Gasoline and Ethanol Fuels

4.1 Introduction

In this chapter, the study compared the combustion characteristics, performance, and emissions of a highly boosted SI engine fueled with EU VI 95 RON E10 gasoline and blends of second-generation bio-gasoline with 5%, 10%, and 20% ethanol. Increasing the ethanol content from 5% to 20% improves efficiency by 2.1% and knock resistance by 16.8% at high loads. Emissions are primarily affected by engine operating conditions, but increasing ethanol from 5% to 20% increased NO$_x$ by 11.02% and THC emissions by 66% at low loads.

4.2 Test Methodology

Tests were conducted on a single-cylinder engine at 3000 RPM to study the performance and emissions of biofuels compared to baseline gasoline at different loads. However, the engine settings remained consistent throughout, with identical cam timing, fuel injection pressure, and timing. The aim was to remove any comparability variation in the load sweeps and to optimise all operational parameters at each load. The study also examined the effects of fuel injection pressure and fuel injection timing. The low-load fuel matrix test was carried out at an engine speed of 2000 RPM and an IMEP of 2.4 bar to simulate average low-load operating conditions.

On the other hand, the high load fuel matrix test was conducted at 16 bar IMEP and 3000 RPM to investigate the engine's performance and emission characteristics sensitivity under different injection timing and pressure. Finally, the emission was analysed over the vast operation regime to study the effect of the ethanol increase over the different operation points. The sets of tests have been summarised in Table 4.1.

Table 4. 1: Biofuels and methanol tests methodologies

Parameter	unit	Load sweep study	Low load matrix	High load matrix
Engine speed	RPM	3000	2000	3000
Indicated mean effective pressure (IMEP)	bar	(2 to 28 bar with 2 bar step)	4.6	16
DI start of injection	degrees BTDCf	300	(275-350 CAD with 25 CAD step)	(275-350 CAD with 25 CAD step)
DI injection pressure	bar	150	(50-200 bar with 50 bar step)	(50-200 bar with 50 bar step)
Intake cam timing(IMOP)	degrees ATDCg	82	82	82
Exhaust cam timing (EMOP)	degrees BTDCg	140	140	140
Relative AFR	-	1 up to exhaust temperature threshold	1	1
Boosted air temperature	°C	40	40	40
Target (CA50)	degrees ATDCf	8 and retreated to avoid knocks	8	retarded to knock limits
Coolant and oil temperature	°C	90	90	90

4.3   Results

In three experiments, we tested various fuels under different conditions to study their effect on engine performance and emissions. The first experiment tested the 95 RON E10 baseline gasoline and biogasoline with different ethanol concentrations at varying load sweeps from 2 bar to 28 bar IMEP and 3000 rpm. We used the same fuel injection pressure and initial injection timings for all tested fuels optimised for baseline gasoline.

The second experiment was conducted at 2000 rpm and 4.6 bar IMEP to investigate the impact of injection parameters on biogasoline fuels with various ethanol contents at low-load engine operation. Finally, we carried out the third experiment at high-power operation with 16 bar IMEP and 3000 rpm to study the impact of injection parameters on engine performance and emissions.

4.3.1 Exploring The Effects of Varying Ethanol Ratios of the Biofuels on Combustion, Efficiency, and Emissions Under Different Loads With Fixed Speeds and Fuel Injection Parameters.

During the test, the engine speed was maintained at a fixed rate of 3000 RPM, while the load varied between 2 bar IMEP and 28 bar IMEP. The engine operating parameters, such as the rail pressure, intake and exhaust valve timings, and start of injection time, were kept constant for each fuel at different operating conditions. These parameters were optimised for the engine's performance during the baseline tests conducted using gasoline. It was observed that the end of the injection was delayed as the ethanol content increased due to the larger volume of fuel being injected. In most conditions, the engine was operated under stoichiometric combustion, with the relative air-to-fuel ratio measured using a Lambda sensor in the exhaust. However, when the load exceeded 24 bar IMEP, the lambda value was reduced to 0.9 to keep the exhaust temperature below 750°C, as seen in Figure 4.1.
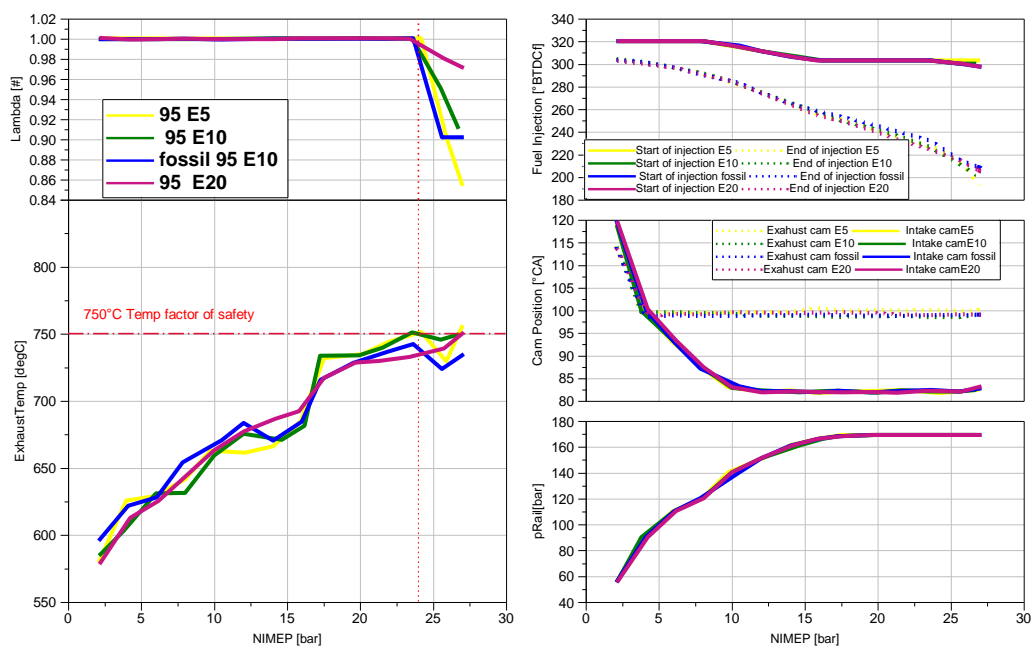
Figure 4. 1: 3000 RPM load sweep data shows the lambda value, Exhaust temperature, fuel injection angle, cam timing, and fuel rail pressure.

In Figure 4.2, the knock intensity is a phenomenon where abnormal and stochastic combustion occurs and limits the efficiency of spark ignition engines. The intensity increased steadily as the engine load increased and reached its peak at 20 bar IMEP. As the load was changed from 2-14 bar IMEP, the burn durations measured by the spark to 10%, 10 to 50%, and 50-90% mass fraction burned were at their fastest combustion at elevated gas pressure and temperature. As a result, the spark timing was delayed, and the MBT could be reached. Above 15 bar IMEP, the spark timing had to be delayed beyond the

MBT to keep the knock intensity below 1.0. This resulted in slower combustion and extended burn durations.
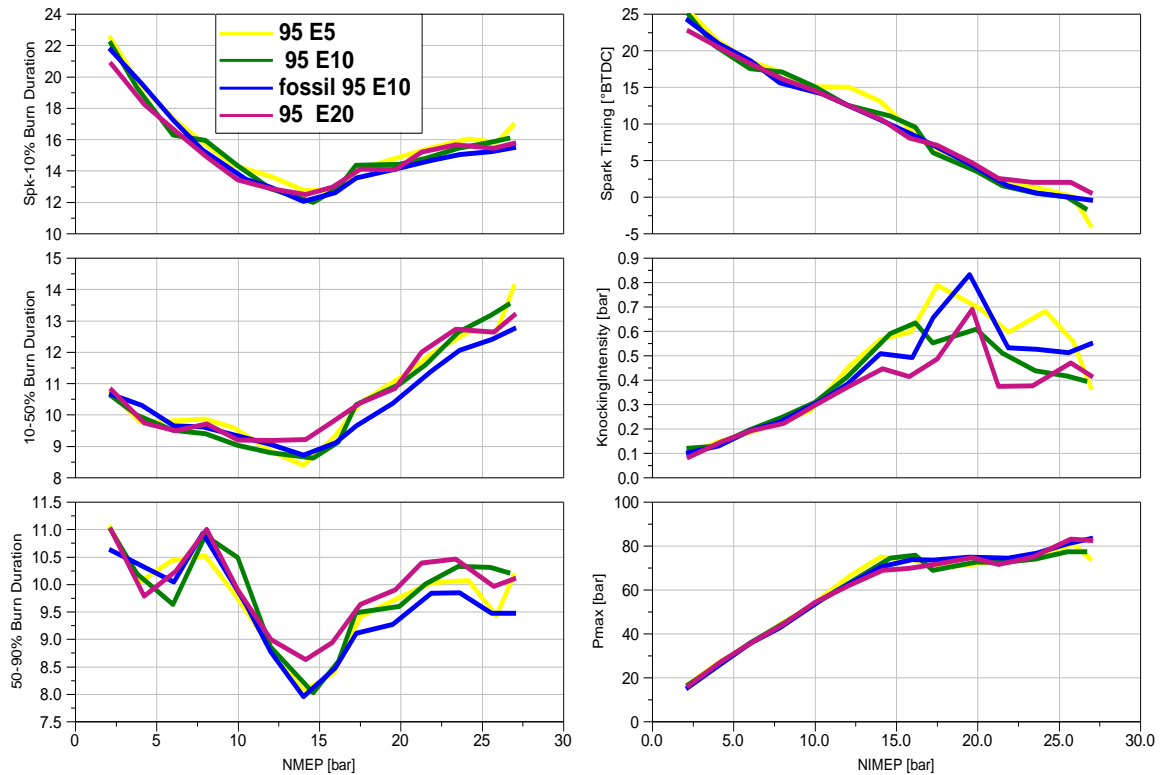
Figure 4. 2: 3000 RPM load sweep data shows spark-to-10% MFB duration, 10-90% MFB durations, spark timing, Knocking intensity, and In-cylinder pressure.

The impact of fuel properties on the combustion characteristics of gasoline and blends of bio-gasoline and ethanol was analysed. The study revealed that at part-load conditions up to 12 bar IMEP, baseline gasoline and bio-gasoline blends exhibited similar combustion characteristics. However, as the load increased, adding ethanol caused an increase in combustion duration while lowering the knock intensity of the engine when it was operated with boosted air. At the highest load of 25 bar IMEP, less fuel enrichment was required to maintain the exhaust gas temperature below the 750c limit compared to baseline gasoline. As a result, higher combustion efficiency is evident in Figure 4.3.
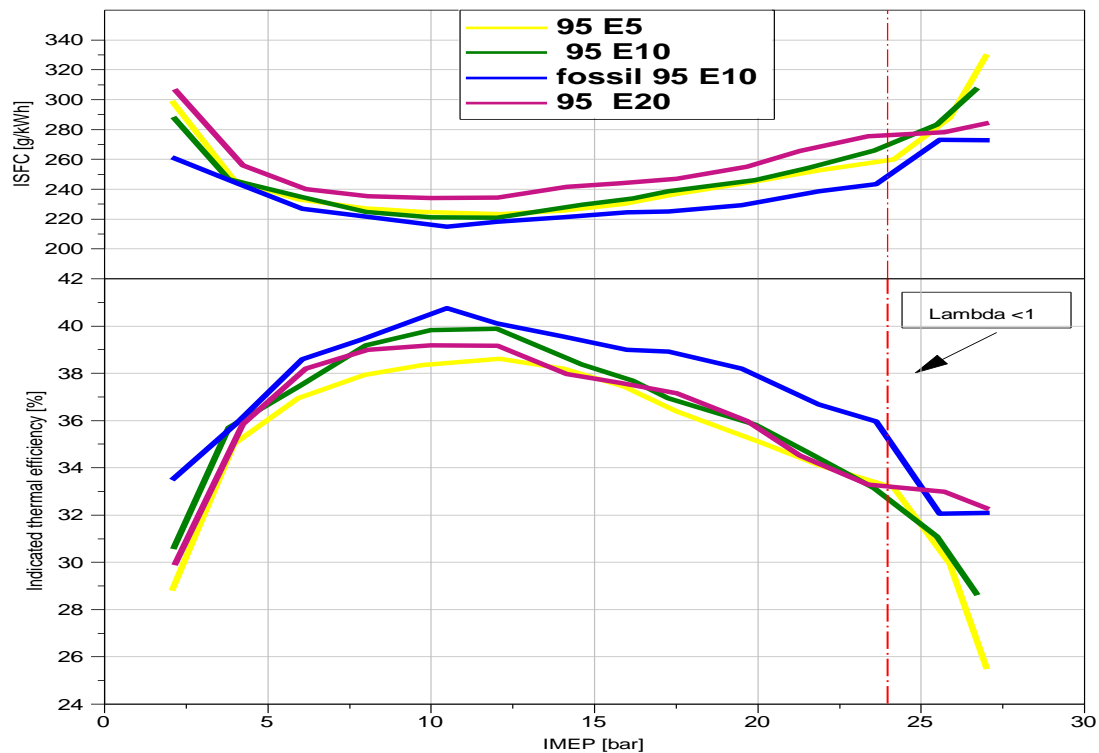
Figure 4. 3: 3000 RPM load sweep data shows the indicated specific consumption and the ITE.

The following information is presented in Figure 4.3, portraying the specific consumption and engine thermal efficiency as a function of load for varying fuel blends. It was observed that fossil gasoline fuel produced superior engine efficiency and lower specific fuel consumption with identical fuel injection parameters and spark timings.

Additionally, Figure 4.4 illustrates the engine-out emissions for different fuel blends at a load function. The increased CO and HC emissions observed at the highest load conditions are attributed to fuel-rich combustion. It was noted that the CO emission was inversely proportional to the lambda value, and the E20 biogasoline produced the lowest CO emission at the highest load. Furthermore, higher HC emissions were observed with bio-gasoline fuel blends due to the heavier hydrocarbon content in bio-gasoline. This heavier composition of bio-gasolines results from the feedstock used in the manufacturing process. It is important to highlight that fossil fuels are further processed to refine aromatic elements to help reduce particles during the combustion process, which can cause harm to human health [150].

The results presented below in Figure 4.4 indicate that biogasoline with a higher ethanol content required less fuel enrichment, leading to lower emissions at maximum load. However, using fuel injection parameters optimized for gasoline caused lower engine efficiencies when running on biogasoline and ethanol blends. Adjusting the fuel injection parameters for optimal engine performance when using biogasoline with a higher ethanol content is recommended.
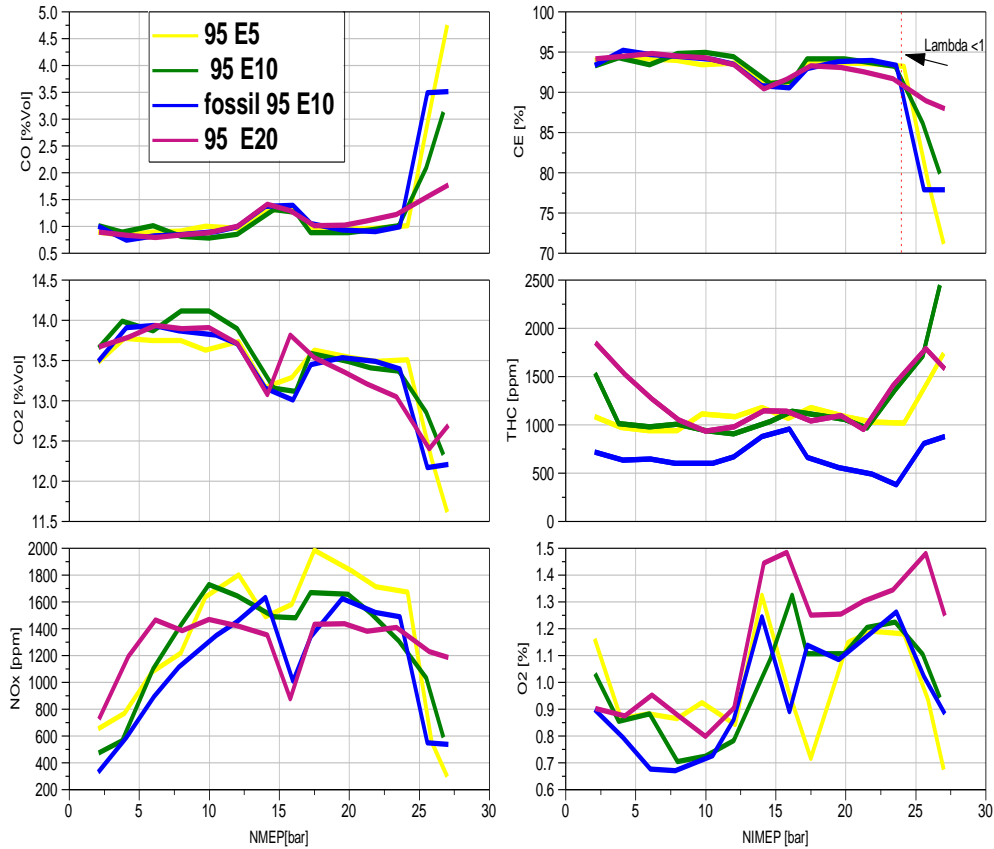
Figure 4. 4: 3000 RPM load sweep data shows the emission captured.

In the analysis conducted on the emissions of DMS 500, Figure 4.5 shows the particulate number (PN) levels recorded during the load. The results have provided a full comparison of the PN emissions of each fuel at similar injection conditions and engine setups at different loads. The results show that second-generation biogasoline fuels have higher PN numbers compared to fossil fuels due to the heavier substance and aromatics in the biogasoline structures due to the production process. However, the study also found that introducing a Gasoline Particle Filter (GPF) into the exhaust system can reduce these PN levels effectively. This indicates that GPF can be an effective measure to mitigate the harmful effects of biofuels on the environment.
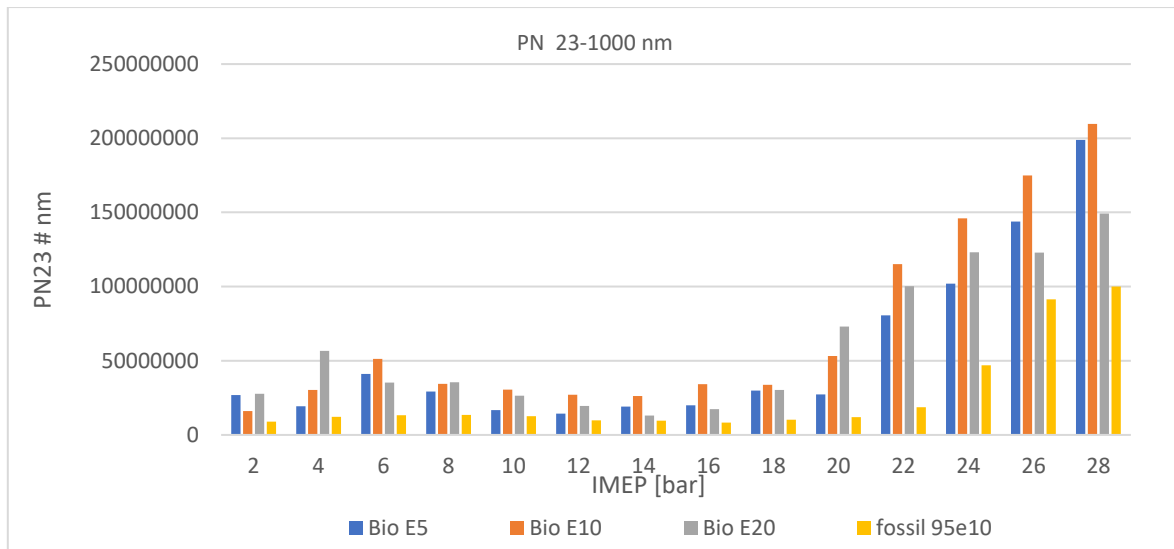
Figure 4. 5: 3000 RPM load sweep data shows the particle numbers for 23-1000 nm size.

Consequently, a decision was made to conduct supplementary experiments to determine the feasibility of enhancing the engine thermal efficiency of bio-gasoline and ethanol blends by optimising the fuel injection parameters during low and high-load operations.

4.3.2 Effect of Fuel Injection Parameters on Combustion, Efficiency, and Emissions of Biogasoline Fuels at low-load Engine Operation

This study aims to analyze the impact of fuel injection pressure and injection timing on engine performance with various biogasoline and ethanol blends under low-load conditions (2.4 bar IMEP and 2000 RPM engine speed). Injection timing ranged from 275 ca BTDCf to 350 ca BTDCf in 25-degree increments, while fuel injection pressure increased from 50 bar to 200 bar in 50 bar increments. Figure 12 displays the results of combustion phasing and duration as a function of fuel injection pressure (y-axis) and injection timing (x-axis). Since spark timings were set to MBT, combustion phasing (indicated by 50% MFB) remained constant at 8 ca ATDC. Notably, there was a minor variation in combustion duration with a given start of injection, and the longest burn duration occurred at 300 ca BTDCf, regardless of injection pressure or ethanol content.

The findings presented in Figure 4.6 indicate that the maximum thermal efficiency increased slightly with a higher ethanol content. However, the lowest thermal efficiency area observed an increase in ISFC due to ethanol's lower calorific value. The thermal efficiency distribution shows that bio-gasoline E20 and E10 attained maximum efficiency at 325 ca BTDCf and 100 bar injection pressure. At the same time, E5 fuel exhibited higher thermal efficiency at a later injection timing and higher injection pressure. Despite significantly varying fuel injection pressure and start injection timings, the thermal efficiency variation remained within 1%, as shown in Figure 4.7.
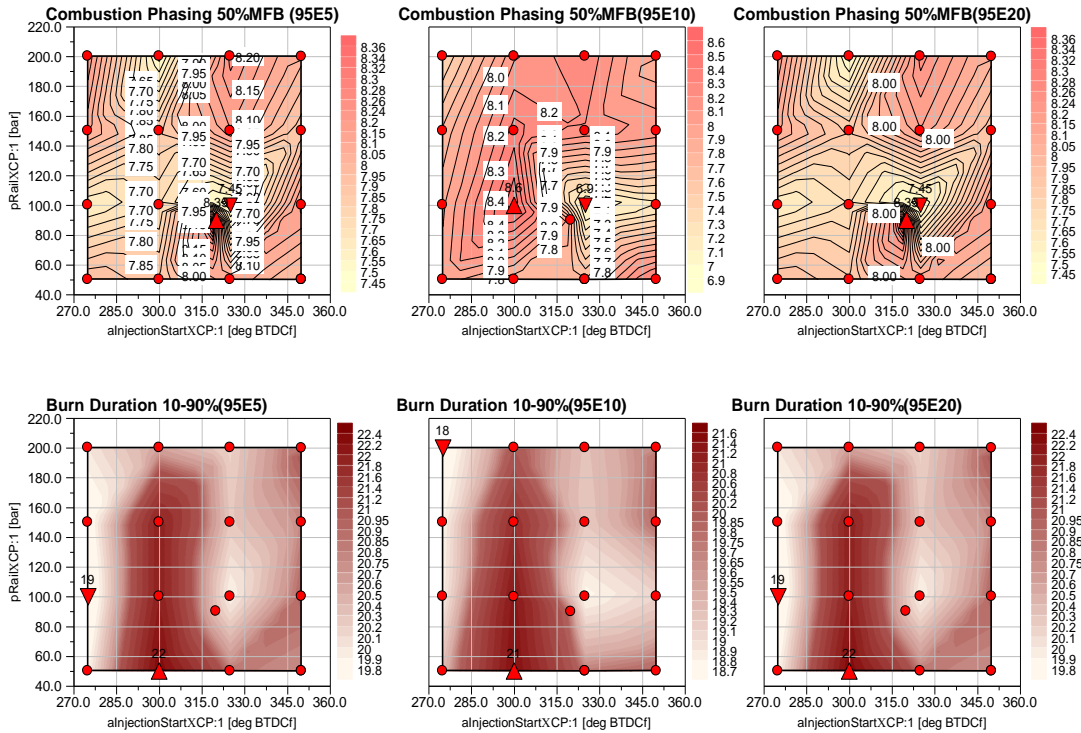
Figure 4. 6: 2000 RPM 2.4bar IMEP, fuel matrix data shows combustion phasing and the burn duration.
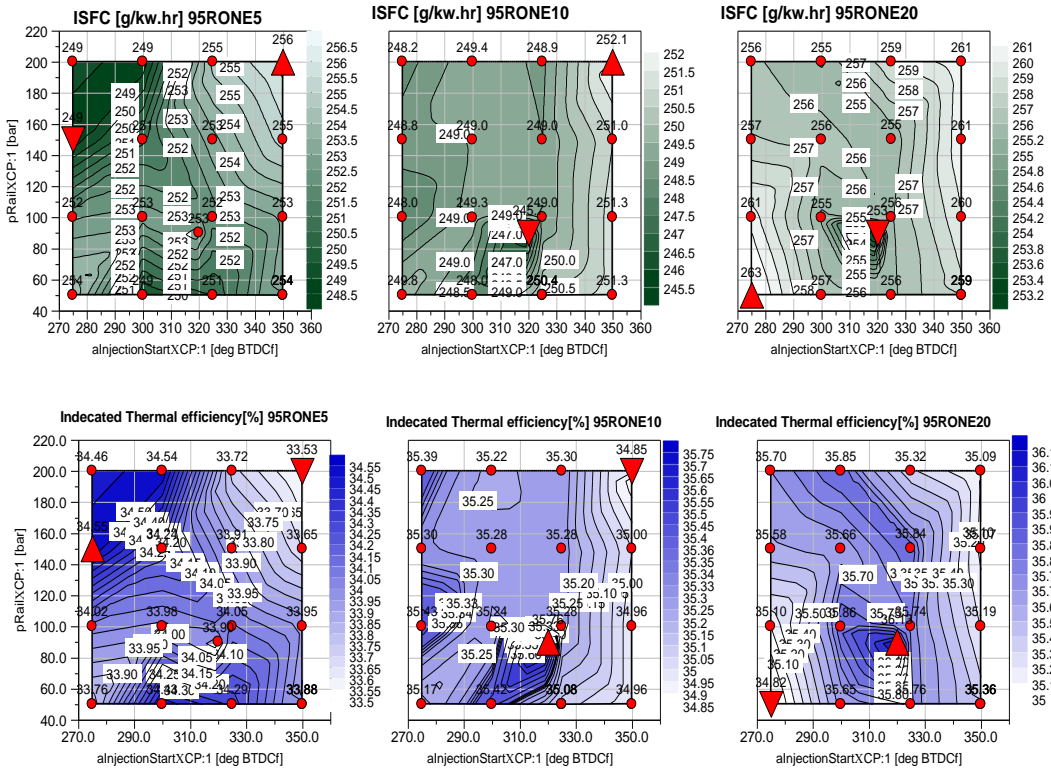
Figure 4. 7: 2000 RPM 2.4bar IMEP, fuel matrix data shows ISFC and ITE.

Figure 4.8 analyses the impact of fuel injection pressure and timing on the THC and NO_x emissions concerning the percentage of ethanol in the fuel. The results showed that the THC emission increased slightly with the percentage of ethanol due to the longer injection duration and delayed injection end, leading to less homogeneous mixtures. E10 and E20

emit more THC than E5, which has 82.9% bio content. E20 biofuel has the most significant emission division at 48.37%, compared to 21.1% for E10. The maximum THC emission was observed at the earliest injection point and 200 bar injection pressure for E10 and E20 biofuels. E5 produced the most THC at 50 bar injection. E20 had the highest NO_x emission variation at 59.3%, and it emitted the least at the latest injection point with the lowest injection pressure due to its faster evaporation rate. The E5 fuel behaved like E10 with retarded injection time, reducing NO_x emissions. The minimum HC emissions were obtained after fuel injection at 325 ca BTDCf for each fuel. The lowest NO_x emission was obtained with E20 with the most retarded injection timing and lower injection pressure due to the lower combustion temperature of E20 and slightly retarded combustion. The fuel injection pressure did little to affect the HC emissions at this part-load and low-speed engine operation.
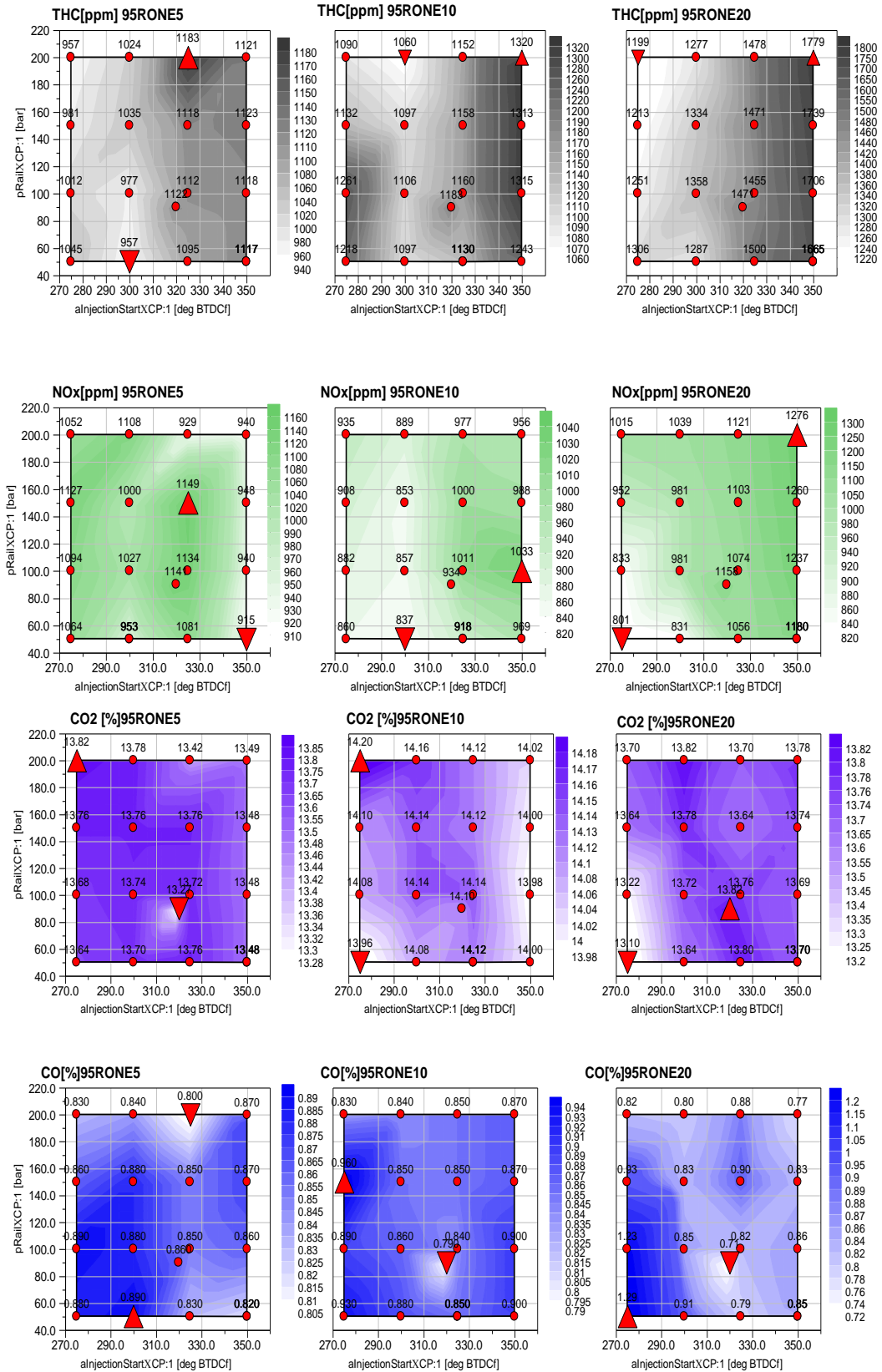
Figure 4. 8: 2000 RPM 2.4bar IMEP, fuel Matrix data shows Emissions data.

4.3.3 Effect of Fuel Injection Parameters on Combustion, Efficiency, and Emissions of Biogasoline Fuels at Higher Power Engine Operation

The objective of the present study was to examine the impact of fuel injection parameters on the performance of three different blends of bio-gasoline and ethanol during high-power engine operation while operating close to the engine's peak island efficiency zone. The study involved 18 test points with stoichiometric combustion at a fixed speed of 3000 RPM at 16 bar IMEP. However, due to knocking combustion at such a high load with an intake pressure of 1.3 bar, the spark timing was retarded, and the combustion stability became a potential concern when more combustion took place well after TDC. Hence, as measured by the CoV (%) in IMEP, the combustion stability was assessed and analyzed, as illustrated in Figure 4.9.
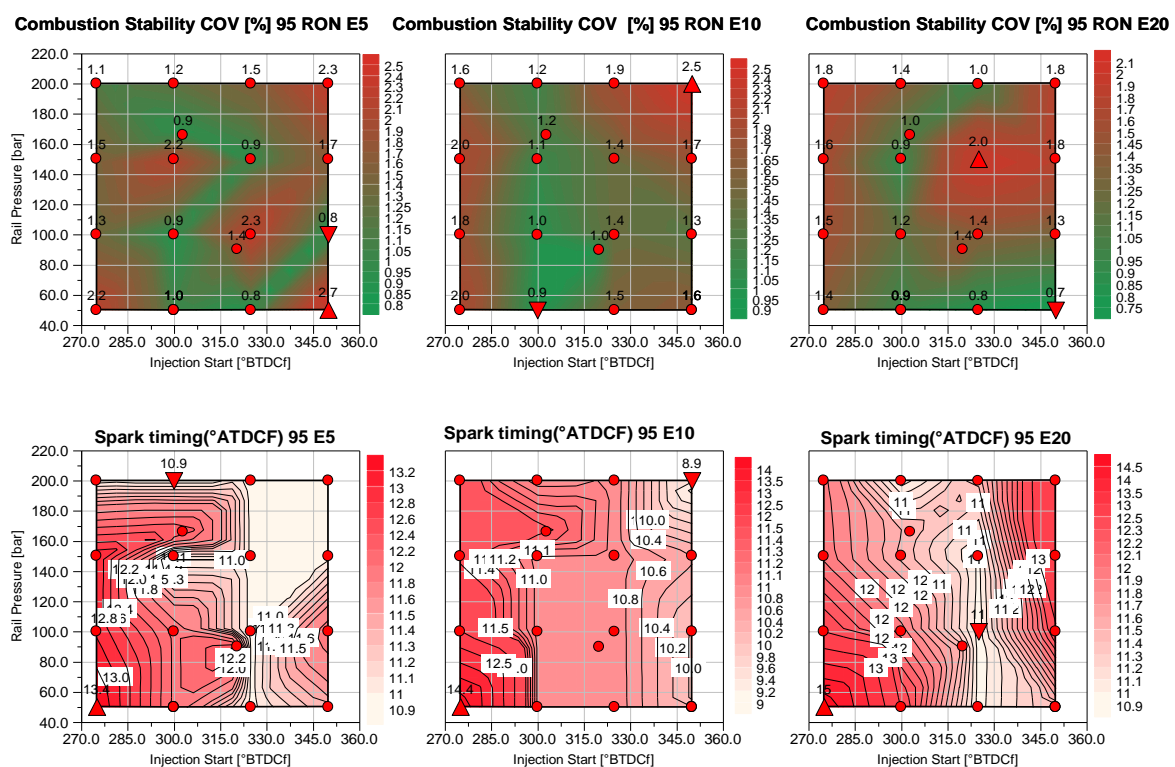
Figure 4. 9: 3000 RPM 16bar IMEP, fuel matrix data shows combustion stability and spark timing.

The experimental findings indicate that E20 fuel exhibits more consistent combustion with lower Coefficient of Variation (COV) values, and the most steady combustion is achieved when fuel injection commences at approximately 300 crank angle degrees before the top dead centre (ca BTDCf) for all three fuels tested. The influence of injection pressure and timing on combustion stability was inconsistent, except for E20 fuel, which demonstrated reduced COV values at lower injection pressure. The results of combustion phasing and burn duration are illustrated in Figure 4.10.
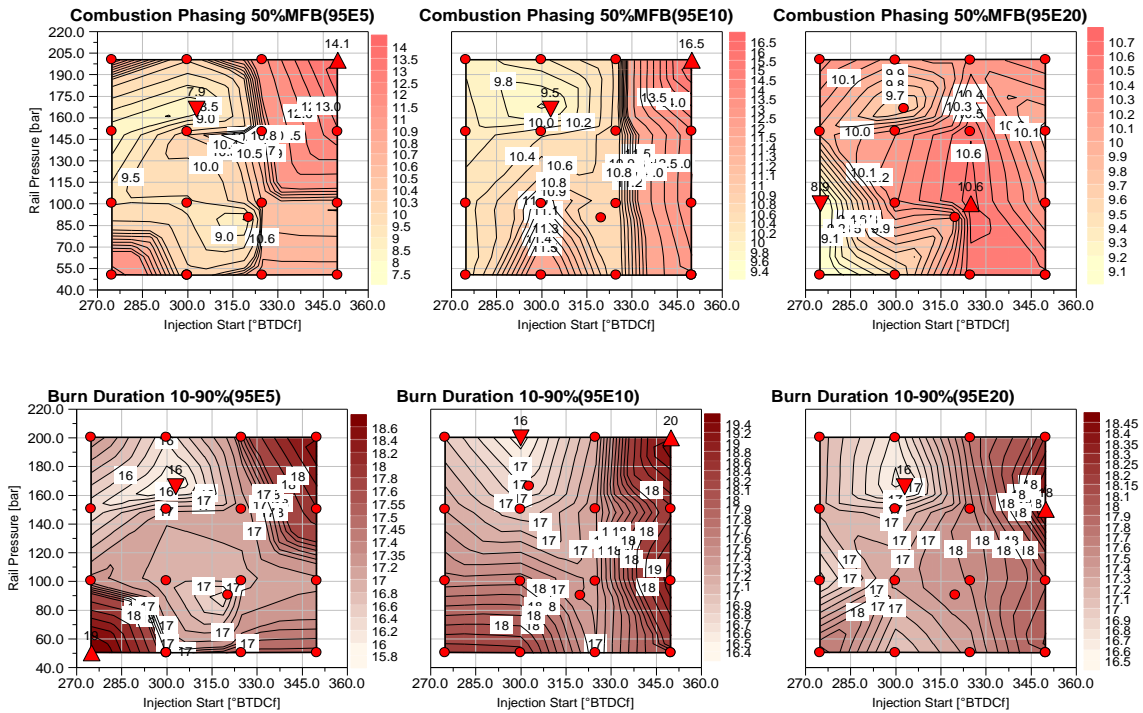
Figure 4. 10: 3000 RPM 16bar IMEP, fuel matrix data shows combustion phasing and the burn duration.

In the experiment, it was observed that E20 fuel had less deviation in combustion phasing at 50% MFB compared to E5 and E10. The earliest injection angle of 350 ca BTDCf at higher injection pressures resulted in the most retarded combustion. Burn duration results were consistent for all three biofuels. During the most stable combustion, 300 ca BTDCf injection timing achieved the minimum burn duration.

Figure 4.11 shows that the highest indicated thermal efficiency was obtained with the highest injection pressure and the start of injection timing of 300 ca BTDCf for all fuels. The thermal efficiency decreased steadily as fuel injection occurred earlier, leading to increased HC emissions, as shown in Figure 4.12. Thermal efficiencies increased slightly across the range of injection pressures and timings tested with increased ethanol content. However, fuel consumption increased due to higher ethanol-content biofuels' lower net calorific value.

It was observed that injection timing and pressure had a more significant impact on thermal efficiency than low-load operation. The variation was approximately 6%, higher than the 4.6 bar IMEP.
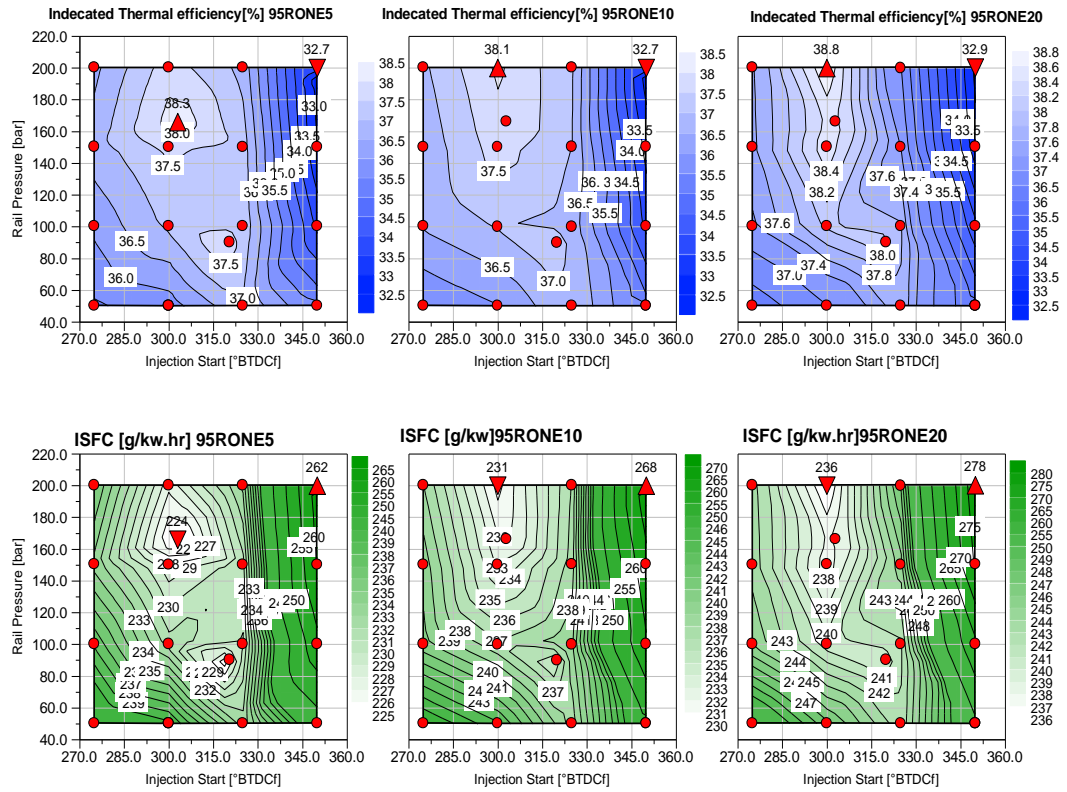
Figure 4. 11: 3000 RPM 16 bar IMEP, fuel matrix data shows ITE and ISFC.
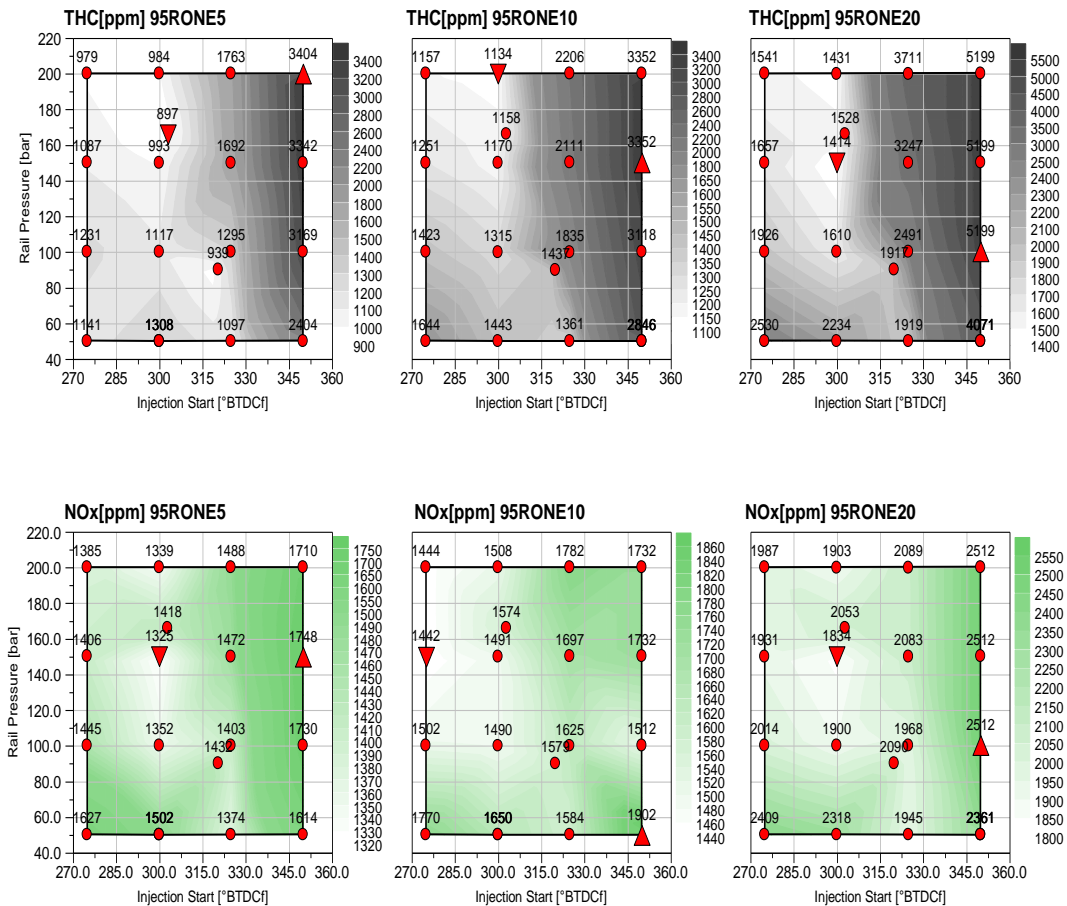
Figure 4. 12: 3000 RPM 16bar IMEP, fuel matrix data shows THC and NOx emissions.

At an injection start of 300 ca BTDCF and an injection pressure of 200 bar, all three fuels achieved their minimum unburnt HC emissions. The HC emissions were highest with the earliest injection timing due to more trapped fuel in crevices, as shown in Figure 4.12. Additionally, the THC increased with higher ethanol fuel. The NO_x emissions also increased with ethanol percentages, likely due to more advanced spark timing. Carbon monoxide emissions increased with retarded injection timing, as shown in Figure 4.13, due to the fuel-rich mixture formed by incomplete mixing and potentially increased impingement onto the piston top. However, the total CO variation was less than 0.5%. E20 produced the lowest CO emissions due to its lower carbon content, and CO_2 emissions remained steady at around 13%.
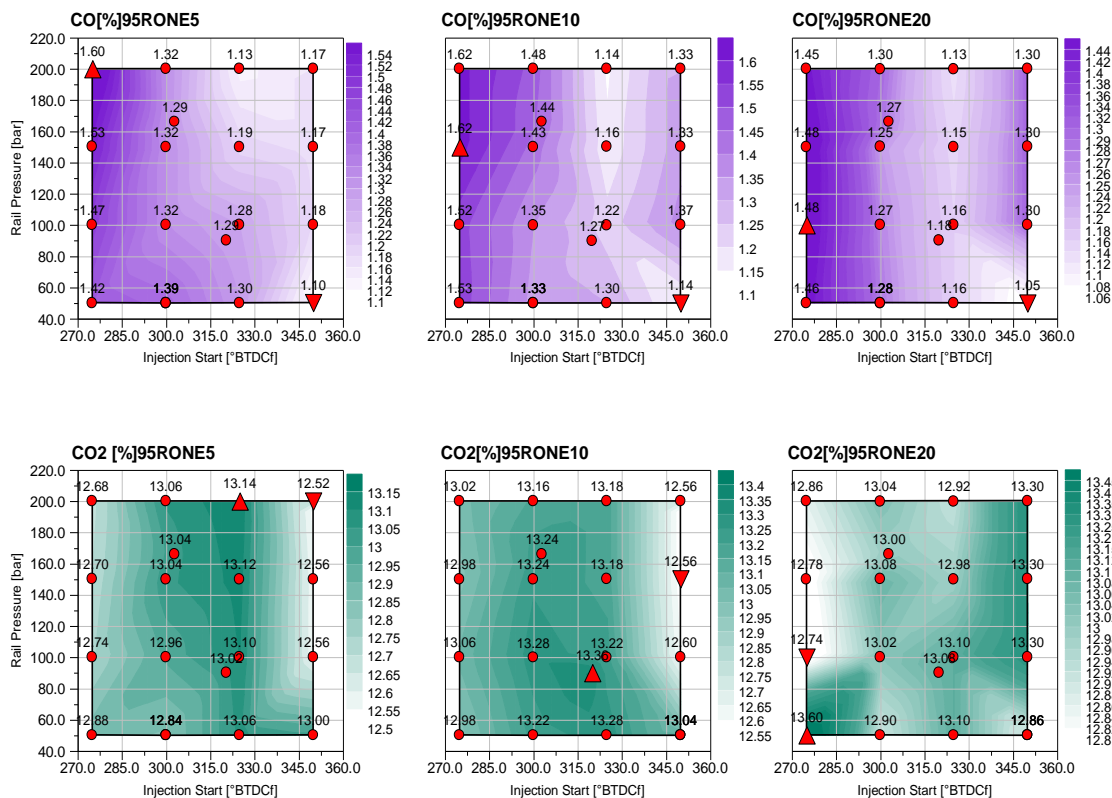
Figure 4. 13: The fuel matrix data of 3000 RPM 16 bar IMEP shows carbon monoxide and dioxide emissions.

4.4   Conclusion

This study conducted three sets of experiments to investigate the effects of biogasoline and its blend with ethanol on the combustion process, thermal efficiency, and emissions in a single-cylinder spark ignition engine. The experiments measured the effects of fuel properties and fuel injection parameters on the engine's performance.

The findings showed that the combustion characteristics of 95 RON E10 gasoline, blends of bio-gasoline, and ethanol were similar at 3000 rpm and loads from 2 bar to 12 bar IMEP. When the engine was operated with natural aspiration and intake pressure below 1 bar, less fuel enrichment was needed, resulting in lower emissions at the highest load with biogasoline E20. However, slightly lower engine efficiencies were obtained from biogasoline and ethanol blends when the fuel injection parameters optimised for gasoline were used.

At low load operation of 4 bar IMEP at 2000 rpm, the combustion duration remained constant as the injection pressure was increased from 50 bar to 200 bar for a given start of fuel injection. The most prolonged burn duration occurred at 300 ca BTDCf, irrespective of the injection pressure and independent of the ethanol content. This maximum indicated that thermal efficiency increased slightly. Overall, the variation of the thermal efficiency was within 1% when the fuel injection pressure and start injection timings were varied.

When the engine was operated at a high load of 16 bar IMEP at 3000 rpm, the injection timing and pressure had a more apparent impact on the thermal efficiency than the low load operation. The variation was about 6%, much higher than the 4.6 bar IMEP. E20 was the most knock-resistant and exhibited more stable combustion. For all three fuels tested, the most stable combustion was obtained with the start of fuel injection at around 300 ca BTDCf, but there was no consistent trend in the change of combustion stability with injection pressure. The burn duration results show a similar trend for the three biofuels. As the ethanol content was increased, the thermal efficiencies were increased slightly across the range of injection pressures and injection timings evaluated.

Chapter 5. The Effect of The Research Octane Number on The Performance and Emission of the second generation biofuels

5.1 Introduction

In this Chapter, two types of biogasoline (99 RON E20 and 95 RON E20) were thoroughly tested in a downsized single-cylinder engine to evaluate their performance, combustion, and emissions in comparison to conventional fossil fuel (95 RON E10) under different engine loads. The study also conducted a detailed injection parameter sweep for biofuels at low and high loads to understand their unique operational characteristics and regimes.

The results showed that both biofuels performed similarly to fossil fuels, with the higher octane number of the biofuels providing more knock resistance and improved thermal efficiency due to spark advance ability—however, more extensive biofuel aromatic content led to more significant hydrocarbon emissions than fossil fuels.

The study also found that both biofuels had stable combustion in low and high-load operations under varying injection pressures and injection start times. However, the 99 Bio E20 had a wider operational range than the 95 Bio E20, but due to high hydrocarbon emissions, especially at high-load operations, an early injection start with more significant injection pressure was not recommended for biofuel.

Overall, the study suggests that both types of biogasoline have promising potential as drop-in replacements for spark ignition engines.

5.2 Test Methodology

The study was conducted in two parts to assess the performance and emissions of biofuels. In the first part, the researchers conducted single-cylinder engine tests at a constant speed of 3000 RPM to compare the performance and emissions of biofuels with baseline gasoline. To ensure precise analysis, load sweeps were performed at the same speed while maintaining consistent engine settings such as cam timing, fuel injection pressure, and timing. The tests were essential to evaluate the engine's characteristics at various loads and optimise all operational parameters for each load.

In the second part of the study, the researchers focused on understanding the impact of fuel injection pressure and the start of fuel injection timings. To achieve this objective, the researchers conducted low and high-load fuel matrix tests, which allowed for a detailed comparison between the two bio-gasolines. The objective was to analyse the effect of higher ethanol content and assess the performance profile of each bio-gasoline under varied injection angles and pressures. The low-load fuel matrix test simulated average low-load operating conditions at an engine speed of 2000 RPM and an IMEP (Indicated Mean Effective Pressure) of 4.6 bar. Similarly, the high-load fuel matrix test was conducted at 16

bar IMEP and 3000 RPM to investigate the engine's performance and emission characteristics under different injection timings and pressures.

The study also analysed emissions over various operating conditions to study the effects of RON of bio-gasoline across different engine operation points. To ensure the reliability and precision of the experiment, all test conditions were maintained under precise conditions with constant water and oil temperatures of 90°C and an intake air temperature of 40°C with absolutely zero per cent humidity. Finally, all test limitations and setup points are summarised in Table 4.1. The study outcomes were reliable and unaffected by external factors, thanks to the precise conditions maintained throughout the tests.

5.3 Results and Discussion

The study involved a lambda sweep test at 3000 rpm to compare the performance of biofuels and fossil fuels. The goal was to evaluate the effectiveness of each fuel type under a range of operating conditions, including high and low fuel matrices.

5.3.1 Assessment of Engine Performance and Emission Characteristics: Bio-fuels vs. Fossil Fuels at 3000 RPM

This study aims to compare bio-gasoline fuels to fossil fuels as a drop-in fuel. The experiment began by setting the engine speed at 3000 rpm and maintaining the optimum cam overlaps at each IMEP load by fixing the cam profile. Additionally, the intake air system is equipped with an external heater with a PID controller to ensure that the operational conditions are fixed for each testing point, with a temperature of 40 degrees Celsius. The injection pressure and angle have been fixed for all testing points, and the engine is running on closed lambda control at the stoichiometric except when the exhaust temperature reaches a high load threshold. To cool down the exhaust, over-fueling strategies must be used.

Figure 5.1 displays the main performance results of the load sweep, ranging from 2 bar IMEP to 28 bar IMEP. The data shows that second-generation biofuels match fossil fuels in terms of thermal efficiency. However, comparative analysis indicates that 99 Bio E20 exhibits slightly higher thermal efficiency than 95 Bio E20, particularly under high-load conditions. This advantage can be attributed to the higher knock resistance of 99 Bio E20, which allows for advanced spark ignition timing without engine knock. This optimised spark timing facilitates a modest yet discernible increase in thermal efficiency, especially during high-load engine operations.
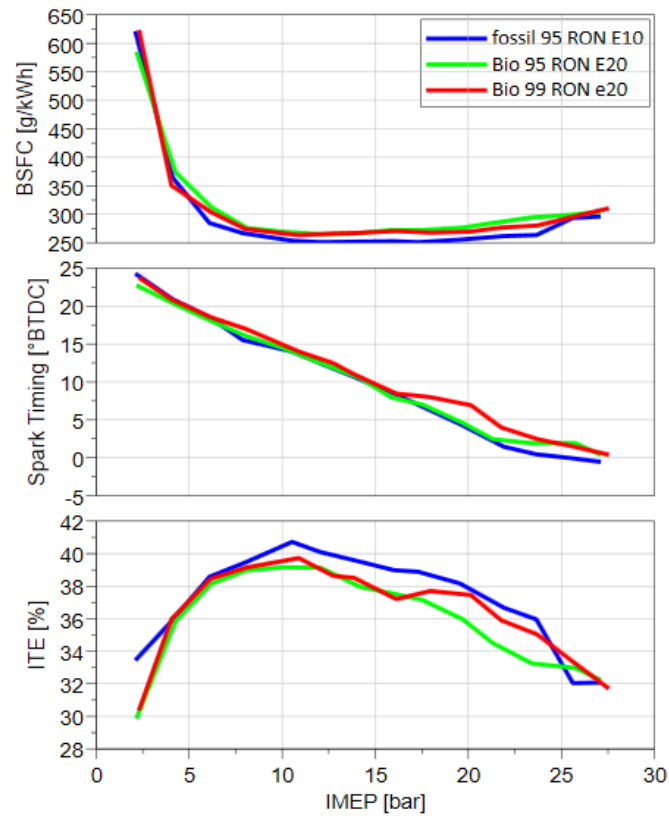
Figure 5. 1: Indicated thermal efficiency, spark timing and BSFC comparison with varying IMEP at 3000 rpm.

Figure 5.2 depicts that the combustion was optimised to operate at MBT, which is 8 degrees at 50% burn. To mitigate engine Knock, the spark timing was shifted at loads above 14 bar IMEP. The graph of knock intensity indicated that the fuel with a 99-octane number had higher knock resistance than the 95-octane number despite both containing a 20% ethanol blend. The burn duration of the three fuels was analogous, as presented in Figure 5.3, and the time from the beginning to 10% burn had a similar trend for all fuels. The graph of 10 to 50% burn duration revealed the minimum burn duration at 14 bar due to operating at MBT before the requirement of spark timing retardation for combating the Knock.
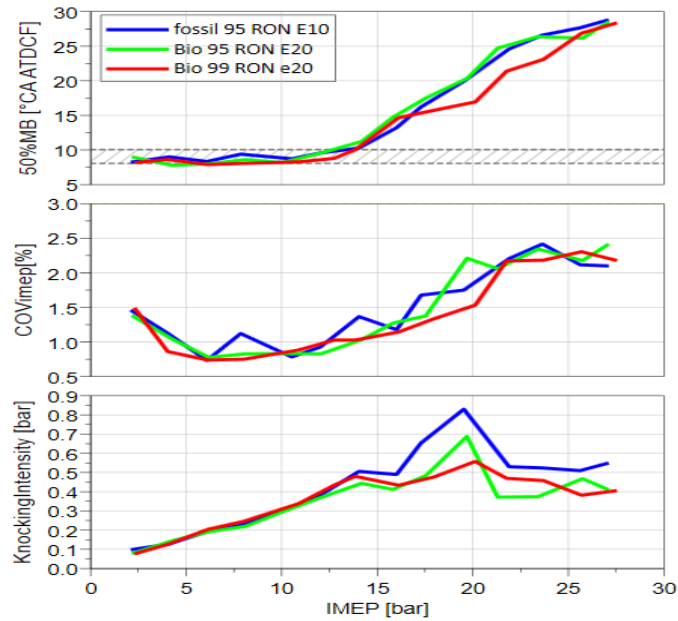
Figure 5. 2: The comparison of 50% burn location, combustion stability, and knock intensity with varying IMEP at 3000 rpm.
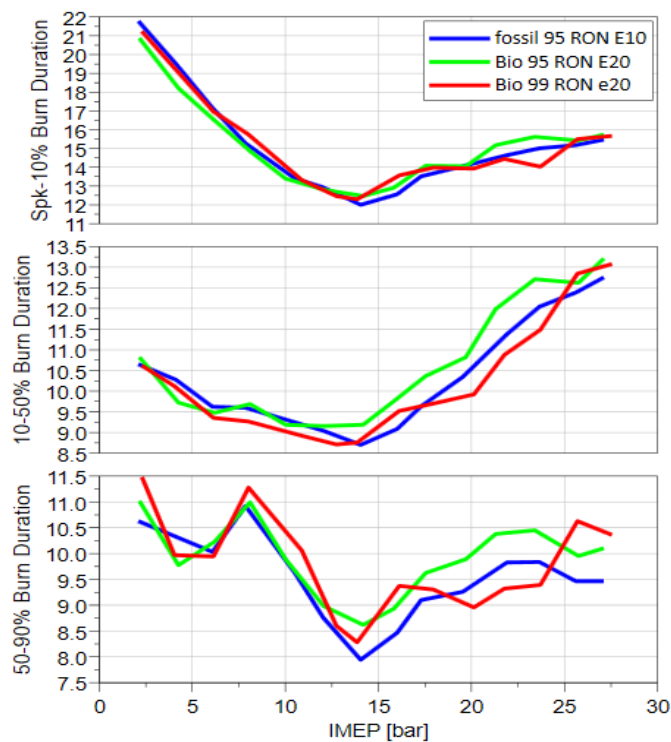
Figure 5. 3: Combustion duration comparison with varying IMEP at 3000 rpm.

According to the emissions results, the lambda value remained constant until the 24 bar IMEP load, after which a rich mixture was introduced to cool down the exhaust pipe. Figure 5.4 illustrates that 99 Bio E20 produced lower NO_x emissions than 95 Bio E20, while CO and CO_2 emissions were comparable for both fuels up to 24 bar IMEP. At higher loads, fuel-enriching strategies played a significant role in the variation of these emissions, as indicated by the lambda in Figure 5.5.
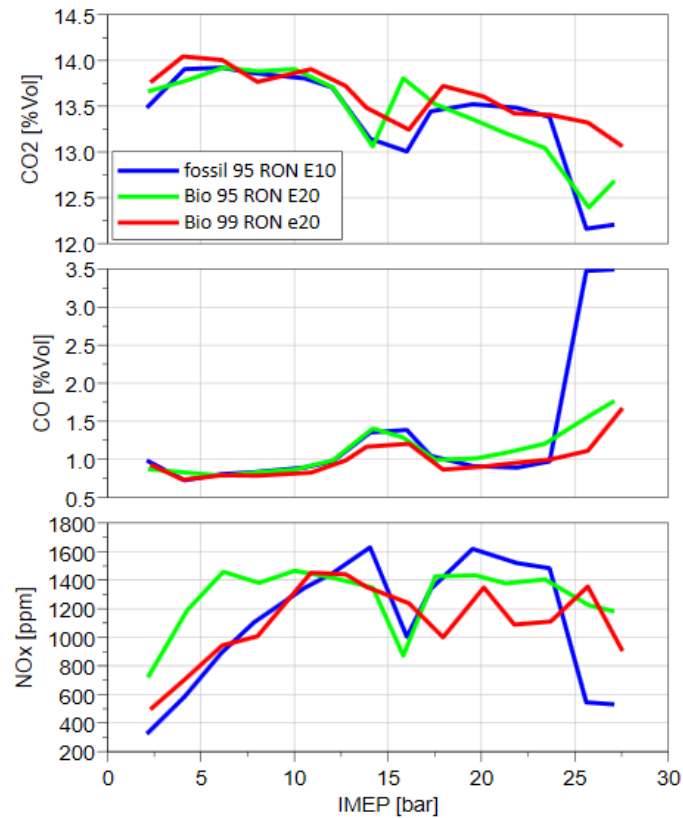
Figure 5. 4: CO_2, CO, NO_x emission analysis.

Figure 5.5 reveals that unburned hydrocarbon emissions had a slight offset due to the heavier chemical substances in the biofuels from the feedstock production process. However, this can be mitigated using advanced emission-captured methods like positive crankcase ventilation or an evaporative emissions control system. Notably, at each load's optimum operation conditions, 99 Bio E20 had lower emissions than 95 Bio E20. Finally, the lambda varied from 24 IMEp to 28 IMEp, depending on the spark angle and the energy each fuel produced to maintain an exhaust temperature below 750 degrees Celsius.
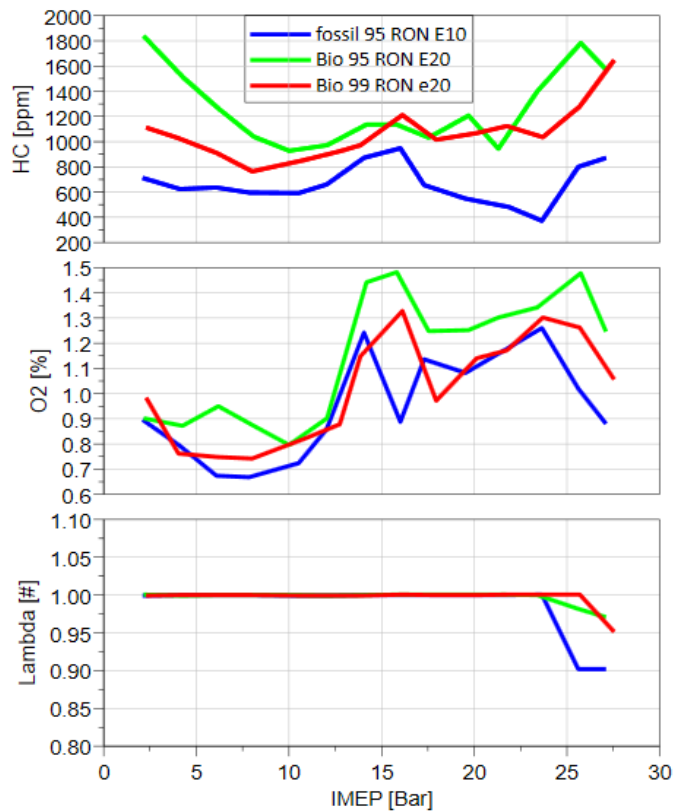
Figure 5. 5: Unburned hydrocarbon, O₂, and lambda value.

The experimental test results indicate that two biofuels have a performance and emission profile similar to fossil fuels. The biofuel's higher octane number leads to higher knock resistance and better thermal efficiency at higher loads due to its better spark ability. The experiment's primary outcome suggests that both biofuels can act as drop-in fuels as they have similar combustion parameters, efficiency, and emissions as fossil fuels. However, the high-octane 99 BioE20 performs slightly better. The next section will examine a fuel matrix study at low and high loads.

5.3.2   Optimisation of Bio-gasoline at Low-load Operation

This experiment aimed to enhance engine performance by meticulously exploring fuel injection variables for biogasoline and octane with varied research octane numbers for low-load operation. We varied the start of injection from 275 CA BTDC to 350 CA BTDC with a 250 CA interval, and the injection pressure was increased from 50 bar to 200 bar with a 50 bar increment at 4.6 bar IMEP and 2000 rpm. This section comprehensively analyses fuel's combustion, performance, and emission characteristics under different injection pressure conditions and timing for low-load engine operation.

Figure 5.6 shows that combustion phasing and burn duration are identical for both fuels when the spark timing is kept at MBT. The combustion phasing, identified by the 50% mass fraction burned (50% MFB), demonstrates a strikingly narrow range of variation, spanning a mere 7 to 9 crank angle degrees (CA). This observation stands steadfast despite fuel injection timing and pressure. Additionally, the analysis of overall burn duration, using the 10–90% mass fraction burned (10–90% MFB) metric, reveals minimal disparities between the two bio-gasoline variants. Notably, the most prolonged combustion duration was

consistently observed at an injection timing of 300 CA BTDC for both fuels, regardless of the variation in injection pressure and RON.

Furthermore, admirable combustion stability was observed even during low-load operations, where maintaining stable combustion can sometimes be more challenging. This stability is reflected in the COV values, which stay comfortably within the specified 3% boundary. The proven combustion stability at low load conditions provides a strong case for considering both 99 Bio E20 and 95 Bio E20 as promising candidates for drop-in fuels in gasoline engines.

The results show that 99 Bio E20 and 95 Bio E20 exhibit commendable combustion stability, identical combustion phasing, and burn duration during low-load engine operations. These findings suggest that both bio-gasoline variants have the potential to be promising candidates for drop-in fuels in gasoline engines.
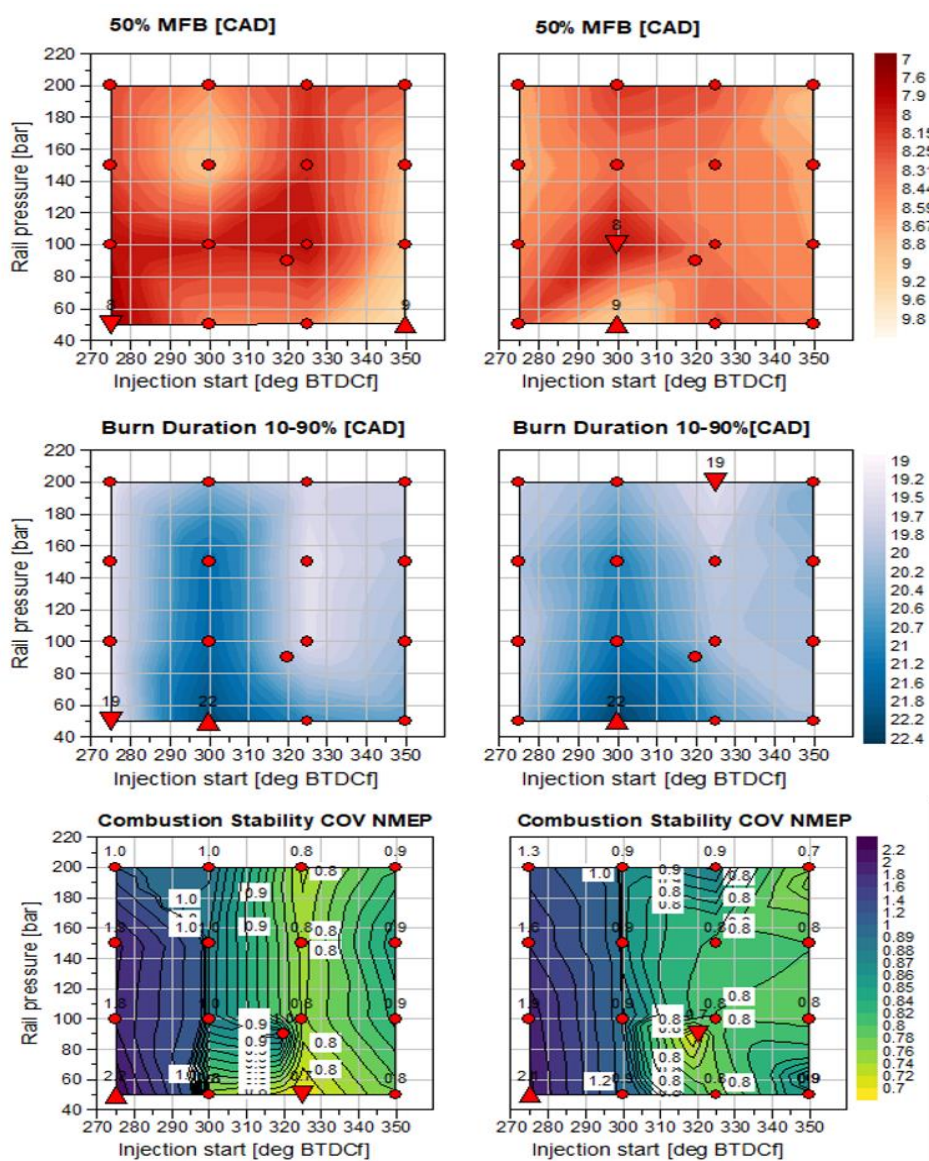
Figure 5. 6: Combustion phasing, Burn duration and combustion stability at 4.6 bar IMEP, 2000 rpm. Left column: 99 Bio E20 and right column: 95 Bio E20. The X-axis represents injection timing, and the Y-axis represents injection pressure.

The engine performance parameters presented in Figure 5.7 are crucial, including indicated specific fuel consumption (ISFC) and indicated thermal efficiency. Interestingly, 99 Bio E20 and 95 Bio E20 have almost identical ISFC values due to their small difference in energy density. However, 99 Bio E20 shows a slightly higher indicated thermal efficiency than 95 Bio E20, which is worth noting. Both fuels exhibit higher efficiency when injection commences between 300-325 degrees crank angle before the top dead centre (CA BTDC) across various operating conditions. However, there is a notable difference in the optimal injection pressure range needed to achieve higher efficiency with each fuel. The image shows a more prominent dark region for 99 Bio E20, indicating that it can deliver improved efficiency over a broader range of injection pressures than 95 Bio E20. The variation in thermal efficiency was minimal, within 1%, even when significant changes were made to fuel injection pressure and the start of injection timings.
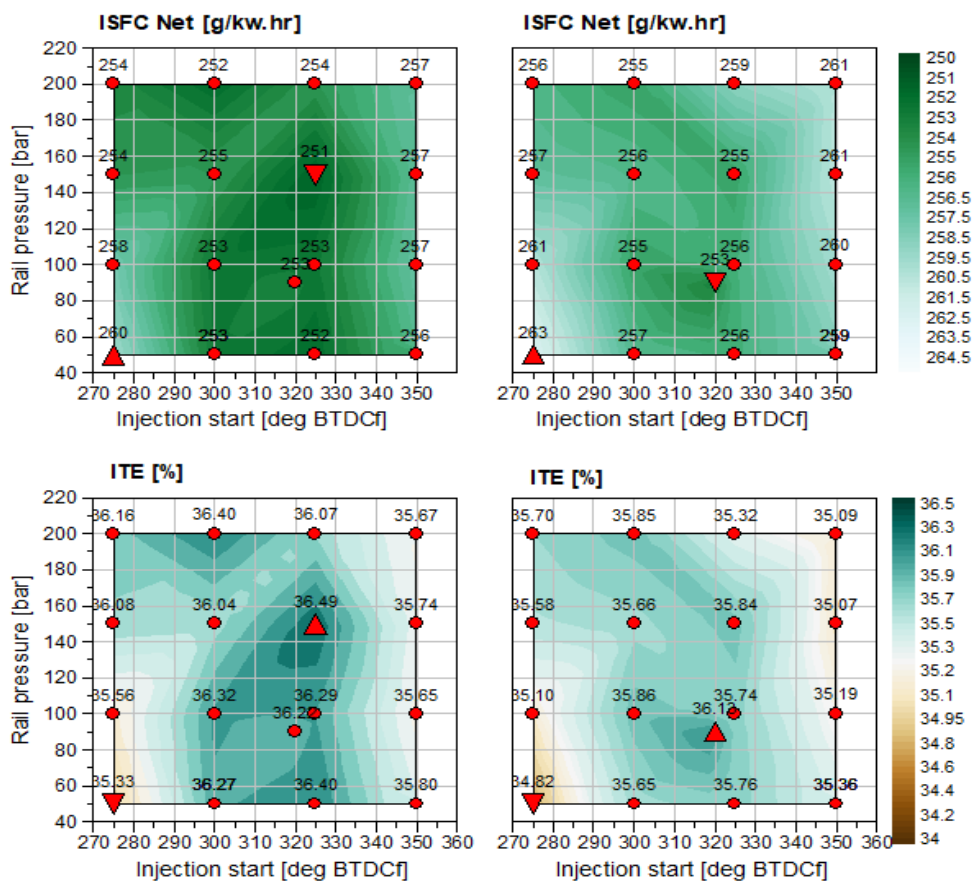
Figure 5. 7: ISFC and indicated brake thermal efficiency comparison for varying injection timing and pressure at 4.6 bar IMEP, 2000 rpm—left column: 99 Bio E20 and right column: 95 Bio E20.

Figure 5.8 displays the engine-out emissions of both fuels under various injection conditions. 95 Bio E20 exhibits marginally higher hydrocarbon emissions than 99 Bio E20. This disparity in HC emissions could be linked to the composition or combustion characteristics of the fuels. The higher initial boiling point of 95 Bio E20 might hinder the fuel's ability to vaporize efficiently, leading to increased HC emissions. One interesting trend is that HC emissions also rise when the injection timing is advanced and injection pressure is increased. This implies that fuel spray impingement on the piston top can cause the wall-wetting effect, increasing HC emissions.

Remarkably, using a slightly delayed injection timing with low injection pressure results in decreased HC emissions for both fuels. This underscores the potential of a more conservative injection approach in reducing HC emissions by promoting optimal combustion conditions. A higher NO_x emission was observed for 95 Bio E20 due to the greater diffusion burning than 99 Bio E20.
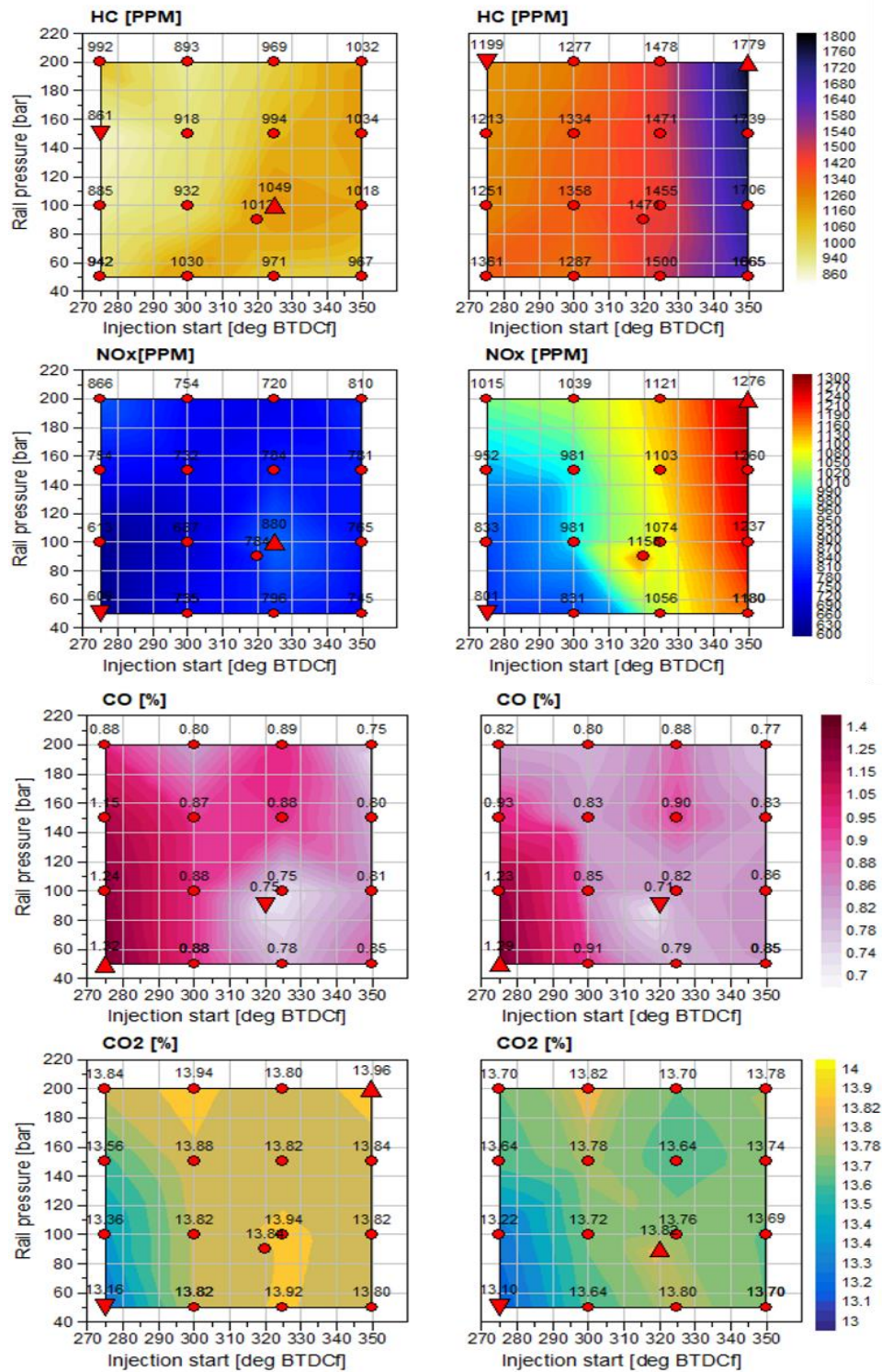
Figure 5. 8: engine-out emission analysis. THC, NO_x, CO and CO_2 comparison for varying injection timing and pressure at 4.6 bar IMEP, 2000 rpm. Left column: 99 Bio E20 and right column: 95 Bio E20.

Figure 5,8 shows the lowest NO$_x$ emissions achieved with delayed injection timing (around 270 CA BTDC) and low injection pressure. This is due to retarded combustion and lower combustion temperatures, which reduce NO$_x$ emissions. For both fuels, similar emissions are observed for CO and CO$_2$. Late injection points have the lowest CO and CO$_2$ emissions, with injection pressure having little effect.

5.3.3 Optimisation of Bio-gasoline at High-load Operation

This section examines the impact of fuel injection parameters on the performance of two biofuels during high-load engine operation. The engine was adjusted to 3000 rpm, 16 bar IMEP, 50-200 bar injection pressure, and 350-275 CA BTDC of SOI to achieve this. The biofuels' combustion behaviour, performance, and emission characteristics were compared under these conditions.

The combustion phasing, as indicated by 50% MFB and 10-90% burn duration, is illustrated in Figure 5.9. Both fuels exhibited combustion phasing variation between 10-14 CA, with no significant difference in behaviour at high-load operation. Figure 5.10 demonstrates the biofuel's exhaust gas temperature and cycle-to-cycle variation during high-load operation. The exhaust gas temperature exceeded the 600-degree Celsius threshold for both fuel types due to the increased fuel mass undergoing combustion. Although a slightly elevated exhaust gas temperature was observed for the 99 Bio E20 variant, the cycle-to-cycle variation for both biofuels remained impressively contained within the 2% range. This observation substantiates the inherent stability of combustion across the various injection pressures and SOI configurations explored in this study. The consistency underscores the robust nature of combustion, reinforcing the reliability of these biofuels under high-load operating conditions.
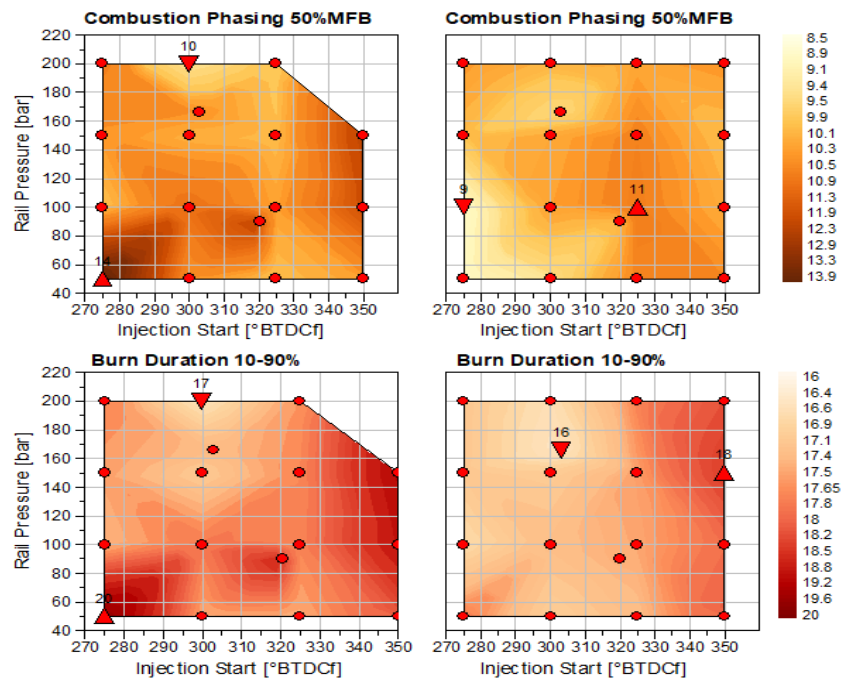
Figure 5. 9: Combustion phasing at high load operation (3000 rpm and 16 bar IMEP). Left column: 99 Bio E20, right column: 95 Bio E20.
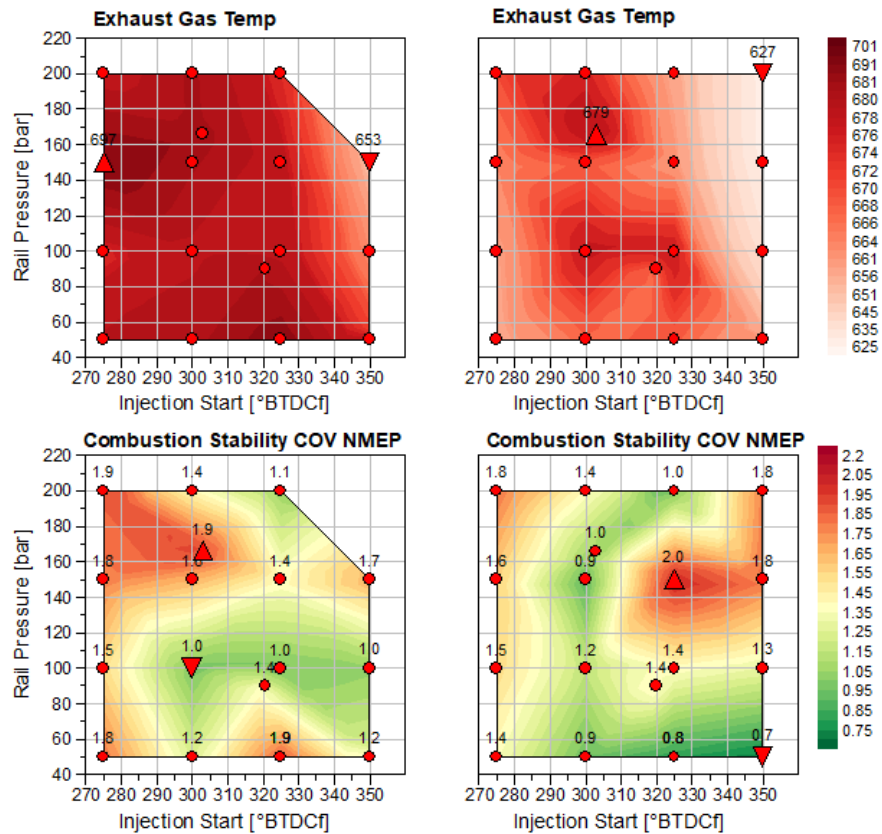
Figure 5. 10: Exhaust gas temperature and COV at 3000 rpm, 16 bar IMEP. Left column: 99 Bio E20, right column: 95 Bio E20.

The graphical representation of the indicated specific fuel consumption (ISFC) and indicated thermal efficiency, as illustrated in Figure 5.11, provides valuable insights into the fuel efficiency of both biofuels. The fuel consumption patterns of both biofuels are similar, resulting in comparable efficiency trends due to their nearly identical calorific values. It is noteworthy that the peak indicated thermal efficiency is approximately 39%. The maximum efficiency for both fuels was recorded when the Start of Injection (SOI) was set at 300 CA BTDC, and the injection pressure varied between 100-200 bar. When injection begins during the valve overlapping period, it leads to higher fuel consumption and reduced efficiency.
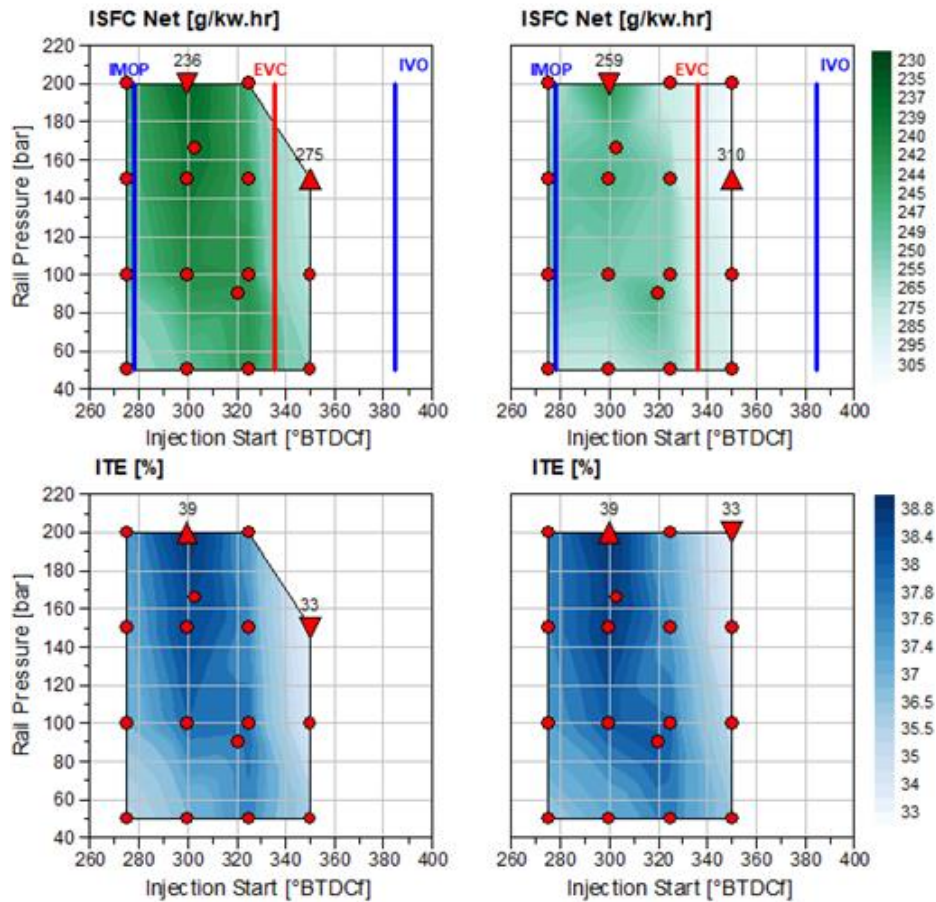
Figure 5. 11: ISFC and Indicated thermal efficiency at 3000 rpm, 16 bar IMEP—left column: 99 Bio E20, right column: 95 Bio E20.

Figure 5.12 displays the engine-out emissions for different fuel types. During the high-load operation, we observed notably high THC emissions at the beginning of the fuel injection. This was due to excess fuel landing on the piston top, creating a fuel film that did not mix well with air, resulting in heavier hydrocarbon emissions for both fuels. For 99 Bio E20, HC emissions increased beyond the analyser's measuring capability during early SOI and higher injection pressure. Therefore, CA BTDC is unsuitable for high-load operation due to extremely high HC emissions during SOI (320-350). We found that delaying the injection start and moderately increasing the injection pressure reduced HC emissions while detecting lower NO_x emissions. Generally, the optimal working zone for emissions is between SOI 280-300 and injection pressure between 120-180 bar.
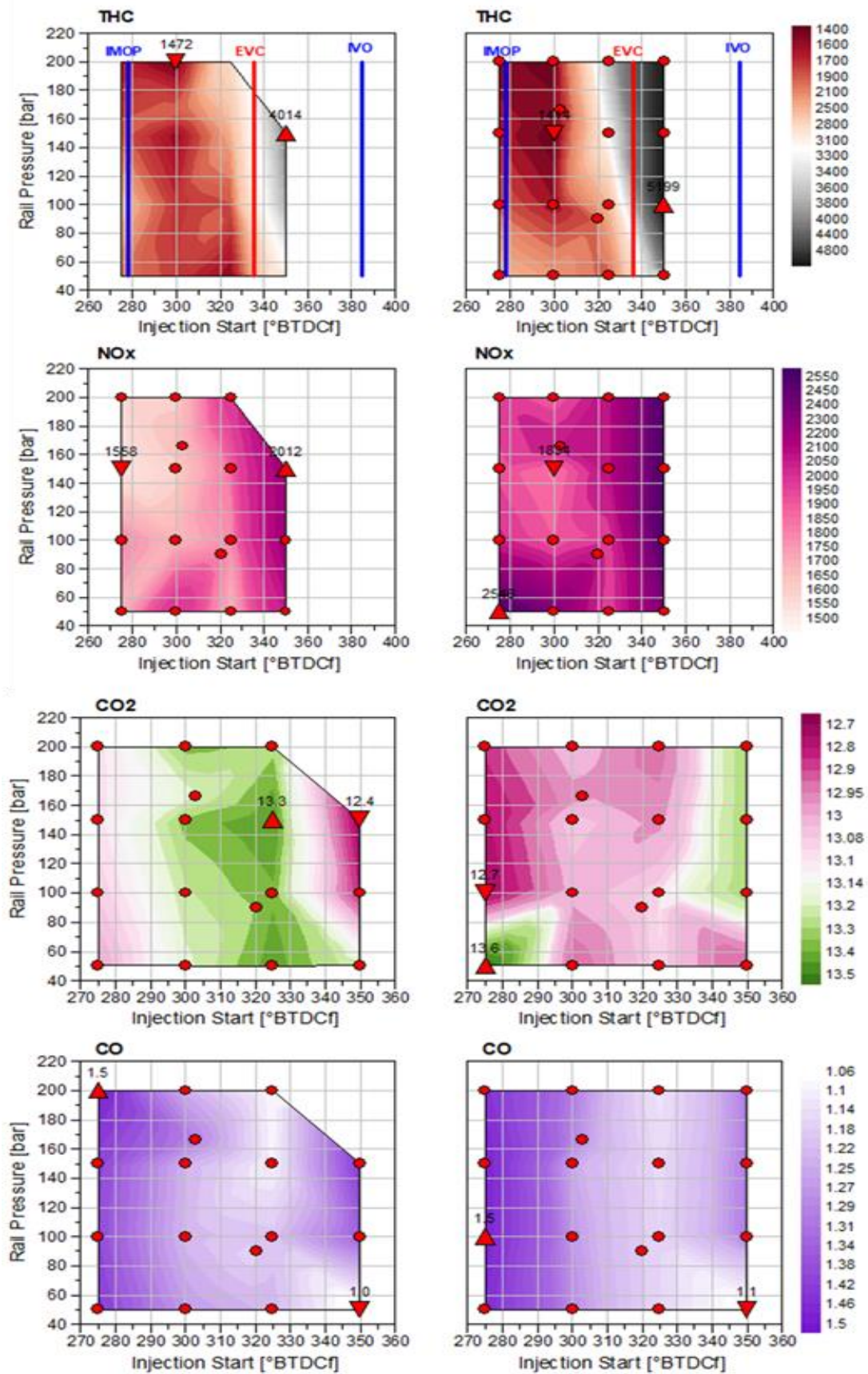
Figure 5. 12: ISFC and Indicated thermal efficiency at 3000 rpm, 16 bar IMEP. Left column: 99 Bio E20, right column: 95 Bio E20.

5.4 Conclusion

This study evaluated the suitability of two new biofuels, 99 Bio E20 and 95 Bio E20, as a drop-in replacement for fossil fuels in spark ignition engines. The research aimed to understand these biofuels' combustion dynamics, performance metrics, and emission characteristics compared to a baseline fossil fuel across different operating conditions. The study involved comprehensive experimentation, including varying injection parameters under low and high load conditions at 3000 rpm.

The research found that biofuels can be used interchangeably with fossil fuels across various operating conditions. The biofuel 99 Bio E20 showed a slightly higher thermal efficiency and knock resistance than the fossil fuel, particularly at high load conditions. However, both biofuels exhibited slightly higher hydrocarbon emissions due to their chemical composition, which contains higher aromatics.

During low-load operation, both biofuels exhibited similar combustion phasing when varying the injection pressure and start of injection. The most extended combustion was seen at SOI 300 CA BTDC at all the injection pressures examined, and the variation in thermal efficiency was within 1%. Notably, 99 Bio E20 has a wider operational regime during low-load operation than 95 Bio E20.

Both biofuels exhibited stable combustion during high-load operation, with similar combustion phasing at different injection pressures and the start of injection. The maximum recorded indicated thermal efficiency was roughly 39% at SOI 300 CA and injection pressures ranging from 100 to 200 bar. However, an early start to injection and higher injection pressure were not recommended due to elevated HC emissions.

The study demonstrated that bioderived gasoline fuel derived from 2nd generation feedstock can be used as a drop-in fuel in existing spark ignition engines with no hardware modifications. The research underscores the importance of biofuels in achieving a zero-carbon future. However, sustainable biofuel production is essential to ensure low-carbon alternatives to traditional fossil fuels while considering land use, water consumption, and biodiversity conservation.

Chapter 6. Effects of Dual Injection Operations on Combustion Performances and Particulate Matter Emissions in a Spark Ignition Engine Fueled with Second-Generation Biogasoline

6.1 Introduction

This Chapter studied the impact of port and direct fuel injections on particulate matter emissions in a boosted spark ignition engine fueled by a biofuel with a high octane number blended with ethanol compared to a fossil fuel baseline. The engine was equipped with two fuel injectors - high-pressure and port injectors. The study found that by reducing direct injection and increasing port fuel injection, particulate emissions were significantly reduced at low-load operations while maintaining the same thermal efficiency and other emissions. On the other hand, at higher load operations, direct injection resulted in a significant reduction in particulate numbers and enabled more stable operation in higher load regions.

6.2 Test Methodology

The experiments were conducted on a single-cylinder engine to evaluate the combustion characteristics of biogasoline and compare its performance and emissions with baseline gasoline. The experiments were carried out at two different engine speeds, 2,000 and 3,000 RPM, to assess the impact of varying loads on engine performance. The water and oil temperatures were set to a constant value of 90℃, while the intake air temperature was maintained at 40°C with no humidity.

The main objective of the experiments was to analyse the effect of the split injection ratio of DI and PFI on engine performance, PM, and other pollutant emissions. The engine experiments were initially performed at a low load operation of 4.6 bar IMEP and 2000 rpm. The injection strategy was swept from 100% DI to 100% PFI with a 20% interval. The engine was run at minimum ignition advance for maximum brake torque (MBT), targeting 50% burn at 8 degrees ATDCf. This was followed by testing the engine at a higher speed of 3000 rpm and a load sweep from 10 bar IMEP to 20 bar IMEP with split ratios from 100% DI to 100% PFI.

Table 6.1 summarises all the boundary conditions and operation constraints for each test. In-cylinder pressure was recorded over 300 engine cycles for the in-cylinder pressure, heat release analysis, and IMEP calculations. The experiments aimed to provide insights into the combustion characteristics of biogasoline and its ability to reduce pollutant emissions.

Table 6. 1: test methodologies for the split injection study

Parameter	unit	Split ratio study	Load sweep study
Engine speed	RPM	2000	3000

Indicated mean effective pressure (IMEP)	bar	4.6	10 to 20 bar
DI start of injection	degrees BTDCf	320	300
PFI start of injection	degrees BTDCf	600	600
DI injection pressure	bar	100	150
PFI injection pressure	bar	8	8
Intake cam timing(IMOP)	degrees ATDCg	100	82
Exhaust cam timing (EMOP)	degrees BTDCg	120	140
Relative AFR	-	1	1
Boosted air temperature	℃	40	40
Target (CA50)	degrees ATDCf	8	8 and retreated to avoid knocks
Coolant and oil temperature	℃	90	90

6.3   Results and Discussion

The upcoming section will evaluate the influence of injection split ratios on the engine's efficiency and emissions while operating with 99 RON E20 biogasoline and 95 RON E10 fossil fuel under various engine conditions.

6.3.1. The Effect of Split Ratio on Combustion Characteristics and Emissions at Low Load

The study aimed to analyse the combustion characteristics and engine emissions by varying injection split ratios from 100% DI to 100% PFI at 20% intervals while keeping the load and speed fixed at 4.6 bar IMEP and 2000 rpm, respectively. To ensure maximum scavenging, the intake and exhaust cam positions were set at 120-degree BTDCg and 100-degree ATDCg, respectively. The air/fuel mixture was maintained stoichiometrically, with PFI and DI injection timings and pressures fixed. The engine was always operated at MBT with both fuels under the same conditions.

As shown in Figure 6.1, the output torque for both fuels remained almost constant, with a minimal variation of 0.6 Nm at each split ratio. The spark timing for biogasoline was fixed at 14 degrees BTDCf, except at 100% PFI, to maintain the CA50 below 8.5 degrees, as depicted in Figure 6. Biogasoline brake-specific fuel consumption (BSFC) was higher at 20% PFI. However, it remained constant at 346 g/kwh, corresponding to 35% Indicated Thermal Efficiency (ITE) (as shown in Figure 6) when the PFI ratio was increased above 60%. The same strategy was applied to fossil fuels, and the spark timing was kept at around 14.25 BTDCf to maintain MBT. The thermal efficiency of fossil fuel was similar to biogasoline at this load for all split ratios. The peak in-cylinder pressure (Pmax) remained almost unchanged over the split ratio sweep. However, biogasoline produced higher Pmax due to the difference in the LHV and ethanol concentrations, as depicted in Figure 6.2.
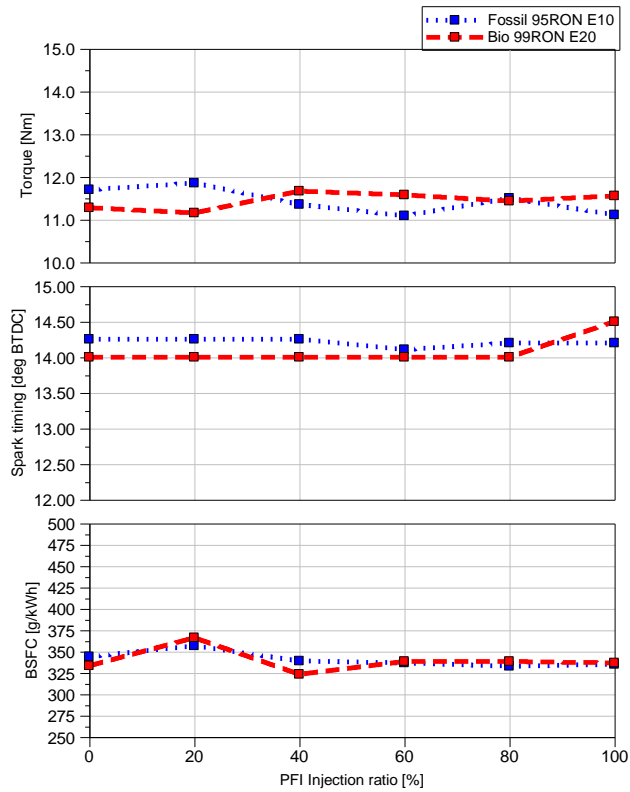
Figure 6. 1: Effect of split ratios on engine torque, spark timing, and BSFC at 4.6 bar IMEP for baseline fossil fuel and biogasoline.
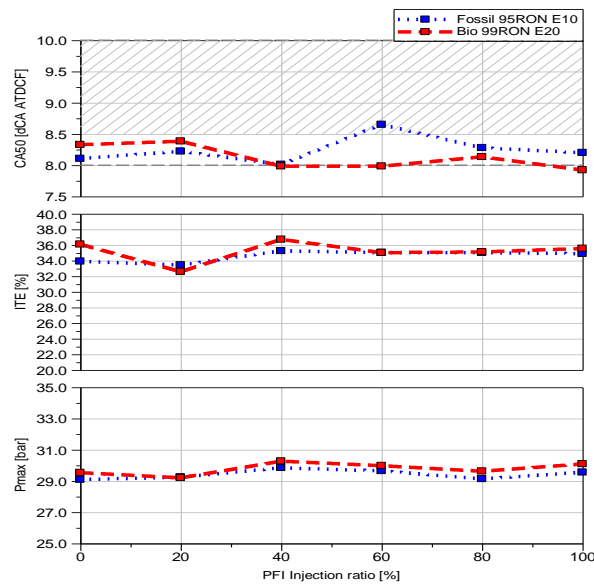
Figure 6. 2: The effect of split ratio on CA50, ITE and Pmax for baseline fossil fuel and biogasoline.

Based on the data presented in Figure 6.3, it can be seen that there is minimal variation between the engine burn points of baseline fossil fuel and biogasoline at both 10% (CA10) and 90% (CA90) split ratios, with a decreasing trend observed as the PFI approaches 100%. Additionally, the engine exhibited stable operation with cycle-to-cycle variation below 0.9% across all split ratios for both fuel types. Notably, the knock intensity remained constant up to 80% PFI, with only a slight increase observed at 100% PFI for biogasoline due to a 0.5-degree spark timing advance to maintain a CA50 of 8 CA ATDCf. It was

observed that fossil fuel burned slightly faster than biogasoline and also demonstrated less knock resistance. These findings suggest biogasoline may be a more suitable alternative in high-load conditions where knock resistance is critical.
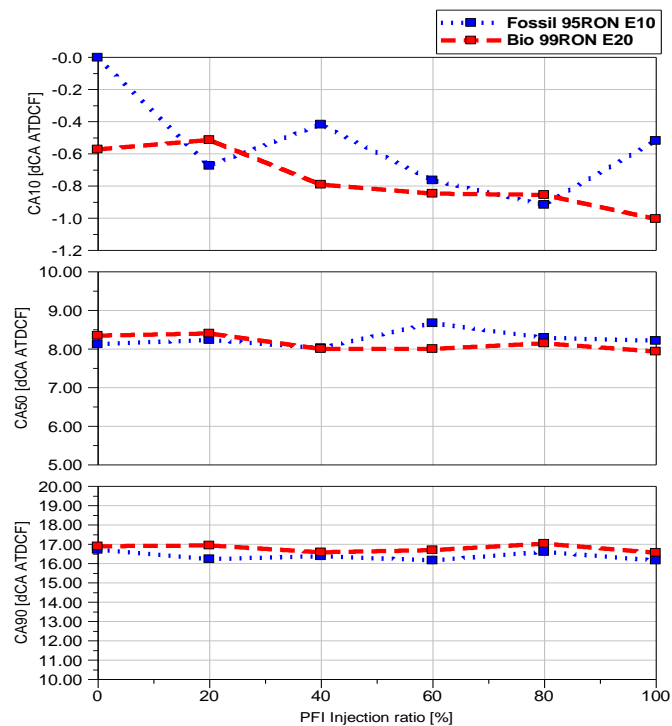
Figure 6. 3: The effect of split ratio on CA10, CA50 and CA90 for baseline fossil fuel and biogasoline.

According to Figure 6.4, engine emissions are affected by the split ratio. At 60% PFI injection, emissions increased by 0.3% compared to 0% PFI, while CO emissions decreased at higher PFI ratios, possibly due to a more uniform mixture. Compared to the same emission level at 0 to 80% PFI split ratio, emissions rose by 20% at 100% PFI and reached 1476 ppm due to DI fuel injection's lack of charge cooling effect. Unburnt hydrocarbon remained unchanged up to 80% PFI but increased by 53% with the 100% PFI injection strategy, likely due to more fuel vapour trapped in the crevice volumes.

The CO_2 emission of biogasoline was 0.5% higher, while the CO and O_2 levels were similar across all fuel split ratios. The NO_x emission showed very little difference between the baseline fossil fuel and biogasoline, while the THC emission was much higher for biogasoline, in line with previous studies.
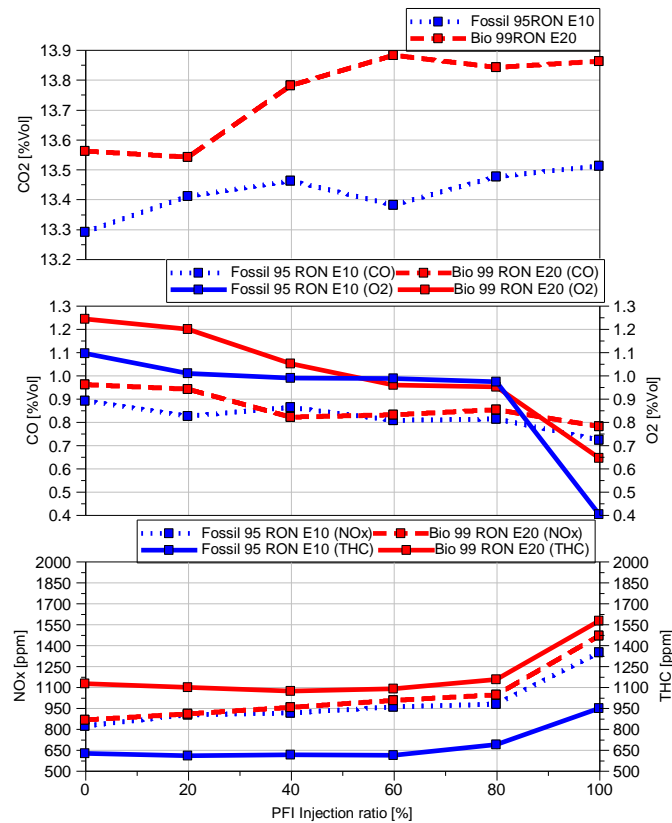
Figure 6. 4: The effect of split ratio on engine emissions for baseline fossil fuel and biogasoline.

As presented in Figure 6.5, the study's findings illustrate the PN levels for particles within the size range of 23 to 1000nm across various injection split ratios for biogasoline and fossil fuel. The results indicate a significant reduction of over 96% in PN when the PFI ratio is increased for biogasoline. Based on the additional emission data presented in Figure 8, the optimal split ratio to minimise PN without increasing other emissions parameters is 80% PFI. While biogasoline has nearly twice the PN of fossil fuel at 100% DI, it produces similar PN levels at 80% PFI.

Figure 6.6 provides a closer look at the spectral density of the PM emission across particle sizes and injection split ratios. The data shows that DI injection produces more particles in the 100nm range, while 100% and 80% PFI produce more particles in smaller sizes ranging from 10 to 20 nm.
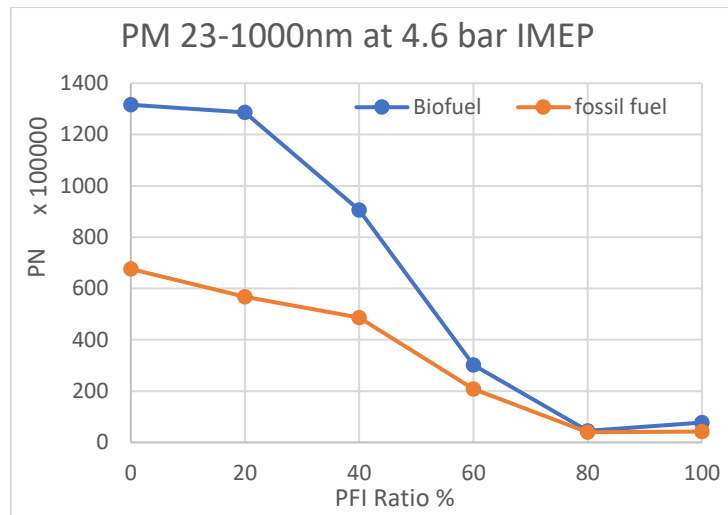
Figure 6. 5: The effect of split ratio on PN for biogasoline and fossil fuel.
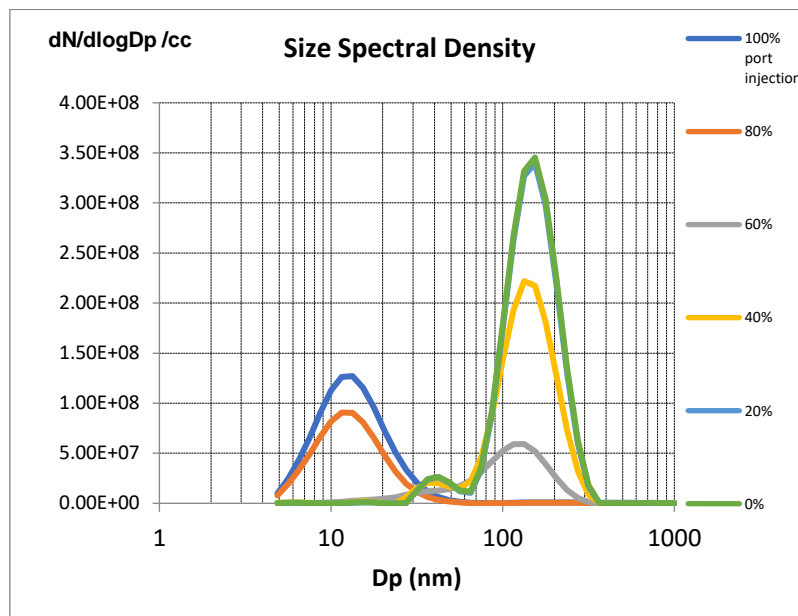
Figure 6. 6: The effect of split ratio on the size spectral density of PM emissions for biogasoline.

The study's experiments have led to a significant discovery regarding engine efficiency and fuel consumption. Specifically, the injection strategy has no effect on these factors at low loads of 4.6 bar IMEP. However, the split ratio does impact emissions. Interestingly, the 100% PFI strategy resulted in the highest NO_x emissions for both fuels. On the other hand, increasing the PFI ratio from 0 to 80% led to a 96% and 84% decrease in PN emissions for biogasoline and the baseline fossil fuel, respectively. Thermal efficiency remained unchanged compared to the 100% PFI strategy. In conclusion, the optimal operating points for both fuels at low loads are 80% PFI and 20% DI, which can maintain consistent NO_x and THC levels while reducing PM emissions. These findings have prompted further investigation into mid- and high-load conditions.

6.3.2. Effect of Split Ratio at 3000 RPM at Mid and High Loads

The engine speed was kept constant during the test at 3000 RPM while the load varied between 10 bar IMEP and 20 bar IMEP. The split ratio was increased stepwise in 20% increments from 0% PFI (100% DI) to 100% PFI. Full PFI reached the cycle-to-cycle stability limit at 19 bar IMEP. Throughout the testing, lambda was fixed at 1, and the exhaust temperature at maximum load was below 750°C. At low to medium loads, spark timings were set to the MBT to maintain CA50 between 8 and 10 degrees ATDCf. However, when the load increased above 14 bar IMEP, spark timing was retarded to prevent knocking combustion. Figures 6.7 and 6.8 show the main engine parameters at different split ratios and load sweeps from 10 to 20 bar IMEP.

The maximum indicated thermal efficiency was achieved with full DI, which was 6% higher than the full PFI at 14 bar IMEP for both fuels. At 10 bar IMEP, the indicated thermal efficiency of biogasoline operation was hardly affected by the variation of port injections. The spark timing was retarded for the PFI operation to avoid knocking combustion at higher loads. The baseline fossil fuel consumed less than biogasoline at 10 bar IMEP due to higher thermal efficiency.

As shown in Figure 6.8, the spark ignition timing of biogasoline at 100% DI operation could be advanced to maintain the CA50 between 8-10 degrees ATDCf at loads up to 14 bar IMEP. In contrast, the full PFI operation had to retard CA50 to avoid the appearance of the knock. Therefore, the spark timing of 100% DI biogasoline at high-load regions was much more advanced than baseline fossil fuel as it has a higher knock resistance.
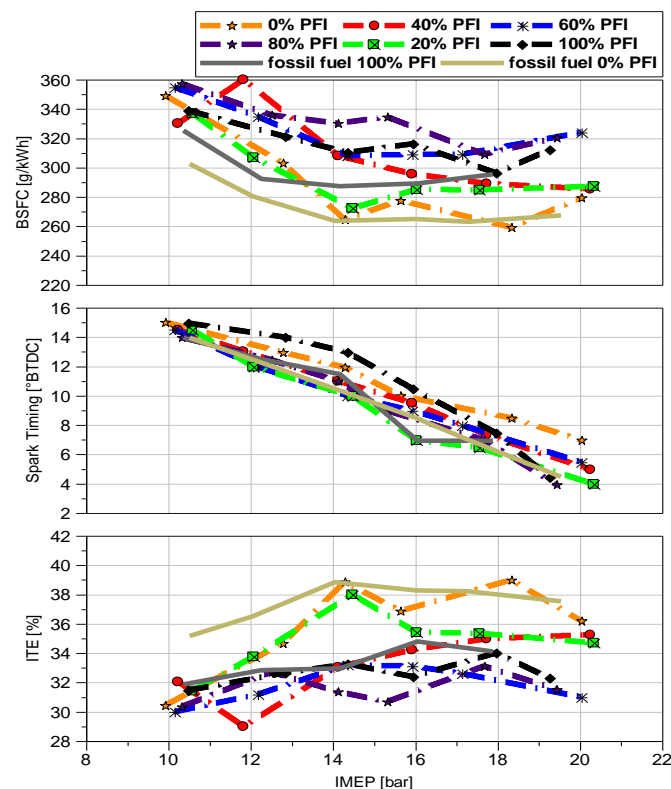
Figure 6. 7: Engine BSFC, spark timing, and ITE at 3000 rpm with different split ratios for biogasoline and baseline fossil fuel.
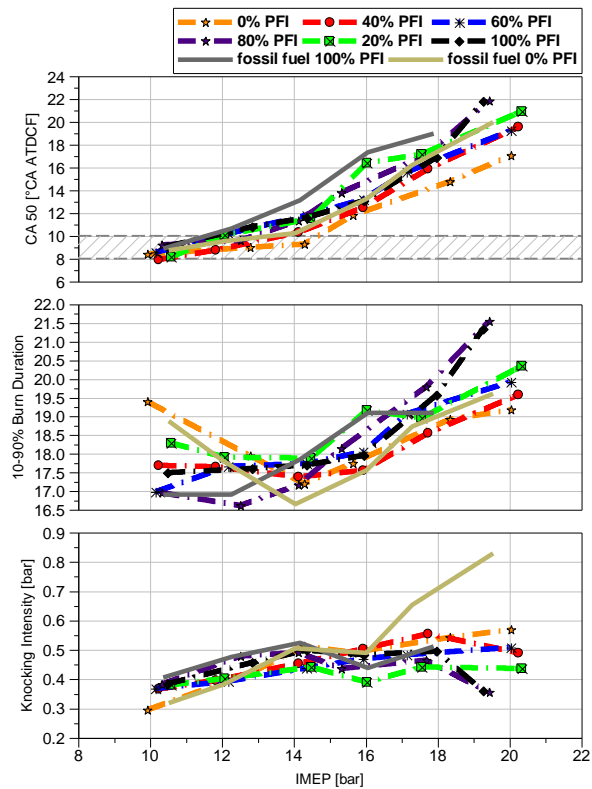
Figure 6. 8: CA50, burn duration and knock intensity at 3000 rpm with different split ratios for biogasoline and baseline fossil fuel.

Figure 6.8 reveals that both fuels had similar burn durations (CA90-CA10) during 100% DI operation. For biogasoline, the burn duration for 80% and 100% PFI operations demonstrated the same trend at high loads when spark timings were retarded. Although the average knock intensity dropped below the threshold at 18 and 20 bar IMEP, the retarded spark timing had to be maintained as occasional knock events were observed under these conditions, as indicated by the higher COV in Figure 6.11.

In all cases, except for the spark to 10% burn duration for the 100% PFI operation, similar trends were observed in the initial, middle, and later burn durations, as shown in Figure 6.9. The spark to 10% burn graph demonstrates that both fuels exhibit a similar trend for 100% DI, while 100% PFI follows a different trend. This difference can be attributed to the absence of stratified injection from DI and a fully homogeneous mixture without enhanced flow motion.

As load increases, Figure 6.10 indicates a consistent trend between the maximum pressure (APmax) location and the peak in-cylinder pressure (Pmax) value, regardless of the split ratios. The spark timing primarily influences the APmax location. Consequently, the 100% DI biogasoline shows the earliest APmax at high load since it has the most advanced spark timing. The maximum pressure rise rate (Rmax) is higher for 100% DI operation due to advanced spark timing and lower for 100% PFI operation at high load due to higher COV.
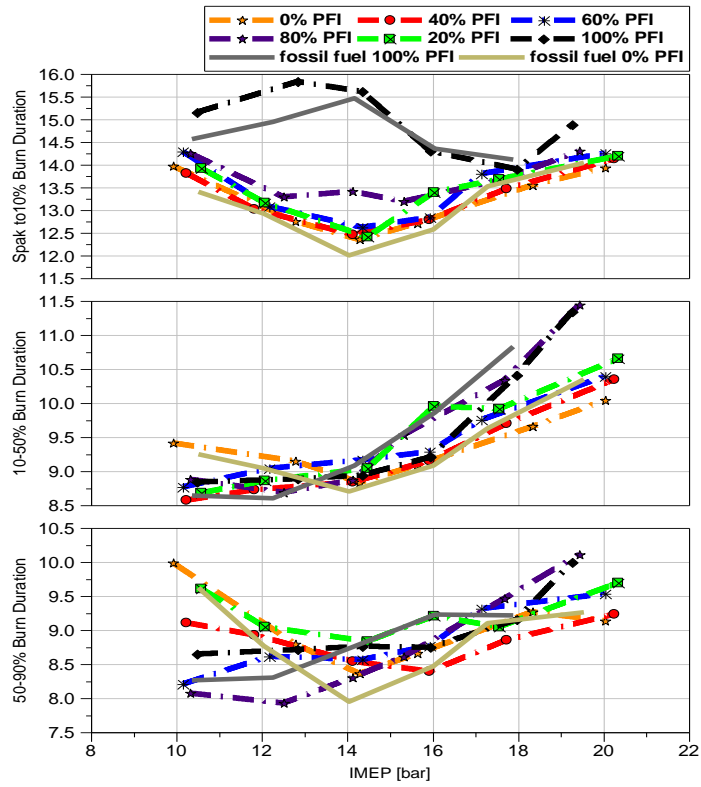
Figure 6. 9: Early burn duration (spark to 10 % burn), middle burn duration (CA10 to CA50), and late burn duration (CA50 to CA90) at 3000 rpm with different split ratios for biogasoline and baseline fossil fuel.
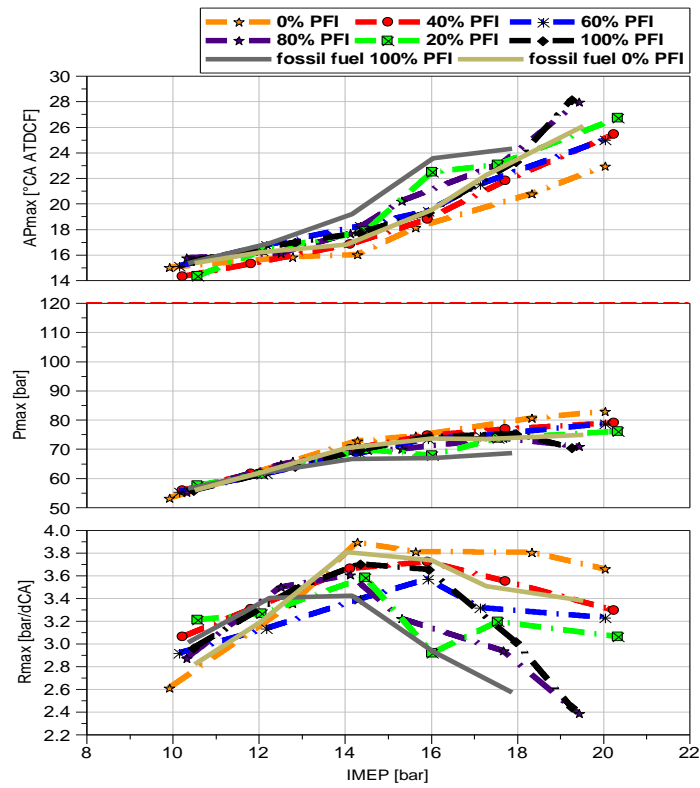
Figure 6. 10: APmax, Pmax and Rmax at 3000 rpm with different split ratios for biogasoline and baseline fossil fuel.

When the exhaust gas temperature exceeds 750°C, extra fuel is injected to cool it down using the fuel cooling effect. Figure 6.11 shows that the exhaust temperature remained below the threshold when the engine ran at lambda 1, indicating that over-fueling is unnecessary for cooling the exhaust system. However, the study discovered that the engine's stability decreased as the PFI split ratio increased, reaching its stability limits at 18.64 bar IMEP during biogasoline 100% PFI operation.

Furthermore, the COV gradually increased as the engine load increased. The baseline fossil fuel with 100% PFI operation reached the stability threshold limits at 15 bar IMEP, whereas bio-gasoline reached the threshold at a higher load of 19 bar IMEP. Additionally, compared to the combustion stability of both fuels at 100% DI, biogasoline demonstrated higher stability due to its marginally higher ethanol percentage.
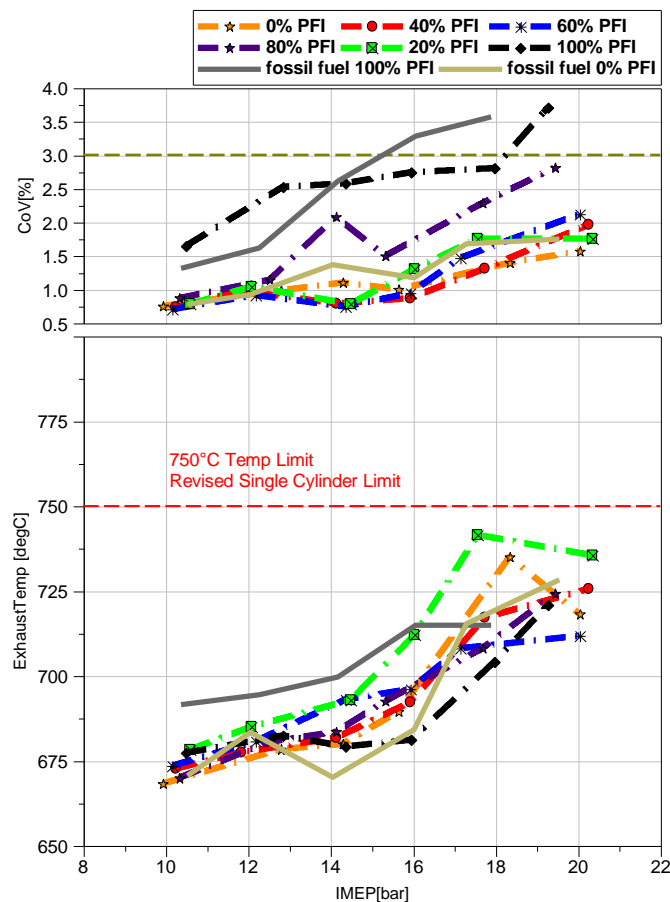
Figure 6. 11: COV and exhaust temperature at 3000 rpm with different split ratios for biogasoline and baseline fossil fuel.

Figure 6.12 displays emissions at varying split ratios. The CO_2 emission remained consistent throughout the load sweep, while fossil fuel emitted slightly less CO_2 (0.4%) than biogasoline. The highest thermal efficiency resulted in the lowest CO_2 levels. Increasing the PFI split ratio increased CO_2 emissions, and the difference between 100% DI and 100% PFI for biogasoline averaged 0.2%. Interestingly, CO emissions exhibited an opposite trend to CO2, with 100% DI in both fuels leading to higher CO emissions due to fuel stratification caused by direct injection.

The highest NO_x emissions occurred with 100% PFI, while direct fuel injection reduced NO_x emissions due to reduced gas temperature due to the larger charge cooling effect. Retarded spark timing prevented knocking combustion at high load operations, leading to

lower NO$_x$ emissions after 18 bar IMEP. Finally, injecting more fuel directly into the cylinder reduced THC emissions, possibly due to less trapped HC in the crevice region. Full DI mode led to lower THC emissions for fossil fuel, thanks to the less charged cooling effect and subsequent lower temperatures.

Data presented in Figure 6.13 showcases the impact of split injection strategies on particle emissions across a range of load conditions for biogasoline. The results indicate that injecting fuel
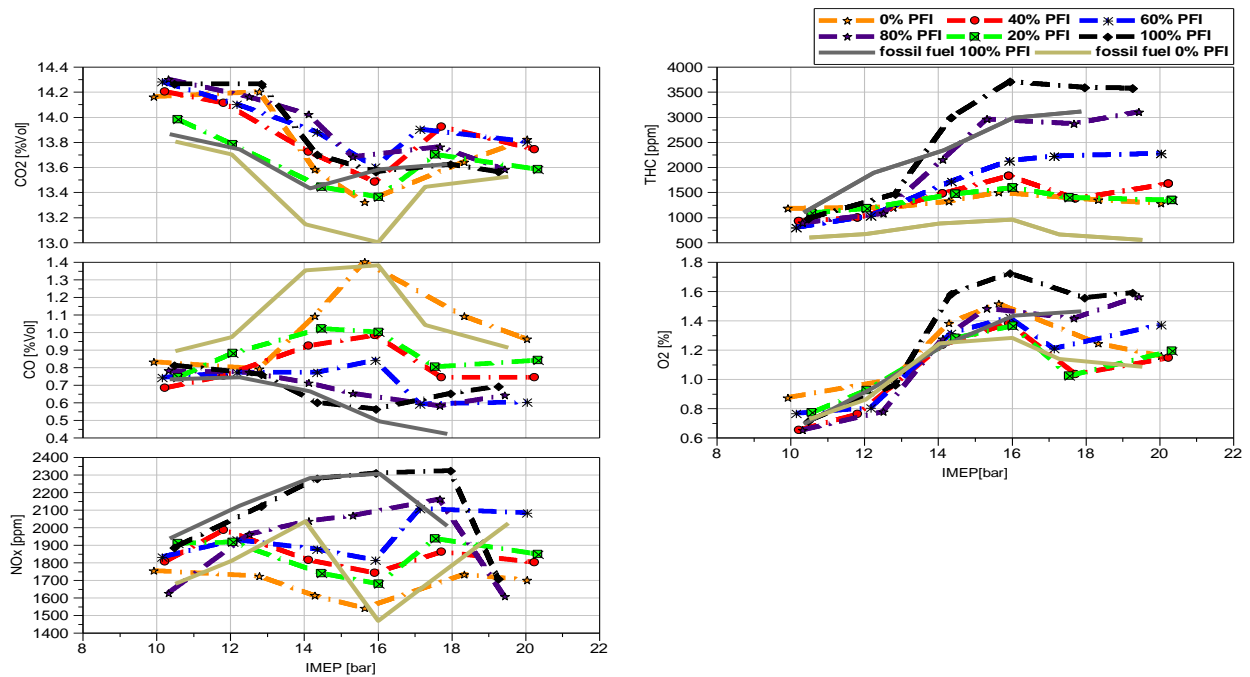
Figure 6. 12: Emission parameters at 3000 rpm with different split ratios for biogasoline and baseline fossil fuel.

predominantly through port fuel injection (PFI) significantly reduces particle number (PN) at low loads of up to 8 bar IMEP, reducing over 86%. However, at high load conditions of 10 bar IMEP or more, increasing PFI ratios to 100%, 80%, and 60% increase PN. In contrast, at the maximum load of 20 bar IMEP, predominantly using PFI to inject fuel resulted in a 64% reduction in PN compared to higher direct injection (DI) ratios.

These findings underscore the critical role of injection split ratio in controlling particle emissions, with PFI demonstrating significant reductions in PN, although not in PM emissions. Figure 6.13 reveals that direct injection may reduce PM emissions at higher loads.

Furthermore, a comparative analysis of PN emissions from biogasoline and fossil fuel reveals that biogasoline benefits more from split injection strategies, with the intersection of 100% DI and 100% PFI PN occurring at 10 bar IMEP, compared to 13 bar IMEP for fossil fuel.

Figure 6.14 presents the size spectral density over the load sweep for 100% DI and 100% PFI operations, highlighting a 64% decrease in PN emission at high load conditions for DI compared to PFI split ratios of 100% and 80%. However, the limited information available

on the detailed composition of RON99 E20 biogasoline and the involved combustion chemistry necessitates further investigation to clarify the reasons for the lower PN of DI operations. Notably, a correlation exists between the high unburnt hydrocarbons in the exhaust and the greater PN number of biogasoline PFI operations, which could be attributed to heavy hydrocarbon compounds in biogasoline forming condensates and solid particles.
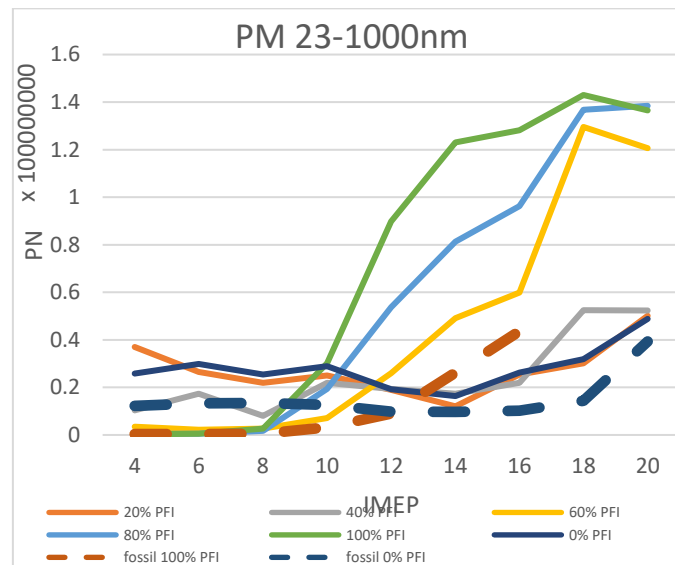
Figure 6. 13: PN results at 3000 rpm with different split ratios for biogasoline and baseline fossil fuel.
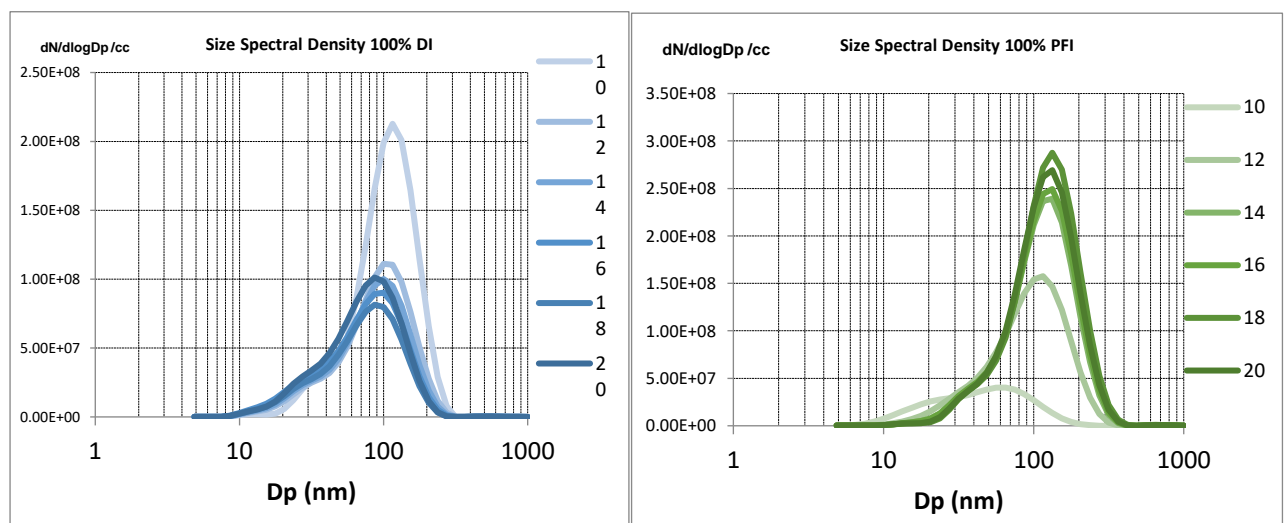
Figure 6. 14: PM size spectral density results at 3000 rpm for biogasoline at 100% PFI and 100% DI at different engine loads.

6.4 Conclusion

Two experiments were conducted to study the performance of biogasoline combustion and PM emissions in a single-cylinder spark ignition engine. The effects of fuel properties and fuel injection strategies on the combustion process, thermal efficiency, and emissions were measured and analysed. The main findings indicate that biogasoline produces more PM emissions due to its heavier components. However, optimal split injection strategies can significantly reduce PM emissions.

Injection strategies have no impact on engine performance under low-load conditions. However, the emissions results show a sudden increase at 100% PFI, but the PN dropped by 86%. The ideal operation point for minimising PN and maintaining emissions at full DI levels is 80% PFI.

Furthermore, when the engine operates at a load higher than 10 bar IMEP at 3000 rpm, DI produces higher thermal efficiency, greater stability than PFI, and lower PN values. Split injection ratios have been more effective in reducing PM emissions at low and mid-load operations for biogasoline than fossil fuel.

Despite its heavier composition, this has significantly benefited biogasoline by reducing and eliminating higher PM emissions. Additionally, biogasoline has achieved nearly the same PN numbers as fossil fuel at the highest operation points.

Future studies can compare fossil gasoline of the same octane number and ethanol concentration (98 RON E20). A comprehensive fuel matrix considering injection pressure and timing variations across different split ratios can also help optimise emissions and performance.

Chapter 7. Hydrogen Fuel System and Engine Testing Facility

7.1 Hydrogen Characteristics

Hydrogen is the lightest element with the symbol H and atomic number 1. It forms a gas consisting of diatomic molecules with the formula H2, commonly known as hydrogen gas, molecular hydrogen, or simply hydrogen. Notably, this element is colourless, odourless, tasteless, non-toxic, and highly combustible. Moreover, hydrogen is the most abundant chemical substance in the universe, accounting for about 75% of all normal matter. The sun and other celestial bodies primarily comprise hydrogen in the plasma state. Most of our planet's hydrogen exists in molecular forms such as water and organic compounds. Each atom of the most common isotope of hydrogen (symbol 1H) possesses one proton, one electron, and no neutrons [151].

7.1.1 Hydrogen Properties and Safety Requirements

Hydrogen has garnered more and more interest in recent years for its near-zero-emission and abundant source. As is summarised by the Hydrogen Council, hydrogen can play significant roles in enabling large-scale renewable energy integration and power generation, distributing energy across sectors and regions, acting as a buffer to increase energy system resilience, decarbonising transportation, decarbonising industrial energy use, decarbonising building heat and power, and providing clean feedstock for industry. Across the seven roles, hydrogen could account for 18% -20 % of total energy consumption by 20. There are five national standards for hydrogen specification in China. GB/T 3634.1-2006 specifies the specifications and requirements of industrial Hydrogen testing, packing, storage, transportation, and safety. It is developed for petroleum, food, fine chemicals, glass and artificial gems manufacturing, metal smelting, cutting and welding. GB/T 3634.2-2011 specifies the specifications and requirements of testing, packing, storage, transportation and safety of pure Hydrogen, high pure Hydrogen and ultrapure Hydrogen. It is developed for electronic, petrochemical, and metal smelting industries and scientific research. GB/T 16942-2009 specifies the specifications and requirements of testing, packing, storage, transportation, and safety of gaseous hydrogen for electronic industries. It is used as a reducing gas, carrier gas for the epitaxy process, and gas for plasma etch. GB/T 34537-2017 specify the specification and requirements of hydrogen and compressed natural gas (HCNG) blends for vehicles. This standard specifies that hydrogen used for HCNG blending should comply with GB/T 3634.1. GB/T 34537-2017. GB/T 37244-2018 is now the only hydrogen fuel specification50, reducing annual CO_2 emission by roughly 60 Gt compared to today's technologies.

Several essential characteristics of hydrogen greatly influence the technological development of hydrogen internal combustion engines, such as

Wide range of flammability

Hydrogen has a wide flammability range (4- 75% versus 1.4-7.6% volume in the air for gasoline) compared to nearly all other fuels. This leads to apparent concerns over the safe handling of hydrogen[152].

Flame velocity and adiabatic flame

Hydrogen burns with a high flame speed, allowing hydrogen engines to approach the thermodynamically ideal engine cycle (most efficient fuel power ratio) when the stoichiometric fuel mix is used.

Minimum ignition source energy

The minimum ignition source energy is required to ignite a fuel-air mix by ignition, such as a spark discharge. Hydrogen and air mix is about an order of magnitude lower than that of a petrol-air mix 0.02 mJ compared to 0.24 mJ for petrol - and is approximately constant over the flammability range.

High diffusivity

The diffusivity of hydrogen is exceptionally high. This ability to spread into the air is significantly greater than gasoline, which is beneficial for two reasons. Creating a homogeneous blend of fuel and air makes it more accessible. Second, if a hydrogen leak occurs, the hydrogen quickly disperses. As a result, hazardous situations can be prevented or minimised [153].

Low density

The most significant effect of hydrogen's low density is that a massive volume of Hydrogen may be required to provide a reasonable driving range without significant compression or conversion to a liquid. Poor density also means the fuel-air mixture has a low energy density, which reduces the engine's power output. As a result, when a hydrogen engine is run lean, problems with insufficient power may occur.

High auto-ignition temperature

The minimum autoignition temperature is required to initiate self-sustained combustion in a combustible fuel mixture without external ignition. For hydrogen, the auto-ignition temperature is relatively high, 585ºC. This makes it difficult to ignite a hydrogen-air mixture based on heat alone without some additional ignition source.

Stoichiometric air-fuel ratio and mixture energy content

The stoichiometric composition of fuel and air provides the chemically precise amount of oxidant to burn all the fuel completely.

Table 7. 1: Hydrogen vs Diesel and Gasoline

Properties	Diesel	Unleaded gasoline	Hydrogen
Formula	$C_nH1.8n$ $C_8–C_{20}$	$C_nH1.87n$ $C_4–C_{12}$	— H_2
Auto-ignition Temperature (K)	530	533–733	858
Min. ignition energy (mJ)	—	0.24	0.02
Flammability limits(vol. % in air)	0.7–5	1.4–7,6	4–75
The stoichiometric air-fuel ratio on mass	14.5	14.6	34.3
Limits of flammability (equivalence ratio)	—	0.7–3,8	0.1–7,1
Density at 16 ◦C and 1.01 bar (kg/m^3)	833–881	721–785	0.0838

Net heating valve (MJ/kg)	42.5	43.9	119.93
Flame velocity (cm/s)	30	37–43	265–325
Quenching gap in NTP air (cm)	—	0.2	0.064
Diffusivity in the air (cm²/s)	—	0.08	0.63
Octane number		92–98	130
Cetane number	44-55	13–17	—

7.1.2 Hydrogen Vs. Gasoline as A Combustion Fluid

Based on the hydrogen properties, it is clear that hydrogen cannot self-ignite once the temperature is less than 585ºC. Also, the air-to-fuel ratio is almost doubled in the hydrogen, meaning less hydrogen is required to burn inside the engine with the same amount of air as seen in Figure 7.1 shows that a hydrogen engine can be more than 117% more efficient than gasoline.

Figure 7. 1: how hydrogen engine vs Gasoline

One main advantage of using hydrogen from a safety perspective away from the fact is that Hydrogen gas does not produce carbon emission, which is the leading gas that affects global warming. Hydrogen has less density compared to the air, which means every time hydrogen leakage happens, it will go to the top as quickly as possible and require a high amount of air and high concentration plus a spark source to make a temporary fire as the hydrogen in the mainline before air mixing cant ignites without high amount of air. An experiment shows the timeline from 3 seconds to 60 seconds result of an automotive fire in the Hydrogen and gasoline tank in Figure 7.2. The photo shows how Hydrogen fire can be limited with a single jet fire to the top without spreading the fire anywhere else. Furthermore, less time is required to fire the whole amount of hydrogen than gasoline, as hydrogen has a high-speed burning rate.

Figure 7. 2: Timeline from 3 seconds to 60 seconds result of having an automotive fire in the Hydrogen and gasoline tank

7.1.3 Hydrogen Safety Issues

Hydrogen is a colourless, odourless gas that is lighter than air. The use of odorants to detect leaks is being investigated. However, all the odorant chemicals considered have been rejected due to concerns regarding their potential to 'poison' the fuel cell membrane catalysts. Furthermore, they may have limited effectiveness for small leaks, as the odorant molecules will inevitably be much larger than the hydrogen molecules. Hydrogen is not expected to cause mutagenicity, teratogenicity, embryotoxicity, or reproductive toxicity. There is no evidence of adverse effects if skin or eyes are exposed to hydrogen; it cannot be ingested. Hydrogen burns with an invisible flame, making detecting a hydrogen fire challenging. This apparent low emissivity of hydrogen flames (total heat flux radiated) may reduce the heat transfer by radiation to objects near the flame, thus reducing the risks of secondary ignition and burns. Hydrogen fires are usually only extinguished once the hydrogen supply has been shut off because of the danger of re-ignition.

It can be concluded that hydrogen is less dangerous or safer compared to other fuels. Hydrogen is different and has to be professionally handled with knowledge of underpinning science and engineering to provide public safety and competitiveness hydrogen. However, based on the main Hydrogen properties, the possibility of having a Hydrogen explosion is not valid as long as the Hydrogen amount needed inside the test cell is less than the minimum Hydrogen Percentage for making fire with oxygen and as long as the Hydrogen leakage from the line to the atmospheric air conditions "no pressure for the explosion.".

7.2 Hydrogen Fuel System Set-up

Therefore, the hydrogen installation plane and the design methodologies with the Hydrogen standards have been adopted in each phase. In this chapter, we will explain our experimental scope, Including the Hydrogen operation conditions compared to the fundamental automotive applications that have existed in the last decade. We divide the hydrogen supplying system into three subzones and treat each zone according to Hydrogen standards. Finally, calculate the maximum fire jet length and the minimum ventilation system requirements according to the standards.

7.2.1 Hydrogen Operation Conditions

The Hydrogen properties vary according to the pressure and the temperature, as shown in Figure 7.3 below.
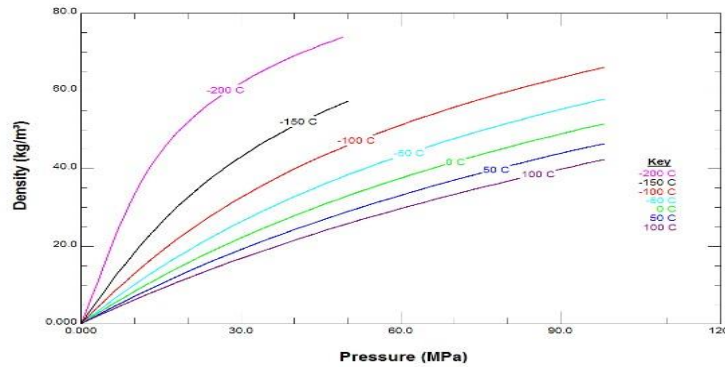
Figure 7. 3: Hydrogen Properties vs Pressure

 As shown in the photo, the density changes with temperature and pressure, but the maximum pressure we will reach will be 50 bar, which is much lower than many Hydrogen operations. Even a Hydrogen fuel cell vehicle that is not stationary equipment carries hydrogen fuel tanks at 70 MPa pressure. Also, one more example shows that our operation points are lower than any Hydrogen application, based on the ISO 19880-1 standard for Hydrogen Fuelling Station and Vehicle Interface Safety, which classified the pressure hazard into four classes, as shown in Table 7.2.

Table 7. 2: classified the pressure hazard into four classes

Pressure Class	NWP (Nominal Working Pressure)	MOP (Maximum Operating Pressure) Highest pressure permitted during normal fuelling	MAWP [C] (Maximum Allowable Working Pressure) Minimum pressure to which component is rated	ITP [A, B] (Integrity Test Pressure)Minimum pressure to which component is tested
	1.00xNWP	*1.25xNWP*	*1.38xNWP*	*1.50xNWP*
H25	25 MPa	31.25 MPa	34.4 MPa	37.5 MPa
H35 [D]	35 MPa	43.75 MPa	48.1 MPa	52.5 MPa
H50	50 MPa	62.5 MPa	68.8 MPa	75.0 MPa
H70 [D]	70 MPa	87.5 MPa	96.3 MPa	105.0 MPa

The maximum pressure in our system needs to be classified as more, not even classified as enough pressure for normal hydrogen vehicle fuelling. However, 95% of experimental operational conditions will be one MPa pressure. Another point must be identified in our hydrogen supply system: hydrogen consumption. Unlike the standard vehicle with a real engine, our test cell facilities have a one-cylinder experimental engine equipped with a separate heating system to reduce the operational time. The average operational Hydrogen consumption will be 3.2 litres/hour. That is why the pipe diameter of the Hydrogen supply is only 6 mm.

7.2.2 Hydrogen Installation Layout

In order to simplify the Hydrogen installation system, we have decided to divide the whole system into three main sub-systems, as shown in Figure 7.4.
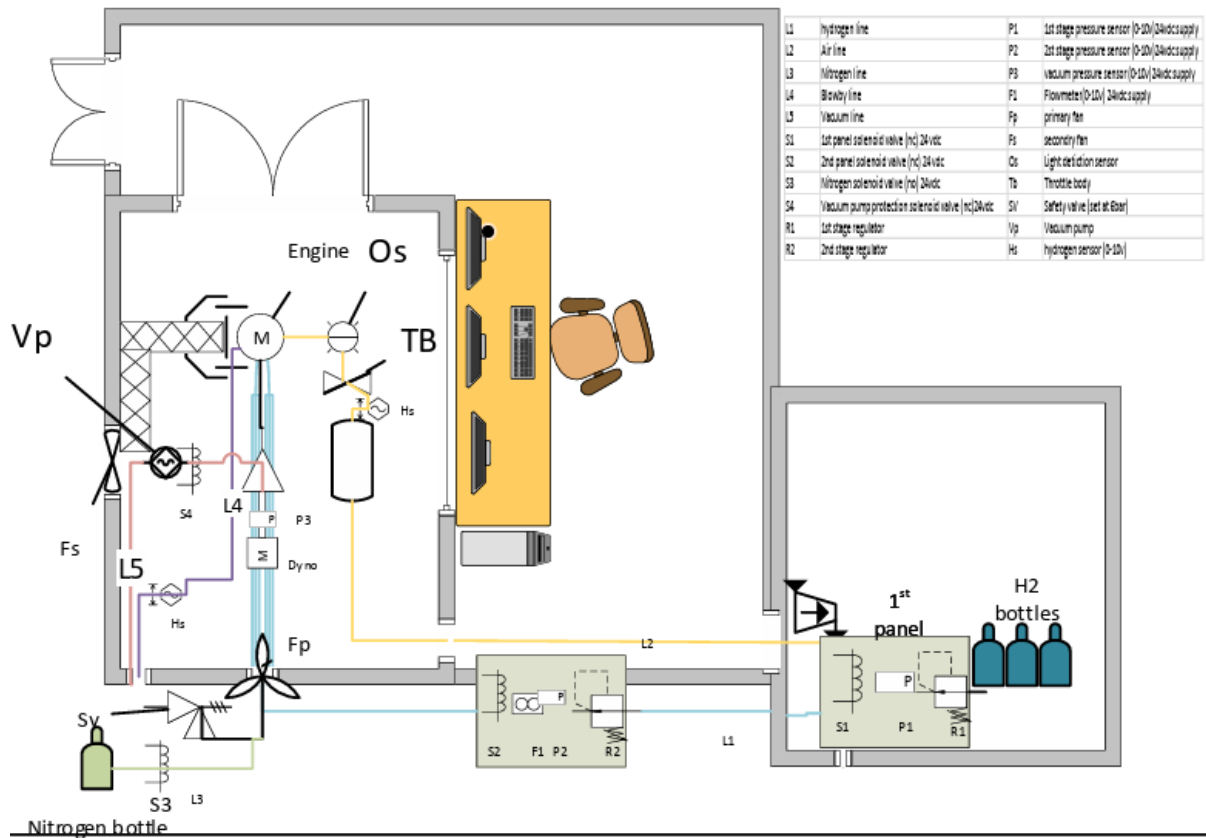
Figure 7. 4: The hydrogen installation system

Zone A is the inside building zone where the Hydrogen supply will go from outside into the engine injection system.

Zone B is defined as the outline line system from the Hydrogen source to the building, including all equipment in the outer line starting from the first fitting on the Hydrogen source to the last fitting on the Building side.

Zone C, which is the operational Hydrogen bottles area.

7.2.3 Hydrogen Supply Methodologies

To provide Hydrogen pressure of 5 MPa in Zone B, the outside 6mm supply line with a total length of 11 meters divided by normally closed safety valves operated mechanically by a Hydrogen differential sensor to isolate and separate the line in case of leakage detection. Start from zone c, where the Hydrogen operational bottles are connected to a unique Hydrogen regulator provided by Swagelok company and hydrogen tested and certified with non-venting set-up—then go to the second stage pressure regulator that reduces the pressure to 1 Mpaa before passing through the filter and the flowmeter. Finally, the hydrogen goes into the test cell via unique double pipes with a vacuum system to provide complete isolation to the hydrogen within the test cell and reduce the Hydrogen leakage possibilities to zero % as any Hydrogen leak will be in the vacuum space between the pipes. As shown in Figure 7.5, the process chart includes the Nitrogen purging system, which will be explained in detail later.
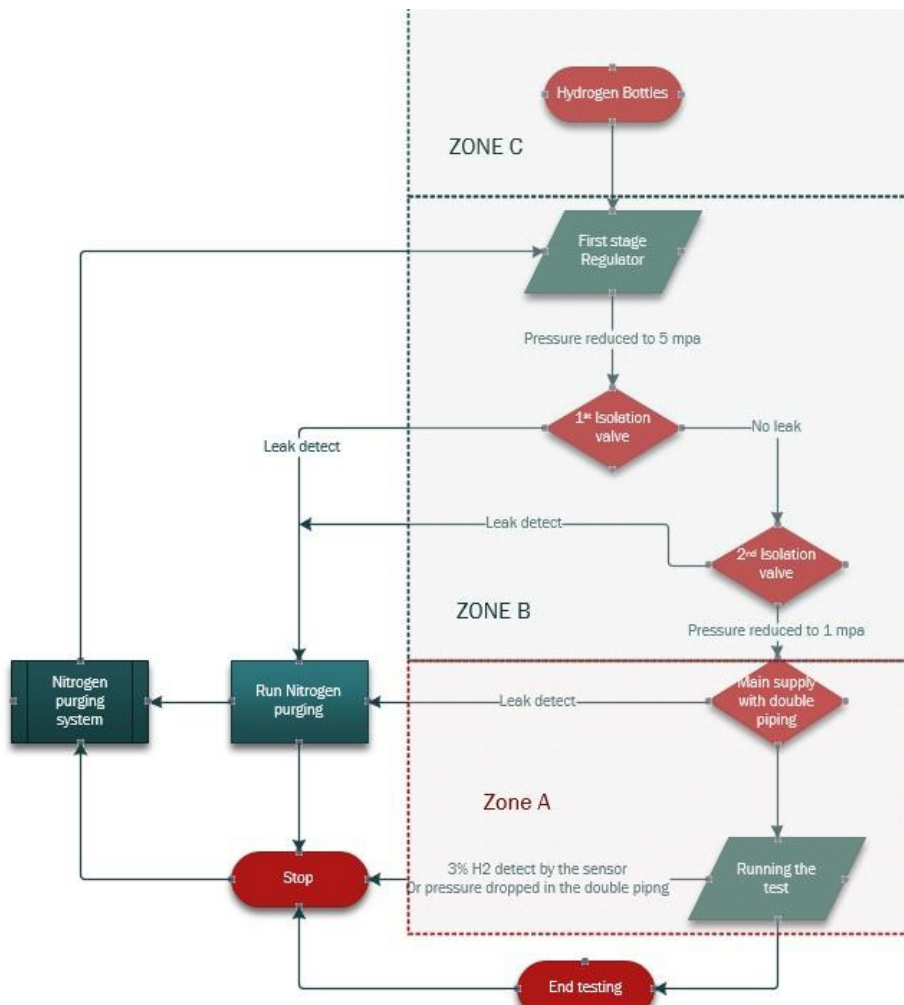
Figure 7. 5: The process chart includes the Nitrogen purging system

7.2.4 Test Cell Ventilation System

The test cell has its ventilation system by an extraction fan that provides more ventilation than recommended, as the test cell volume is 31.3 $m3$, t; ashen by area method, the CFM should be 430 while the fan provides 650 cfm. Also, the fan location is 2.3 meters to the top, which makes it able to reject the air at the top first, where any Hydrogen leak will go to the top first.

7.3 Standards Safety Measures for Hydrogen

This section will introduce the safety standards used in all Hydrogen design and installation processes. All standards have been used in each zone—furthermore, All design aspects and considerations are from theoretical and practical sides—finally, the installation test standards and inspection with maintenance for each system component.

7.3.1 Hydrogen Safety Standards

In the beginning, hydrogen has many applications and conditions, such as liquid hydrogen or fuel cells. The primary Hydrogen safety standard is ISO/TR 15916:2015, "Basic considerations for the safety of hydrogen systems.". For Hydrogen use in the laboratory, the principal UK standard is the Installation permitting guidance for hydrogen and fuel cell stationary applications: UK version. These two standards cover all Hydrogen sections

regarding understanding and design safety considerations. However, more specific standards have achieved a correct design approach according to the zone definition and the phase. Fore zone c, which is the Hydrogen supply bottles area, and both BRITISH COMPRESSED GASES ASSOCIATION standards involved CODE OF PRACTICE 4 GAS SUPPLY AND DISTRIBUTION SYSTEMS, and CODE OF PRACTICE 44 THE STORAGE OF GAS CYLINDERS. For zone B, piping installation and fitting standards have been involved.

Also, for the testing phase for Hydrogen supply pre-commissioning Hydrogen Piping and Pipelines ASME Code for Pressure Piping, B31 ASME B31.12-2011. Finally, for the Hydrogen detection standard, HSE Gas detection is used.

7.3.2 Hydrogen Leakage Characteristics

According to the information we have acquired so far, we can refer to the HSE standard to identify the characteristics of Hydrogen leakage. The maximum operating pressure in zone B, which is 6 mm outside the piping system, is 5 Mpa, and the total distance from the Bottles to the double pipes is 11.7m, split by two isolation valves. In case of leakage in the 6 mm outside piping, the isolation valves will cut the Hydrogen supply, and the amount of Hydrogen leakage to the outside environment will be half 11.7m multiplied by the 6mm cross-sectional area. The total amount of Hydrogen leakage is 0.16 litre, the Hydrogen density at 5 MPa is 4 kg/m3, and the total Hydrogen mass that could be leaked to the outside is 0.64 grams.

The second step is to understand the shape of the Hydrogen leakage. Furthermore, as mentioned earlier, hydrogen has a lower density, and it always goes to the top and mixes with air till the saturation becomes less than 8 %, then it becomes non-flammable. From the HSE standard, we can calculate the length of the Hydrogen jet leakage, as shown in Figure 7.6.
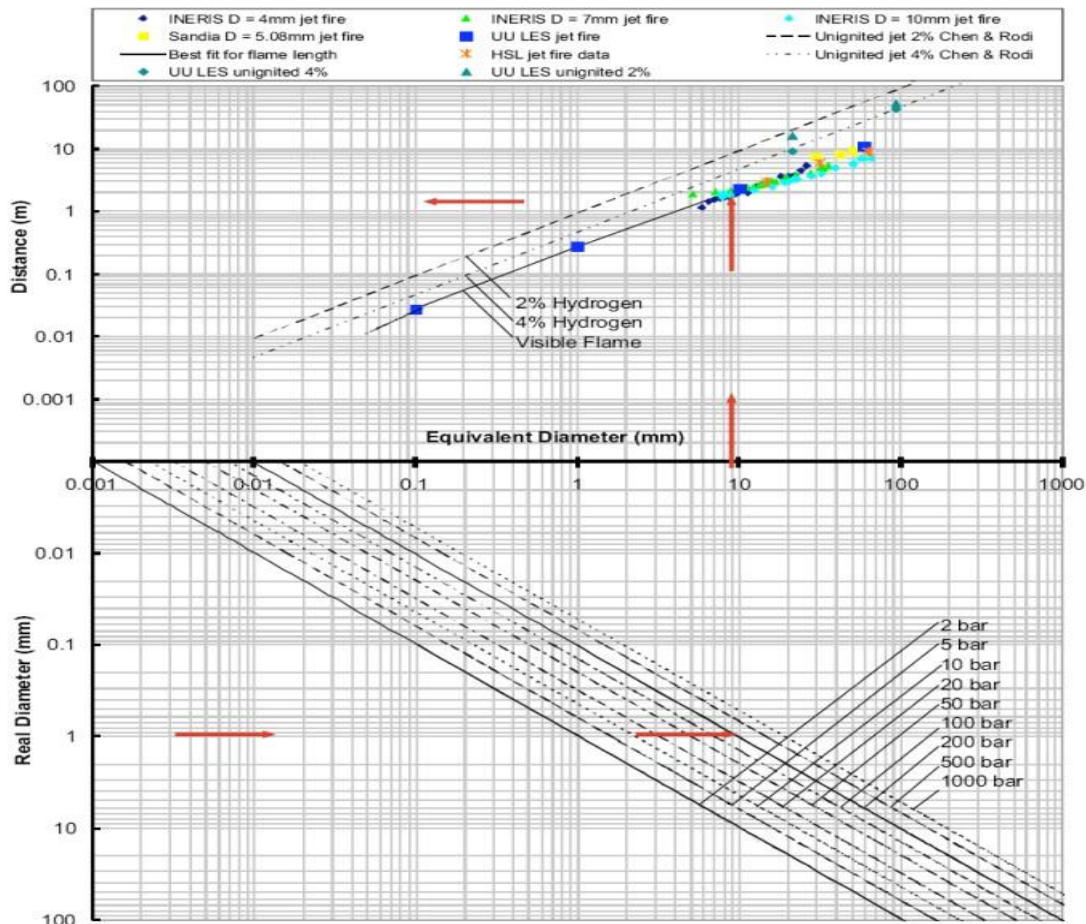
Figure 7. 6: Calculate the length of the Hydrogen jet

In our case, with an actual diameter equal to .6 mm, which is 10% of the pipe size at 50 bar, we will have 0.6 meters of Hydrogen jet leakage.

One final consideration that needs to be considered is the total leakage time, and by knowing the pressure difference between the air and Hydrogen line from the Ideal compressed gas formula, the total time required to leak all hydrogen, "0.16 litres", is 1.7 seconds.

7.3.3 Hydrogen Storage Health and Safety Installation (Zone C)

It starts from the Hydrogen bottles area, located outside of the building and surrounded by a wooden structure with a total area of $24m2$. The Number of Hydrogen bottles will be only three without having any storage area for spare bottles to reduce leakage opportunities, and they will be replaced by the provider company every five to seven weeks according to the test consumption.

However, following the UK BCGA CODE OF PRACTICE 44, THE STORAGE OF GAS CYLINDERS, which explains that firewall bricks must isolate the gas bottles from two sides as a minimum required and three as a recommendation. Shown in figure 7.7 is an example of how the operational bottles outside look.

Figure 7. 7: The operational bottles outside

The department has decided to demolish the wooden structure, replace it with firewall resistance bricks from three sides, and ensure all ignition sources are three meters away. Finally, the three bottles will be inside a metal cage and stand alone without mixing the Hydrogen bottles with different types, as shown in Figure 7.8.

Figure 7. 8: Mixing the Hydrogen bottles with different types

7.3.4 Hydrogen Supply System (Zone B)

The bottles will have the first stage regulator attached directly to the bottles, then 4.8 meters of 6 mm hydrogen pipe connected to a ground metal structure. Then attached to the building through the first isolation valve; however, from the jet leakage characteristics, we know the length of the jet and the final direction, which is the top, but in case of having a leakage from different angles in the pipe itself, it will take a certain distance then turn to the top. To provide complete protection in angular jet leakage and keep the Hydrogen jet path to the top and away from direct connection to the building, we have designed the U-shaped metal mounting with a 30 cm offset distance from the building, as shown in Figure 7.9.
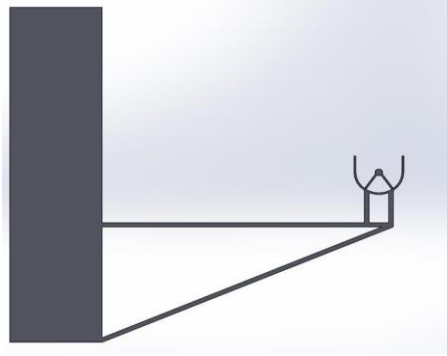
Figure 7. 9: U shape metal mounting with a 30 cm offset distance

The height of the supply pipe will be 1.7 meters from the ground to avoid any sparking source. Finally, another factor that needs to be considered is the exhaust pipe coming from the test cell to the outside with a maximum temperature equal to 120; however, the flash temperature of hydrogen equals 585, but for extra safety percussion, we decided to add thermal insulator layers around the exhaust pipe to reduce the temperature from 120 to 35 only, as shown in figure 7.10.

Figure 7. 10: Exhaust pipe

7.3.5 In-cell Hydrogen Supply System (Zone A)

Once hydrogen passes through the second isolator valve, it goes directly to the test cell inside a 50 mm larger pipe, failing the gap between them with negative pressure air to have the ability to since any leakage by direct pressure increasing which will lead to cut the Hydrogen supply and run the nitrogen purging system. The vacuum double piping system is not required in gas Hydrogen use; however, by using this approach, we can entirely prevent and isolate the hydrogen system from the test cell, as shown in Figure 7.11.
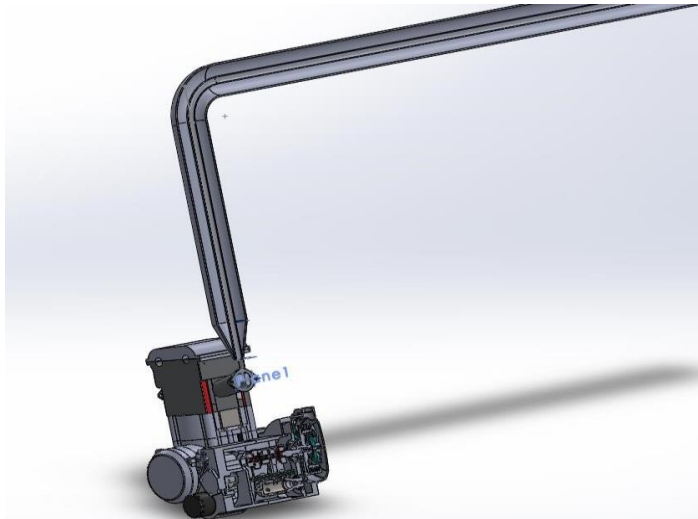
Figure 7. 11: 3D design for double piping

One last point has been considered in case of Injector failure inside the air intake port. To overcome this issue, a pneumatic gate valve is attached before the air intake and actuated by a hydrogen sensor or optical sensor to close and isolate the airline if the Hydrogen sensor reads or the optical sensor sees a backfire coming from the intake port side.

7.3.6 Hydrogen Installation Standard Test

Before running the system and installing all lines, the Hydrogen line test will be performed according to the ASME B30.1 and BCGA CP4 standards. Various tests involve applying pressure to the pressure system (or sub-assembly) that can be performed depending on the materials used, the construction method and the pressure system's design. Pressure testing aims to apply stored energy to an assembly to verify its strength, integrity, and functionality. For this document, the various types of pressure testing include:-

1-Standard pressure test. This test is used when all pressure components' safe working limits are known.

To be in line with the Design Code. 2-Proof pressure test. This test is carried out when the safe working limits of any of the components under pressure cannot be accurately calculated or is in doubt, for example, when an existing pressure system is modified.

3- Leak test. This test is performed after a successful standard or proof test has been carried out, As shown in Figure 7.12.
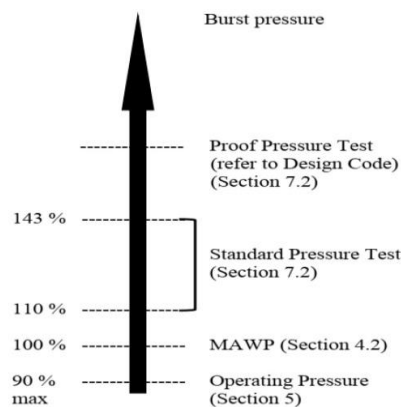
Figure 7. 12: Standard pressure tests

7.3.7 Hydrogen Equipment Specifications

All Hydrogen equipment is provided with a Hydrogen certificate, including the electronic pressure sensors, flow rate meter, regulators, and piping with fittings. Moreover, All pieces of equipment will be certified for higher pressure than our operation point for extra safety, as shown in the example Figure 7.13.

Figure 7. 13: Hydrogen equipment

7.3.8 Hydrogen Installation and Testing Consultancy

All Hydrogen lines and sub-assembly will be assembled and tested by an expert through a third-party consultancy company. All sub-assembly tests will be performed according to the standards on the Brunel site or the company side, and we will connect the sub-assembly to the pipe fitting and make the standard leak test before running the Hydrogen project. Figure 7.14 is an example of the sub-assembly system.
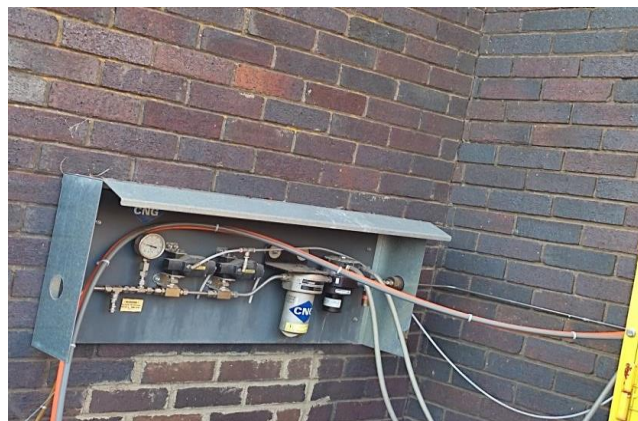
Figure 7. 14: Sub-assembly system

7.4 Hydrogen Prevention and Detection Systems

As we explained, our system with the highest safety standards and detecting Hydrogen leakage is the primary key to reacting and controlling the leak. Also, the reaction method to the Hydrogen leakage is crucial as the timing is critical to contain the fire before attaching other flammable objects. Finally, discuss some unique safety features that have been implemented.

7.4.1 Hydrogen Detection Systems

The hydrogen detection system starts from the working principles, which are supposed to be reliable and efficient. A pneumatically actuated customarily closed isolation valve is introduced to our system, and a differential pressure sensor actuates them in the outside supply line. As the pipe length is more than 11.5 meters and it is exposed to the air, makes

the Hydrogen sensing process relatively harder for the Hydrogen sensor, unlike the differential sensor, which will immediately detect the pressure drop due to the Hydrogen leakage and mechanical close the insolation valve in less than 0.3s.

A Hydrogen sensor has been installed and connected to the main Brunel firefighting network inside the test cell.

Furthermore, the Hydrogen pipe that goes from the second isolation valve to inside the test cell will be isolated inside a larger pipe with a vacuum pressure system to increase the system's sensitivity and ensure it is fully sealed from the test cell environment.

7.4.2 Hydrogen Purging System and Automated Shutdown System Strategies.

Nitrogen gas is inflammable and can also operate as an isolator gas in case of hydrogen leakage detection. Therefore, a purging system is designed to detect the leakage and react to the minimum pressure drop in less than 0.01 seconds. The general idea of using a vacuum system is to improve the system leakage sensitivity and create a fully robust mechanical detection system that can detect any pressure drop without laying on any other aspects, such as sensor signal, electric wiring, and any detection actuator. Also, the purging system is not only operating with an emergency shutdown system, but the purging process is part of the standard shutdown procedures. Finally, the purging process has been upgraded to include purging the line from outside (Zone B) till the high engine end (Zone C), leaving no Hydrogen in the line.

An automated shutdown system is designed to react to any leakage detection in all zones, immediately isolate the line, and turn on the purging process. However, understanding how critical this process is led to designing the system in a method that allows this process to happen in case of system failure by selecting isolation valves in the "normally closed position" and the nitrogen valve in the "normally open position" that means if any fault happens the purging system is designed to run immediately. Figure 7.15 shows the logic of the automated PLC shutdown system.
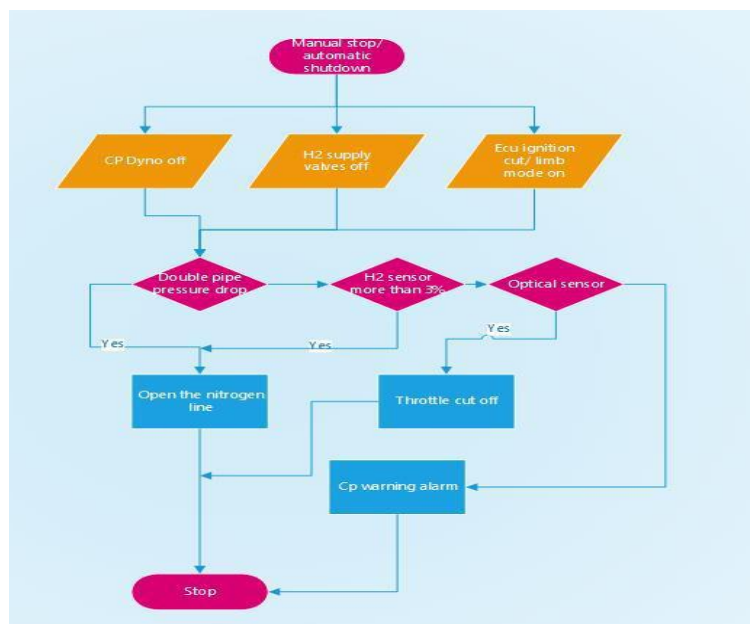
Figure 7. 15: The automated shutdown logic diagram.

7.4.3 Remarkable Safety Points

Considering the low, let us summarise the main safety features of our Hydrogen supplying system.

Hydrogen amount and low pressure needed to six main points:-

1- Zero Hydrogen storage. Connecting only three bottles without any spare bottles reduces the risk of leakage.
2- Minimum fittings. Selecting inline equipment with the same size achieves fewer fittings and reduces leakage possibilities.
3- Vacuum system. Total system isolation with a vacuum pressure to get extreme sensitivity is the same technique adopted by NASA for cryogenic liquid Hydrogen.
4- No Hydrogen in the line. Including outside lines by purging the line after testing leaves no chance to have any risks; also, reduce the total hours per week from having Hydrogen in the outline from 168 to 17 hours.
5- The emergency system runs at any failure. Include the emergency system by designing the system to run in case of signal failure.
6- Complete Hydrogen Isolation in the building. Using double piping and Negative pressure monitoring to ensure they are sealed means if we get fire inside the building and have Hydrogen leakage simultaneously, there is no interaction between both.

7.4.4. Hydrogen Fuel Supply System Summary

in conclusion, we have a standard approach for using Hydrogen, and we have our approach, which is more strict to provide a fully isolated system. Also, providing a safe environment is the project's main priority, and the main concern was ensuring the work environment was safe. Moreover, I would like to compare standards recommendations and our approach for more enhanced safety measures in this summary.

Standards Recommendations

According to all international standards and UK standards, they advise us to have an excellent ventilation system inside the building as hydrogen leakage is inevitable. Also, for hydrogen bottles, they advise us to follow the standards, keep all storage bottles in a safe area, and provide a good ventilation system with a three to eight meters safe distance. Regarding hydrogen detection, the standards recommend using multiple sensors in the building or protecting the hydrogen leakage. For hydrogen piping, the main recommendation is to keep the line at a certain distance away from flammable sources and use specific certificate materials.

our approach

Starting from Having zero Hydrogen storage, isolate the hydrogen operation bottles with fire-resistant brick walls from three sides. Then, isolating the hydrogen 6 mm line with a U-shaped metal structure for no fire jets in different angles creates an offset to the building for no attachments between the jet leakage and the building surface. Consider the outside media by changing the line height to avoid any interactions with ground risks, isolating the exhaust line for extra safety, and adjusting the shutdown system to purge the whole line and keep the outside line empty. Inside the building adopting the double piping system because minimising the risk of having Hydrogen was not enough, and we prefer the complete isolation technique. Also, double the system sensitivity using the vacuum system

that reacts to any pressure loss to ensure the double piping is isolated to the test cell environment. Designing the automatic shutdown system to run in case of emergency or system failure creates no chance of hydrogen gas leakage without running the nitrogen purging system or even Hydrogen leakage. The system can run in case of double pips leakage or system failure. Finally, add extra sensors with High-speed vulvae to trace and isolate the system in case we have Hydrogen leakage inside the engine and connected to the automatic shutdown system.

7.5 H$_2$ Engine Testing Facility Setup

The experimental facility has relied on liquid fuels for the past few years. However, transitioning to hydrogen as the primary fuel source requires significant modifications. This will enable various operational techniques, such as hydrogen PFI and DI technologies. One main challenge during this transition was determining the new risk assessment for the hydrogen supply line. It was crucial to ascertain the hydrogen source's location, given its capacity to store liquid fuel within the same test cell.

Unlike automobile and transportation applications, the operation of the test cell using hydrogen necessitates an isolated and permanent site for safely storing the hydrogen bottles. This ensures that there are no potential hazards within the test cell. The chosen solution involved securely isolating and adequately ventilating the bottles outside the test cell. They were in a semi-enclosed space without a ceiling and surrounded by fire shields.

To further reduce the potential risk of leakage within the test cell, it is advantageous to have all supply line accessories, such as pressure regulators, sensors, flow meters, and shutdown valves, located outside the test cell. This arrangement restricts the number of connections and significantly minimizes any potential risks.

7.5.1 H$_2$ Engine Setup

Figure 7.16 shows the SI single-cylinder engine diagram from MAHLE Powertrain. It was used to test hydrogen performance and emissions in two injection configurations: central direct injection and port fuel injection. The engine features a MAHLE adaptable electronic control unit (ECU), allowing seamless transitions between PFI and DI engine operation. For direct and side-port fuel injection, the engine uses DI-CHG10 injectors from Phinia, which enable hydrogen injection ranging from 200 to 1000 kPa in the PFI system and 1000 to 4000 kPa in the DI system. To address potential hydrogen-related risks, the engine incorporates a forced crankcase ventilation system that feeds into an extraction hood and is monitored by a hydrogen sensor. If the hydrogen concentration exceeds 3%, the PLC system initiates a warning, and at 4%, the hydrogen supply is cut off.

The engine also features fully variable valve timings for both intake and exhaust cams, allowing flexibility in determining the optimal valve timing and overlap configuration for each injection system. Additionally, the ECU enables adjustments to fuel injection timing and pressure, giving the ability to control the start or end of the injection process as needed. Finally, the engine includes an external boosting system with a maximum boost pressure of 400 kPa and an external air heater to regulate intake temperature accurately.
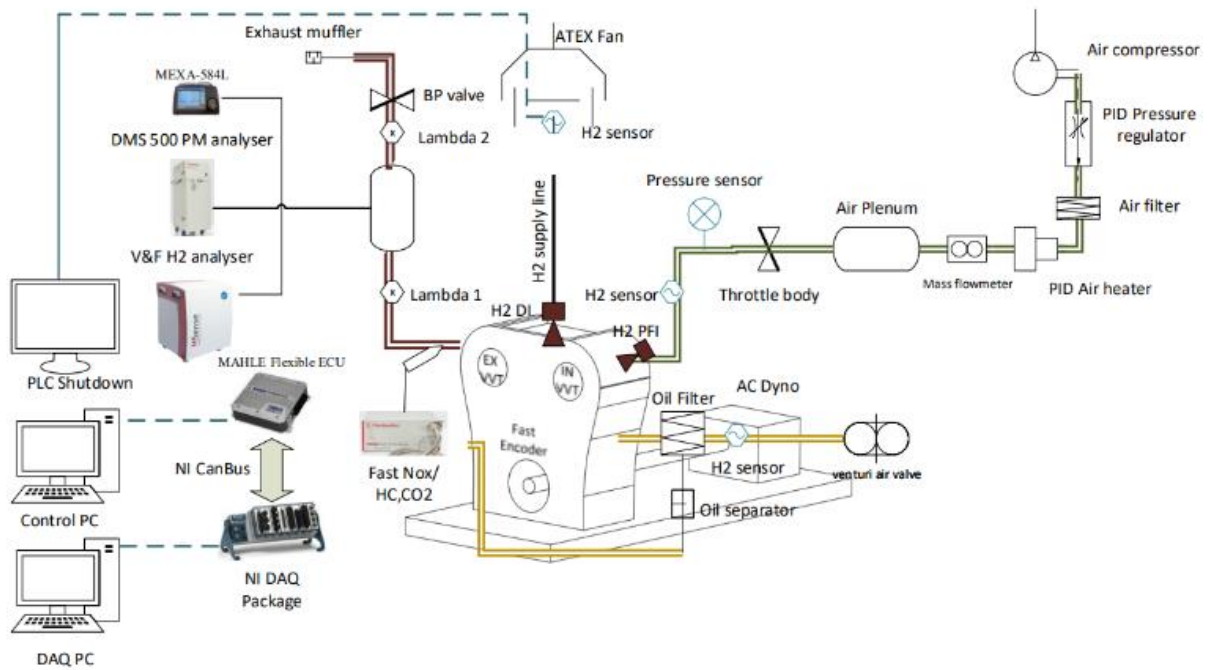
Figure 7. 16: Schematic of H2IC test cell setup

7.5.2. Hydrogen Fuel Supply

Supplying hydrogen begins with the hydrogen bottles in a confined area connected to a first-stage control panel. A pressure sensor monitors the hydrogen gas pressure as it is reduced. Before reaching the hydrogen flowmeter, the hydrogen line is connected to a solenoid valve. Placing the hydrogen flowmeter downstream of the initial stage helps avoid any potential pressure drops affecting the final pressure delivered to the injector. In the second stage control panel, a pressure regulator further reduces the hydrogen pressure to the PFI or DI injection pressure. This panel is outfitted with a pressure sensor and a safety solenoid valve, which work together to isolate the line and minimize the amount of H_2 in the pipeline in the event of hydrogen leakage.

To prevent any hydrogen leaks in the hydrogen pipe from entering the room, two double vacuum tubing systems were designed and installed for the PFI and DI hydrogen supply lines between the fuel injector and the external hydrogen pipes. This ensures that any leaked hydrogen is isolated within the double vacuum tube. A pressure sensor is also installed to detect hydrogen leakage in the space between the inner and outer hydrogen pipe. If hydrogen leakage is detected, a nitrogen-based purging system is activated to remove the leaked hydrogen. See a visual representation of this setup in Figure 7.17.
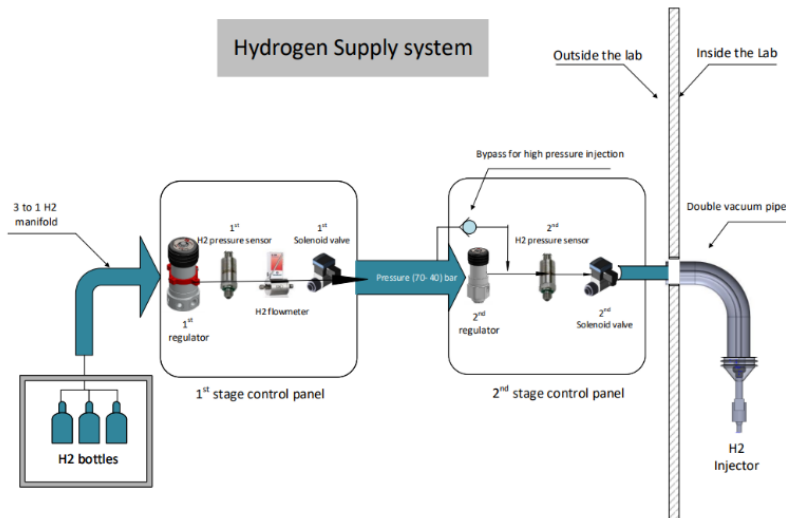
Figure 7. 17: H2 Supply line.

7.5.3. Emission Analysers

Throughout the emission testing process, various instruments were utilized to measure a range of pollutants present in the exhaust emissions. Specifically, CO/CO_2 and oxygen (O_2) concentrations were measured using a HORIBA (MEXA-584L). In order to accurately quantify any particulate matter emissions in terms of particle size and number, a Cambustion DMS 500 fast particle analyser was employed. To additionally measure steady-state emissions, Rotork Analysis Model 523 flame ionization detection (FID) HC analysers were utilised.

To measure the instantaneous NO and NO_2 emissions, a fast NO_x emissions analyser was connected to the back of the exhaust valves using a 1.2-meter emissions pipe. Finally, to measure the hydrogen concentration in the exhaust or H_2 slip, a V&F hydrogen analyser was utilised[154], [155].

In summary, a comprehensive set of advanced instruments was employed to provide accurate and reliable measurements of various pollutants in exhaust emissions.

7.5.4. DAQ System

There are 138 input channels receiving signals from the sensors and measurement equipment in the engine test room. However, the sampling rate for each sensor depends on the sensor's priority and the reading's value. For instance, the in-cylinder, intake, and exhaust gas pressures are sampled in the crank domain, whilst the other sensor outputs are recorded in the regular time domain. Thus, a hybrid selection of NI cards encompasses fast and standard USB NI cards. These cards can automatically synchronise within the NI-based combustion analyser, Valieteck. Furthermore, it uses an NI to CANBus communication card to transfer signals from the ECU, as shown in Figure 7.18. The phenomenon of in-cylinder pegging is achieved by comparing the in-cylinder pressure value with the intake pressure from the fast response sensor at a crank domain degree of 100 before top dead centre firing (BTDCf). The TDC location is identified using an encoder signal and calibrated during the motoring process and self-system check [156].

The indicated thermal efficiency is calculated from the Fuel's Lower heating value multiplied by the hydrogen flow rate. That is divided by the Indicated power, calculated from the in-cylinder pressure sensors and IMEP, as shown in equation 7.1.

$$ITE(\%) = \frac{Indecated\ Power\ (Kw).\,3600}{Fuelflow\left(\frac{Kg}{hr}\right).\,\text{CalorificValu}(\frac{KJ}{Kg})}$$

(7.1)

The assessment of combustion cyclic variability is determined by the coefficient of variation of indicated mean effective pressure (COVIMEP) over 300 cycles, as per Equation 7.2.

$$COV_{IMEP}(\%) = \frac{\sqrt{\dfrac{\sum_{i=1}^{n}(IMEP_1 - IMEP_{mean})^2}{n-1}}}{IMEP_{mean}}$$

(7.2)

The lower net value (LNV) is introduced to identify partial combustion or misfiring instances, and it is calculated based on the ratio of the minimum IMEP to the averaged IMEP over 300 cycles, as shown in Equation 7.3.

$$LNV_{min}(\%) = \frac{IMEP_{min}}{IMEP_{av}} * 100$$

(7.3)
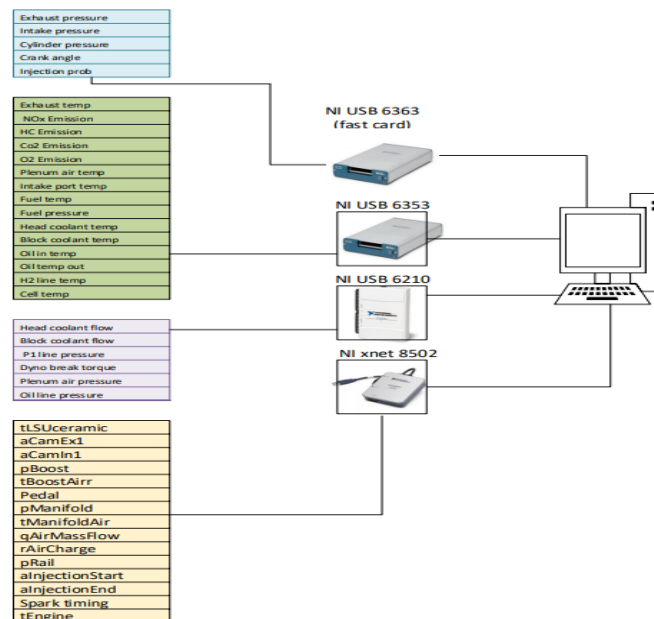
Figure 7. 18: Schematic of DAQ system

Chapter 8. The Potential of Hydrogen in an Externally Boosted Spark Ignition Engine- Performance and Emissions

8.1 Introduction

In this chapter, the single-cylinder boosted spark ignition engine was run over a wide range of lambda values to determine the optimal operating point for hydrogen and demonstrate its benefits over gasoline combustion. A load sweep test was performed at 2000 rpm, and the performance and emission results were compared between gasoline and optimized hydrogen combustion.

An in-depth analysis was conducted by varying fuel injection time and pressure, allowing for exploration of their effects on fuel performance and emissions. This provided valuable insights for further optimization.

8.2 Test Methodology

The experimental procedure involved testing a boosted spark ignition engine under different fuel conditions. Specifically, the central direct injection (DI) fuel supply system was swapped from gasoline to hydrogen while maintaining the same cam timings and intake temperature at a constant value of 38 degrees Celsius. The oil and water coolant temperatures were kept constant at 90 degrees Celsius using external heaters.

To determine the optimum air-fuel ratio (AFR) for each fuel, the first experiment was conducted at a fixed load and engine speed, varying the AFR from stoichiometric to lean limits. Once the optimum AFR for each fuel was established, the second test was carried out to study engine performance and emissions under different loads. The effects of fuel injection pressure and timing on engine performance and emissions were also investigated.

In all tests, the highest average in-cylinder pressure and maximum pressure increase rate (Rmax) were limited to specific thresholds for safety. The stability of engine operation was ensured by maintaining a coefficient of variation of the indicated mean effective pressure (COVimep) value at 3%. Combustion phasing was adjusted to occur at a specific point after the top dead centre (ATDC) gross by setting the spark timing to the Maximum brake torque (MBT).

Lambda values, which indicate the ratio of air to fuel in the engine, were determined using two wide-band sensors in the exhaust line. These sensors were calibrated using O_2 measurements obtained from the Horiba emission analyser, and the accuracy of the lambda values obtained from the sensors was verified by checking them against those calculated from the exhaust gas analysers. Table 8.1 shows the experimental step of each experiment test for the gasoline and the hydrogen DI.

Table 8. 1: Engine test conditions for gasoline vs. hydrogen

Engine parameters	Unit	λ sweep test	Engine load sweep test	Fuel matrix

Engine Speed	rpm	2000	2000	2000
Engine Load	kPa	1000	Sweep from 200 Kpa to engine limit with 200 kps step	1000
λ	-	Sweep from 1 to engine limit	2.75 for H2 1 for gasoline	
Intake Cam positions	ATDCg	97	97	97
Exhaust Cam positions	BTDCg	102	102	102
Start of injection DI	BTDCf	150 for hydrogen 300 for gasoline		SWEEP
Injection pressure DI	kPa	3000 for hydrogen 10000 for gasoline		SWEEP
Intake air Temp	^{0}C	40	40	40

8.3 Results and Discussion

8.3.1 Lean Burn Comparison Between Gasoline and Hydrogen Combustion

This study aimed to demonstrate the lean-burn capabilities of hydrogen and gasoline spark ignition combustion engines. The engine was operated at a medium load of 1000 Kpa IMEP, and the air-fuel mixture was precisely regulated to increase the lambda value. Eventually, the engine was pushed to its lean-burn limits for gasoline and hydrogen fuels.

Figure 8.1 presents the study's findings, showing the engine's operational limits as a function of lambda values. These limits were established using three critical criteria: Rmax, LNV, and partial burn's lowest net value percentage.

Hydrogen combustion exhibited a rapid increase in Rmax to the 600 kPa limit when approaching the stoichiometric air-fuel mixture at lambda 1, owing to its faster burning rate. To prevent this, measures were taken to retard the spark timing, as shown in Figure 8.2.

On the other hand, gasoline combustion's Coefficient of Variation in IMEP drastically increased when operated beyond lambda 1.5, resulting in great cyclic variability that exceeded the acceptable 3% limit of COVimep. The sharp reduction in the LNV percentage suggested an increased occurrence of misfire cycles at these lean operational conditions. Therefore, gasoline engines should not operate beyond lambda 1.5.

In contrast, a much leaner air/fuel mixture could achieve hydrogen engine operation. Even at a lambda value of 3.75, the hydrogen combustion process remained highly stable, with

a slight drop in LNV after lambda 3. This indicates that hydrogen combustion can achieve leaner air-fuel mixtures and remain highly stable compared to gasoline combustion.
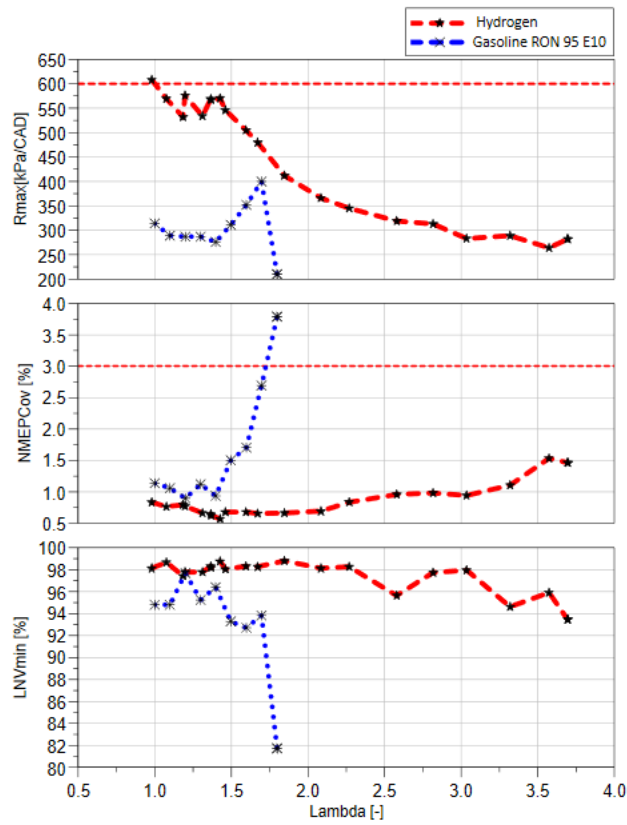
Figure 8. 1: Engine operational limit for gasoline and hydrogen for different lambda value
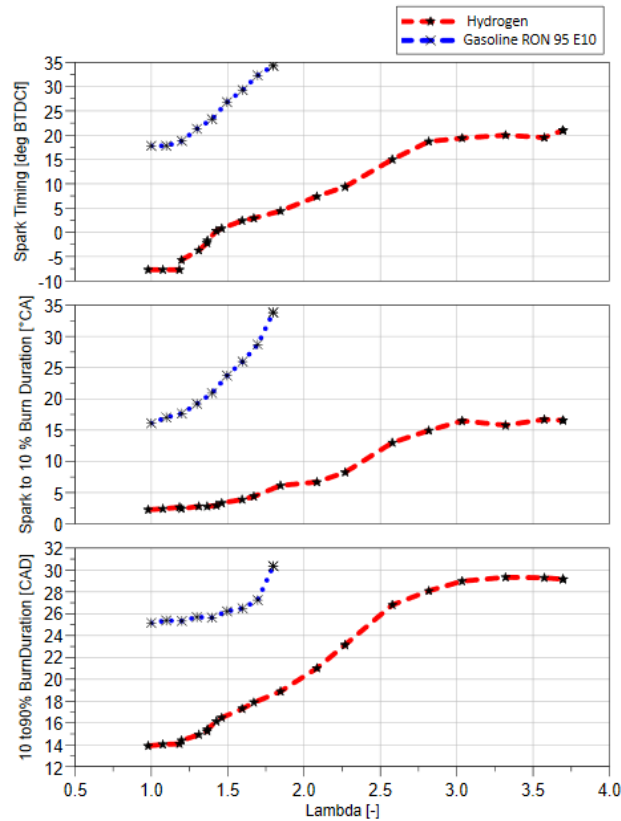
Figure 8. 2: The comparison of Spark timing and burn duration for gasoline and hydrogen under varying lambda conditions.

Figure 8.2 depicts the spark timing and initial and main combustion durations for gasoline, with spark timings remaining at MBTs. For hydrogen engine operation, the spark timings were set at MBT spark timing for leaner mixtures below lambda 1.5. However, as the mixture became richer than lambda 1.5, the spark timing had to be adjusted to prevent Rmax from approaching the engine's 600 kPa limit, ensuring safe operating conditions. Notably, when the lambda value for hydrogen was 1, the spark started after the compression Top Dead Center (TDC) to stay within the engine's functioning limits, although at the expense of engine performance.

The centre graph shows the time from spark timing to 10% burn, demonstrating that hydrogen combustion started much faster than gasoline combustion. Under lean conditions, there was a significant delay in initiating combustion with gasoline. The 10% hydrogen burn duration at a lambda value of 2.75 matched the speed achieved by gasoline under the stoichiometric condition, showing the superior capability of the hydrogen engine to operate with extremely lean conditions for maximum efficiency and little NOₓ emission.

The bottom graph of Figure 8.2 shows the main burn duration from 10-90%, with similar trends observed between hydrogen and gasoline combustion. At lambda 1.5, the total combustion duration (0-90%) of hydrogen and gasoline was about 20 CAs and 50 CAs, respectively.

Figure 8.3 compares gasoline and hydrogen engine performance regarding indicated thermal efficiency and hydrogen slip for different lambda values. The data shows that the highest hydrogen slip in the exhaust occurred near stoichiometric operation due to

delayed combustion and lower combustion temperature. However, the hydrogen slip remained low between lambda values of 1.2 to 2.5 before starting to rise again due to slower combustion of leaner mixtures.

It is worth noting that the gasoline engine had higher indicated thermal efficiencies than the hydrogen engine when the lambda value was less than 1.8. This is because the MBT spark timing for all operations optimized gasoline combustion. In contrast, hydrogen combustion was significantly retarded for near stoichiometric operations to prevent the excessive rate of pressure rise caused by the rapid heat release rate of hydrogen. Additionally, increased PMEP values, as shown in Figure 8.3, contributed to this difference.

On the other hand, the hydrogen engine produced higher efficiency when the lambda value was more than 2.3. The highest efficiency of 41% was achieved at a lambda value of 3.25. This was due to slower combustion of leaner mixtures, resulting in a lower heat release rate and pressure rise.
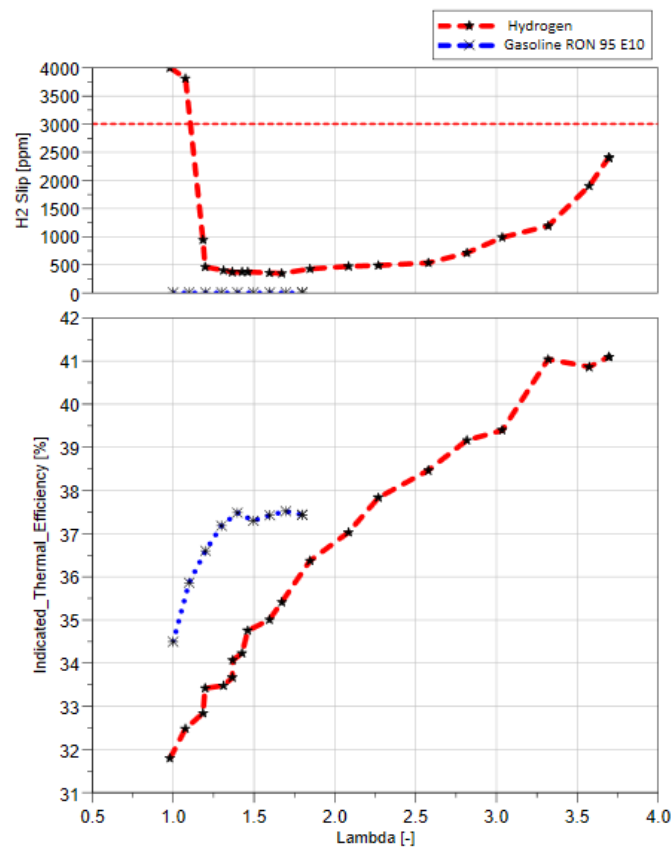
Figure 8. 3: Indicated thermal efficiency and hydrogen slip comparison

In the comparison shown in Figure 8.4, the PMEP and intake manifold pressure of gasoline and hydrogen fuels were compared at various lambda values. It was observed that both fuels had similar intake pressure within the lambda range of 1 to 1.5, which was slightly lower than atmospheric pressure and resulted in negative PMEP values. However, due to the charge cooling effect, the gasoline fuel exhibited slightly lower PMEP values than hydrogen.

When the lambda values exceeded 1.5, the boosting rig increased the intake pressure above atmospheric pressure, resulting in positive PMEP values. It is important to note that

the boosting rig played a significant role in producing positive PMEP values, and the intake pressure of both fuels was significantly increased beyond atmospheric pressure. This led to improved engine efficiency and performance, as evidenced by the significant increase in PMEP values for both fuels.
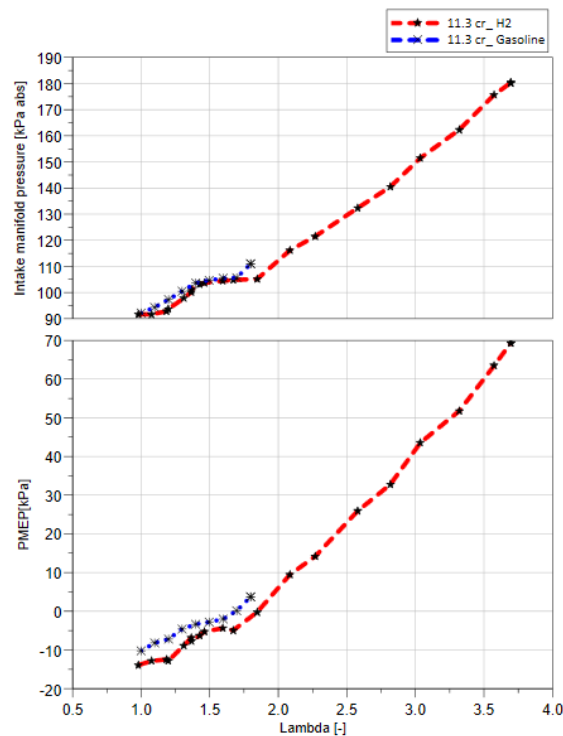
Figure 8. 4: PMEP and intake manifold pressure comparison.

Figure 8.5 shows gasoline and hydrogen combustion's NO_x and exhaust gas temperature results. The lower NO_x hydrogen emission at lambda 1 can be explained by hydrogen being operated with significantly delayed spark timing. The peak combustion temperature was effectively reduced due to this change, resulting in lower NO_x emissions but higher exhaust gas temperatures. These elevated exhaust gas temperatures can have advantages, especially in the context of an existing turbocharged engine. The increased exhaust gas temperature can improve turbine performance in the turbocharger, potentially increasing its efficiency and overall engine performance. The maximum NO_x emission of hydrogen combustion was measured at a lambda value of 1.5, whereas the maximum NO_x formation of gasoline combustion occurred at lambda 1.2. As the lambda was increased to 2.5, the NO_x emission of hydrogen combustion reduced below 50 ppm. Near zero NO_x emission, i.e., less than ten ppm was observed beyond lambda 3.

The data presented in Figure 8.6 details the emissions of HC, CO, and CO_2 resulting from gasoline and hydrogen combustion processes with varying lambda values. The study reveals that in gasoline combustion, emissions decreased as the mixture became leaner, except near the lean-burn limit of lambda 1.5, where HC emissions increased due to partial burning. In contrast, hydrogen combustion produced zero emissions across all lambda values studied.

These findings suggest that lean-burn combustion is highly beneficial for hydrogen engines, leading to higher efficiency and near-zero NO emissions. To identify the optimal combination of minimal NO_x emissions, highest thermal efficiency, and lowest H_2 slip, a

hydrogen engine was tested with a lambda between 2.75 and 3. A lambda of 2.75 was chosen for subsequent studies due to the negligible improvement in thermal efficiency and NO$_x$ emissions beyond lambda 3, which increases the possibility of incomplete combustion. Additionally, operating beyond lambda 3 requires increased boosting pressure and higher ignition energy.

In conclusion, the study highlights the advantages of hydrogen combustion over gasoline combustion in terms of emissions. It emphasises the importance of lean-burn combustion for optimal performance in hydrogen engines.
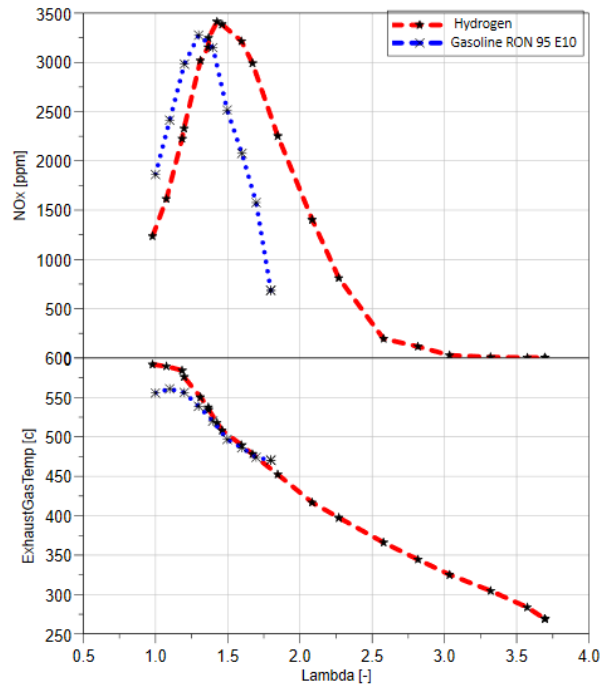
Figure 8. 5: Fast NO$_x$ emission and exhaust gas temperature
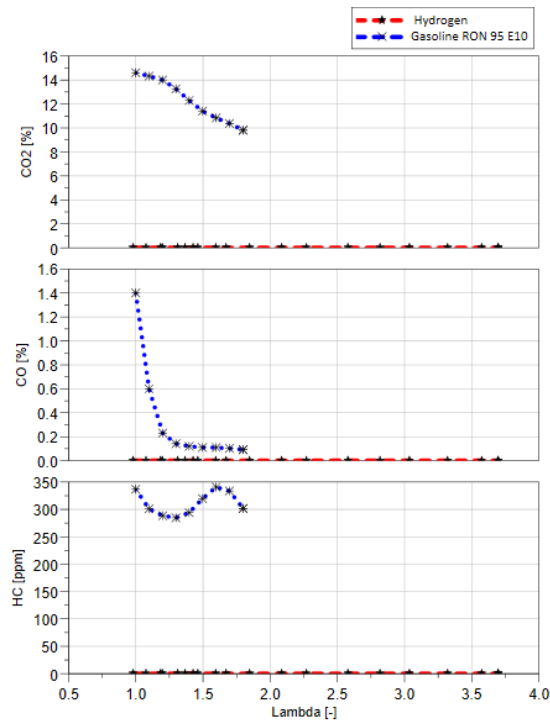
Figure 8. 6: HC, CO and CO$_2$ emission comparison between gasoline and hydrogen for different lambda values.

8.3.2 Assessment of Gasoline and Hydrogen Performance and Emission at Different Loading Conditions

This section delves into a detailed analysis of gasoline and hydrogen engines' performance and emission characteristics. Our experiments were conducted under various load conditions while ensuring a consistent engine speed of 2000 rpm. We conducted gasoline combustion at a stoichiometric air-fuel ratio while the hydrogen engine operated at a lambda value of 2.75.

Our findings showed that the hydrogen engine outperformed the gasoline engine in terms of efficiency across the entire load range, thanks to its lean-burn combustion. Figure 8.7 illustrates that the hydrogen engine consistently achieved higher efficiencies at all loads. The maximum load of the hydrogen engine was limited by the maximum in-cylinder pressure, as seen in the figure. Since the H$_2$ injector could not operate under 10 bar injection pressure, the hydrogen engine was limited to 4 bar IMEP. The maximum ITE achieved by the hydrogen engine was about 41% at 800 kPa load. However, we observed a slight reduction in efficiency as the load increased further due to increased pumping work.

On the other hand, gasoline engine operation showed a significant decline in ITE after reaching 12 bar IMEP. This decline was primarily due to the need for spark retardation to control engine Rmax limit at these elevated loading conditions, as shown in Figure 8.7 (c). This led to a significantly retarded 50% mass fraction burned (50% MFB). The retarded gasoline combustion beyond 12 bar IMEP also resulted in unstable combustion, as shown by the increased cyclic variation and the occurrence of misfire depicted by the lower LNV value.
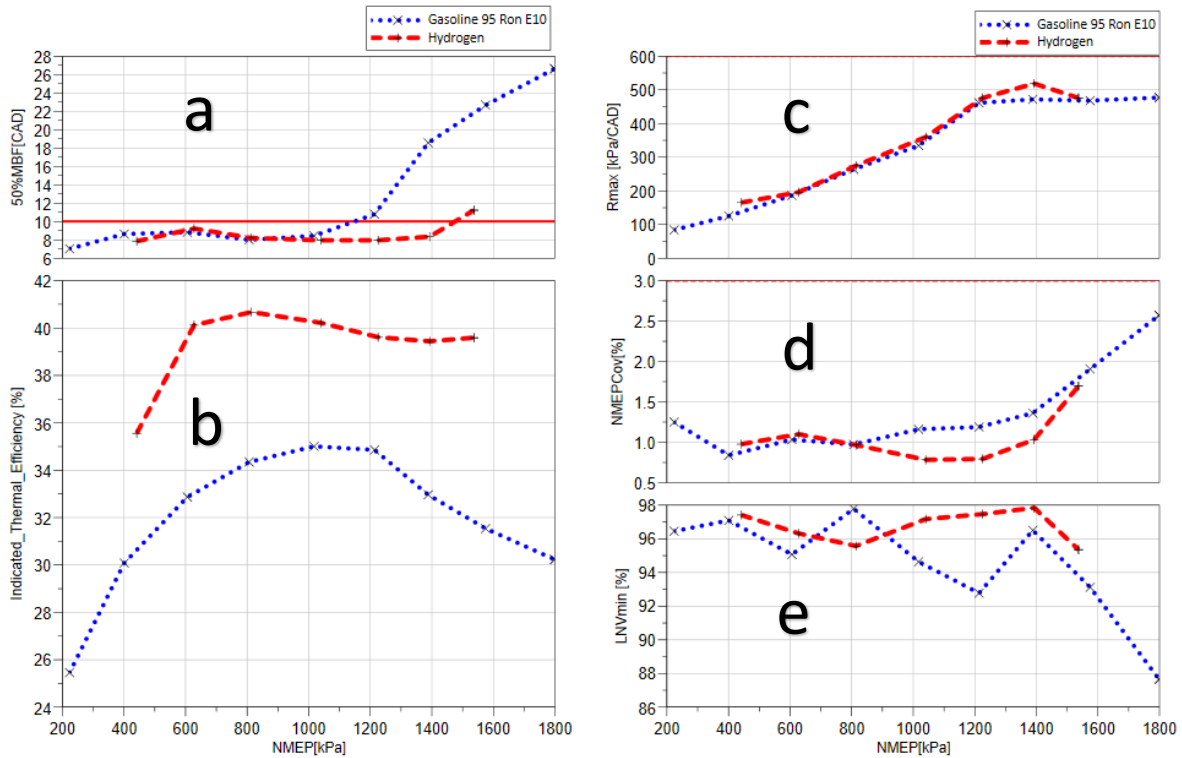
Figure 8. 7:Engine performance and combustion characteristics compare gasoline and hydrogen at varying loading conditions. Gasoline was operated at lambda one and hydrogen at lambda 2.75. (a) 50% mass fraction burned (b) Indicated thermal efficiency (c,d,e) Engine limits and combustion stability

Figure 8.8 shows the observed maximum in-cylinder pressure, the intake manifold pressure and the PMEP values as a load function. As the load increased, the intake pressure and Pmax increased as more fuel was burnt. Hydrogen engine operation experienced higher Pmax probably due to faster combustion characteristics of hydrogen and higher boost. Also, hydrogen has higher PMEP compared to gasoline for all loading conditions. It is worth mentioning that these results were obtained when the gasoline engine was under stoichiometric conditions (lambda 1) whilst the hydrogen was operating at lambda 2.75. The current engine design limit of 120bar Pmax thus limited the maximum load of hydrogen engine operation. However, higher output can be obtained from a DI hydrogen engine with a higher Pmax and higher boost pressure.
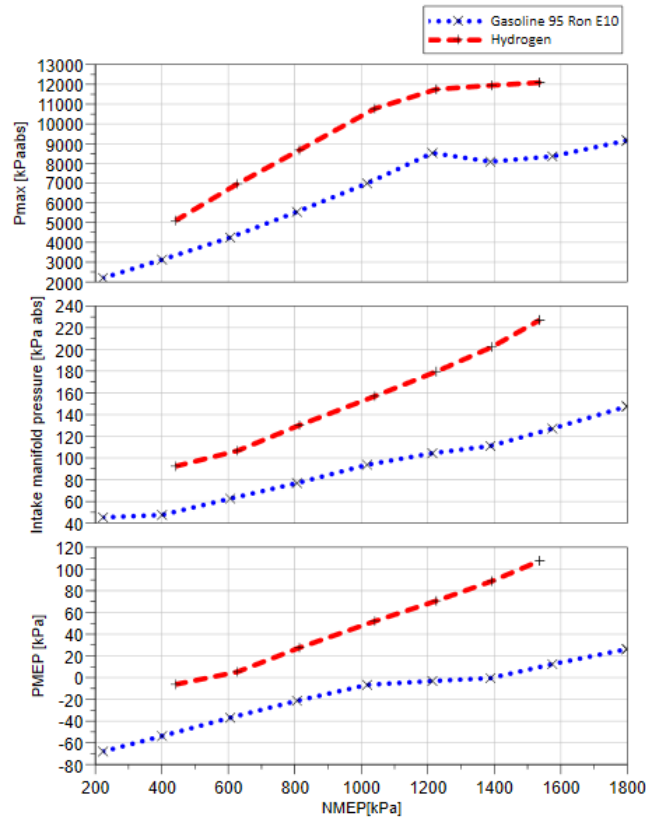
Figure 8. 8: Maximum in-cylinder pressure, manifold pressure and PMEP comparison with varying loading conditions for gasoline and hydrogen fuel

Figure 8.9 depicts a comprehensive overview of engine-out emissions and hydrogen slip in the context of gasoline and hydrogen combustion under various loading situations. During low to medium-load operation, hydrogen engine operation produced negligible NO_x emission. Even at high loads, the increase in NO_x for hydrogen remained below 100 ppm. The gasoline engine's NO_x emission was increased from 1200ppm to 2000ppm. The hydrogen engine's exhaust had no CO, CO_2 and HC emissions. As shown in Figure 11, the hydrogen concentration in the exhaust decreased with load as the more complete combustion took place at a higher combustion temperature.
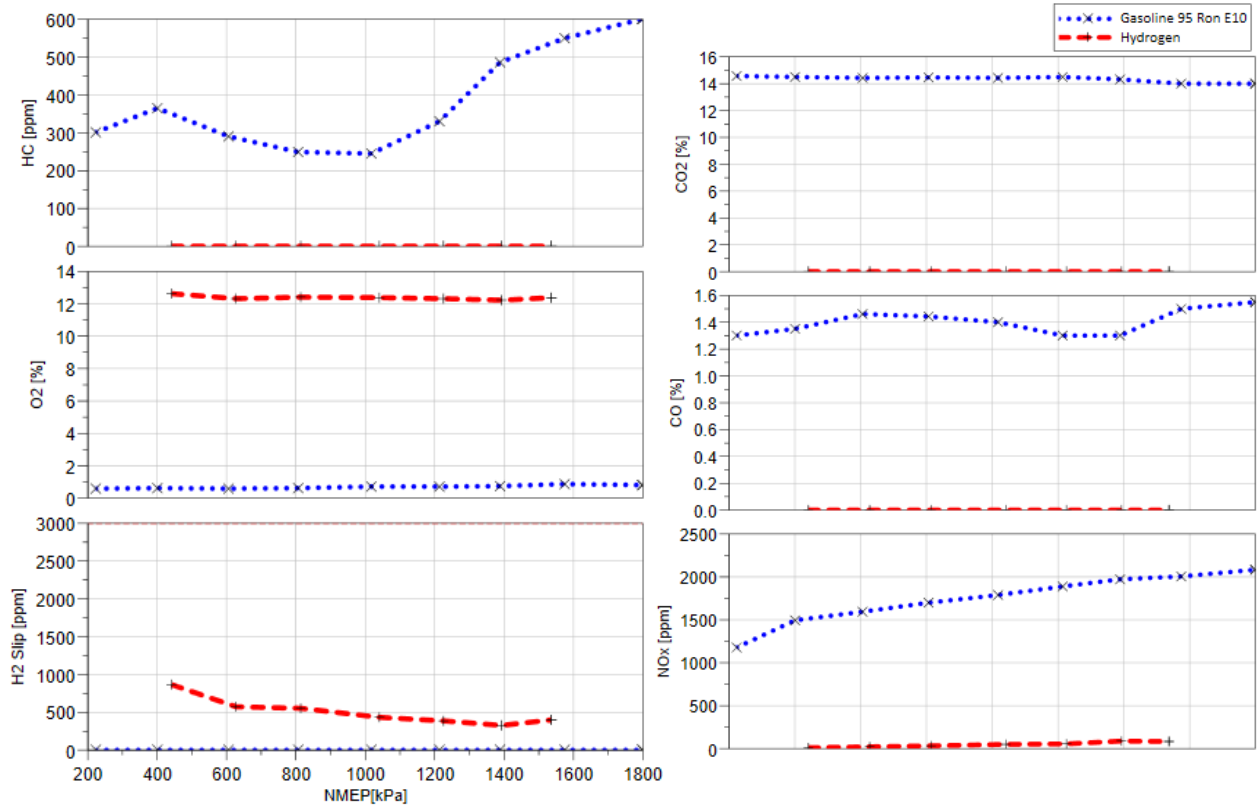
Figure 8. 9: Hydrogen slip and engine-out emission comparison between gasoline and hydrogen combustion for the load sweep.

8.3.3 Assessment of Gasoline and Hydrogen Performance and Emission Over Fuel Injection Matrix

This section will explore the impact of injection pressure and timing on the performance and emission characteristics of direct injection (DI) gasoline and hydrogen engines. The hydrogen injection pressure was varied between 10 and 40 bar, while the gasoline engine operated between 50 and 200 bar. As the hydrogen was injected in a gaseous form, its start of injection could be delayed up to 100 degrees before the top dead centre (BTDC). In contrast, liquid gasoline had to be injected earlier to ensure proper atomization and evaporation. The engine experiments were conducted at a constant speed of 2000 rpm and a load of 10bar IMEP, while the air-to-fuel ratios were maintained at stoichiometric levels for gasoline and lambda 2.75 for hydrogen.

Figure 8.10 illustrates both fuels' indicated thermal efficiency contours across various injection timings and pressures. The graph suggests hydrogen injection began around 180 crank angle degrees (CAD) later than gasoline injection. It is important to note that the start of hydrogen injection could be delayed with higher injection pressure without affecting the pressure differential during the injection process. However, the earliest injection timing of hydrogen was limited by the possibility of backfiring due to escaping hydrogen into the intake port.

Regarding thermal efficiency, hydrogen engines exhibited about 2.8% higher efficiency in all conditions. Meanwhile, the gasoline engine achieved 1.8% higher indicated thermal efficiency in the higher injection pressure region of 150 to 200 bar with very late injection

compared to the early and low-pressure areas. On the other hand, the hydrogen engine was less sensitive to the injection pressure and timing and produced higher efficiency with a higher pressure of 30 to 40 bar and late injection.

In conclusion, injection pressure and timing significantly impact the performance and emission characteristics of DI gasoline and hydrogen engines. Understanding these effects can aid in optimising engine design and operation for improved efficiency and reduced emissions.
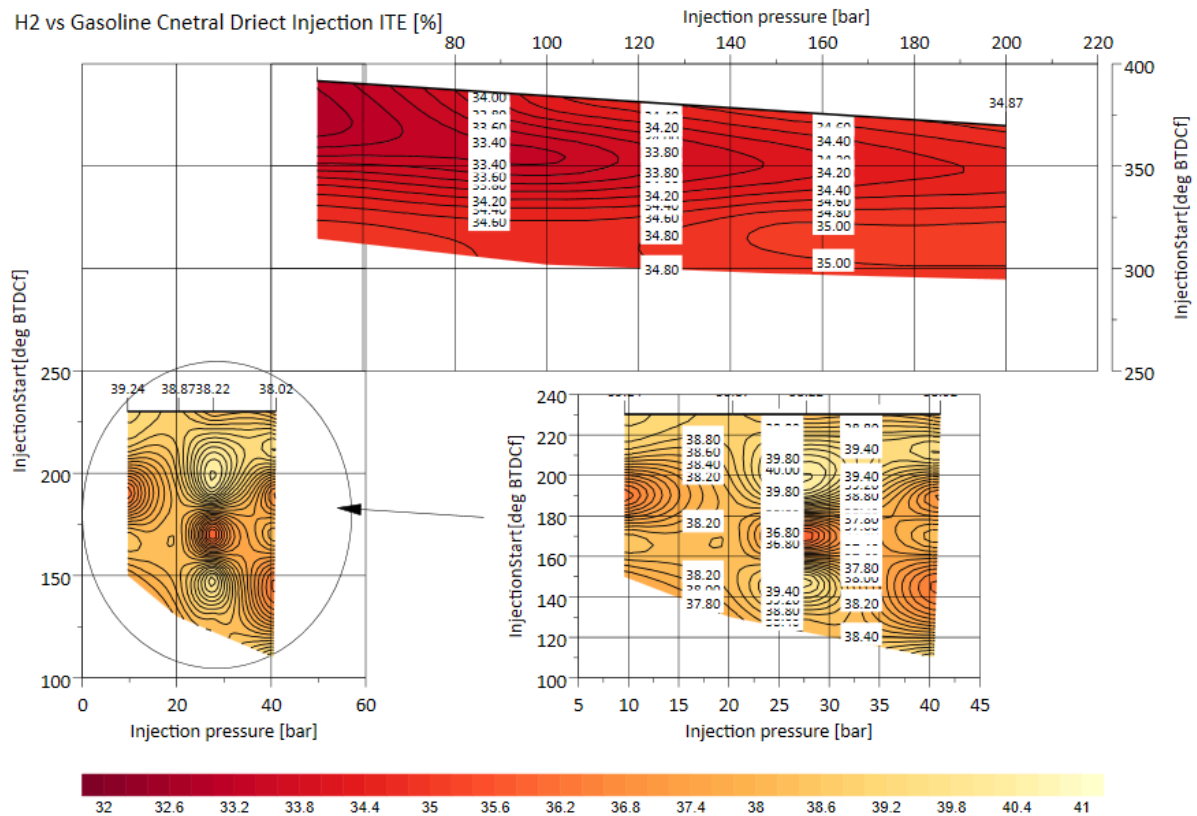
Figure 8. 10: ITE for hydrogen and gasoline at 10 bar IMEP and 2000 rpm speeds vs injection pressure (bar) and injection start angle (BTDCf)

Figure 8.11 shows the variations in the indicated specific fuel consumption (ISFC) with injection pressure and timings for both hydrogen and gasoline. The hydrogen engine had an average ISFC of 78.7 g/kw.hr with very small variations in the injection parameters. The gasoline engine was operated with a much higher ISFC between 245-257 g/kw.hr, thanks to gasoline's much lower calorific value (47MJ/kg) than hydrogen (143MJ/kg) and to lower gasoline combustion engine operation efficiency.
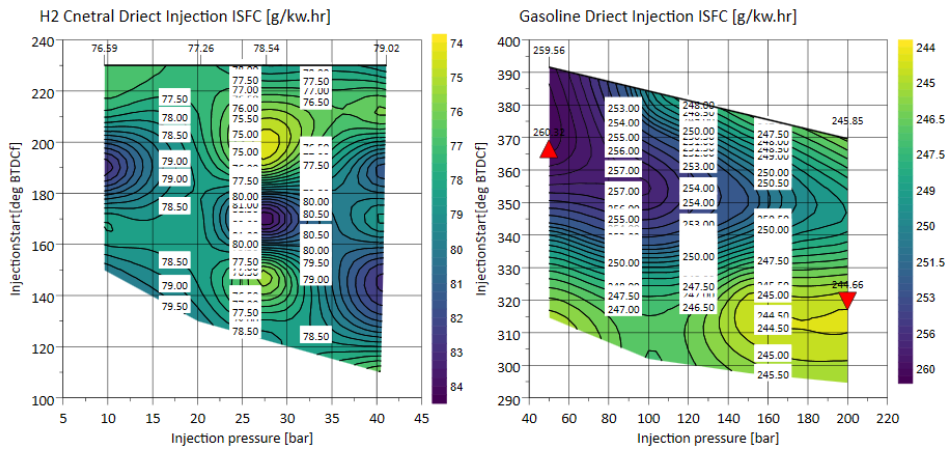
Figure 8. 11: ISFC (g/kw.hr) for hydrogen vs gasoline over the injection matrix.

The experiment presented in Figure 8.12 aimed to study the effect of injection pressure and timing on cyclic variations in hydrogen and gasoline engines. The coefficient of variation (COV) for hydrogen was observed to be more sensitive to the injection pressure than the injection timing. Interestingly, the operation of the hydrogen engine exhibited slightly higher cyclic variation at injection pressures ranging from 30 to 40 bar. This was attributed to shot-to-shot variations in hydrogen injection, as the injection duration became shorter at increased injection pressure.

On the other hand, the operation of the hydrogen engine produced more stable combustion than the gasoline engine at lower injection pressures. This was in contrast to the gasoline engine, which was found to be more sensitive to injection timing than injection pressure. Specifically, earlier injection led to more stable combustion in the gasoline engine, likely due to better fuel mixing with air over a longer period.

Overall, the experiment results highlight the complexities involved in optimising the performance of internal combustion engines. The findings suggest that different fuels and engine types require different injection strategies to achieve optimal combustion stability.
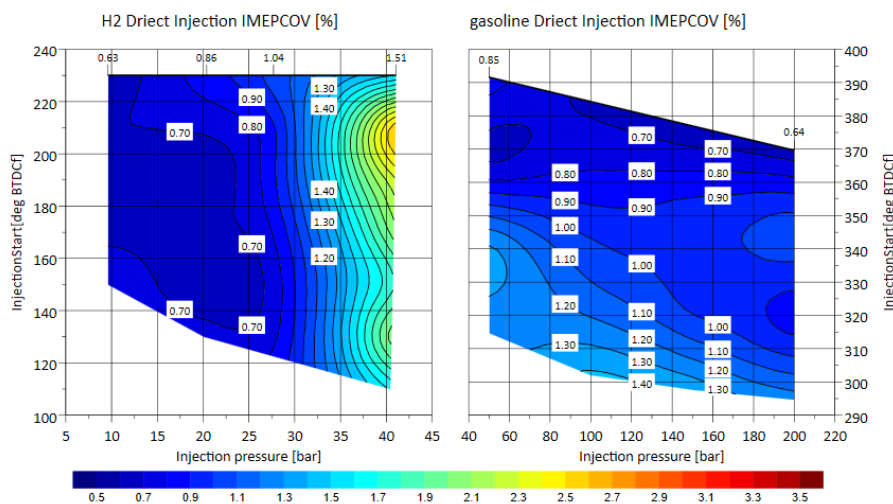
Figure 8. 12: IMEPcov (%) for hydrogen vs gasoline over the injection matrix.

In the presented research study, Figure 8.13 showcases the primary combustion duration of 10 to 90% MFB (Mean Fraction Burned). It's important to note that the hydrogen and

gasoline engines were operated under varying mixtures – the hydrogen engine was powered by a lean variety (l=2.75). In contrast, the gasoline engine was run on a stoichiometric mixture. Interestingly, both engines had similar combustion durations despite the varying combinations. It's worth mentioning that the most delayed injection timings (located in the lower right regions) resulted in slightly longer combustion durations for both fuels. This could be due to the slower burning rate of the mixture caused by lower temperature and pressure conditions.
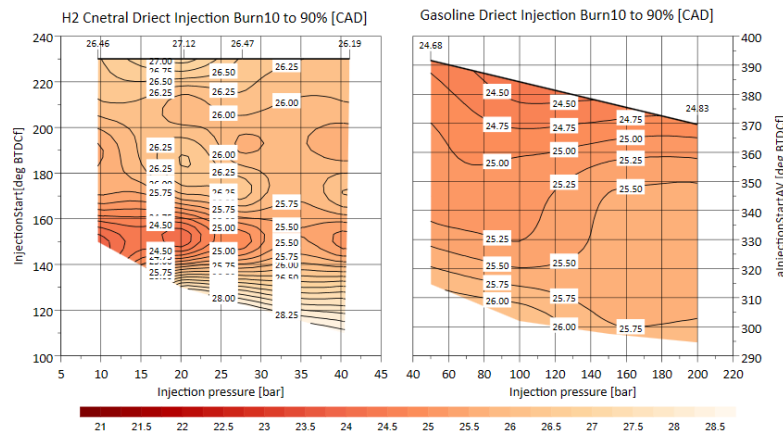
Figure 8. 13: the 10 to 90% burn duration (CAD) for hydrogen (λ=2.75) vs gasoline (λ=1.0) over the injection matrix.

Figure 8.14 shows the intake pressure for hydrogen and gasoline engine operation. At 10 bar IMEP, the stoichiometric gasoline operation could be achieved at near atmospheric pressure or wide-open-throttle. Because of its lean-burn operation, the hydrogen engine was supplied with significantly higher intake pressures. As the start of hydrogen injection was retarded towards the intake valve closure timing, the boost pressure decreased because the hydrogen gas displaced less air. The boost pressure had to be increased with the hydrogen injection pressure for a given injection timing, indicating more air was displaced by the gaseous hydrogen.
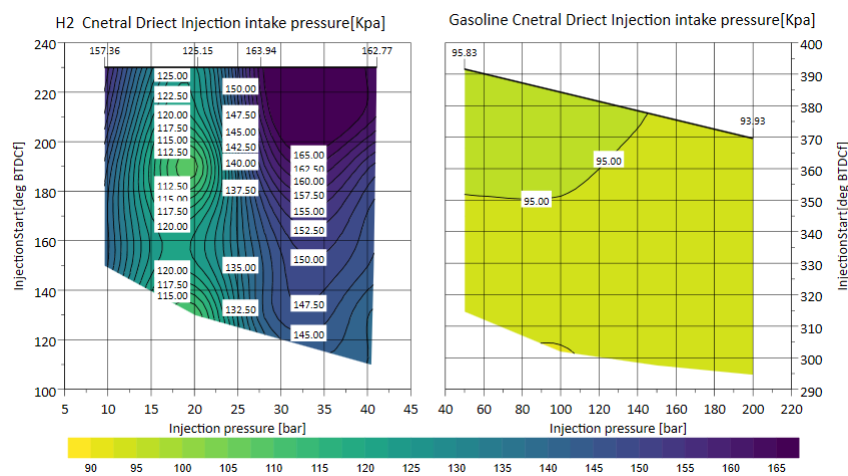
Figure 8. 14: Intake pressure for hydrogen vs gasoline over the injection matrix.

Figure 8.15 depicts the impact of fuel injection timings and pressures on NOₓ emissions from hydrogen and gasoline engines. On average, the stoichiometric gasoline engine

produced NOₓ emissions of over 1500ppm, while the lean-burn hydrogen engine typically generated less than 100ppm NOₓ emissions, which increased slightly with delayed hydrogen injection. The injection delay into the second half of the compression stroke increased the likelihood of an inhomogeneous mixture, resulting in higher combustion temperature from a richer variety than the averaged lambda=2.75, leading to increased NO formation.
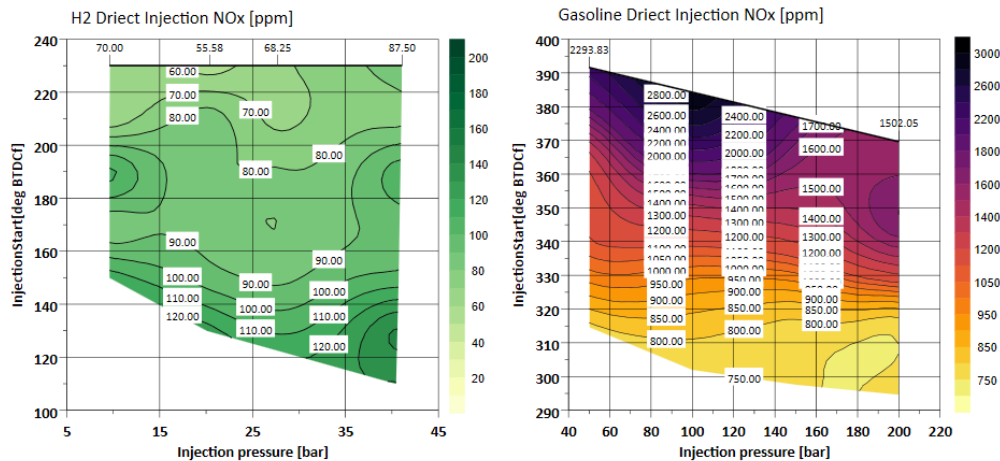
Figure 8. 15: NOₓ emission (ppm) for hydrogen vs gasoline over the injection matrix.

Figure 8.16 shows the unburnt fuel concentration in H₂ slip and HCs in the hydrogen and gasoline engine's exhaust. The hydrogen slip was hardly affected by the injection timings and pressure except for the slightly higher value observed at the most retarded and high injection pressures region at the bottom right in the left graph. In comparison, the injection timing mostly affected the HC emission and reached its maximum value at the lowest and earliest injection point of 50 bar and 395 degrees BTDCf.

As observed in all the other tests, the emission analysis showed that the hydrogen engine eliminated all CO, CO₂, and HC.
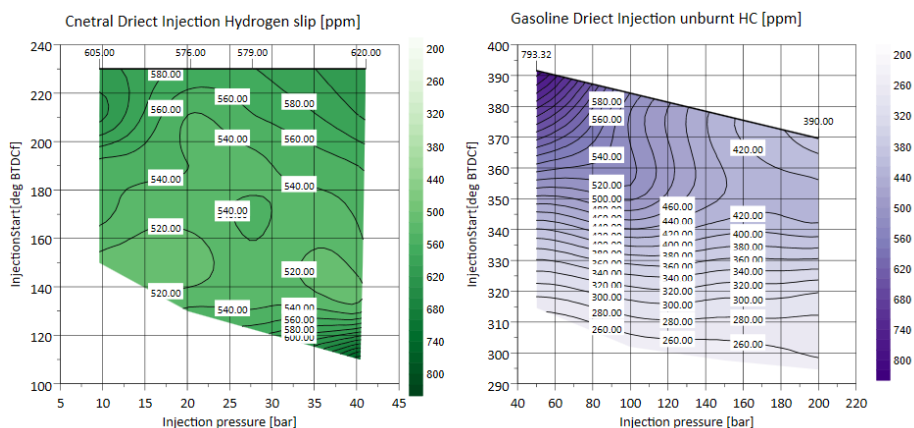
Figure 8. 16: H2 slip and the HC emission (ppm) for hydrogen vs gasoline over the injection matrix.

8.3.4 Unlock The Potential of The Hydrogen at Wide Engine Load

From the previous three sets of testing, it is evident that hydrogen has tremendous potential to operate within a much wider lambda and nearly the same load range. However, it is essential to note that the tests were conducted at a fixed lambda of 2.75 for minimum boost, lower NOₓ, and higher efficiency selection criteria. With an optimised injection timing and pressure at low load, the engine can operate in a stable region and at maximum load. If the combustion begins to rise toward lambda 1, it will drop the in-cylinder peak pressure and allow the hydrogen to operate up to new engine limits. The reason for repeating the test, as indicated in Figure 8.7, is that the gasoline has been running up to the engine stability point, and combustion has been retarded to avoid the engine-knocking phenomenon. Hydrogen, on the other hand, is showing very stable combustion. Based on the lambda sweep test, the hydrogen DI technologies could run near stoichiometric combustion, albeit with a tradeoff of higher NOₓ generation. This issue could be eliminated by adopting an EGR or an after-treatment system.
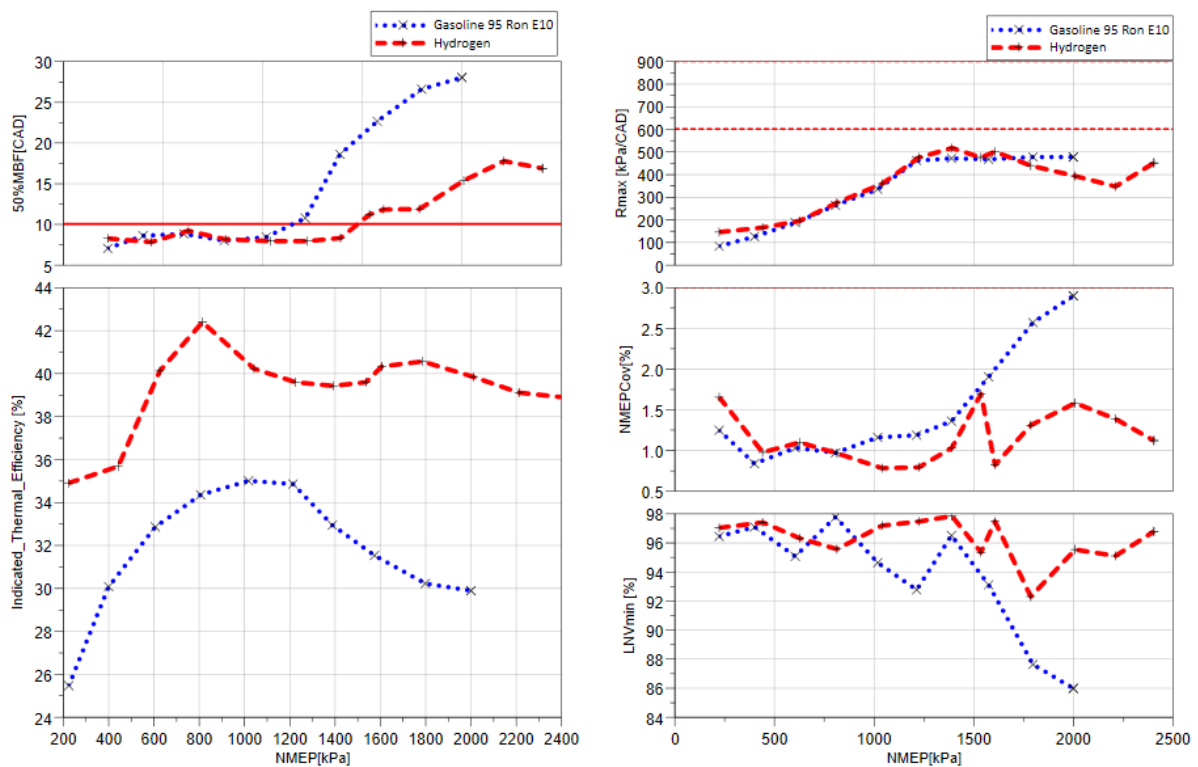
Figure 8. 17. Hydrogen vs Gasoline at 2000 rpm load sweep with optimum injection and lambda

Figure 8.17 demonstrates the load sweep at 2000 rpm, and the lambda for hydrogen is fixed at 2.75 between IMEP 2 to 16 bar, then dropping the lambda to maintain the engine within the in-cylinder peak pressure. From 16 to 24 bar, the lambda is drooped by 1, and the COVIMEP for hydrogen still shows very stable combustion. At low load, the injection pressure is dropped to 10 bar injection, which allows better hydrogen mixing at low load and reflects on higher engine stability at low load. Overall, the Hydrogen DI has overcome the gasoline load by optimising the hydrogen injection matrix and applying a flexible lambda strategy.

8.4 Conclusion

This study conducted a comprehensive investigation to compare the performance, combustion and emissions of the direct injection gasoline and hydrogen spark ignition on the same engine. The results have demonstrated that hydrogen can be easily adapted to the current SI engine to eliminate CO_2, CO and HC emissions.

The DI hydrogen engine can operate in an extensive range of relative AFRs ranging from lambda1.0 to 3.8, whilst the DI gasoline engine was limited to lambda1.6. The hydrogen engine produced ultra-low NO_x emissions (less than 50 ppm) when it was operated with mixtures leaner than lambda=2.5.

The DI hydrogen engine should be operated with a very lean mixture for better thermal efficiency than the gasoline engine. At Lambda 2.75, the hydrogen engine operated at higher thermal efficiency than the gasoline engine by at least 5%, from low to high load conditions. It is important to acknowledge that this study used an engine originally designed and optimised for gasoline operation. Given this context, it is reasonable to anticipate even greater performance gains with a dedicated engine specifically optimised for hydrogen operation. Such an engine would likely exhibit superior efficiency and overall performance, underscoring the potential for further advancements in hydrogen engine technology.

The DI hydrogen engine's performance and emissions were much less affected by the fuel injection pressure and timings than the SI gasoline engine at the WOT condition (10bar IMEP). However, the injection of gaseous hydrogen during the early intake process displaced more air and, hence, higher boost pressure than the gasoline engine. Additionally, a slightly higher boost pressure was needed as the in-cylinder hydrogen injection pressure was increased from 10-40 bar.

Overall, hydrogen has the potential to be the next-generation zero-carbon alternative fuel for medium-duty spark ignition DI engines with minor modifications to the existing infrastructure.

Chapter 9. Hydrogen Engine Insights: A Comprehensive Experimental Examination of Port Fuel Injection and Direct Injection

9.1 Introduction

In this chapter, the results will be presented and discussed on the performance and emissions of a boosted spark ignition hydrogen engine with either both port fuel injection and direct injection systems.

The study aims to evaluate the benefits of the direct injection system over the port fuel injection system by analyzing the air-to-hydrogen ratio at different speeds and conducting load sweep tests. Additionally, the study assesses the impact of valve timings on combustion, engine performance, and emissions for each injection system.

Overall, this study provides valuable insights into the performance and emissions of a hydrogen-fueled engine, highlighting the benefits of the direct injection system over the port fuel injection system and the impact of valve timings on engine performance.

9.2 Test Methodology

The experimental testing involved the operation of an engine using two distinct hydrogen injection systems, namely port fuel injection and central direct injection, at three different engine speeds (1500, 2000 and 3000 rpm), different engine loads, and relative air-to-fuel ratios (λ). Table 9.1 summarises the engine test conditions for the three investigations: the λ sweep test, engine load sweep test, and cam envelope sweep test.

The first experiment, the λ sweep, was conducted by exploring the effect of different λ values (ranging from 1.5 to above 3) at a fixed engine load of 1000 kPa IMEP (a mid-load simulation) and a fixed intake and exhaust cam position of 97 CAD ATDCg and 102 CAD BTDCg, respectively. The second experiment, the engine load sweep, was conducted for a range of engine loads from 400 kPa to 1600 kPa (low to high engine operation) at a fixed λ value of 2.75 and fixed intake and exhaust cam positions of 97 CAD ATDCg and 102 CAD BTDCg, respectively. The last experiment, the cam envelope sweep, was performed for a wide range of both intake (75-120 CAD ATDCg) and exhaust (80-125 CAD BTDCg) cam timings at a fixed λ value of 2.75, fixed engine load and speed of 1000 kPa IMEP and 2000 rpm, respectively.

To ensure accurate control, the intake temperature was regulated using an inline air heater with PID control within 0.3 degrees, maintaining it at 38 degrees Celsius. The oil and water coolant temperatures were also fixed at 90 degrees, with external heaters, and PID correlates with a 3-degree variation.

The injection pressure and start of injection were generally set at 3000 kPa and 150 CAD BTDCf, respectively. The injection pressure was reduced to 1000 kPa for engine loads below 800 kPa IMEP to ensure stable combustion. The PFI was held constant at 1000 kPa, and the end of injection was fixed at 200 CAD BTDCf to ensure that the PFI took place after the intake valves opened, minimizing the hydrogen buildup in the intake that could cause backfire.

The limits of the highest average in-cylinder pressure and maximum pressure rise rate (Rmax) were set to 12000 kPa and 600 kPa/CAD, respectively. COV_{IMEP} of 1.5% was used to

determine stable engine operation, and the combustion phasing (50%MB) was set between 8 and 10 CAD ATDCg for optimal combustion.

The relative air-fuel ratios (λ) were measured by two wide-band sensors in the exhaust line calibrated with O_2 measurements from the Horiba emission analyzer and then compared with a λ calculated from the hydrogen flow rate minus the H2 slip and air flow rate. Finally, all three testing sets were conducted using full DI and repeated with the exact operating conditions using PFI.

Table 9. 1: Engine test conditions for H2ICE PFI vs DI

Engine parameters	Unit	λ sweep test	Engine load sweep test	Cam envelope sweep test
Engine Speed	rpm	1500, 2000, 3000	1500, 2000, 3000	2000
Engine Load	kPa	1000	SWEEP	1000
λ	-	SWEEP	2.75	2.75
Intake Cam positions	ATDCg	97	97	SWEEP
Exhaust Cam positions	BTDCg	102	102	SWEEP
Start of injection DI	BTDCf	150	150	150
End of injection PFI	BTDCf	200	200	200
Injection pressure DI	kPa	3000	1000 at low load, 3000 from 800 kPa IMEP	3000
Injection pressure PFI	kPa	1000	1000	1000

9.3 Results and Discussions

This study examines an SI engine's performance and emissions characteristics fueled by DI or PFI. The λ values were adjusted at different speeds to determine the optimal λ for each technique. Once the optimal λ was identified, it was set at various engine speeds during load variations.

9.3.1 Effect of Lambda on PFI and DI H2 Engine Performance and Emissions at A Constant Mid-load.

An experimental study was conducted to assess the performance and emissions characteristics of an H2 engine. The engine was evaluated at a fixed load of 1000 kPa IMEP and three different engine speeds (1500rpm, 2000rpm, and 3000rpm). The study aimed to determine the minimum λ value and the lean-burn limit for PFI and DI operations by varying the relative air-to-fuel ratio λ.

The top graph of Figure 9.1 illustrates that, in most cases, the maximum thermal efficiency was attained when the spark ignition timing was set to MBT (minimum ignition advance for Best Torque), with the 50%MB ranging between 8-10 CAD after the TDC, except with the richest and leanest mixtures. However, when the λ value was reduced to less than 1.5 at 2000rpm, the combustion rate significantly increased, and hence the spark timing had to be retarded to keep the Rmax below the limit of 600 kPa per crank angle shown in Figure 9.2.

The results indicate that the maximum thermal efficiency was achieved within the λ range of 2.5 to 3.5, and DI operation had slightly higher ITE than PFI operation, as shown in Figure 9.1. In addition, PFI and DI operations were characterized by stable combustion, with less than 1.5% variate the injection over a broad range of λ values. Nevertheless, the cyclic variation slightly increased when the λ was increased towards the lean operation limits.

At rich operation points (low λ), the PFI operation experienced a backfire in the intake due to the ignition of hydrogen in the intake by the hot burnt gas escaping the cylinder during the valve overlap period. Therefore, PFI operation was limited to a minimum λ of 1.5. In contrast, the DI operation could be operated with lower λ without backfire because of the absence of hydrogen in the intake system when hydrogen was injected directly into the cylinder later in the intake process at a much higher injection pressure of up to 4,000 kPa.

The bottom graph in Figure 9.2 shows that the pressure rise rate increased with lower λ due to faster combustion. In order to keep Rmax below the limit of 600 kPa per crank angle, the spark timing was retarded. Finally, the drop in LNVmin and sudden rise in COVIMEP at 3000 rpm DI λ 3.75 was caused by one partial burn cycle among 300 cycles, as shown in Figure 9.2.
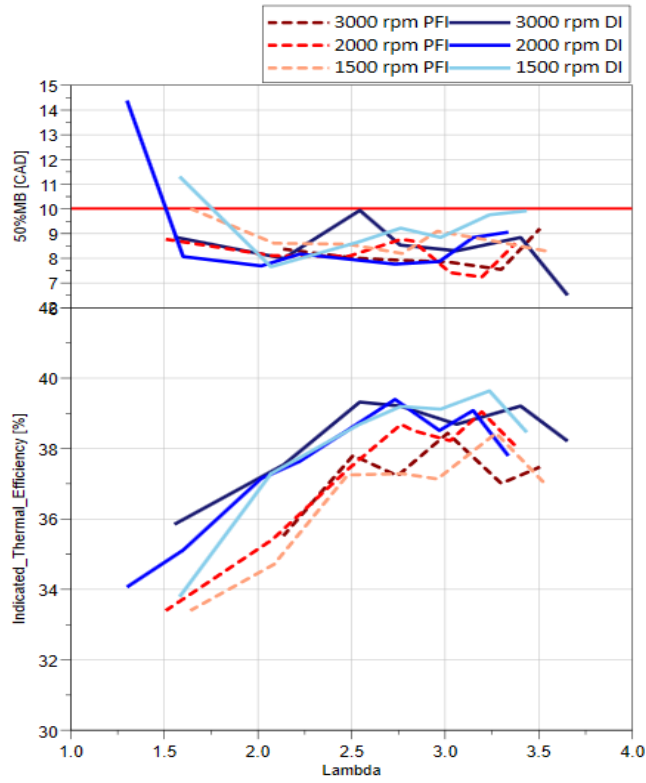
Figure 9. 1: The thermal efficiency of direct injection (DI) and port fuel injection (PFI) systems at different λ values and the 50% mass burn rate.
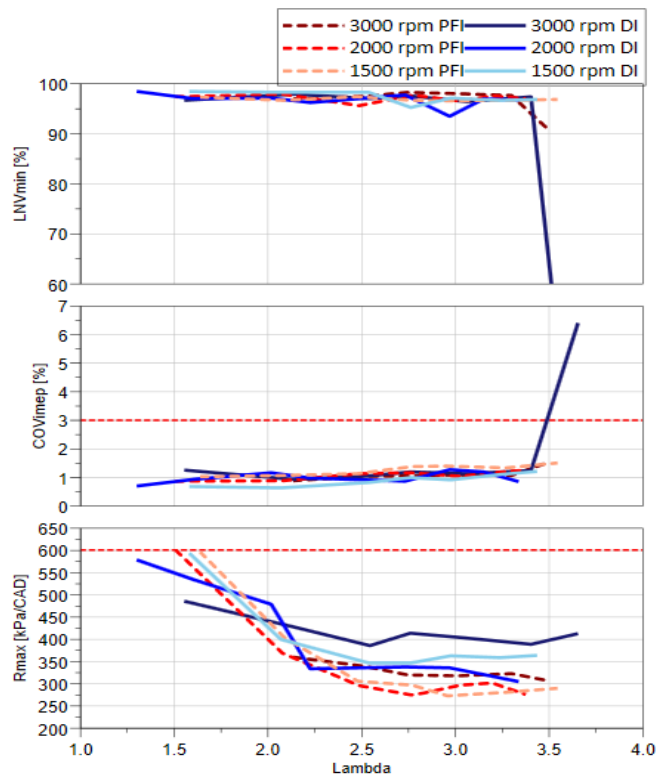
Figure 9. 2: operational constraints associated with different speeds and λ values in DI and PFI systems.

Spark timings and burn durations are presented in Figure 9.3, where all spark timings occurred at MBT except for the operation with λ lower than 1.5, which required retarding the sparking after top dead centre firing to limit the pressure rise rate within 600 kPa per crank angle. MBT timings became more advanced with increasing engine speed during PFI operation as expected, resulting in longer combustion duration and increased initial flame development and main combustion duration in terms of crank angles. The same trend was observed during DI operation when λ was less than 2, with 2000rpm operation exhibiting longer combustion duration and more advanced spark timings than other engine speeds. Direct injection operation generally resulted in longer combustion durations than equivalent PFI operation. PFI and DI hydrogen engine operations produced zero CO_2, CO, and HC emissions.

As illustrated in Figure 9.4, NO_x emissions were less than 10 ppm between λ=3.0 to 3.5 and no more than 50 ppm between λ=2.75 to 3, and increased rapidly from λ 2.5 to 1.5. At 1500rpm, DI operation produced higher NO_x emissions below λ 2.0, possibly due to burning a slightly richer mixture formed during direct injection operation. PFI operation resulted in more H2 concentration in the engine's exhaust gas than DI operation, likely due to hydrogen being trapped in crevices during compression stroke. More H2 was measured at lower engine speeds during PFI operation, minimally affected by engine speed when hydrogen was directly injected into the cylinder.
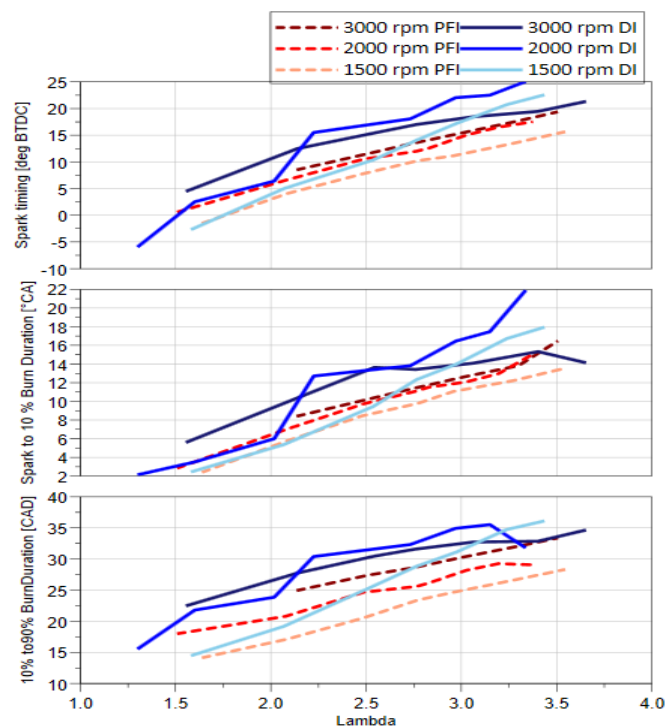
Figure 9. 3: The parameters of spark ignition and burn duration.
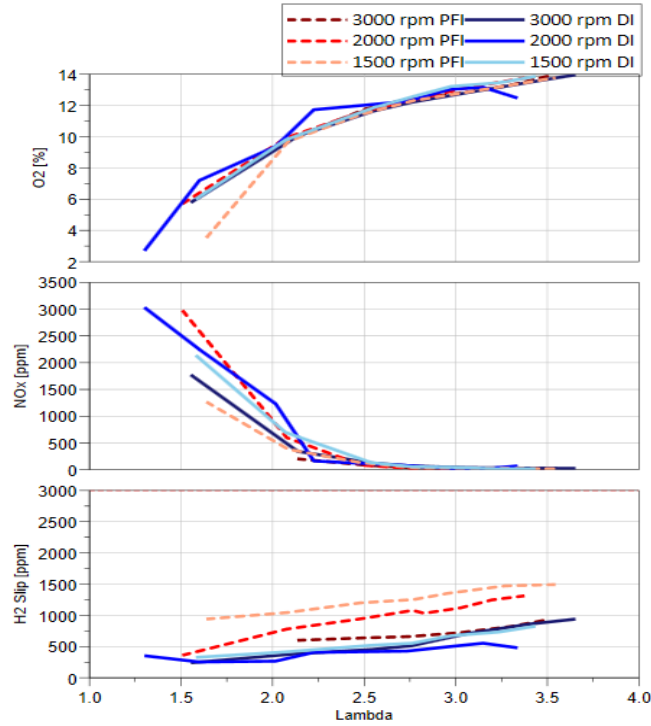
Figure 9. 4: The main three outputs from the exhaust line are oxygen, NOₓ, and H2 slip.

In order to quantify the error of measured λ by the lambda sensors in the exhaust due to the presence of unburned fuel, measurements of exhaust gas components can be used to calculate the actual air-to-fuel ratio and λ in the cylinder in a controlled experimental setting. To assess the influence of H_2 slip on the measured emissions-based λ, a particular air-fuel ratio equation for H_2 was formulated based on Equation 9.4[157].

$$H_2 + A\left[O_2 + {}^{79}/_{21}\, N_2 + Z.(H_2O)\right] \rightarrow c.H_2O + d.H_2 + e.O_2 + f.NO + g.N_2 \tag{9.1}$$

By utilising the atom balances for hydrogen and oxygen, along with the equations for emissions volume concentration, a solution for variable A can be obtained.

$$A = \frac{1 - [H_2] + [O_2] + {}^{1}/_{2}\,[NO]}{z - [O_2]\left(\frac{200}{21} + 2.z\right) - [NO]\left(\frac{200}{42} + z\right) + [H_2]\left(\frac{79}{21} + z\right)} \tag{9.2}$$

$$z = \frac{100}{21}.HR.\frac{M_{Air}}{M_{H_2O}} \tag{9.3}$$

$$AFR = 2.A.AFR_{stoich} \tag{9.4}$$

The wet exhaust volume concentrations for O_2, H_2, and NOₓ are denoted as $[O_2]$, $[H_2]$, and $[NO]$, respectively. HR represents the humidity ratio, whereas M_{air} and M_{H2O} are the molar masses for air and water, respectively.
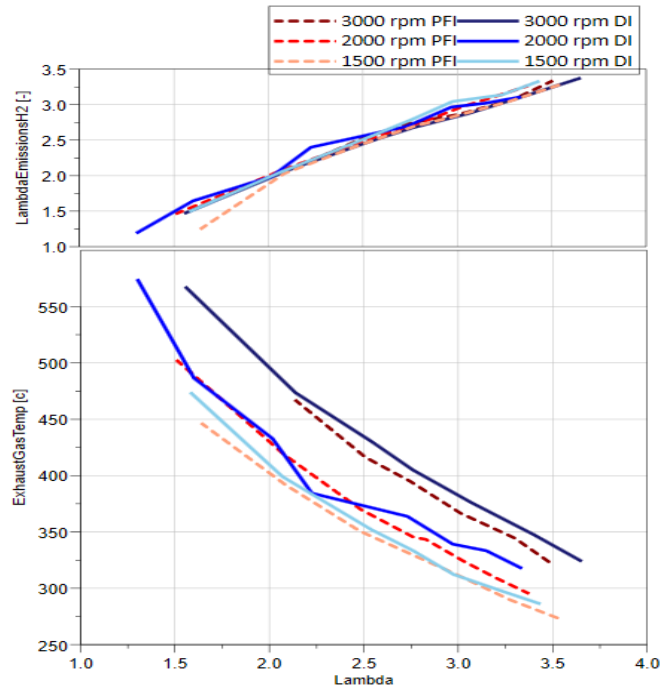
Figure 9. 5: The relationship between the estimated and measured λ emission based on λ values and the exhaust gas temperature

Figure 9.5 displays the correlation between the in-cylinder λ values obtained from emissions measurements and those from lambda sensors. The two sets of λ values matched up until λ 3, except the lowest λ at 1500rpm due to a dip in O_2 concentration detected by the lambda sensor. Beyond λ 3, the in-cylinder λ values were slightly lower than the lambda sensor readings due to the lambda sensor's reduced accuracy with higher O_2 concentrations. As demonstrated in the lower graph of Figure 8, DI operation resulted in slightly higher exhaust gas temperatures due to slower combustion and delayed end of combustion.

The results of the λ sweep test, conducted at various speeds, indicate that DI hydrogen operation demonstrated slightly higher ITE than PFI operation due to lower pumping loss and fewer hydrogen slip emissions. Neither PFI nor DI hydrogen engine operations produced CO_2, CO, or HC emissions. Both injection strategies facilitated stable engine operation across a wide range of λ values, although backfire limited PFI operation to λ 1.5 or higher.

Based on the λ sweep test findings, it was determined that the ideal operational λ range for achieving minimal NO_x emissions, optimal thermal efficiency, and reduced H_2 slip is between λ 2.75 and 3. Therefore, λ 2.75 was selected for additional engine testing under different operating conditions, as it required less air boosting for high load and maintained low NO_x emissions.

9.3.2. Comparison of PFI and DI Hydrogen Engine Performance and Emission With Load Sweep Operating Conditions at A Fixed Lambda

This study examined PFI and DI strategies' effectiveness and emission levels under various engine speeds and loads while maintaining a fixed λ 2.75. Figure 9.6 displays the ITE results for PFI and DI strategies across different engine loads and speeds. Additionally, Figure 9.7 outlines the operating constraints, including 50%MB, LNVmin, COV_{IMEP}, and Rmax. Figures 9.9 and 9.10 provide insight into the emissions and intake air pressure, respectively. Finally, Figure 9.11 compares measured and calculated λ and O_2 concentrations.

The data from Figure 9.6 indicates that ITE increased with engine load for both PFI and DI operations, with an efficiency peak occurring from 1000 kPa onwards due to reduced pumping work. DI operation demonstrated higher ITE than PFI, ranging from approximately 2.5 percentage points at lower loads to 1.5 percentage points at higher loads. This is likely due to the increased volumetric efficiency generated by higher injection pressures offered by the DI technology. Additionally, engine speed affected ITE in both systems, particularly at low and medium engine loads, with lower speeds resulting in higher thermal efficiencies up to the load point of 1000 kPa, which corresponded to the wide-open-throttle position.
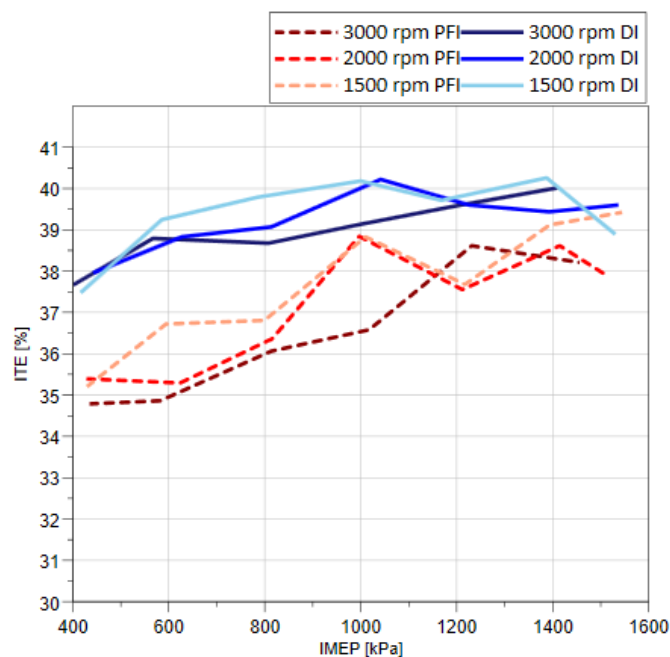
Figure 9. 6: Indicated thermal efficiency of DI and PFI systems at different engine loads and speeds.

According to the data in Figure 9.7, both PFI and DI engines demonstrated highly stable combustion across low to high-load operations, with COVIMEP remaining consistently below 1.5% and 50 50%MB between 8-10 CAD after TDC. However, at very high engine loads (IMEP > 1400 kPa), the DI system exhibited an exception with a retarded 50%MB to keep Rmax below 500 kPA/CAD, as illustrated in Figure 11. A minor anomaly in the LNVmin minimum peak was observed at 800 kPa IMEP with the DI system, but it did not affect

COVIMEP. The LNVmin minimum peak was attributed to a single partial burn cycle. During the experiments, it was found that the DI injection pressure needed to be adjusted (lowered to 1000 kPa) for engine loads under 600 kPa, as higher injection pressures tended to cause increased cycle-to-cycle variations. Possible factors contributing to this variation include cyclic changes in fuel injection and mixture formation due to in-cylinder flow fluctuations.
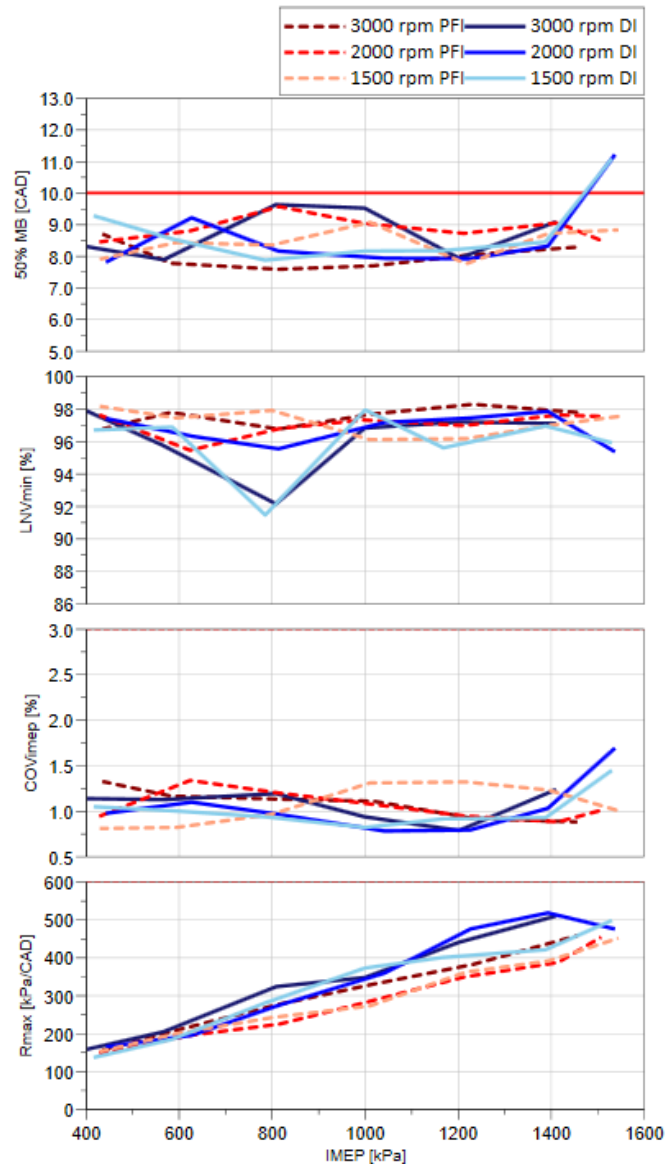
Figure 9. 7: Operational constraints associated with DI and PFI systems at different engine loads and speeds

Similar to the experiment results in the previous section, central direct injection operations had longer burn durations than port fuel injection for both the spark to 10% and 10% to 90% of the mass fraction burned period. Moreover, the combustion duration increased, and the minimum advance for best torque spark timings became more advanced as the engine load increased. These trends differ from those observed in the spark ignition gasoline engine, where a higher load results in a shorter combustion duration due to faster flame speed when gas temperature and pressure are higher, resulting in less spark advance. These findings suggest that hydrogen flame speed is less influenced by in-cylinder pressure and temperature than gasoline combustion and that

hydrogen combustion is slowed down at higher gas pressure. Another possible explanation is the stratification of the in-cylinder charge due to more retarded spark timing; however, further optical measurements are necessary to confirm this.
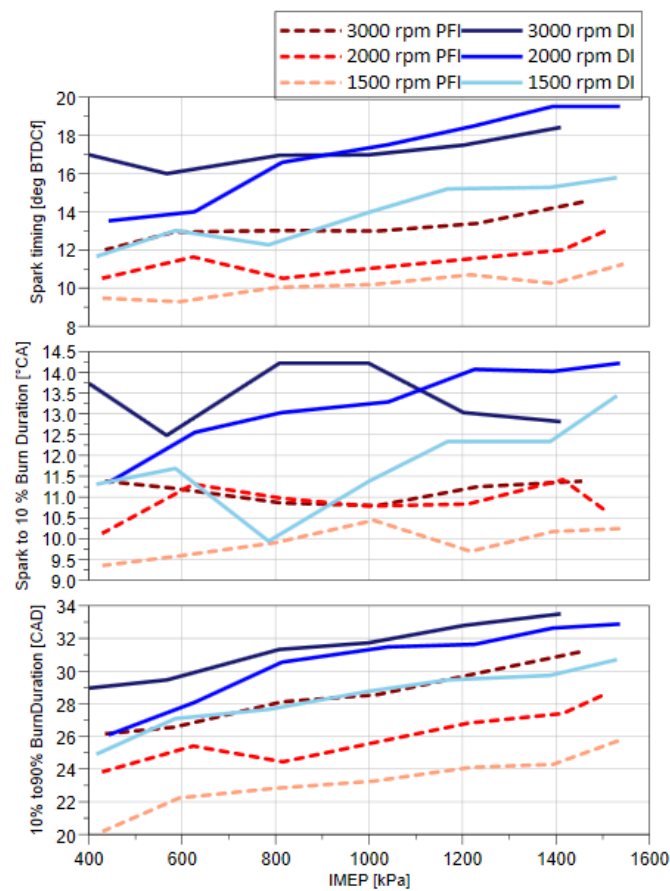
Figure 9. 8: The parameters of spark ignition and burn duration of DI and PFI systems at different engine loads and speeds

In Figure 9.9, it can be observed that NO_x emissions began to increase beyond 1200 kPa IMEP for the DI operation despite remaining relatively low (below 150 ppm). This can be attributed to the partially stratified charge in the cylinder resulting from the delayed end of injection, which allowed for more hydrogen to be injected. Consequently, the combustion of a slightly richer mixture would generate more NO and associated emissions. The previous section shows that the DI operation resulted in higher exhaust gas temperatures due to delayed combustion. In contrast, the higher H_2 slip from the PFI operation may have been caused by increased H_2 trapped in the crevice volume.
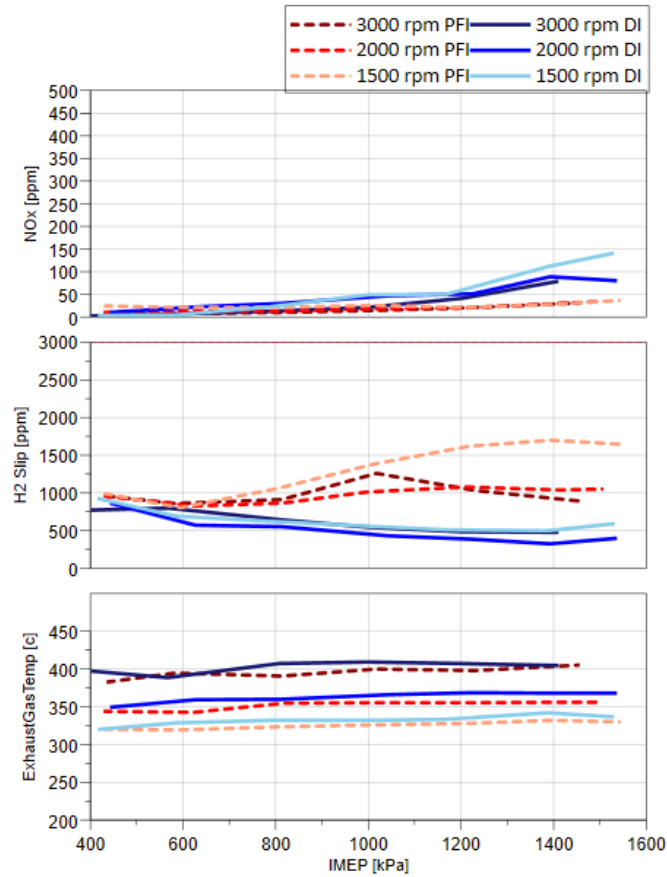
Figure 9. 9: Exhaust emissions and temperatures generated by DI and PFI systems at different engine loads and speeds

A notable discrepancy was discovered during the experiment between DI and PFI systems regarding the intake air pressure. Figure 9.10 illustrates that PFI necessitates greater pressure boosting to attain the same operating conditions (λ and engine load) as DI. This phenomenon can be attributed to PFI injecting hydrogen into the manifold during the intake stroke, displacing the airflow at the intake pressure. In contrast, the direct injection of hydrogen occurs within the cylinder at the start of the compression stroke (150 CAD before TDC) without disrupting the pre-existing air in the cylinder after the intake valves have been closed. As a result, PFI requires a higher pressure boost for an equivalent air and fuel mixture within the cylinder, compared to DI.
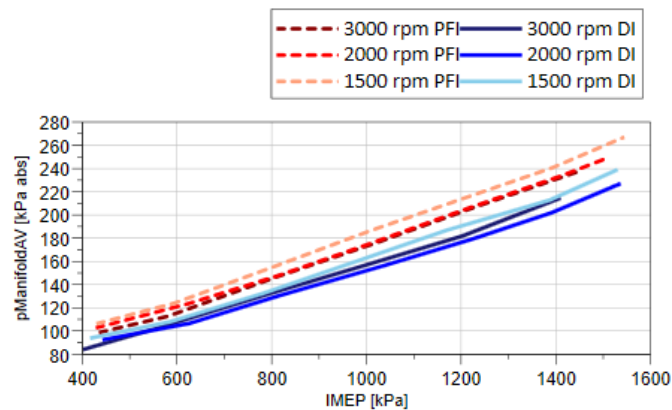
Figure 9. 10: Intake air pressure of DI and PFI systems at different engine loads and speeds

As evidenced in the preceding section, the relative air-fuel ratios, measured and calculated, were in harmony for various λ values, barring exceedingly lean operation. Given that λ was a constant in this experiment, as outlined in the Methodology section, it was imperative to compare the λ measured by S1/S2 with the calculated λ and O_2 concentration from the Horiba analyser. Figure 9.11 demonstrates that both λ values and O_2 remained constant when the engine load was altered, thus attesting to the precision of the experiment's findings.
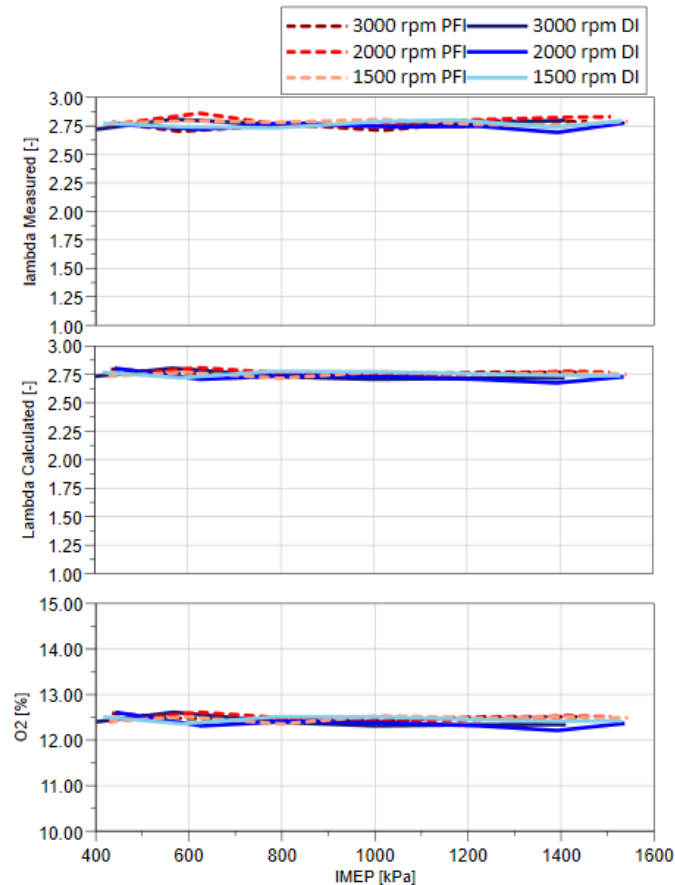
Figure 9. 11: Measured and calculated λ as well as O_2 concentration generated by DI and PFI systems at different engine loads and speeds

Through conducting engine load sweep tests at various speeds, valuable insights into the performance of Direct Injection (DI) and Port Fuel Injection (PFI) systems have been gained. The results demonstrate a subtle difference in their performance, with DI exhibiting a slightly higher Indicated Thermal Efficiency (ITE) than PFI. Moreover, both injection methods displayed impressive combustion stability across various engine loads and speeds, as observed in the λ values sweep experiments.

However, there is a crucial distinction between the two injection systems, and that is in the boosting pressure. DI requires lower intake pressure, which places less strain on the boosting system. This characteristic makes DI a more efficient and dependable choice compared to PFI. Therefore, DI would be preferable if the goal is to optimize engine performance while minimizing the demand on the boosting system.

9.3.3.Investigation of The Benefit of The High-pressure Late Injection of The DI vs PFI Over A Full Cam Envelope.

After analysing previous sections, it has been established that DI outperforms PFI hydrogen when considering both performance and emissions. This section will explore the relationship between DI and variable valve timing controls. The test was conducted at a consistent speed and load of 2000 rpm and 1000 kPa IMEP, respectively. To remove the impact of the relative air-fuel ratio on performance and emissions, the λ was held at a constant value of 2.75. The intake valve maximum lift timing was shifted from 117 degrees ATDCg to 87 degrees ATDCg with a 10-degree step, while the exhaust cams were shifted from 122 to 92 degrees BTDCg, as shown in Figure 9.12. The experiments were conducted at 16 different matrix points, spanning from minimum to maximum overlap.

Valve overlap near the TDC intake increased significantly, leading to a more efficient scavenging effect during high-load operation. This matrix was conducted for both PFI and DI operations, and by examining the maximum valve overlap setup, we can evaluate the impact of alternative valve timings on hydrogen performance and emission parameters for both injection methods. Additionally, this study will aid in determining the optimal cam configuration for each injection system and compare the potential DI benefits of cam overlap to PFI.
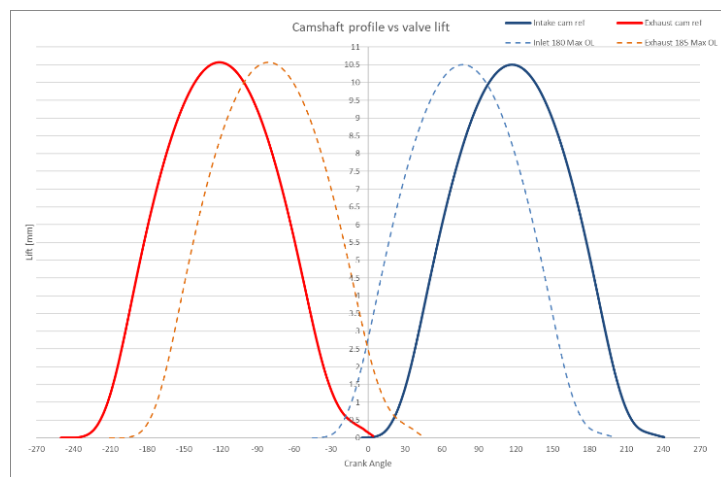
Figure 9. 12: Intake and exhaust cam profile with maximum and minimum overlap.

The graph in Figure 9.13 displays the correlation between the H2 slip in the exhaust line and the intake and exhaust cam envelope. In the PFI system, H2 slip increased as valve overlap grew in the lower left region, reaching over 3000 ppm with the exhaust cam peak retarded at 92 CAD BTDCg and the intake cam advanced at 82 CAD ATDCg. However, to prevent λ sensors from overheating due to burning unburned hydrogen in the exhaust gas, the exhaust and intake cams were limited to 102 CAD BTDCg and 97 CAD ATDCg, respectively, during PFI operation. This configuration resulted in an H2 slip value of 1000 ppm, similar to the previous λ sweep test value. Direct hydrogen injection began at 210 CAD ATDCg after the complete closure of the intake valve, allowing for optimal overlap. Comparing PFI and DI systems, it is clear that the DI system produced approximately 50% less H2 slip across the tested valve timing matrix. It is worth noting that a minor non-linear variation in H2 slip in the DI system, caused by a reduction in exhaust timing of less than 200 PPM, may be attributed to the chamber's boundary conditions and the mixture's state.
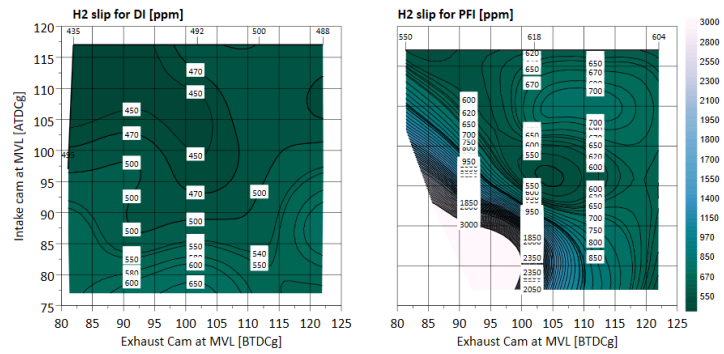
Figure 9. 13: H2 slip of each injection system over the valve timing matrix
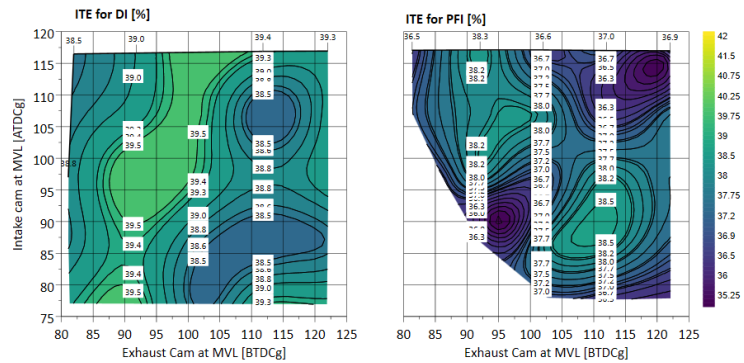
Figure 9. 14: Indicated thermal efficiency of each injection system over the valve timing matrix
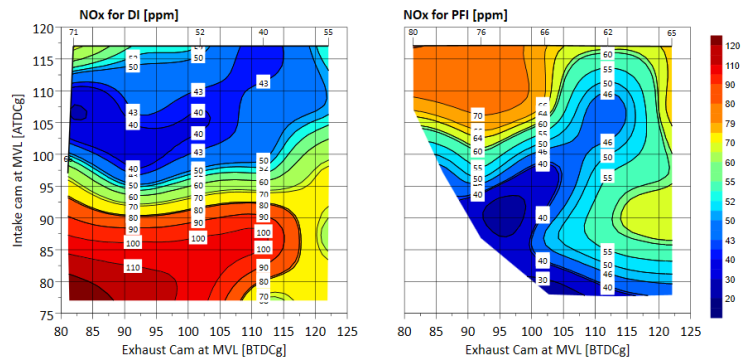
Figure 9. 15: NOₓ emissions of each injection system over the valve timing matrix
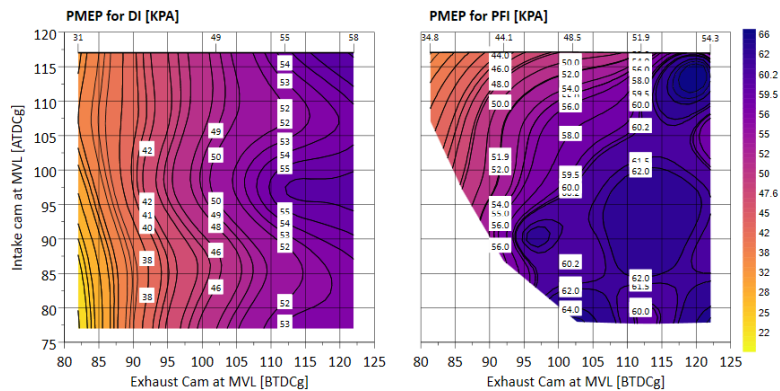
Figure 9. 16: PMEP of each injection system over the valve timing matrix

Comparing the thermal efficiencies of different injection systems across the cam matrix, Figure 9.14 reveals that the performance of the PFI operation with a fixed end of injection at 200 CAD BTDCf is more affected by cam timings. At the peak overlap period, the ITE of the PFI operation declined by 4% due to the short-circuiting of hydrogen through the exhaust valves. The PFI system achieved maximum thermal efficiency when the maximum lift of exhaust valves was at 102 CAD BTDC, and the maximum lift of intake valves was at an angle of 82 CAD ATDC. Consequently, these valve times were adopted for comparing the DI and PFI operations.

Figure 9.15 depicts the impact of valve timings and their overlap on NO_x emissions. The PFI operation showed lower NO_x emissions, consistent with earlier results. The highest peak level of NO_x during the PFI operation was observed when the ITE was the highest due to higher combustion temperature. The NO emissions decreased towards the maximum overlap period region in the bottom left, where more H_2 slip was found. In contrast, the DI system exhibited slightly higher NO_x emissions, all below 100pm, likely due to the higher temperature combustion in the partially stratified mixture. The NO emissions appeared to increase with the earlier closure of the intake valves, thanks to the slightly increased effective compression ratio and higher gas temperature. The maximum NO emissions were with the maximum overlap setting.

Figure 9.16 highlights the significant difference in PMEP between the PFI and DI hydrogen engines. The higher PMEP values of the PFI operation were caused by the increased compression work due to higher intake pressure, as shown in Figure 13, and hence increased compression work. This increase explains PFI's lower ITE values than DI operations. Moreover, the PMEP values increased with the earlier exhaust valve opening, consistent with the decreasing ITE values from left to right in the graphs.

9.4 Conclusion

The present study has evaluated the performance and emissions characteristics of both H2 DI and PFI systems. The assessment included investigations into the influence of different lambda values and loads at various engine speeds to examine each system's performance enhancements and operational capabilities. Additionally, the study explored the potential advantages of incorporating delayed and high-pressure injection into direct injection systems, particularly in combination with the optimised valve overlap setups.

The main findings can be summarised as follows:

1. The current downsized SI gasoline engines can be readily converted to operate with hydrogen using either a DI or a PFI fuelling system. Compared to gasoline engines, both PFI and DI hydrogen engines exhibit consistently higher thermal efficiencies due to their lean burn operation within the lambda range of 2.5 to 3.7. While the PFI H2 engine can operate within a lambda range of approximately 1.5 to 3.7, the DI H2 engine can function within a much broader lambda range, including stoichiometric mixture, without encountering any backfire issues.

2. The DI H2 operation exhibited superior performance compared to PFI across the entire load and lambda sweep in terms of thermal efficiency. This can be attributed to the lower pumping works and reduced H_2 slip in the exhaust.

3. H2 DI operation required less boosting than the PFI setups, thanks to its higher volumetric efficiency. This translates to reduced pumping work and lower demand on the boosting system.

4. Both DI and PFI operations produced zero emissions of carbon dioxide (CO_2), hydrocarbons (HC), and carbon monoxide (CO). Additionally, both systems demonstrate ultra-low and near-zero NO_x emissions from lambda 2.5 to 3.7.

5. The DI H_2 system could be used with positive valve overlap for improved scavenging effects with little hydrogen slip. Further, a higher injection pressure of 40 bar contributes to an enhanced combustion process in high-load conditions.

6. The parameter of engine stability, LNV_{min}, was found to display a higher sensitivity and better representation of the overall engine ability compared to COV_{IMEP}. The DI and PFI operations exhibited exemplary stability across a wide range of lambda up to lean limits, where a sudden partial burn occurred without any initial sign of instability.

Additional studies on the potential benefits of passive and active pre-chamber have also been conducted, and the results will be presented in a future paper.

Chapter 10. Evaluation of Central-mounted and Side-mounted Direct Injection H2 Engine Operations

10.1 Introduction

An extensive examination was conducted to assess the performance, combustion, and emissions of a single-cylinder direct injection hydrogen spark ignition (SI) engine equipped with either a side-mounted direct injection (SDI) or a centrally installed direct injection (CDI) injector. The first part of the investigation analysed the engine's performance and emissions characteristics under CDI and SDI operations with varying injection timings and pressures. Subsequently, the performance and emissions were compared between CDI and SDI operations at different engine speeds and relative air-to-fuel ratios (lambda) using the optimised injection pressure and timings. Furthermore, the study evaluated the hydrogen engine's performance and emission attributes with the CDI and SDI setups at a fixed λ value of 2.75 across a broad range of engine loads.

10.2 Test Methodology

The testing process involved running an engine with either a CDI or SDI injector at a fixed load of 10 bar IMEP and a speed of 2000 rpm. The lambda value was set to 2.75 based on previous studies, which showed that this value delivers optimal performance with minimal air boost requirements and reduced levels of NO_x.

The first test aimed to determine the optimal injection pressure and timing for each hydrogen injector installation. The performance and emission sensitivity of the engine to the injector location were also evaluated. The testing points were operated at a target 50% mass fraction burnt (50%MB) at 8 degrees ATDCf. Spark timing was adjusted to operate at the Maximum Brake Timing (MBT) except when the engine reached one of the limits, which forced the operator to retire the spark.

The optimal injection configuration of each injector installation was identified based on the first test's results and applied to subsequent tests at 10 bar IMEP with different air/fuel ratios at low, mid, and high engine speeds. The performance and emission characteristics were evaluated at different loads ranging from 4 to 16 bar IMEP at three engine speeds to study the benefits of maximum cam overlap with a DI late injection.

To ensure accurate control, the intake temperature was fixed at 38 degrees Celsius using an inline air heater with PID control. The oil and water coolant temperatures were also fixed at 90 degrees with external heaters. The limits of the highest average in-cylinder pressure and maximum pressure rise rate (Rmax) were set to 12000 kPa and 600 kPa/CAD. A COVIMEP of 1.5% was used as the threshold for stable engine operation.

The λ values were measured by two wide-band lambda sensors in the exhaust line, calibrated with O_2 measurements from the Horiba emission analyzer, and then compared to a λ calculated from the H2 slip exhaust to validate the measured values. Finally, both intake and exhaust cams were fixed in both λ sweep and engine load sweep tests to

maintain the same scavenging effect before varying the cams. Table 10.1 summarises all test conditions.

Table 10. 1: Test conditions for CDI vs SDI.

Engine parameters	Unit	Fuel matrix	λ sweep test	Engine load sweep test
Engine Speed	rpm	2000	1500, 2000, 3000	1500, 2000, 3000
Engine Load	kPa	1000	1000	SWEEP
λ	-	2.75	SWEEP	2.75
Intake Cam positions	ATDCg	97	97	97
Exhaust Cam positions	BTDCg	102	102	102
Start of injection DI	BTDCf	SWEEP	150	150
Injection pressure CDI	kPa	SWEEP	3000	1000 at low load, 3000 from 800 kPa IMEP
Injection pressure SDI	kPa	SWEEP	2000	2000

10.3 Results and Discussion

This study presents a comprehensive analysis of the performance and emission attributes of downsized, highly boosted spark-ignition engines that operate solely on hydrogen using two different injection methods: central direct injection (CDI) and side-direction injection (SDI). We have gained valuable insights into engine operation under varying injection conditions by thoroughly assessing the fuel matrix. This leads to a better understanding of optimised injection parameters, including injection pressure and timing, as outlined in Section 4.1. By modifying λ values at different speeds under optimised conditions, we have identified engine combustion operation parameters and emissions while also investigating the impact of lambda variation on engine performance and emissions, as demonstrated in Section 4.2. The optimal λ has been identified using the results from the second phase. In the third phase of the experiment, optimal lambda has been maintained at a constant level across various engine speeds during load variation. This has allowed us to investigate the effect of load variation on engine performance with greater accuracy and precision.

10.3.1 Investigation of Fuel Matrix for Optimisation of Engine Operation at Different Injection Conditions

The primary objective of this study is to determine the optimal operational point for comparing spark-ignition direct injection (SDI) and compression-ignition direct injection (CDI) by varying the injection pressure and timing at a fixed load of 10 bar IMEP and engine speed of 2000 rpm. The air-fuel ratio (AFR) was set to 2.75, based on previous studies that showed NO_x emissions of less than 50 ppm. The boosted pressure was set between 130 and 170 KPA absolute. The cam timing was kept constant throughout the experiment.

The experiment involved varying the injection pressure between 10 and 40 bar for each setup, with a 10-bar step change and the injection timing between 230 to minimum and late injection angle, which varies due to higher injection pressure enabling later injection with a step of 10 degrees. The start of injection timing was varied between 230 degrees BTDCf and the delta pressure across the injector limited the end of injection. Thus, a higher pressure enabled late injection and reduced the risk of reverse flow across the injector.

Figure 10.1 illustrates the combustion stability analysis based on the coefficient of variation (COV) in IMEP. It is observed that the cyclic variation increased with the injection pressure for both CDI and SDI. Notably, the CDI maintained the COV in IMEP to less than 1.0 when the injection pressure was set between 10 to 30 bar injection. On the other hand, the SDI achieved similar stable operations with injection pressure between 10 to 20 bar. In general, the CDI exhibited slightly lower cyclic variability than the SDI. The SDI could not be operated at higher injection pressures above 35 bar. Furthermore, the SDI operations were limited to late injection timings when the injection pressure exceeded 30 bar. The differences in combustion stability between the SDI and CDI could be attributed to differences in in-cylinder motion and the distance and angle of the injection position.
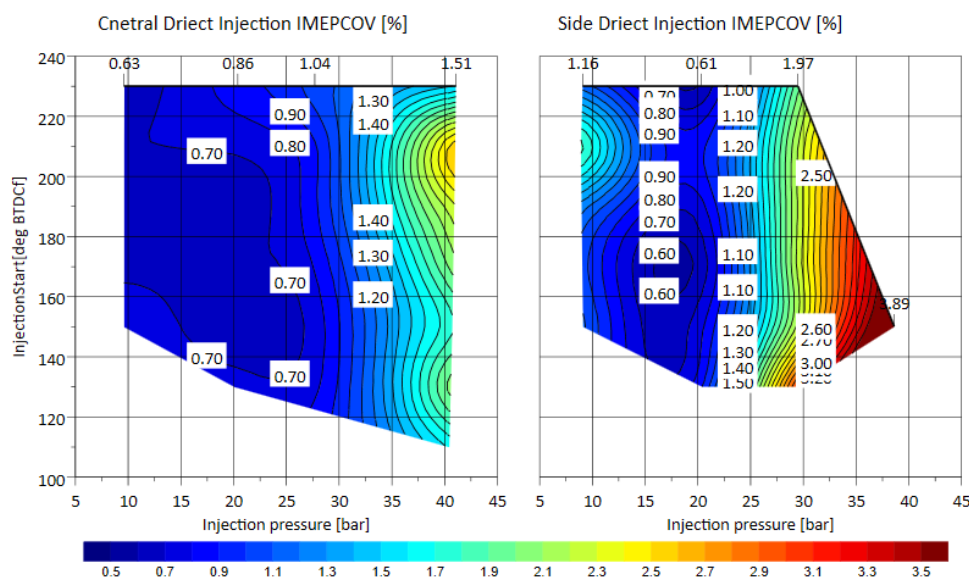
Figure 10. 1: COVIMEP [%] values at 2000 rpm and KPa IMEP for CDI and SDI

According to the data depicted in Figure 10.2, the thermal efficiency (ITE) of the CDI (compression-ignition diesel engine) was consistently 1.8% higher than that of the SDI (spark-ignition gasoline engine). Despite injection timing and pressure variations, the ITE remained relatively stable when the SDI was utilised. Conversely, the CDI exhibited some fluctuations in ITE, with the best thermal efficiency achieved at an intermediate injection pressure of 25 bar and an early injection of 200 degrees BTDC (before the top dead centre). These results suggest that implementing the CDI may improve thermal efficiency compared to the SDI and that optimising injection pressure and timing can further enhance the CDI's efficiency.
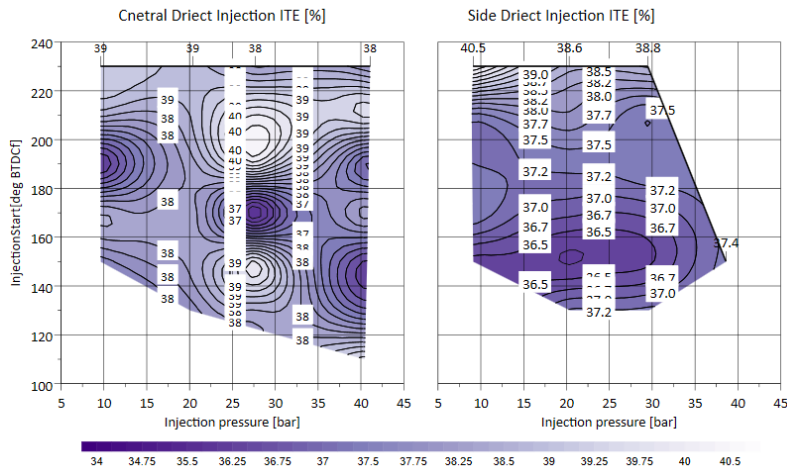
Figure 10. 2: ITE [%] values at 2000 rpm and 1000 KPa IMEP for CDI and SDI

Figure 10.3 illustrates the burn durations between 10% and 90%, which were analysed. The results indicate that the CDI operations had slightly longer main combustion durations than the SDI operations by 2.5 CAs. One possible reason for this is the improved mixing criteria of the CDI, which may lead to an increased likelihood of rich mixing pockets in the SDI. Furthermore, the CDI showed slightly longer burn durations at late injection angles. Overall, the burn durations of the SDI were less affected by fuel injection timings than the CDI.
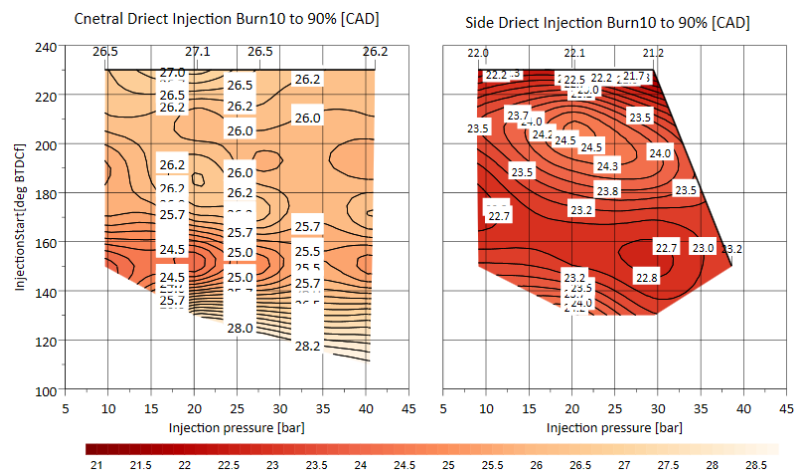
Figure 10. 3: The 10% to 90% burn duration [CA] values at 2000 rpm and 1000 Kpa IMEP for CDI and SDI

Figure 10.4 compares CDI and SDI's Pumping Mean Effective Pressure (PMEP) values. The findings indicate that CDI had almost 10 KPa lower PMEP values than SDI under identical injection conditions. This suggests that CDI has superior mixing criteria and lower pumping loss, which may account for the higher ITE observed in Figure 5. PMEP decreases when injection timing is delayed due to reduced air displacement during the intake process and in-cylinder conditions resulting from injected hydrogen.
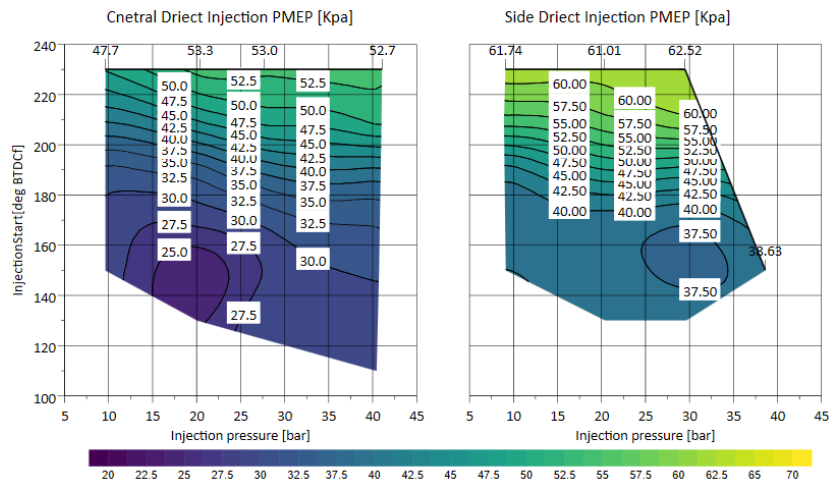
Figure 10. 4: PMEP [KPa] values at 2000 rpm and1000 KPa IMEP for CDI and SDI

The combustion of hydrogen results in only two exhaust emissions, namely NO_x and H_2 slip. The NO_x emission across the fuel matrix map is demonstrated in Figure 10.5. The CDI operations showed a slightly lower NO_x emission than the SDI operations. Due to the shorter mixing time, the increased NO_x emissions in the late injection region of the CDI operations were likely caused by the combustion of a slightly richer mixture. Similarly, NO_x emissions increased significantly with the retarded injections, particularly at lower injection pressures, where the injection duration was longer, and less time was available for fuel and air mixing to complete before ignition occurred.
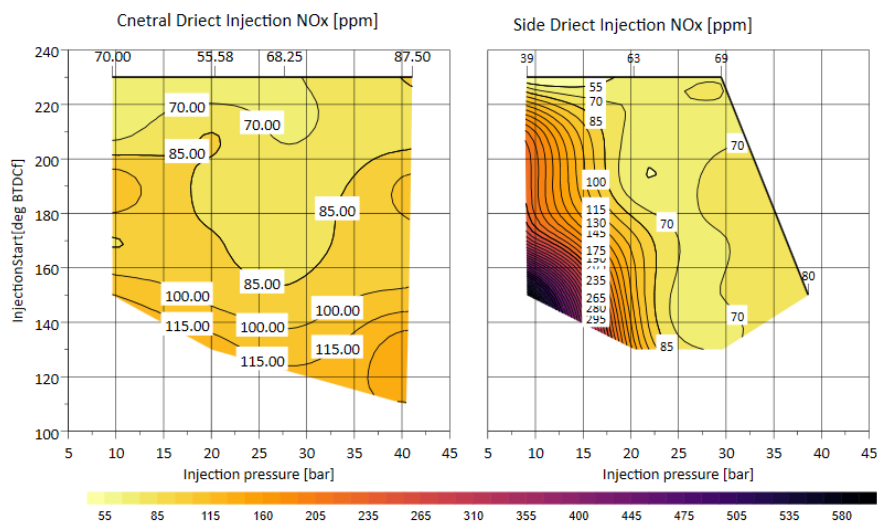
Figure 10. 5: NO_x [ppm] engine-out emissions at 2000 rpm and 1000 KPa IMEP for CDI and SDI

Figure 10.6 presents a graph illustrating the concentration of hydrogen in the exhaust, measured in ppm. The level of hydrogen slip is directly related to the efficiency of

combustion. The data indicates that the unburned hydrogen resulting from CDI operations was approximately 50% lower than that of SDI operations. Injection timing and pressure had little impact on the emission of unburned hydrogen from CDI operations. On the other hand, in the case of SDI operations, reduced injection pressures led to higher levels of unburned hydrocarbons, and the highest hydrogen slips were detected with the most delayed injection timings. As depicted in Figure 8, the region where SDI has higher NO_x emissions is also where the H_2 slip is more significant. These findings confirm the hypothesis that inadequate mixing of air with fuel in rich pockets contributes to increased NO_x emissions, especially when hydrogen slip is higher. The results suggest that the CDI system is superior to the SDI system in reducing hydrogen slip and minimising NO_x emissions.
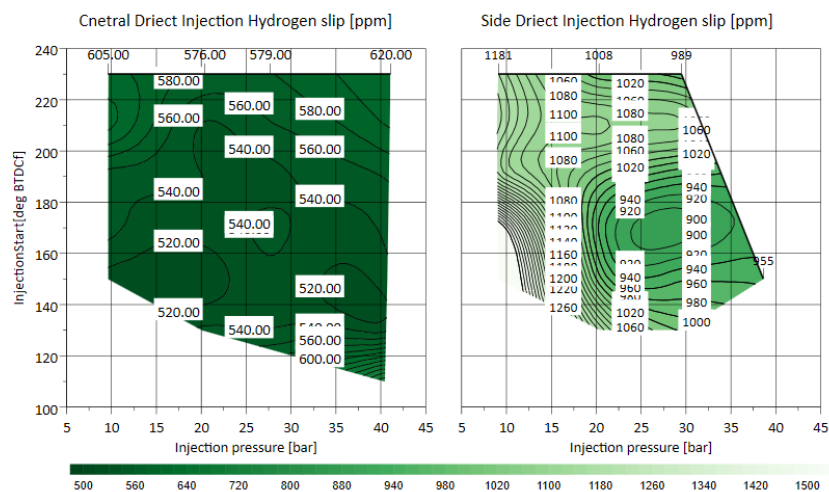
Figure 10. 6: The hydrogen concentration in the exhaust gas [ppm] at 2000 rpm and 1000 KPa IMEP for CDI and SDI.

The above results have demonstrated a CDI hydrogen engine's superior performance and reduced emissions compared to the SDI engine, regarding the reduced cyclic variability, higher thermal efficiency, and lower NO and unburned hydrogen emissions.

To understand the effect of injector positions, further studies are being carried out on the hydrogen injection and mixing processes through 3D-CFD simulations and high-speed imaging analysis in an optical engine.

10.3.2. Engine performance and emissions of the CDI and SDI operations at different engine speeds and air/fuel ratios

The present study compared engine performance and emissions of conventional and single diesel injection (CDI and SDI) operations across different engine speeds and varying air-to-fuel ratios (lambda). Specifically, the study evaluated performance and emissions at 1500, 2000, and 3000 rpm with lambda values ranging from slightly lean-burn (greater than 1.5) to ultra lean-burn (as low as 3.5) operation points.

Previous results indicate that the optimal region for CDI is at a 30-bar injection pressure with a start of injection timing of 150 degrees before the top dead centre (BTDCf). In contrast, SDI can function at the same start of injection timing, but the higher coefficient of variation necessitates a lower injection pressure of 20 bars only. For higher load and speed operation points, the start of injection for SDI may need to be retarded to 160 degrees BTDCf to avoid the risk of reverse flow due to the higher in-cylinder pressure.

Figure 10.7 illustrates that CDI and SDI setups enable the engine to operate in a wider range of lambda values. The lowest lambda or richest mixture limit was determined by the rate of maximum pressure rate of 600 kPa/CAD, as shown in Figure 10.8. The lean-burn limit was set at the LNVmin threshold of 89%. At and beyond the lean-burn limit, some misfires and partial burning cycles were detected. This is particularly noticeable at a lambda value of around 3.5 for Central DI. In most cases, the spark timing (ST) was set to the Minimum ignition advanced for Best Torque (MBT).

Moreover, Figure 10.7 shows that the highest thermal efficiency was achieved from lambda = 2.75 to 3.6 while fluctuating slightly between 36 and 40 for both CDI and SDI. CDI operations exhibited slightly higher thermal efficiency than SDI for a given lambda value in this range. The indicated thermal efficiency (ITE) decreased as the relative air-to-fuel ratio was reduced from 2.5 to 1.5, and CDI maintained higher efficiency than SDI operations.

The decrease in thermal efficiency with lambda is mainly due to the reduction in the specific gas ratio of the mixture, as stated by the standard Otto cycle analysis, and the slightly increased heat loss from higher combustion temperature gases. Additionally, as the relative air-to-fuel ratio was decreased beyond lambda=2.0, the spark timing had to be retarded to reduce the maximum rate of pressure rise, delaying the 50% MB point away from the optimum point.
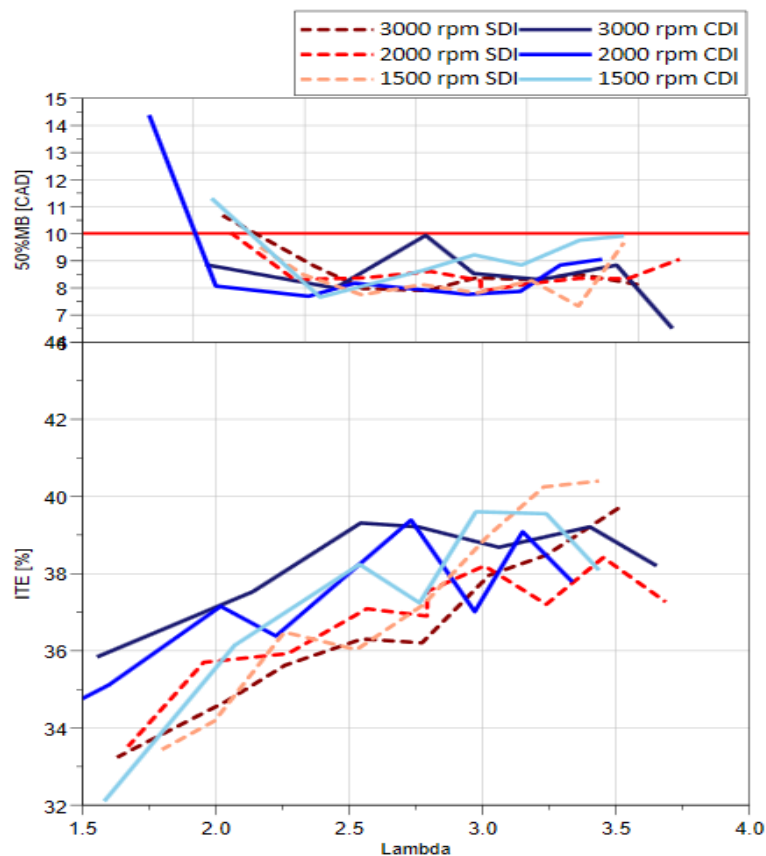
Figure 10. 7: The 50% mass burn rate and thermal efficiency results for both CDI and SDI systems at different λ values and engine speeds

The data presented in Figure 10.8 shows the results of experiments conducted on the LNVmin, COV of IMEP, and Rmax of both central and side direct injection strategies for different engine speeds over the lambda range from 1.5 to 3.5. The hydrogen side direct

injection (SDI) and the central direct injection (CDI) setups exhibited highly consistent and stable combustion throughout the extensive lambda range, showing less than a 1.5% variance. However, it is worth noting that the COVIMEP experienced a slight increase (up to 0.5%) as the lambda moved towards lean operating limits. The engine experienced sudden misfires due to leaner combustions, which caused it to operate in a dangerous region. Despite the instability and superpipe misfire, capturing this phenomenon and conducting testing under these conditions is essential to explaining the trend at CDI 3000 rpm and understanding the root cause of misfires, enabling appropriate solutions.
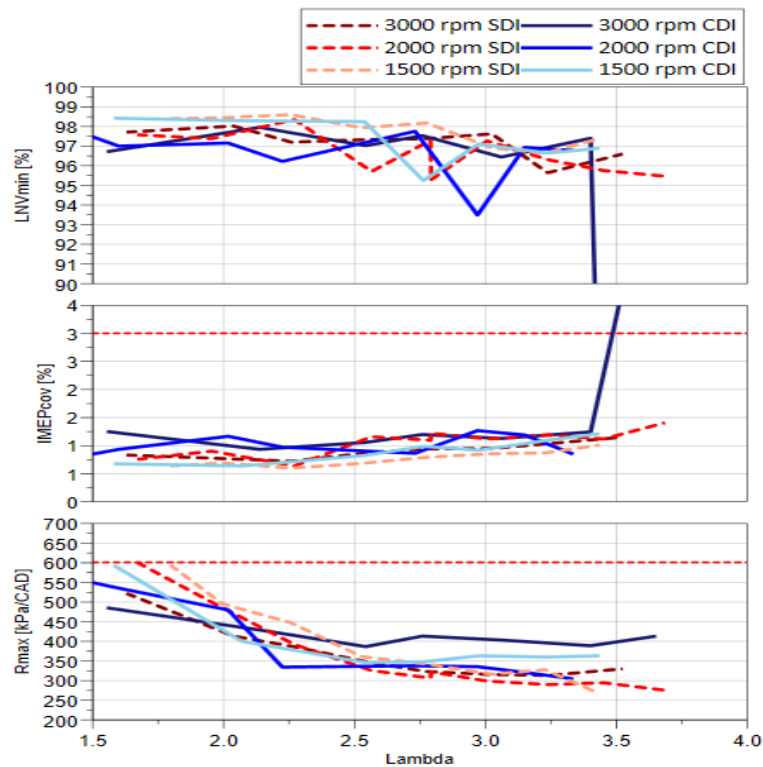
Figure 10. 8: Engine lowe net value, coefficient of variation, and the maximum pressure rise rate.

The SDI operations had slightly lower cyclic variation. As the lambda value was reduced to 1.75 and lower, the spark timing had to be retarded, as shown in Figure 10.9, to prevent the pressure rise rate from exceeding the limit of 600 kPa per crank angle. Figure 10.8 shows the characteristics of spark timing and burn duration in three different graphs. As the lambda was decreased, the flame speed increased, and combustion durations were reduced, leading to more retarded MBT spark timings. Additionally, more retarded spark timings than MBT were used to avoid excessive rates of pressure rise when the lambda value was less than 1.75. The SDI operations were generally characterised by a slightly shorter combustion duration, probably due to the faster burning of a slightly stratified charge mixture. This disparity can be attributed to variations in injector position, hydrogen distribution and mixing within the cylinder, and the impact of CDI's tumble motion charge effect compared to SDI. To validate these observations, computational fluid dynamics (CFD) and optical diagnostics are used in an optical engine analysis to study the in-cylinder mixture formation process.
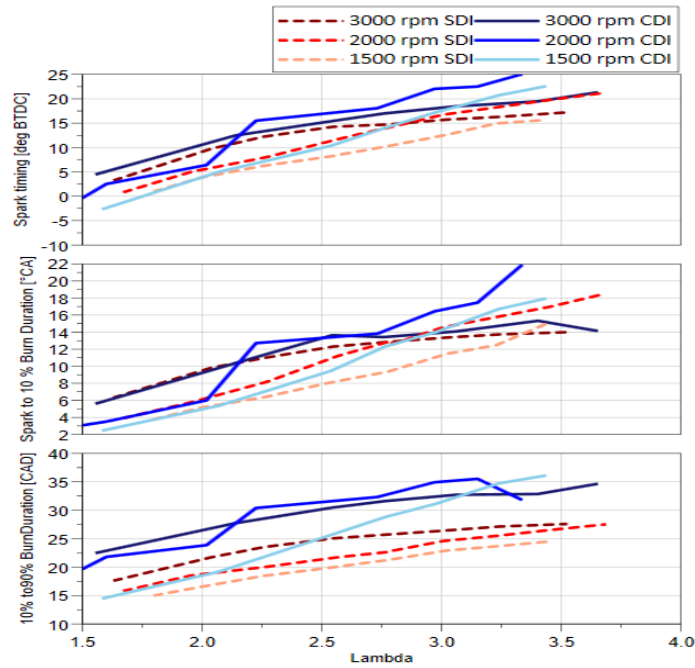
Figure 10. 9: The spark timings and burn durations for both CDI and SDI operations

This disparity can be attributed to variations in injector position, hydrogen distribution and mixing within the cylinder, and the impact of CDI's tumble motion charge effect compared to SDI. To validate these observations, computational fluid dynamics (CFD) and optical diagnostics are used in an optical engine analysis to study the in-cylinder mixture formation process.
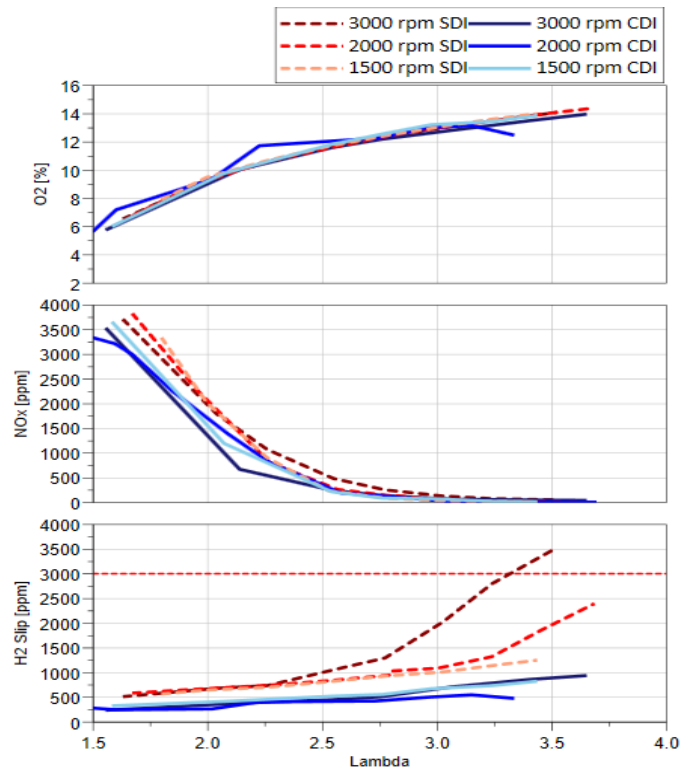
Figure 10. 10: Engine-out emissions of O_2[%], NO_x[ppm], and H_2 slip[ppm]

To assess the accuracy of the measured air-fuel ratio (λ) by the lambda sensors, exhaust gas composition was used to calculate the air-fuel ratio (AFR) based on the hydrogen combustion, as shown in Figure 10.11 The lambda values were carefully measured and found to align with those derived from the exhaust gas composition. Nonetheless, a minor discrepancy arose beyond λ three due to the differing traits of λ and O_2 sensors, which display a sharper curve about O_2 concentration. This divergence becomes more noticeable when examining NO emissions levels below 10 ppm. Consequently, emission analysers experience elevated uncertainty in such scenarios, particularly in leaner conditions.
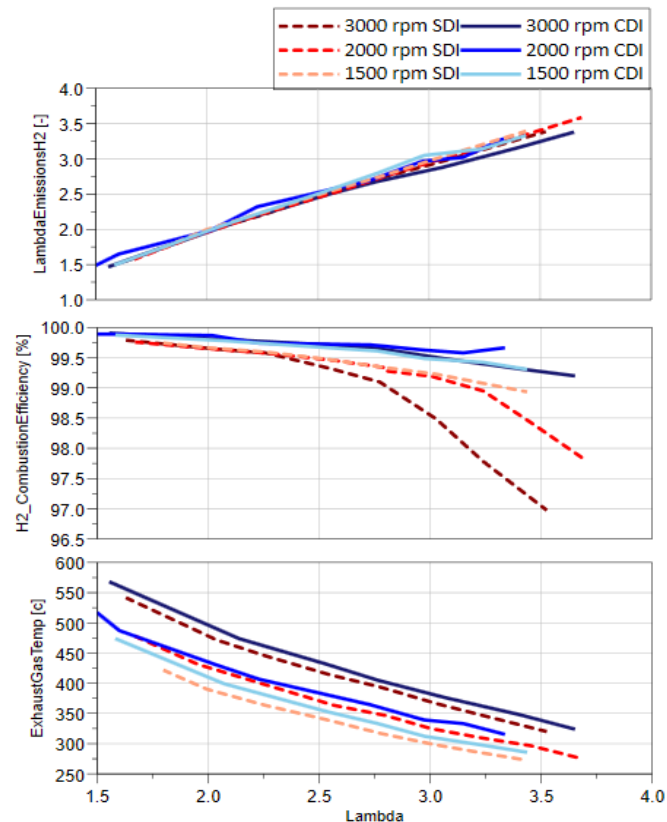
Figure 10. 11: The relationship between the estimated and measured λ emission based on λ values and the exhaust gas temperature

The combustion efficiencies decreased with lambda as more unburned hydrogen was left in the exhaust due to lower combustion temperatures with leaner mixtures. The CDI setup has been proven to outperform the SDI setup in terms of wider engine operation range, from near stoichiometric to very lean-burn operations and higher thermal efficiencies. Notably, the CDI setup displayed significantly lower hydrogen slip in the exhaust and lower NO_x emissions than the SDI operations. These results indicate that the CDI setup exhibits improved combustion efficiencies, resulting in lower unburnt hydrogen and higher exhaust gas temperatures due to retarded end of combustion. The decrease in exhaust temperatures with lambda values is expected due to the lower combustion temperature of leaner mixtures. Based on the analysis of these results, further experiments were conducted to examine the performance and emissions of both CDI and SDI operations for a fixed lambda value of 2.75, which achieved maximum thermal efficiency, minimum NO_x emissions, and hydrogen emissions simultaneously.

10.3.3 Engine Performance and Emissions of The CDI and SDI Operations at Lambda 2.75

This section assesses the performance and emission characteristics over various engine loads, from low to high levels. The evaluation applied to SDI and CDI setups and was carried out at a fixed λ value of 2.75.

Figure 10.13 illustrates the 50% MB points and the ITE for both injector setups, indicating that the CDI operations exhibited consistently higher thermal efficiencies than the SDI operations by around 1%-4%. The difference in ITE between the CDI and SDI was more pronounced at lower load operations, and the effect of engine speed on ITE values was more significant for the SDI operations. The ITE decreased at light load operations due to increased pumping works.

Moreover, the decrease in ITE was observed at a relatively high load of 1000 KPa IMEP when the engine was operated with the side injector compared to CDI operations that maintained high efficiencies until the load was reduced below 600 KPa IMEP. The 50% MB points were kept around 8 CAD by the MBT spark timing in most cases except the highest load point of 1500kPa when the 50% MB of fuel exceeded 10 CAD at the very high load limit of 1500 Kpa.

The results in Figure 10.14 explain the range of load operations, where COVIMEP was around 1.5% and increased towards both high and low-load operations. In the case of SDI, the limit of 3% was reached and exceeded at 3000 rpm at low engine loads of IMEP < 600. This is also reflected by the lower LNVmin value at the same conditions for SDI. Additionally, the limited range of the direct injectors with a minimum injected pressure of 10 bar caused higher instability at very low loads, such as 100 and 200 KPA IMEP.

Finally, Figure 10.12 indicates that the SDI fuel injection system has marginally higher pumping losses than the CDI system.
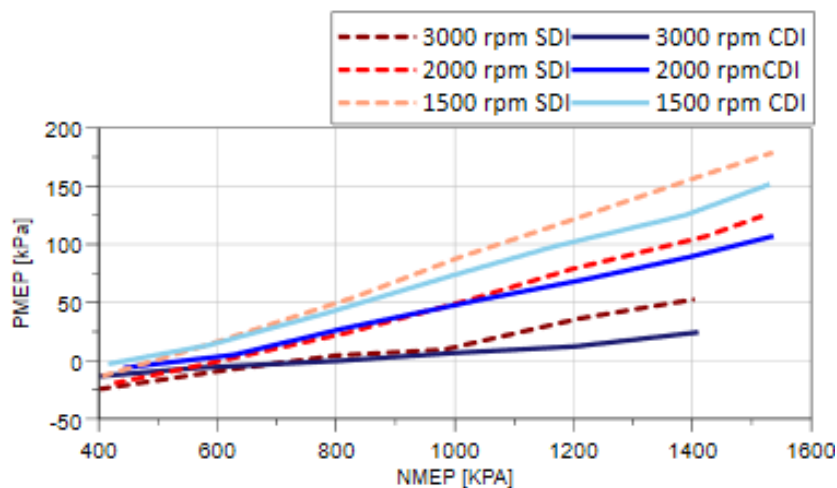
Figure 10. 12: PMEP vs load sweep for SDI and CDI at different speeds
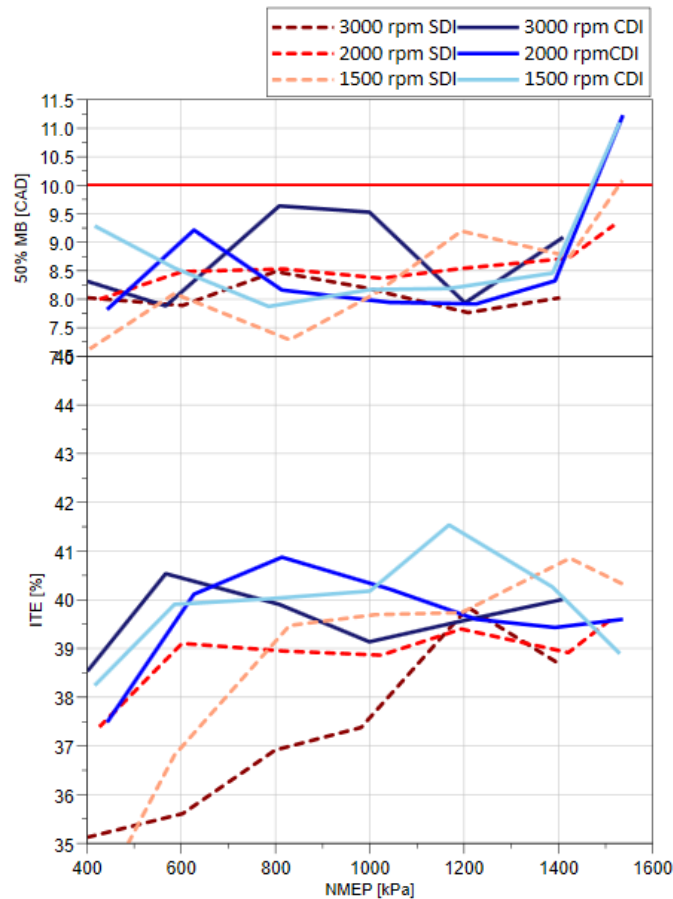
Figure 10. 13: 50% Mass fraction burned points and Indicated thermal efficiency as a function of load and speed at a constant lambda 2.75

In Figure 10.15, the start of injection timing, spark to 10%, and 10% to 90% of mass fraction burnt duration in crank angles are depicted to illustrate the combustion characteristics. CDI consistently exhibited longer burn duration than SDI, similar to the λ sweep experiment. While the combustion durations in crank angles increased with engine speed, they remained almost constant in absolute times. It is worth noting that the combustion duration was slightly increased with load, indicating slower hydrogen combustion at elevated pressure.

Moving on to Figure 10.16, the oxygen percentage O_2 (on the top), the NO_x emissions (in the middle), and the H2 Slip (at the bottom) are shown. Across all engine load conditions, higher hydrogen concentration was detected for SDI operations, contributing to the lower ITE of SDI operations highlighted previously. As engine load increased, the NO_x emission for both SDI and CDI increased due to higher combustion temperatures, but the NO_x level remained under 100 ppm in the low load range of 400 to 800 Kpa. As the load increased above 1200Kpa IMEP, the NO_x emissions increased rapidly for both SDI and CDI operations. In addition, the NO_x dependency on engine speed was more pronounced in SDI operations than in CDI. Finally, it can be observed from Figure 10.12 that the O_2 percentage for both CDI and SDI methods remained almost constant at 12.5% since lambda was kept constant at the value of 2.75.
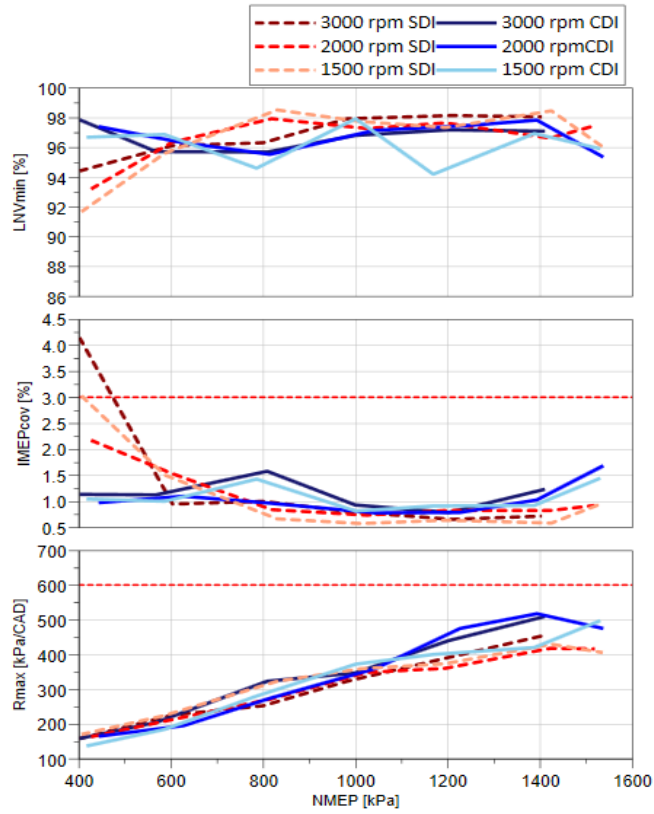
Figure 10. 14: Operational constraints as a function of load and speed at a constant lambda 2.75
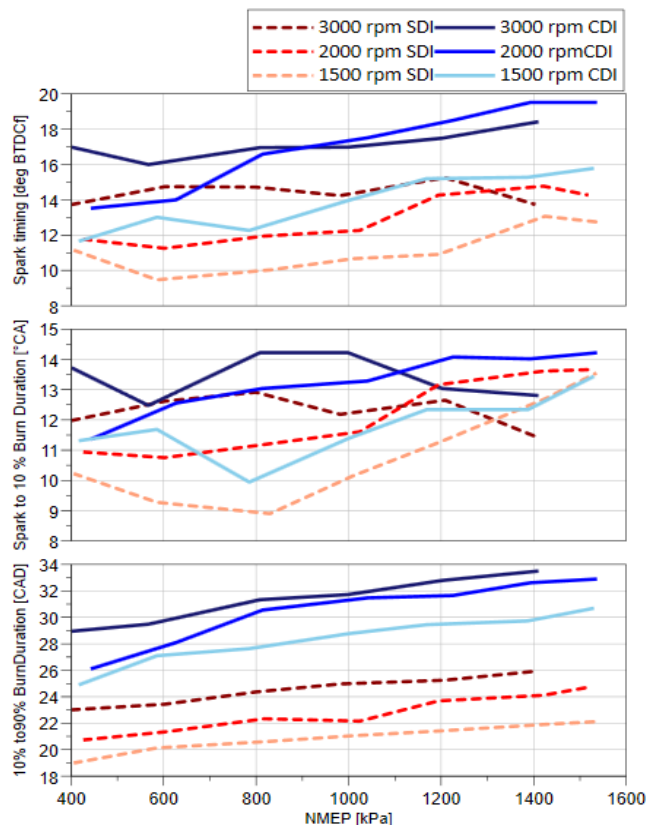
Figure 10. 15: The spark ignition timing and burn durations as a function of load and speed at a constant lambda 2.75
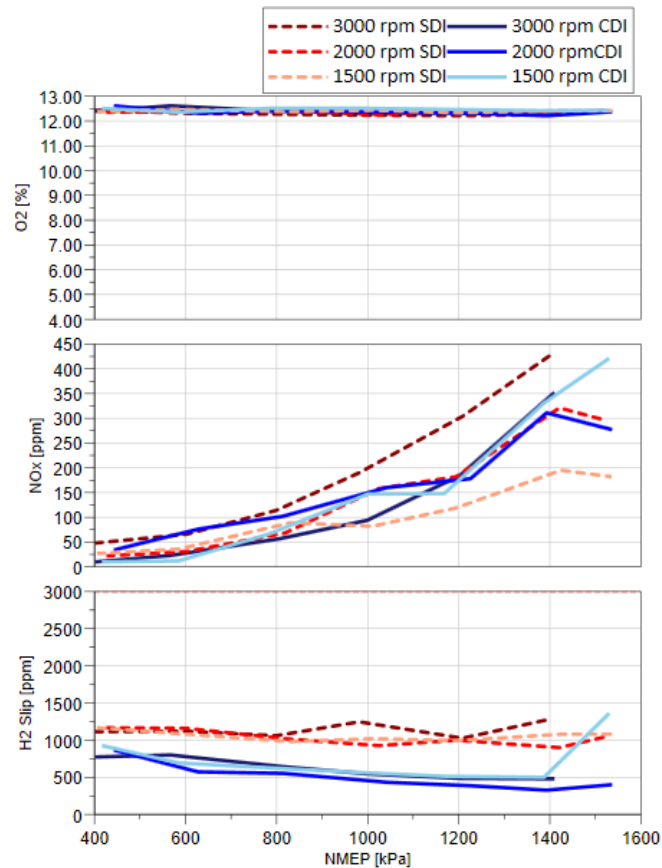
Figure 10. 16: The main three outputs from the tailpipe, Oxygen, NO$_x$, and H$_2$ slip as a function of load and speed at a constant lambda 2.75

In Figure 10.17, there was an exact match between the lambda values measured by the lambda sensor and those calculated by the exhaust gas analysis. The graph demonstrates that while the lambda sensor readings remained at 2.75, the calculated lambda values remained within an acceptable error margin of around 0.05, ranging from 2.7 to 2.8. Moreover, at the same speed condition, the exhaust gas temperature was noticeably higher in CDI mode than in SDI mode, consistent with the lambda sweep experiment.

Regarding higher engine speeds, the Exhaust Gas Temperature (EGT) tends to depend more on engine speed when the engine load increases from low to high values. This is due to the greater heat release per unit of time at these higher engine speeds.

Based on the engine load sweep test at constant lambda and various speeds, we can confidently conclude that CDI operations have superior efficiency, load range performance, and fewer NO$_x$ and hydrogen emissions compared to SDI operations in all load conditions, albeit with only a small difference.
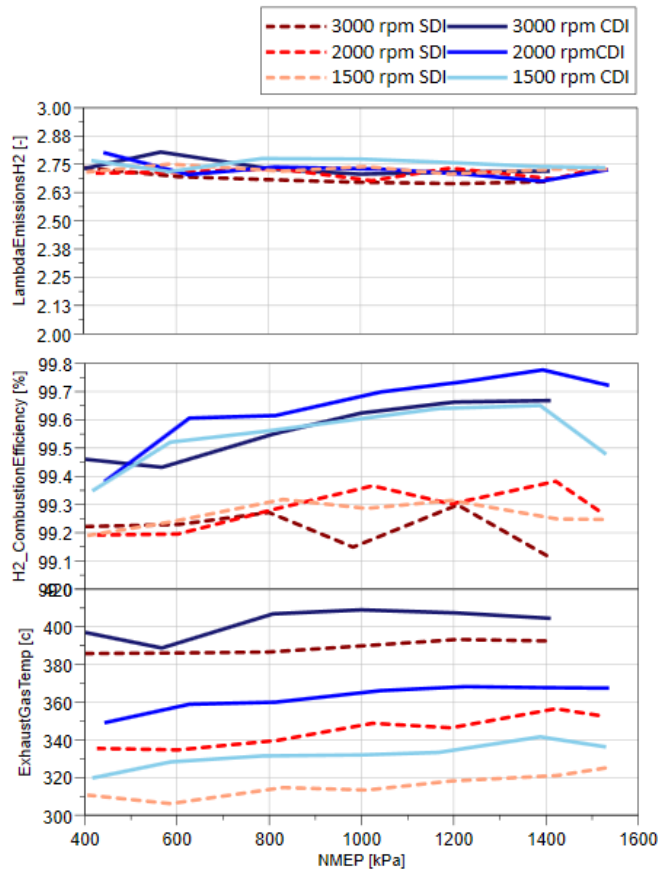
Figure 10. 17: The hydrogen combustion efficiency and exhaust gas temperature as a function of load and speed at a constant lambda 2.75

10.4 Conclusion

This study presents the results of extensive engine experiments conducted on a single-cylinder hydrogen direct injection spark ignition engine. The study aimed to analyse the effect of the hydrogen injector's location on the engine's performance, thermal efficiency, NOₓ, and hydrogen emissions. The same engine and test equipment were used for the investigation.

The study demonstrates, for the first time, that the centrally mounted hydrogen direct injection injector (CDI) setup enables the hydrogen engine to achieve superior performance over the side-mounted injector (SDI) operations across different engine speeds and loads at different relative air-to-fuel ratios. The highest thermal efficiency was obtained in the lambda range of 2.75-3.5. The CDI hydrogen engine achieved higher thermal efficiency than the SDI operations, ranging from 1.5% at higher load to 4% at lower load operations when the relative air-to-fuel ratio was kept constant at 2.75.

The CDI and SDI hydrogen engine setups could operate with a wider range of air-to-fuel ratios. However, the CDI setup enabled the hydrogen engine to operate with even wider operations, extending the lean-burn limit to lambda=3.8. The peak cylinder pressure and maximum pressure rate limited the stoichiometric operation. Additionally, the hydrogen engine could be operated with a wider range of injection timings and injection pressure

between 10 and 40 bar, whereas the SDI operations were better suited with injection pressure around 20 bar and more restricted injection timings.

The SDI operations were characterised by shorter combustion durations than the CDI by several crank angles but slightly lower combustion efficiency by 0.2-0.5%, associated with higher hydrogen slip in the exhaust.

The two injection systems' emission characteristics were similar, with increased NO_x emissions with engine speed and load. NOx levels remained under 100 ppm in the low load range of 400 to 800 kPa IMEP. As the load increased above 1200 kPa IMEP, the NO_x emissions increased more rapidly. However, the CDI operations produced 50% less NO_x emissions and much less H_2 slip than the SDI operations when the hydrogen engine was operated at a constant lambda of 2.75.

The study's findings suggest that the hydrogen injector's location plays a significant role in the direct injection hydrogen engine's performance and emissions. The observed differences in both engines' performance and emissions are believed to be mainly caused by the in-cylinder mixing processes. CFD studies and high-speed optical measurements are being carried out on a single-cylinder optical engine with either a centrally-mounted or a side-mounted hydrogen injector to better understand the impact of the hydrogen injection process.

Chapter 11.Experimental Investigation of NO_x Emission Characteristics in Hydrogen Internal Combustion Engine

11.1 Introduction

A comprehensive study was carried out to assess the NO_x emissions for a hydrogen ICE with different injection modes compared to gasoline. The study involved varying the relative air-to-fuel ratio (AFR) from stoichiometric to the lean-burn limit in a boosted spark ignition (SI) engine fuelled with gasoline or hydrogen. A fast NO_x emissions analyser was employed to measure the instantaneous NO and NO_2 emissions in the engine exhaust.

The study offers a comprehensive analysis of NO_x emissions at multiple levels. It begins with an analysis of steady-state averaged emissions, followed by an analysis of average crank-angle domain NO_x distribution and emissions, along with in-cylinder pressure analysis. Furthermore, time and cycle analyses assess NO_x emissions' temporal and cyclic variations.

Therefore, this study conducted a comprehensive assessment across three phases.

This study provides valuable information on NO_x emissions from hydrogen and gasoline combustion in the same engine, which can help design cleaner and more efficient engines.

The present study employed an ultra-fast response NO_x analyser, specifically the Cambustion CLD50 fast $NO\&NO_2$ analyser, for conducting the experiments. This analyser is distinct from standard analysers in that it has a response time of approximately five milliseconds in the configuration used in these experiments and is sensitive to tens of parts per billion. Thus, it is well-suited for measuring transient NO and NO_2 in the exhaust of H_2 combustion engines, where very low NO_x levels can be attained, but sudden operating condition changes can cause spikes in NO_x levels. The exhaust flow rate and pressure will produce varying delays in various engine load and lambda scenarios. Furthermore, the 1.2-meter length and the T90 response time consistently introduce an inherent delay. To address this issue, the commencement of the NO_x measure ramp is synchronised with the exhaust valve opening time within the crank domain.

11.2 Test Methodology

This research aims to thoroughly analyse the NO_x emission characteristics of conventional gasoline and hydrogen combustion engines. The study considers the NO_x formation mechanism and its dependency on the AFR. The engine was operated at a mid-load and speed point of 10 bar IMEP and 2000 RPM, respectively. The lambda values for each fuel were varied from lambda=1 to the maximum lean points.

The study employed a fixed intake temperature of 38 °C to maintain consistency, while oil and water temperatures were maintained at 90 °C. The intake cam maximum opening was set at 97 degrees after the gas exchange top dead centre (ATDCg), while the exhaust cam was fixed at 102 degrees before the gas exchange top dead centre (BTDCg). Moreover, the injection timing and pressure were optimised for each fuel to ensure that both fuels operated at the maximum brake torque (MBT) point.

As described in Chapter 7, a Cambustion fast NO$_x$ emissions analyser was connected to the back of the exhaust valves using a 1.2-meter emissions pipe. And a sampling rate of 0.25 per crank angle.

This research compares the engine performance characteristics and constraints of hydrogen and baseline gasoline fuel under identical engine configurations, intake temperature, and air humidity conditions. The table in the study provides details of the operating conditions at test points. Table 11.1 shows the operation conditions at test points.

Table 11. 1: The operation points for the fast NO$_x$ engine-out emissions

Engine parameters	Unit	λ sweep test
Engine Speed	rpm	2000
Engine Load	kPa	1000
λ	-	SWEEP
Intake Cam positions	ATDCg	97
Exhaust Cam positions	BTDCg	102
Start of injection H2 DI	BTDCf	150
Start of injection gasoline DI	BTDCf	300
Injection pressure H2 DI	kPa	3000
Injection pressure gasoline DI	kPa	100000
Intake air Temperature	°C	40

11.3   Results and Discussions

The results are presented in two stages: first, the results associated with PFI and GDI fuelling during lambda sweeps, and second, the study evaluates NO$_x$ emissions within the average crank-angle domain to demonstrate the average levels of NO$_x$ emissions observed across 300 cycles, including analysing NO$_x$ emissions using in-cylinder data in the time domain enables the observation of fluctuations in NO$_x$ levels over a specific period.

11.3.1 Impact of Lambda on Average NO$_x$ Emissions

This section presents a study that explores the performance and NO$_x$ emission characteristics of a specific vehicle (identified as H2 ICE) compared to baseline gasoline engines across a broad range of relative AFRs. To ensure consistency, all operation points at different relative AFRs were fixed at 50% burn of 8 degrees ATDCf to maintain MBT. With cam timing fixed for each fuel, the scavenging effect from the overlap was fixed. Figure 11.1 displays the Indicated Thermal Efficiency (ITE) of central DI H2 and gasoline fuel over various lambda values up to the limits of the COV in IMEP. The results illustrate the vast relative AFR map of hydrogen compared to the narrow range of gasoline

operations. Hydrogen DI operates from stoichiometric combustion to a maximum relative AFR of 3.8, with COV in IMEP below 1.6%.

Meanwhile, gasoline DI managed to operate up to lambda of 1.6 at 2% COV and a maximum lambda of 1.8 at 4.2% COV. The ITE results indicate that hydrogen has a higher ITE of 41% compared to gasoline's 37.4% at the leanest operating points. However, the lower ITE of hydrogen at stoichiometric operations is due to a higher hydrogen slip from the exhaust system. It is important to note that the engine was designed and built for gasoline fuel and adopted hydrogen without any modifications. The study also found that the value of the H2 slip increases with leaner combustions, but it remains below the threshold.
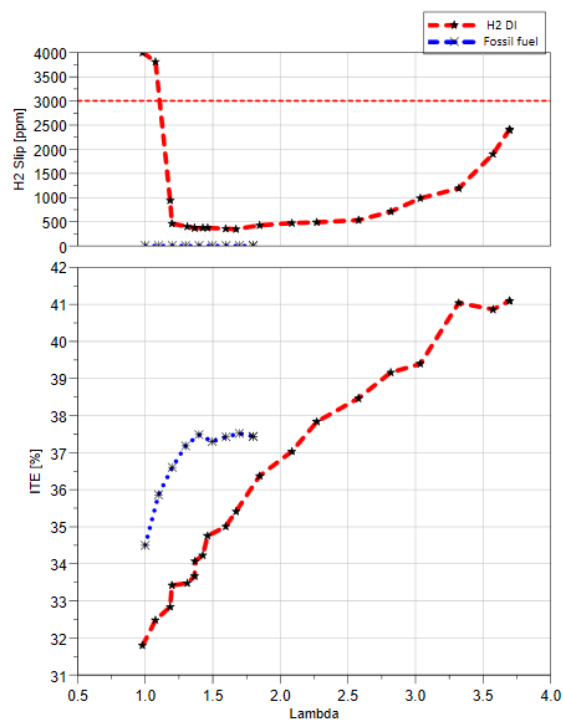
Figure 11. 1: Hydrogen slip in the exhaust and Indicated thermal efficiency for gasoline vs hydrogen at different lambda.

The data presented in Figure 11.2 illustrates the mean NO_x emission captured by the fast NO_x emission analyser in the exhaust port while varying the relative AFR for hydrogen DI and PFI compared to gasoline DI. The results indicate that hydrogen usage leads to a negligible NO_x emission above lambda 3. NO_x levels drop below 50 ppm from lambda 2.75, and an exponential increase in NO_x emission is observed when lambda reduces from 2.5 to 1.4, with peak NO_x emissions captured.

The graph in the study shows slightly lower NO_x emissions for the hydrogen PFI system than the hydrogen DI system. This is due to the complete burn and the higher thermal efficiency of the DI system, which results in a higher in-cylinder gas temperature that causes higher NO_x at the same load. However, at lambda 2.75, the difference is almost negligible, and at lambda 3, the NO_x emissions fall below 10 ppm for both hydrogen injection systems. Additionally, the NO_x emissions for the PFI system match those of the DI at a lambda of 1.5 where the backfire starts appearing in the intake line for the PFI.

Furthermore, a comparison of NO_x emissions between the direct injection systems of hydrogen and gasoline reveals that at stoichiometric combustion operations, the NO_x

emission is lower in hydrogen than gasoline by almost 41%. This is due to H_2 slip at lambda 1, resulting in lower thermal efficiency and lower peak cylinder temperature. The study also observed that the lambda point of the peak NO_x emissions of each fuel was different, with gasoline at lambda 1.3 and hydrogen at lambda 1.38. This is influenced by the fuel properties that directly affect the NO_x formation mechanisms.

This section aimed to identify the NO_x emissions characteristics and the ITE of both hydrogen and gasoline engines. The presented data indicate the average NO_x emissions at each testing point.
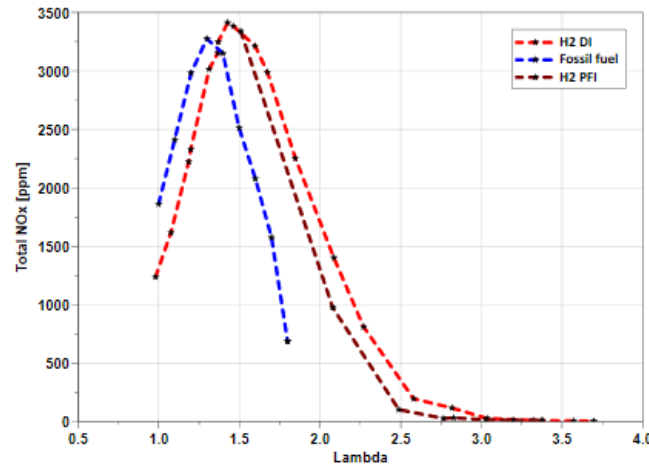
Figure 11. 2: NOx emission for gasoline and hydrogen at different lambda values with fixed load and speed of 10 bar IMEP and 2000 rpm.

11.3.2. Analysis of NO_x Emissions in The Crank-angle Domain

This section presents the NO_x emission data and in-cylinder pressure in the crank-angle domain to illustrate the NO_x emission characteristics and distribution. Additionally, the study breaks down the NO_x emissions to analyse the distribution of NO and NO_2 separately over the crank-angle domain. Furthermore, the study directly compares the NO_x emission and in-cylinder pressure under very lean operation conditions by comparing the hydrogen DI and PFI systems. The aim is to provide an in-depth understanding of NO_x emission behaviour and distribution in the crank-angle domain, which could help improve engine performance and develop emission control strategies.

Figure 11.3 shows the NO and NO_2 emissions from the hydrogen DI system with a very lean combustion of lambda 3.3. The graph illustrates the distribution of NO and NO_2 in the crank-angle domain and the averaged in-cylinder pressure over 300 cycles. The results indicate that the NO_2 levels are approximately 4 particles per million (ppm). Meanwhile, NO emissions are below 2 ppm. The effect of the exhaust opening event is visible at around 170 degrees after the firing top dead centre (ATDCf), corresponding to the exhaust valve opening timing. At this operating point, the NO2 emissions are higher than NO due to the higher error gain of NO_2. However, both NO and NO_2 values are within the measurement range, indicating that both emissions are negligible.
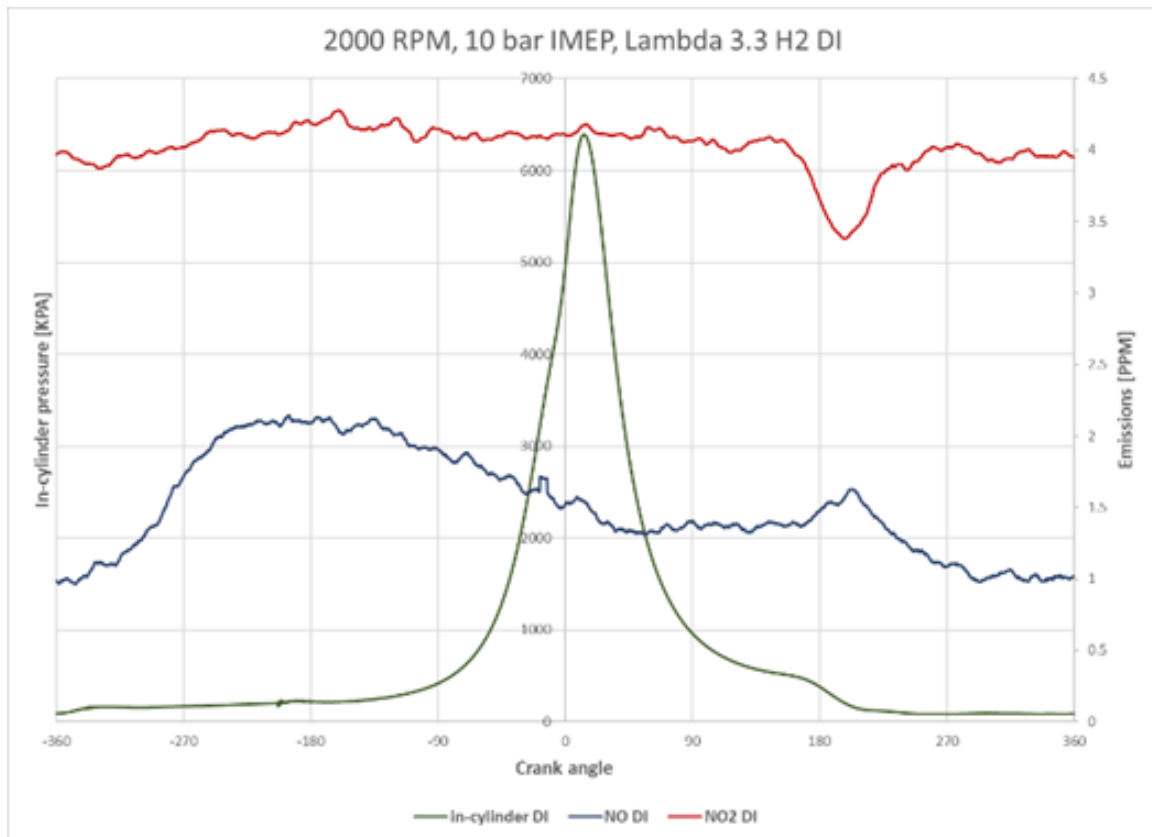
Figure 11. 3: Averaged NO and NO_2 emissions for DI hydrogen in the crank-angle domain at lambda of 3.3.

The correlation between emissions and in-cylinder pressure at a lambda of 2.75 is displayed in Figure 11.4, which is considered the optimal point for engine operation due to the lowered requirement for boosted air and minimized NO_x emission. The figure illustrates that the hydrogen DI and PFI systems generated nearly identical in-cylinder pressure, with a peak pressure of 6878 KPa at 6 degrees ATDCf. Notably, NO emissions contribute to 80% of the total NO_x emissions, with NO_2 accounting for only 20%.

Additionally, the results indicate that the DI system produces 14 ppm higher NO_x emissions than the PFI system, indicating a higher thermal efficiency. Intriguingly, NO distribution across the crank-angle domain shows saturation on the exhaust opening side, with the NO peak detected during the intake stroke. This delay is due to the overall low NO concentration.

This information is critical for researchers and engineers in the automotive industry, as it provides valuable insights into the impact of fuel injection systems on engine performance and emissions.
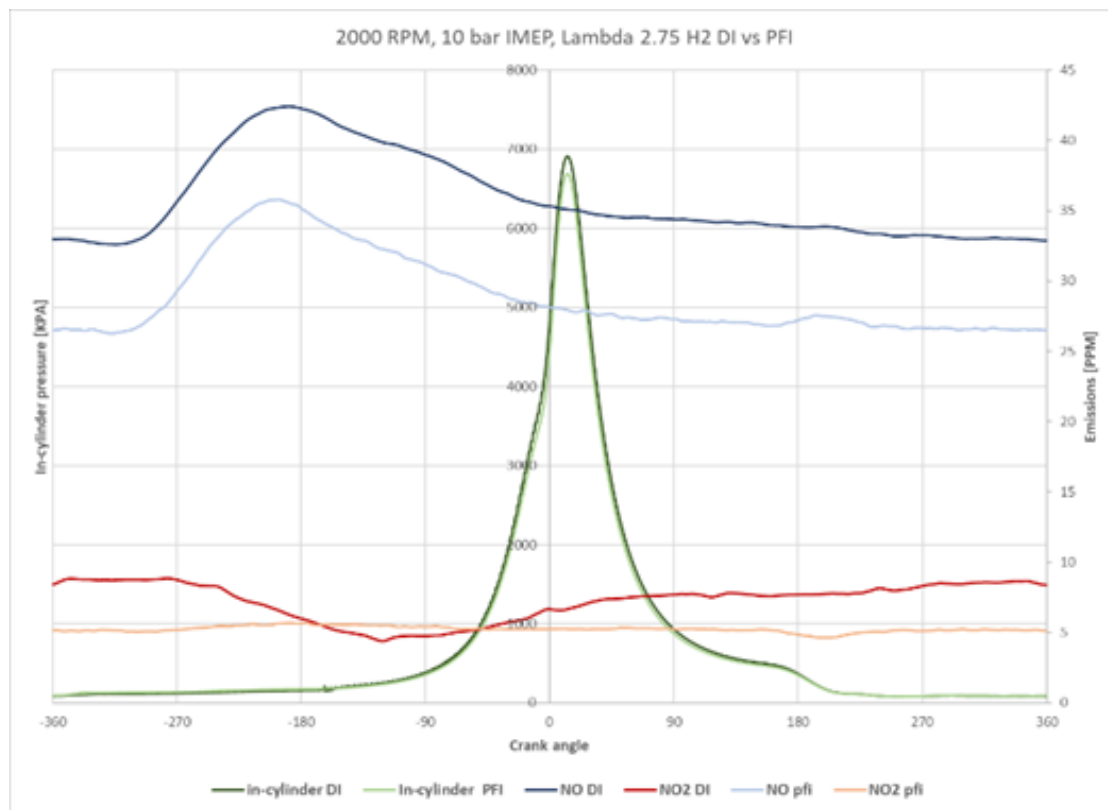
Figure 11. 4: Averaged No and NO_2 emission for DI and PFI hydrogen in the crank-angle domain at lambda value 2.75.

The data presented in Figure 11.5 showcases the rapid NO and NO_2 emissions characteristics at a lambda of 1.5 with the hydrogen DI system. It is worth noting that this particular lambda has the highest NO_x emissions, emphasizing the importance of monitoring and adjusting spark timing carefully to ensure efficient and safe engine operation. The accompanying diagram illustrates a significant NO spike occurring at 156 degrees ATDCf, approximately 5 degrees after the exhaust valves' opening time. Moreover, it shows that the NO peak location corresponds with the exhaust valve opening peak.

These findings indicate the crucial role of spark timing in minimizing NO_x emissions in engines, particularly at high lambda values. Optimizing spark timing while considering the exhaust valve timing is vital in reducing NO_x emissions and ensuring safe and efficient engine operation.

In Figure 11.6, we compare NO_x emissions directly over the crank-angle domain for the hydrogen and gasoline DI systems at lambda 1.3, where a peak of NO_x emissions was observed for gasoline fuel. Both fuels exhibit less than 10% fluctuation levels over the cycle. However, hydrogen's NO_x emissions are 9.3% lower than gasoline.

Furthermore, in-cylinder pressure data reveals operational differences between the two fuels. Gasoline demonstrates a lower in-cylinder pressure of almost 1000 kPa than hydrogen. Additionally, the retarding of spark ignition timing for hydrogen operation is indicated by the location of peak in-cylinder pressure, which is approximately 13 crank angle degrees after the peak in-cylinder pressure for gasoline. This feature significantly impacts the ITE of the hydrogen DI system when operating at this lambda configuration.

Therefore, it is crucial to consider the operational differences between different fuels when optimizing engine performance and efficiency.
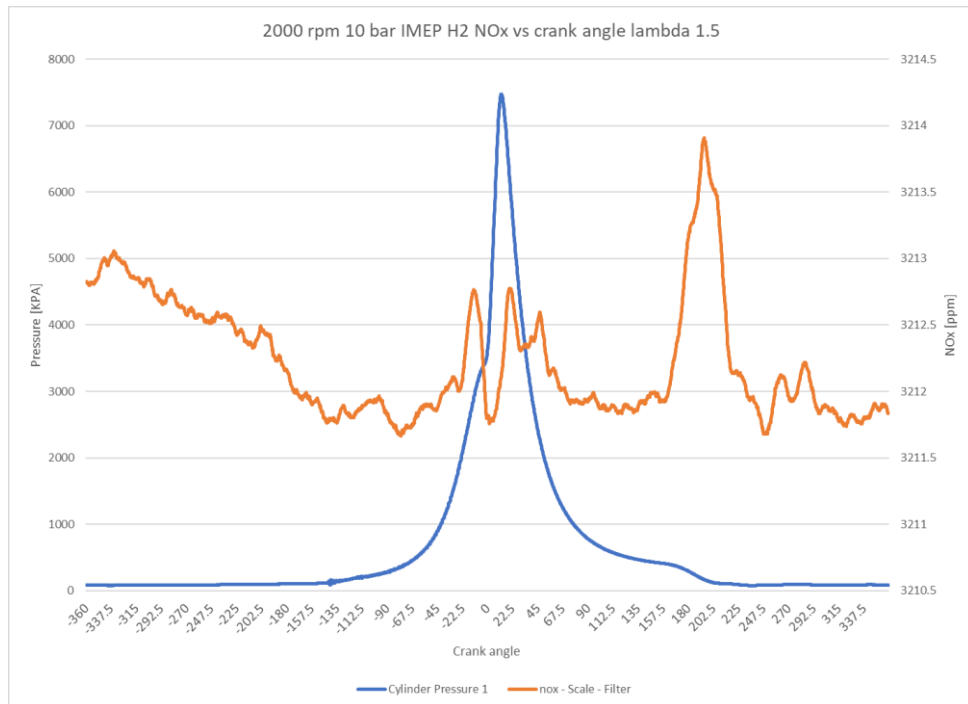
Figure 11. 5: NOₓ emission distribution for DI hydrogen in the crank-angle domain at a lambda of 1.5.
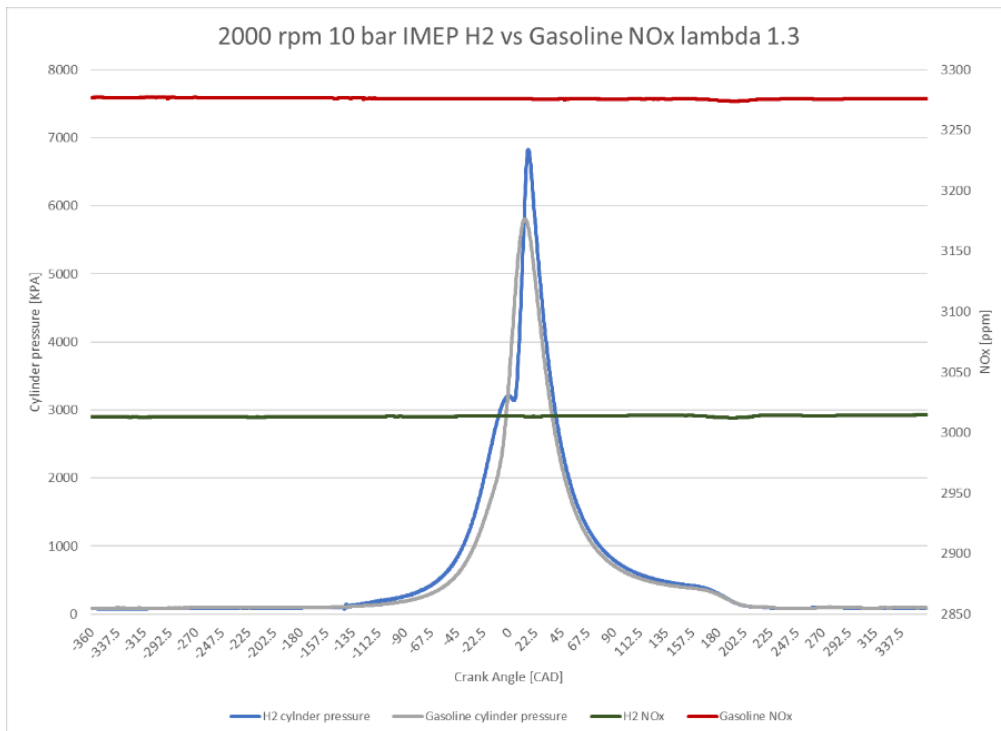
Figure 11. 6: NOₓ emission for DI hydrogen and DI gasoline and in-cylinder pressure traces in the crank-angle domain at a lambda of 1.3.

Figure 11.7 shows the NOₓ emissions for both hydrogen and gasoline systems at lambda 1, the stoichiometric ratio, across the crank-angle domain. The data reveals that for hydrogen, spark ignition is significantly delayed to almost 5 degrees ATDCf to keep the

maximum pressure rise rate within the allowable limits. Interestingly, hydrogen operations have 370 ppm lower NO_x levels than gasoline. This difference in combustion characteristics is further highlighted by the in-cylinder pressure, which shows a higher pressure for hydrogen with delayed ignition to maintain engine limits. The study emphasises the importance of ignition timing and fuel characteristics in managing NO_x emissions, especially with hydrogen fuel. This analysis provides comprehensive insights into NO and NO_2 emissions distribution and the differences between hydrogen and gasoline fuels under varying conditions using in-cylinder pressure data. The study confirms negligible NO_x emissions at lambda 3.3 and a direct comparison between hydrogen DI and PFI at lambda 2.75 with NO_x emissions around 50 ppm.
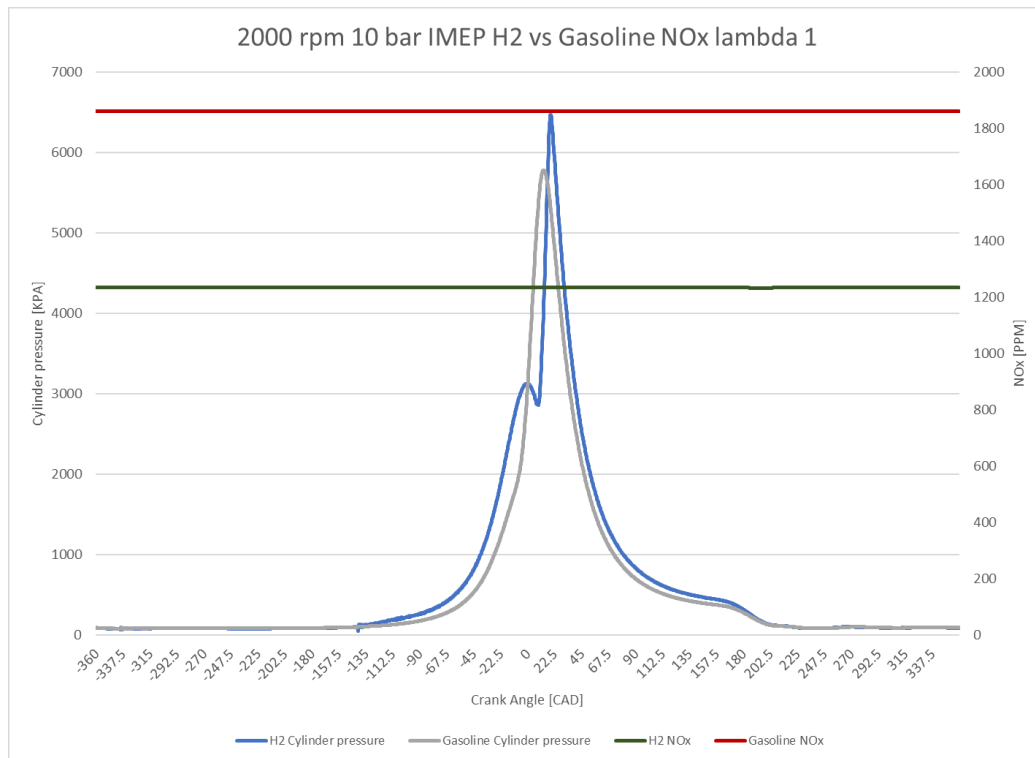
Figure 11. 7: NO_x emissions for DI hydrogen and DI gasoline and in-cylinder pressure in the crank-angle domain at lambda of 1.

11.3.2 Analysis of NO_x Emissions in The Time Domain

After conducting a thorough analysis of the performance and emissions of hydrogen and gasoline operations by averaging 300 cycles, a crank-angle domain analysis was performed to show the averaged data. However, this section delves deeper into the investigation and aims to comprehensively understand the cycle-to-cycle NO_x emissions characteristics. The objective is to fully comprehend the dependency of NO_x on other combustion parameters, such as the peak in-cylinder pressure and the engine cycle-to-cycle variations (CCVs).

To achieve this, we analysed the in-cylinder pressure and NO_2 emissions of 15 cycles at lambda 2.75 in the time domain, and the results are displayed in Figure 11.8. The data indicate that high NO and NO_2 fluctuations are observed, even though the engine Coefficient of Variation (COV) in IMEP was less than 0.6%. The NO emission shows a minimal variation of 20 ppm, as the overall NO_x emissions at lambda 2.75 are close to zero.

The location of the peak NO$_x$ varies based on cycle-to-cycle dynamics, indicating a significant impact of cycle-to-cycle variability on NO$_x$ emissions.

In conclusion, this detailed analysis provides valuable insights into the cycle-to-cycle NO$_x$ emissions characteristics and the impact of other combustion parameters on NO$_x$. These insights can be used to optimise engine performance and reduce harmful emissions.
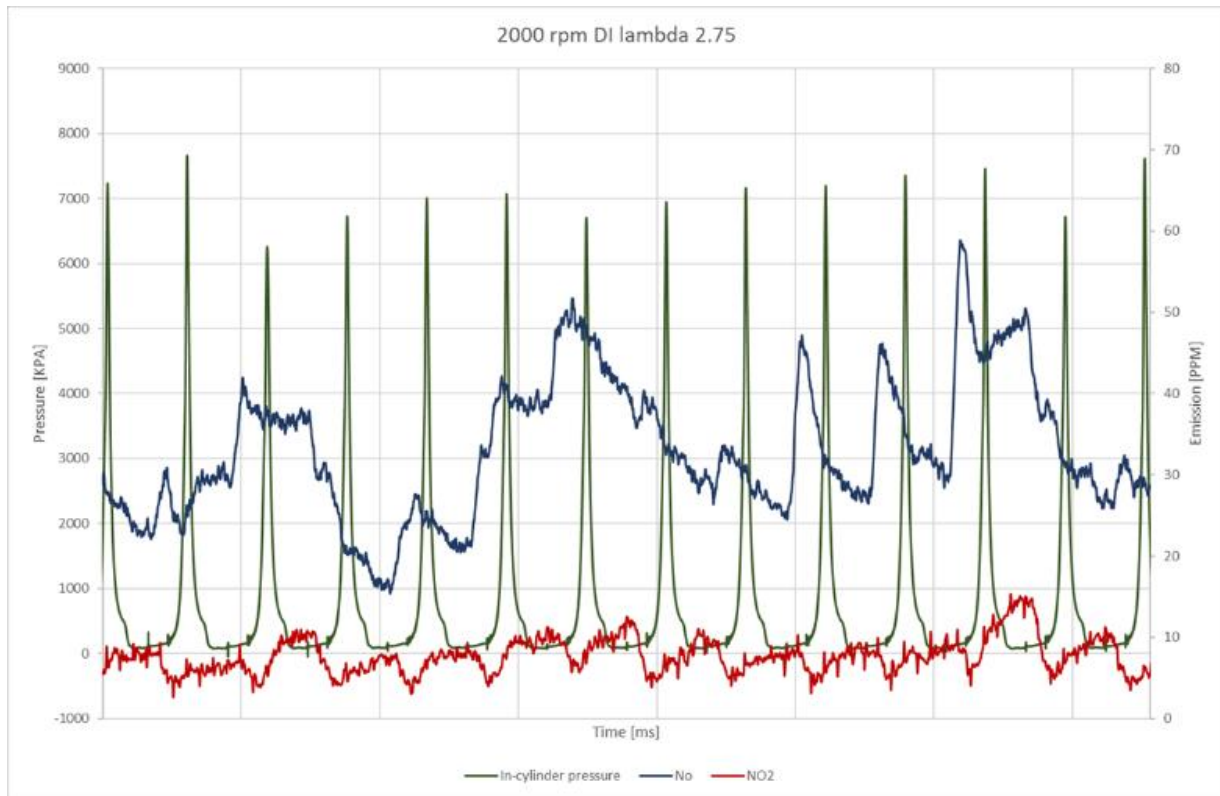
Figure 11. 8: NO$_x$ emission and in-cylinder pressure for DI hydrogen in the time domain at a lambda 2.75.

Figure 11.9 displays the average NO$_x$ emissions over 200 cycles and the NO$_x$ variations indicated by the COV of NO$_x$. Besides, both gasoline and hydrogen DI systems at lambda of 1.3 are directly compared in Figure 11.9. The data demonstrates that hydrogen has constant NO$_x$ emissions with minor oscillations of less than 0.5% on average. In contrast, gasoline has unstable NO$_x$ emissions with higher levels of cycle-to-cycle variations, therefore greater COV in NO$_x$, as shown in Figure 11.9, and equation 11.1 provides the cov$_{NOx}$ calculation.

$$COV_{NOx}(\%) = \frac{\sqrt{\frac{\sum_{i=1}^{n}(NOx_1 - NOx_{mean})^2}{n-1}}}{NOx_{mean}} \qquad (11.1)$$
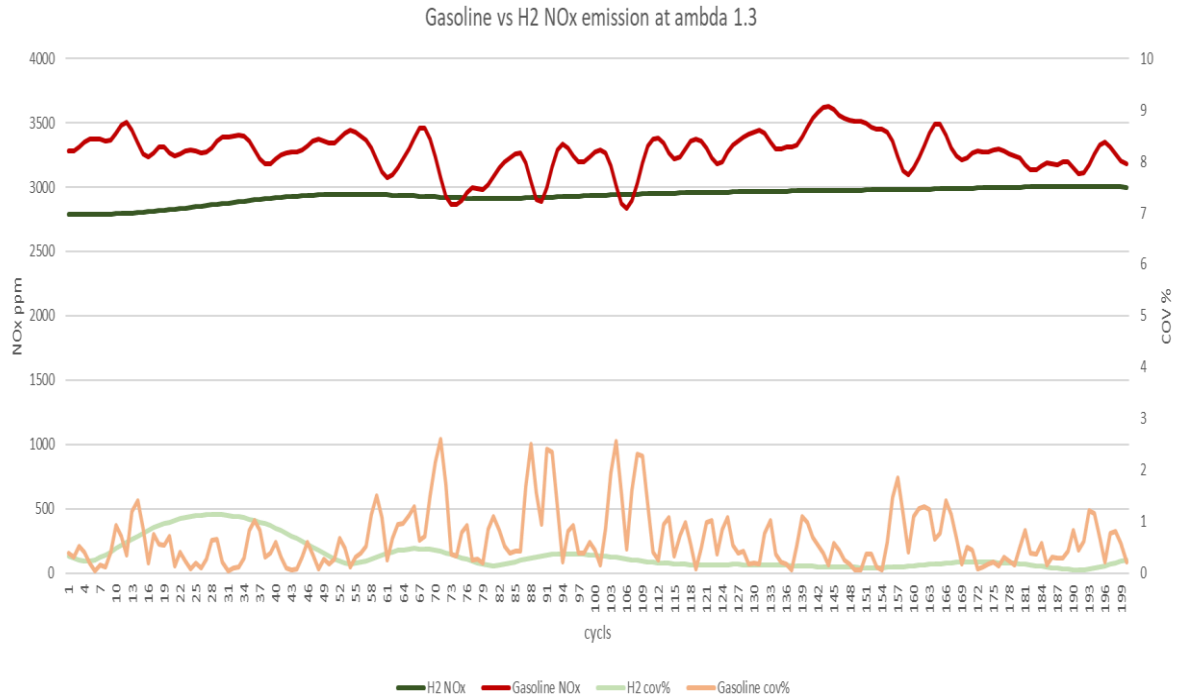
Figure 11. 9: NO_x emission and NO_x variation for DI hydrogen and DI gasoline across 200 cycles at a lambda of 1.3.

Figure 11.10 compares peak in-cylinder pressure and NO_x emissions for each cycle at a relative Air-Fuel Ratio of 1.3. The findings indicate that while the Coefficient of Variation (COV) in Indicated Mean Effective Pressure (IMEP) is less than 1% for both fuels, the peak in-cylinder pressure variation in gasoline Direct Injection (DI) is considerably higher than that in hydrogen DI. This is evident in gasoline DI's wider peak in-cylinder pressure distribution. Furthermore, the figure shows that hydrogen fuel generates higher peak in-cylinder pressure while emitting lower NO_x emissions.
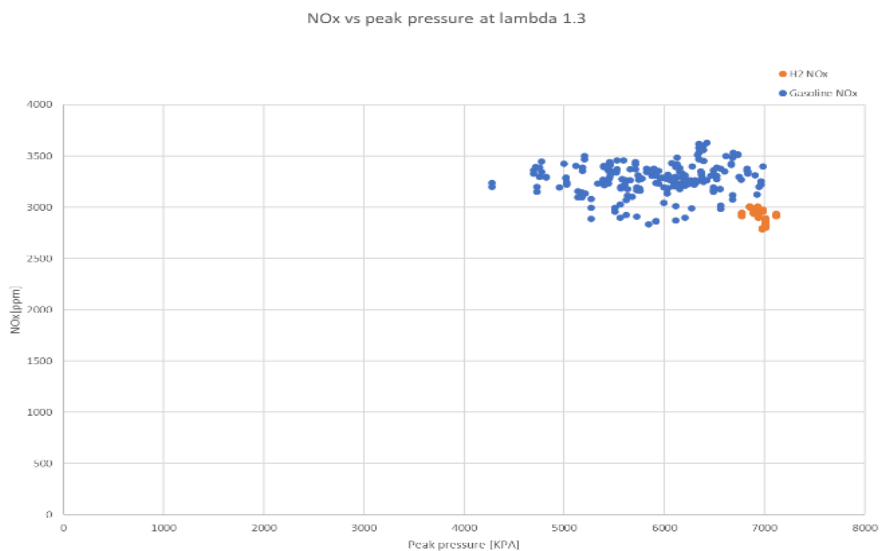
Figure 11. 10: NO_x emission and peak cylinder pressure for hydrogen DI and gasoline DI at lambda of 1.3.

In Figure 11.11, the NO_x emissions of gasoline and hydrogen DI are compared at a lambda of 1. The results show that gasoline produces higher NO_x emissions and oscillation levels

than hydrogen. Although the engine is primarily optimised for gasoline as the primary fuel, hydrogen exhibits more stable NO_x emissions with a lower COV of NO_x per cycle and lower average NO_x levels.

Figure 11.12 compares the in-cylinder peak pressure to NO_x emissions for 200 cycles under stoichiometric conditions. The data indicates that gasoline exhibits higher in-cylinder pressure variation and greater oscillation of NO_x emissions than hydrogen. In contrast, hydrogen demonstrates stable peak in-cylinder pressure and lower NO_x emissions. These findings provide strong evidence for the benefits of hydrogen fuel in reducing NO_x emissions compared to gasoline. The results provide clear evidence for the benefits of hydrogen fuel in reducing NO_x emissions compared to gasoline.
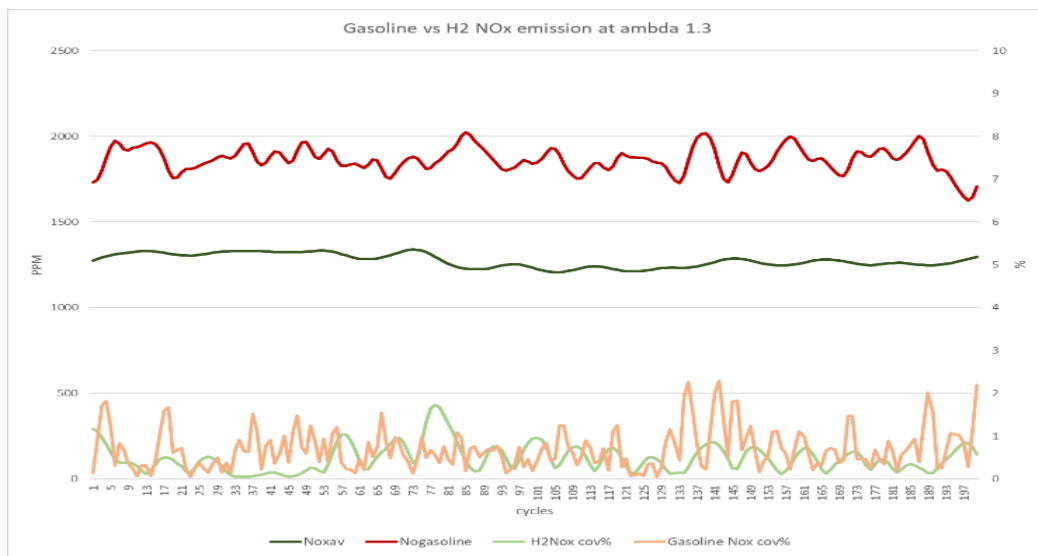
Figure 11. 11: NO_x emission and NO_x variation for DI hydrogen and DI gasoline in 200 cycles at a lambda of 1.
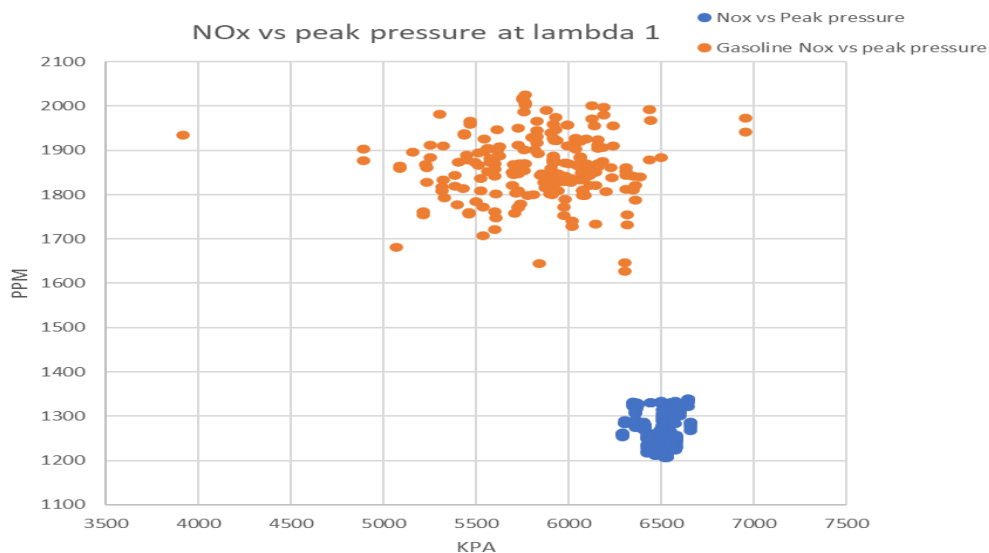
Figure 11. 12: NO_x emission and peak cylinder pressure for hydrogen DI and gasoline DI at lambda of 1.

The information presented in Figure 11.13 compares NO_x emissions at varying cylinder pressures and COV of NOx at a lambda of 1.8, the maximum for gasoline. The graph illustrates that gasoline exhibits a greater fluctuation in peak cylinder pressure under

these lean conditions than hydrogen, resulting in elevated COV of NO$_x$ This difference can be attributed to the combustion properties of gasoline, which generate a less uniform air-fuel mixture and a longer combustion time.

Figure 11.14 displays results obtained under stoichiometric conditions. The data indicates that gasoline has a wider range than hydrogen and is associated with significantly higher NO$_x$ emissions and a greater COV of NO$_x$ during each cycle. This is due to the higher temperatures and pressures reached during combustion, which promote NO$_x$ formation. Conversely, hydrogen demonstrates a consistent in-cylinder peak pressure and lower NO$_x$ emissions, with the COV of NO$_x$ remaining below 1.7%. This is due to hydrogen's faster combustion rate, which results in a more uniform air-fuel mixture and a shorter combustion duration.

Furthermore, the data suggests that higher in-cylinder peak pressure corresponds to increased NO$_x$ emissions and a greater COV of NO$_x$, reaching 2.3%. These results indicate that hydrogen offers significant advantages over gasoline due to its lower NO$_x$ emissions and consistent in-cylinder peak pressure. As a result, hydrogen-powered engines have the potential to reduce emissions and enhance engine efficiency, making them a promising solution.
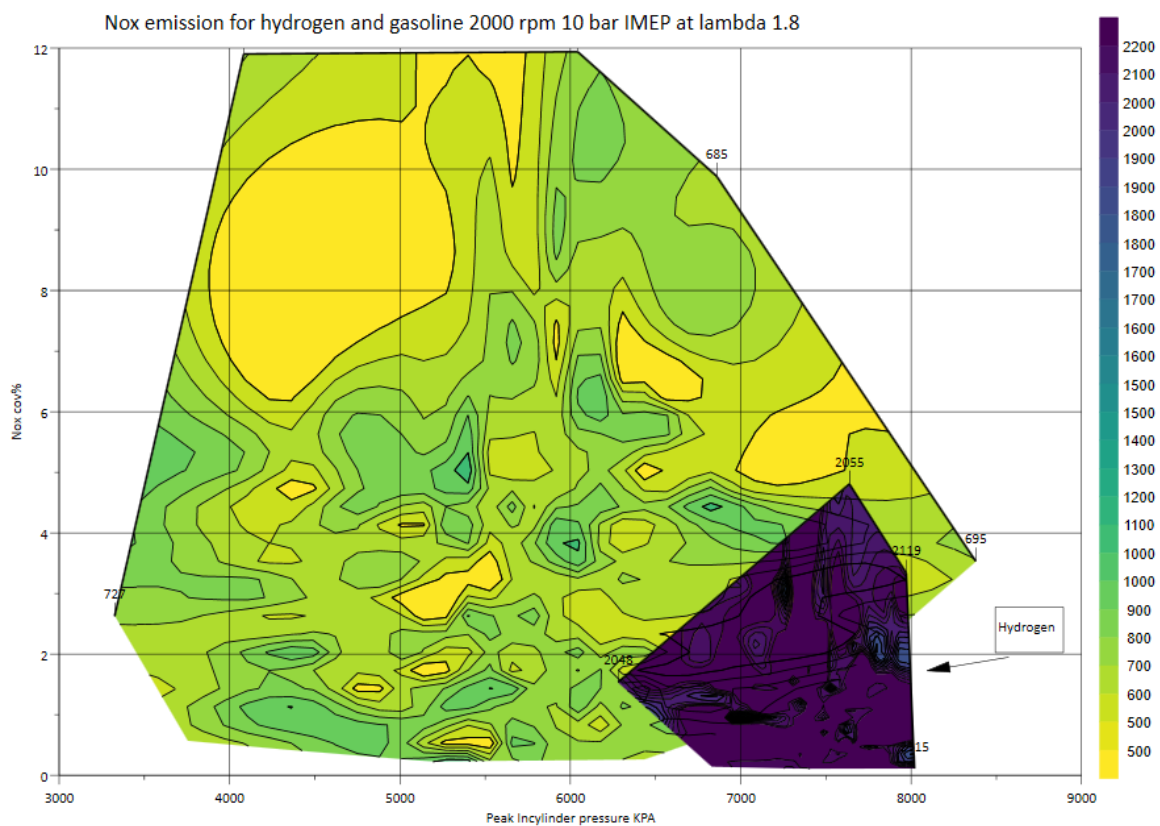
Figure 11. 13: Variations of NO$_x$ emission with peak cylinder pressures for hydrogen DI and gasoline DI at lambda of 1.8.

Figure 11. 14: Variation of NOₓ emission with peak cylinder pressures for hydrogen DI and gasoline DI at lambda of 1.

The previous diagrams have compared the relationship between in-cylinder peak pressure, NOₓ emissions, and COV of NOₓ for hydrogen and gasoline. These comparisons have evaluated the primary NOₓ characteristics at a lambda of 1.8 and 1. Since lambda one is considered the optimal AFR for gasoline, it's worth noting the results at the optimal lambda for hydrogen, which is 2.75. Figure 11.15 shows the NOₓ emission characteristics at lambda 1 for gasoline and lambda 2.75 for hydrogen. The data shows a higher peak in-cylinder pressure for hydrogen, with almost no NOₓ emissions. The average NOₓ emissions for hydrogen are less than 55 ppm, compared to 1850 ppm for gasoline.

Figure 11. 15: Variation of NOₓ emission with peak cylinder pressures for hydrogen DI and gasoline DI at optimum lambda for each fuel.

11.4   Conclusion

The study explores the primary NO_x emissions characteristics of a hydrogen-fuelled spark ignition (SI) engine designed and optimised for gasoline fuel. The results indicate that using hydrogen fuel has improved combustion stability and reduced cycle-to-cycle variations in peak in-cylinder pressure and NO_x emissions. Additionally, the hydrogen fuel has resulted in higher thermal efficiency and almost zero NO_x emissions at a lambda value of 2.75 without requiring excessive boosting or further modifications to the existing ICE platform.

Hydrogen fuel has a much wider operation lambda range than gasoline, particularly evident in its ability to operate from lambda 1 to almost lambda 4. This feature allows for the adoption of hydrogen fuel in various ICE applications. A direct comparison between the NO_x emissions of hydrogen and gasoline at the stoichiometric operation point shows that the former produces less emissions, which enables existing after-treatment systems to remove NO_x from the exhaust tailpipe more effectively.

When comparing the evolution of NO_x emissions over the crank-angle domain for hydrogen DI and PFI systems, it is observed that the PFI system produces slightly less NO_x. This is considered an advantage for existing SI engines that use gasoline PFI and are looking to adopt hydrogen fuel. However, the main limitation of the PFI hydrogen system is the occurrence of backfire when operated with near stoichiometric mixtures.

The time analysis of the NO_x emissions characteristics reveals that DI hydrogen engine operation produces much better engine stability and less NO_x variations than gasoline. Even at the optimum operation point for gasoline, hydrogen engine operation has proven to be more stable with less NO_x emissions and lower NO_x emission fluctuations between cycles.

Chapter 12. Experimental Assessment of The Possible Carbon Dioxide and Hydrocarbon Emissions on a Downsized Spark Ignition Engine Using H$_2$ Fuel

12.1 Introduction

In the previous studies, the researchers experimented with different methods of introducing lubricant oil to observe its effects on particle emissions from compressed natural gas and gasoline spark-ignition engines. The study included testing three distinct forms of introducing the oil and two fuel-injection modes, namely port fuel injection and direct injection, to replicate the various ways lubricant oil could enter the combustion chamber. The oil was injected into the intake manifold or the combustion chamber for the compressed natural gas tests. The oil was mixed with the fuel for the gasoline port-fuel-injection and direct-injection tests[158], [159].

Extensive research has been conducted on NO$_x$ generation in recent years, but limited attention has been given to the emissions of CO$_2$ and HC produced by lubricants. As a result, many uncertainties remain in this field. Clear evidence is needed to better understand the relationship between lubricant emissions and load or operational points. This study seeks to address this knowledge gap by examining the dependence of lubricant emissions on load and operating points to comprehensively understand the complex relationship between lubricant emissions and hydrogen engine operation. The findings of this study will have significant implications for the automotive industry, particularly in the efficient use of hydrogen in ICEs. The industry can develop better strategies to minimise environmental impact and enhance ICE performance by understanding lubricant emissions and their impact on hydrogen engine operation.

The objective of the study was to detect any carbon dioxide (CO$_2$) and hydrocarbons (HC) from lubrication oil at various loads and air-to-fuel ratios (AFRs) using a fast emissions analyser. The analyser captured a sample per 0.25 crank angle degree and correlated in-cylinder pressure with exhaust pressure to determine the delay time. The study included load and AFR sweeps in both time and crank domains and a comprehensive evaluation of emission spikes over 200 cycles.

The test cell has an ultra-high-speed flame ionisation detector (FID), which can identify unburned hydrocarbons and is equipped with NDIR 500 to capture the CO$_2$ in the crank domain. The FID50 fast FID is specifically designed to cater to both engine and non-engine applications, offering an impressive 15 ms T10-90 response time and four samples per crank degree, thanks to Cambustion. This type of FID is typically used to measure THC in pre- or post-catalyst engine exhaust, detect leaks quickly in HC gas-carrying pipelines, conduct mobile THC measurements, wind tunnel measurement of HC tracer gas mixing and dispersion, feedback control of biogas production, and other process control applications.

The fast FID analyser is a quick and efficient solution for capturing transient HC and CO$_2$ emissions responses. However, during the steady-state operation of a hydrogen ICE engine, the NDIR and FDI analysers showed almost zero HC and CO$_2$ emissions. This is

unusual since hydrogen is a zero-carbon fuel. Nonetheless, it is important to note that the lubricant oil in the chamber is expected to produce HC and CO_2 emissions over a few cycles. The ultra-fast FDI 150 kit analyser has a short heated line and fast response time to capture these emissions. This allows it to capture HC and CO_2 spikes over the cycles and correlate emissions standard deviations with in-cylinder pressure fluctuations.

12.2 Test Methodology

The present study aims to analyse the spikes in hydrocarbon (HC) and Carbon Dioxide (CO_2) emissions during an engine that uses 100% hydrogen as a combustible fuel. The unburnt hydrocarbon results from the unburnt lubricant oil slipping from the oil seal, while the CO_2 emissions represent the burnt oil.

The researchers performed two sets of tests to understand the dependence of lubricant oil emissions. The first set of tests was the lambda sweep test, conducted at 2000 rpm and 10 bar IMEP, marking the mid-speed and mid-load point on the engine map. This test aimed to evaluate the CO_2 and HC emissions under different relative AFRs to frame the emission characteristics at different burn conditions.

The second test was the load sweep test, performed at a fixed lambda of 2.75 and a speed of 2000 rpm, representing the mid-speed and optimum lambda. It was found that the learn lambda will require more boosted air, consequently dropping the overall efficiency. Also, the rich region will produce higher NO_x emissions.

To add more accuracy to the measurements, a delay correlation was added by combining the three fast pressure sensors in the intake, exhaust, and in-cylinder pressure to calculate the delay time between the exhaust valve opening and the emissions reading due to the length of the heated line. The delay time was an average of 1.75 crank degrees at 2000 rpm.

Table 12.1 below shows the full engine operation condition. The tested points were eventually set at the maximum brake torque (MBT), attainable at 50% mass friction burn of 8 degrees ATDCF. To keep all boundary conditions unchanged and prevent any impact on the heat loss, the oil and coolant temperature was kept constant at 90 degrees Celsius, using an external proportional-integral-derivative (PID) controller. Furthermore, the inducted airline was outfitted with an external heat and dryer to maintain zero per cent humidity and 37 degrees of air temperature using a PID controller with a fluctuation of 1 degree.

In summary, the study aimed to provide a detailed analysis of the HC and CO_2 spikes that occur during the operation of an engine using 100% hydrogen as a combustible fuel. The researchers conducted two sets of tests to comprehend the dependence of lubricant oil emissions and added a delay correlation to the measurements to provide more accuracy. The study also considered several boundary conditions to maintain consistency and ensure reliable results.

Table 12. 1: test parameters for CO_2 and Hc emissions capture

Engine parameters	Unit	λ sweep test	Load sweep test
Engine Speed	rpm	2000	2000
Engine Load	kPa	1000	SWEEP

λ	-	SWEEP	2.75
Intake Cam	ATDCg	97	97
Exhaust Cam	BTDCg	102	102
Start of injection	BTDCf	150	150
50% MBF	ATDCf	8	8
Injection pressure	kPa	3000	3000
Coolant and oil temperature	°c	90	90
Intake Air temperature	°c	38	38

12.3 Results and Discussions

The report's results section will be divided into two comprehensive sections to analyse the collected data thoroughly. The first section will describe the average 300-cycle performance and emissions for the load and lambda sweeps, with a specific focus on the dependence of averaged HC and CO_2 emissions on load and lambda variations. The analysis will delve into individual cycles to identify HC and CO_2 emissions spikes and their frequency over a 200-cycle period.

The report's second section will investigate peak HC and CO_2 emissions in a single cycle at different operation points. This investigation will involve correlating the standard deviation of HC and CO_2 with the peak in-cylinder pressure fluctuations. By doing so, this section aims to provide a clear understanding of the factors that contribute to peak emissions and identify potential strategies for reducing them.

12.3.1 The Emission and Performance of The H_2 DI Engine

Throughout the load sweep test, the engine maintained a steady speed of 2000 rpm, while the 50% mean burn fraction (MBF) was fixed at the ideal spark advance for maximum torque (MBT) of 8 degrees after top dead centre (ATDC). However, to avoid exceeding the cylinder's peak pressure limit of 120 bar, the spark timing had to be slightly delayed at higher loads. To keep nitrogen oxide (NO_x) emissions low and maintain minimum air boost, the lambda value remained fixed at 2.75.

Figure 12.1 shows a graph of the thermal efficiency plotted against the indicated mean effective pressure (IMEP) values. These values ranged from 4 to 16 bar IMEP, while the 50% MBF remained at around 8 degrees with a slight fluctuation of 1 degree. As illustrated in Figure 12.2, the 50% MBF increased at higher loads as the cylinder's peak pressure approached its limit of 120 bar.

The Indicated Thermal Efficiency (ITE) values were consistently high throughout the load sweep test, averaging 40%. The higher injection pressure at lower loads caused a higher Coefficient of Variation of Indicated Mean Effective Pressure (COV_{IMEP}). The maximum ITE of 41.7% was achieved at an IMEP of 800 Kpa. Due to the engine's excellent knock resistance, the ITE remained stable at higher loads.
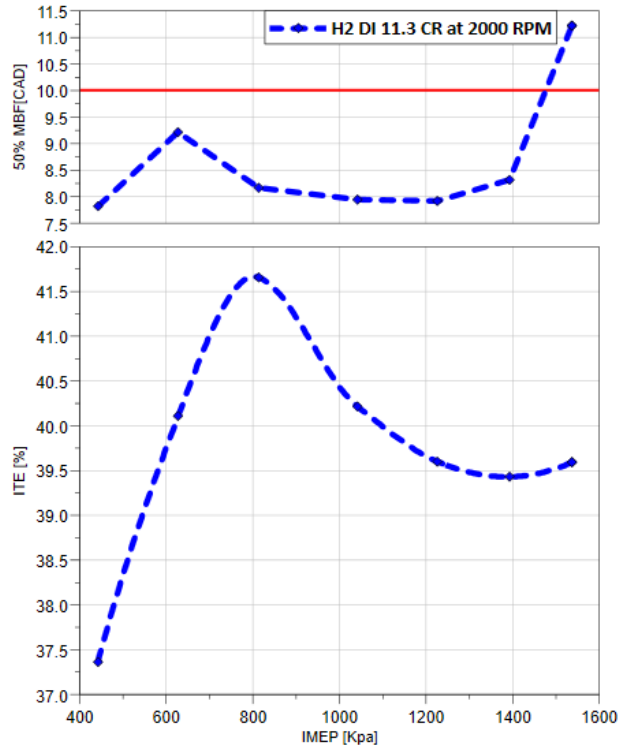
Figure 12. 1: The ITE [%] and the 50% MBF[ATDCf] vs IMEP [Kpa] at 2000 rpm and 2.75 AFR.

The combustion parameters and operation limitations are displayed in Figure 5. In Figure 12.2 (a), the graph for COVIMEP at different loads demonstrates a stable trend with less than 2% variations. Additionally, the in-cylinder Pmax trend shows an increase in the peak pressure as the load increases up to the threshold point of 120 bar. The pressure rise rate (Rmax) graph reflects higher rates as the load increases up to 14 bar IMEP, followed by a slight drop due to spark retarding to maintain the peak in-cylinder pressure within limits.

In Figure 12.2 (b), the spark timing graph displays the spark location at various loads, with retardation occurring at higher loads to maintain 50% MBF at the MBT region up to 14 bar IMEP. Further retarding is necessary to keep the engine under the operation limit. The middle graph indicates the spark to 10% burn duration, following the 10 to 90% burn duration trend.
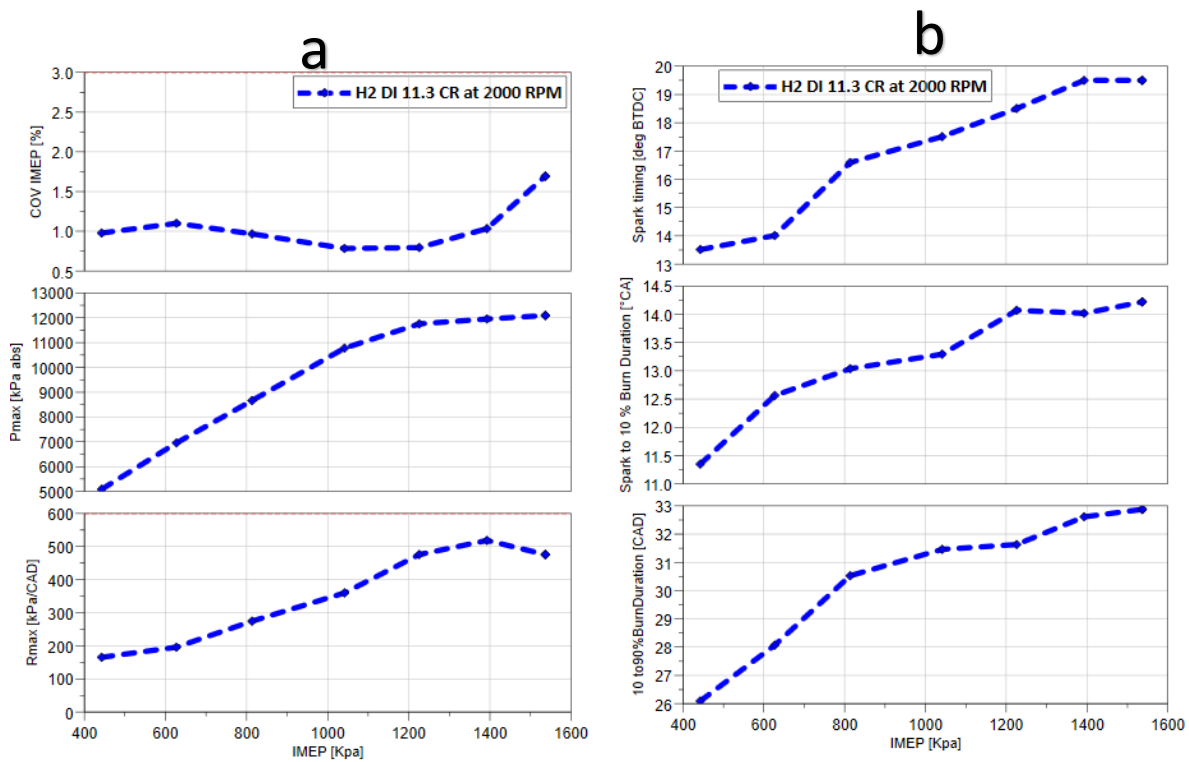
Figure 12. 2: (a) Engine limitations of COVimep[%], Pmax[Kpa Abs], and Rmax [Kpa/CAD] and (b) Engine burn characteristics of spark timing [BTDCf], Spark to 10% brun [CAD], and 10 to 90% brun duration.

An analysis was conducted on the engine-out emissions of the hydrogen spark ignition (H_2 SI) engine concerning the Indicated Mean Effective Pressure (IMEP) load sweep, as shown in Figure 12.3. Results indicate that fast carbon dioxide (CO_2) emission did not correlate with the load, and the highest CO_2 value measured was within the acceptable limit, at 32 ppm. The fast hydrocarbon (HC) concentration was found to be insignificant. The lambda value, which indicates the air-fuel ratio, consistently fluctuated at 0.41 over the target lambda of 2.75. Oxygen (O_2) measurements showed a strong correlation with the lambda values. The nitrogen oxide (NO_x) emission slightly increased as the load increased due to increased heat generation but remained at low levels, registering between 10 and 97 ppm. H_2 slip from the exhaust increased with lower loads. The trade-off between lower H_2 slip and higher NO_x at higher loads shows that a lower H_2 slip leads to a higher H_2 burnt rate and NO_x generation.
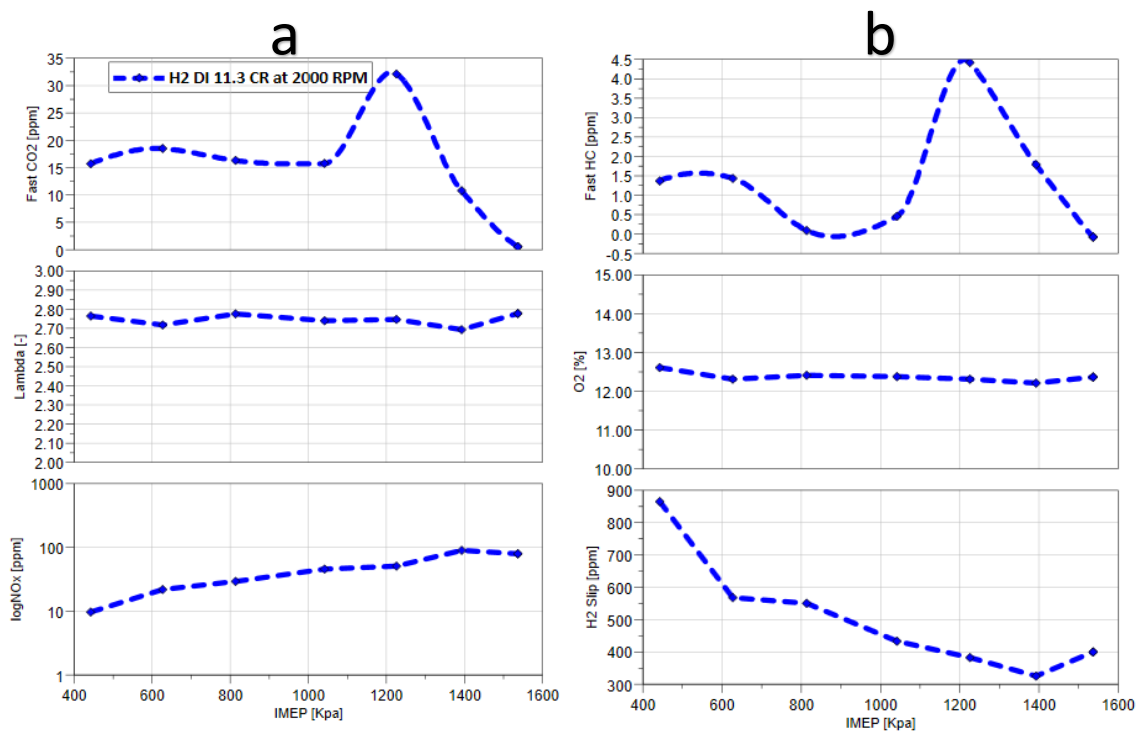
Figure 12. 3: Engine-out emission vs load sweep.

The data from the previous figures shows the hydrogen direct injection (DI) system's exceptional efficiency. Even during wide load operation, the system maintains an impressive Indicated Thermal Efficiency (ITE) of over 39.5%, as seen in Figure 12.1, with minimal engine variation of less than 2% (Figure 12.2).

One of the system's most significant advantages is its superior knock resistance and lean-burn operation, allowing combustion maintenance at the Maximum Brake Torque (MBT) during higher loads. This is not possible with carbon-based fuel without spark retarding to avoid knock. The hydrogen DI system's lean-burn operation allows it to run with a high air-to-fuel ratio, reducing fuel consumption and emissions.

Furthermore, the fast Flame Ionisation Detector (FID) emission output shows minimal Carbon Dioxide (CO_2) and hydrocarbon (HC) emissions, even with load fluctuations. This feature is particularly impressive since the hydrogen DI system can run at high loads without causing knock, a common issue with traditional carbon-based fuels.

Moving onto the second lambda sweep. The aim is to maintain a constant speed and load, specifically 2000 rpm and 10 bar IMEP. The primary objective of this study is to examine the effect of air-fuel ratio (AFR) on hydrocarbon (HC) and carbon dioxide (CO_2) emissions in the engine. We've fixed the load and speed with 50% MBF around 8 degrees to keep the engine running smoothly and efficiently.

To conduct this experiment, by utilising an H2 DI system. This system boasts several advantages, such as eliminating the fire in the intake ducts that typically occurs due to injection starting at 150 degrees BTDCf. Additionally, it helps to eliminate hydrogen slips from the cam valve overlaps. To ensure optimal combustion, we need to significantly retard the spark since hydrogen has a higher flame velocity resulting from higher Rmax.

The ultimate goal of this experiment is to gain detailed insights into the engine's behaviour under varying AFR conditions and to evaluate the effectiveness of the H2 DI system in minimising emissions.

Figure 12.4 depicts the relationship between the in-cylinder Integrated Total Energy (ITE) with 50% Mass Burn Fraction (MBF) and lambda swept from 1.2 to lambda four. The maximum ITE is observed to be 40.5% within the lambda 2.5 to 3.4 range. However, the ITE is slightly reduced by less than 1% at the extremely lean region due to the higher H2 slip, as demonstrated in Figure 12.6 (b). Furthermore, a lower ITE was captured at the less lean area due to the spark timing returning to almost 10 degrees after the top dead centre before combustion, as shown in Figure 12.5. The 50% MBF, in Figure 12.4, demonstrates consistency at around 8 degrees but massively increases at the rich operation points to maintain the Rmax when limits, which explains the sudden ITE drop.

In Figure 12.5, the graph displays the engine limitations and combustion characteristics at various relative air-fuel ratios (AFRs). Figure 12.5 (a) demonstrates the primary operation limitations, such as the Coefficient of Variation of Indicated Mean Effective Pressure (COV$_{IMEP}$), the maximum in-cylinder pressure, and the maximum pressure rise rate. The combustion COV$_{IMEP}$ remains relatively stable during lean operation, with a slight increase under leaner conditions, but remains under 3%. As the engine is introduced to more lean operation and boosted air, the maximum in-cylinder pressure (Pmax) increases. When the operation moves towards stoichiometric combustion, the Rmax increases, forcing a significant spark retardation to maintain the engine under the Rmax limits of 600 Kpa. The spark timing graph on the other side indicates the retardation process that occurs during rich combustion and a spark at the Top Dead Centre (TDC) in lambda 1.5. Then, to maintain Rmax within the limits, the spark is almost 10 degrees After Top Dead Centre (ATDCf). Finally, the burn duration trend suggests that lean combustion has a longer burn duration, which correlates with the previous analysis.
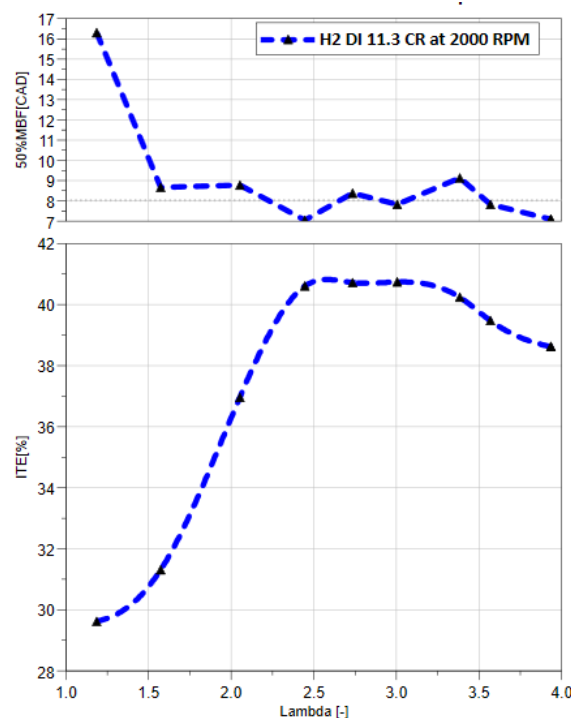
Figure 12. 4: ITE [%] and 50% MBF [CAD] vs lambda sweep at 10 bar IMEP and 2000 rpm
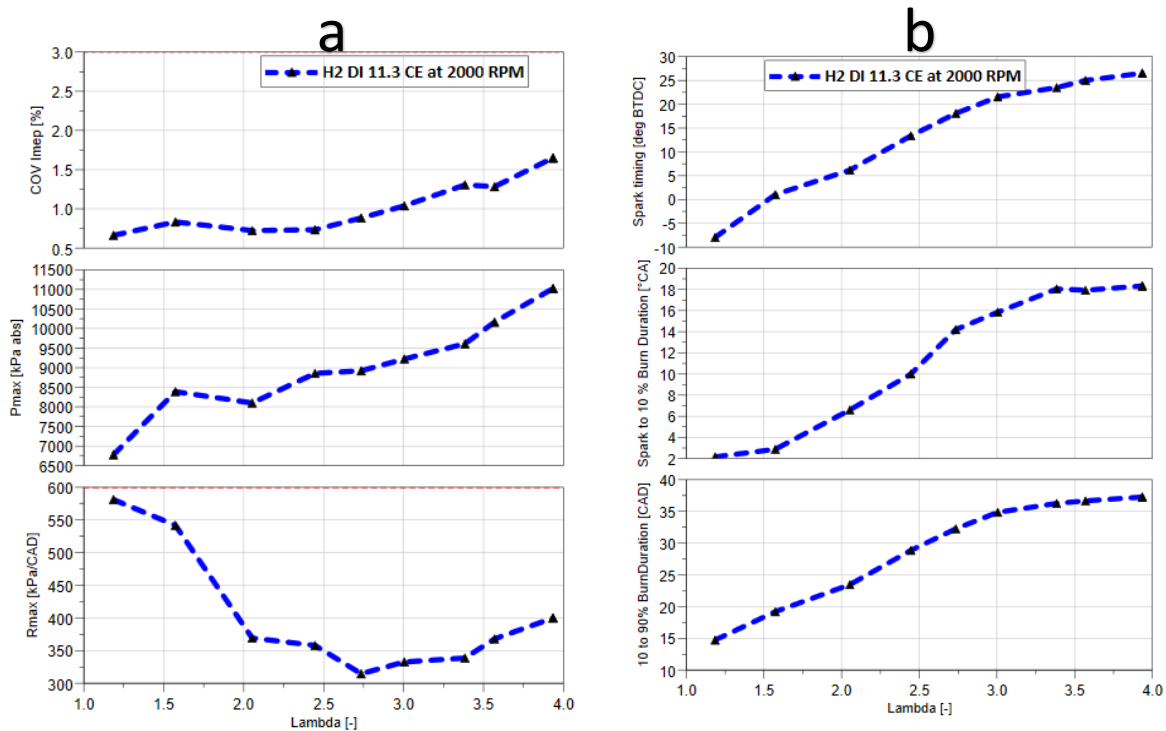
Figure 12. 5: Engine limitations in the left side of COVimep[%], Pmax[Kpa Abs], and Rmax [Kpa/CAD] engine burn characteristics in the right side of spark timing [BTDCf], Spark to 10% brun [CAD], and 10 to 90% brun duration vs lambda sweep.

The data presented in Figure 12.6 highlights the relationship between engine-out emissions and intake pressure, as captured by the manifold intake pressure, which is also utilised for in-cylinder pressure pegging. The fast HC and CO_2 trends illustrate a trade-off, with lean combustion increasing averaged CO_2 emissions by 16 ppm, while simultaneously causing the HC to drop from 6 ppm to nearly zero. The emission output of the average 300 cycles can be considered as near-zero emissions under the lambda variation. Additionally, the O_2 output is correlated with the lambda measured from the wide band lambda in the exhaust, which is employed for quality checks. The NO_x emissions from lambda 3 to 4 show a single digit in ppm, while from lambda 2.5 to 3, they range from 100 to 10 ppm and increase exponentially to reach the peak NO_x around lambda 1.5. The decrease in NO_x emissions as the lambda increases is attributed to lower in-cylinder temperature during lean operations. This causes lower combustion efficiency and more hydrogen slip. In the extremely lean case (lambda=3.9), there is a very high hydrogen slip rate; hence the thermal efficiency at this operation condition drops (as shown in Figure 12.4). Finally, the intake pressure demonstrates the necessary boost to achieve the same load at varying AFRs.
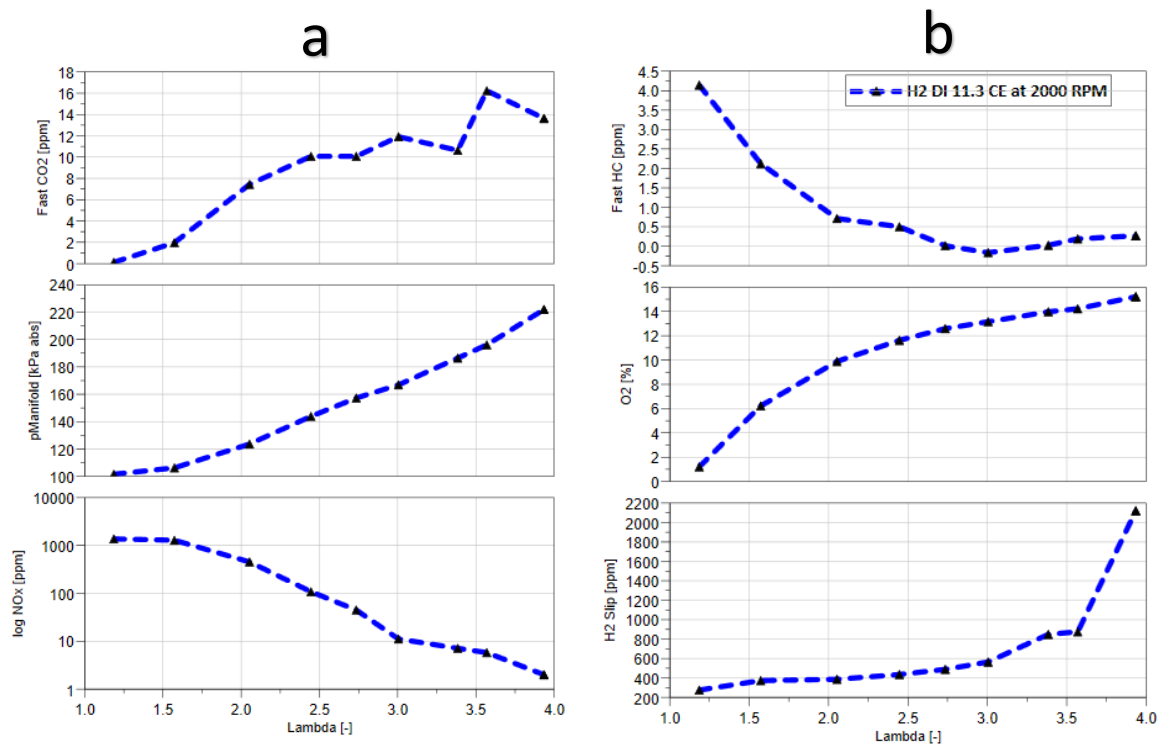
Figure 12. 6: Engine-out emission and Intak pressure [Kpa Abs] vs lambda sweep.

Based on the lambda sweep analysis, hydrogen DI technology can maintain engine stability even while operating at stochiometric operations and a variety of air-to-fuel ratios. Additionally, the ultra-fast FID indicates that HC and CO_2 emissions are minimal, suggesting that the impact of lubricant on emissions is negligible. However, examining the trends of HC and CO_2 emissions in the cycle analysis section is recommended to gain a more thorough understanding of the situation. Although both studies show CO_2 and HC emissions that are almost non-existent, it is important to conduct further investigation to address the trends observed in the lambda sweep analysis. Analysing individual cycles may be worth considering, as CO_2 and HC emissions can be affected by introducing lubricant species into the cycle. By doing so, we can better comprehend the underlying factors contributing to emission trends and develop more effective solutions to minimize emissions and promote sustainable energy practices.

12.3.2 HC and CO_2 Emissions Analysis in The Cycle Domain

This section will analyse the HC and CO_2 emissions per 0.25 crank angle degree during a single cycle. Our primary objective is to compare the spikes that occur throughout 200 cycles at steady-state operating points. For the study, we will use the previous operation points logged in the load and lambda sweep and maintain the engine speeds at 2000 RPM. This investigation aims to identify high levels of hydrocarbons and carbon dioxide and establish a correlation between the frequency of these occurrences and a more accurate depiction of lubricant emissions.

Figure 12.7 illustrates the maximum HC and CO_2 emissions in parts per million (ppm) for each engine cycle. The data is collected over 200 cycles, spanning 720 degrees of crank rotation, to obtain more accurate measurements of lubricant emissions. The diagram depicts the emissions captured at an IMEP of 10 bar and a lambda value of 2.75 while the

engine ran at a speed of 2000 rpm. The peak average trend of CO_2 is directly related to the average value depicted in Figure 12.6, with a deviation of 9 ppm and significant variability in the cycles. The highest recorded increase in maximum cyclic CO_2 levels is 35 parts per million (ppm), while the average value is only 10 ppm. These findings support the theory that the emission value of lubricants follows a cyclical pattern.

In contrast, the HC emission remains almost negligible, with two significant spikes occurring during the 200 cycles, measuring 15 and 10 ppm, respectively. The overall result demonstrates the disparity in the HC and CO_2 attributes, with the HC spikes exhibiting significantly greater overshooting compared to the average values of CO_2.
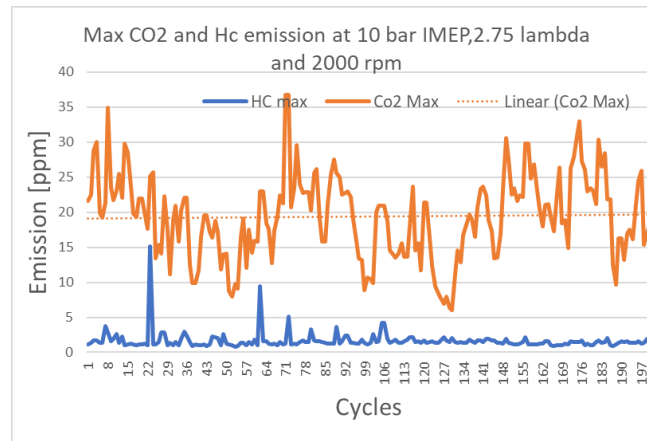
Figure 12. 7: Cycle peak emissions of HC and CO_2 with the linear trend of the peak CO_2.

Figure 12.8 compares the average HC emission per cycle and the maximum HC per cycle with each cycle's peak in-cylinder pressure. This comparison aims to evaluate the combustion stability at a consistent load and speed of 10 bar IMEP and 2000 rpm while maintaining the air-fuel ratio (lambda) at 2.75. Such an evaluation aims to determine the accuracy of utilising average data in reflecting the presence of spikes. This analysis shows that utilising averaged data does not accurately reflect the actual existence of the spikes, highlighting the importance of measuring and analysing the maximum HC per cycle in assessing the overall combustion stability.
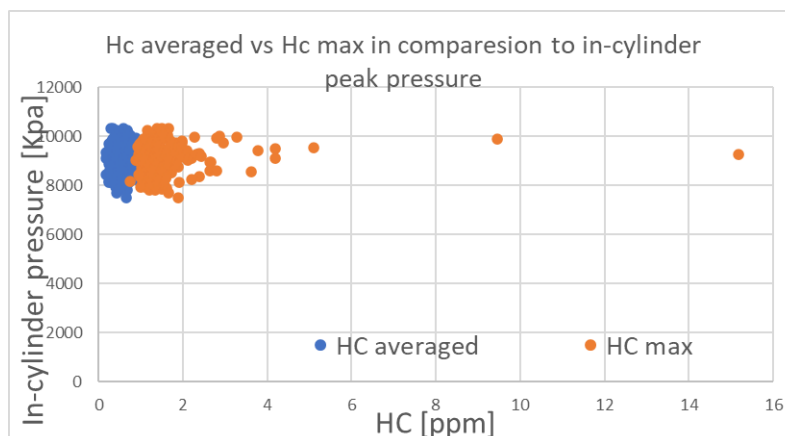
Figure 12. 8: HC averaged vs max at 2000 rpm,10 bar IMEp and lambda 2.75 vs In-cylinder peak pressure.

The relationship between peak in-cylinder pressure and emissions spikes was investigated by observing HC and CO_2 max over 200 cycles at 2000 rpm and 10 bar IMEP, with 1.2 AFR

and near stoichiometric combustion. Figure 12.9 represents the result of the study. The average maximum HC was observed to be 5ppm, which is consistent with the findings of previous tests. Emission spikes were detected in only two consecutive cycles, and the CO_2 max emission fluctuated between 15 to 0 ppm over the 200 cycles. Furthermore, the study did not reveal any direct correlation between the peak in-cylinder pressure and the emission characteristics of CO_2 and HC.
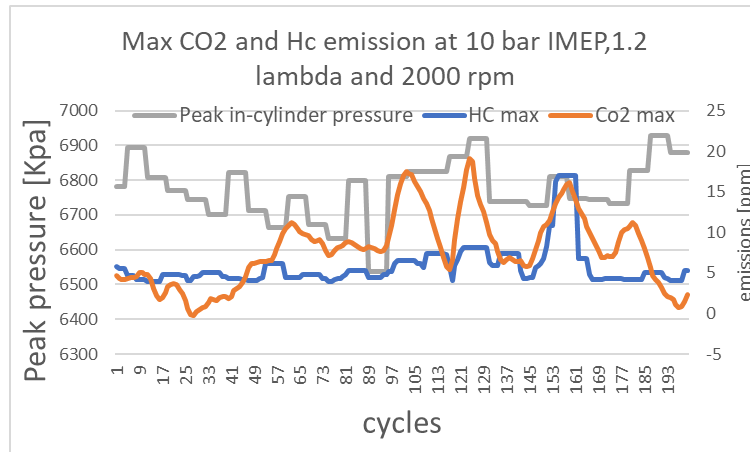
Figure 12. 9:Cycle peak emissions of HC and CO_2 with the peak in-cylinder pressure.

In the previous charts, we maintained a constant load of 10 bars while adjusting the lambda between lean to rich values. However, in Figure 12.10, we set the lambda at 2.75, maintained a speed of 2000 rpm, and applied a load of 16 bar IMEP. This chart offers valuable insights into the emission behaviour under these circumstances, particularly CO_2 and HC emissions. CO_2 emissions ranged from 0 to 10 ppm, with an average CO_2 maximum of 5 ppm. In contrast, maximum HC emissions remained near zero, with frequent HC spikes per cycle. While the spikes appeared in more than six cycles, their peak value was below 20 ppm, nearly zero-emission. These observations indicate that the engine operates efficiently and produces minimal emissions under these conditions.
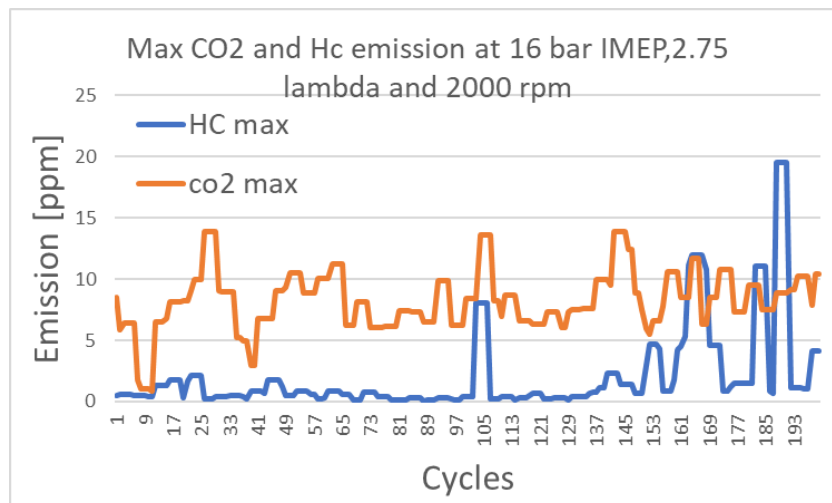
Figure 12. 10:cycle peak emissions of HC and CO_2 at 16 bar IMEP.

To better represent the emission spikes of each cycle, we should analyse the peak HC and CO_2 values individually rather than relying on averaged data. However, a key question is the severity of the spike values for each cycle. Propose analysing the HC spikes to answer

this question, as they are more easily identifiable than CO2 spikes. For this purpose, an HC emission standard deviation (SD) function is introduced, which calculates the standard deviation of the HC in each cycle to determine if the HC max is occurring frequently or only once per cycle. The HC standard deviation equation, represented in equation 12.1, is based on identifying the maximum value ratio to the mean emission value.

$$SD_{HC} = \sqrt{\frac{\sum_{i=1}^{n}(HC_1 - HC_{mean})^2}{n-1}} \qquad\qquad (12.1)$$

To visualise this analysis, Figure 12.11 shows a 3D graph with the peak in-cylinder pressure on the x-axis, the HC SD on the y-axis, and the maximum HC on the z-axis.

Figure 12.11 shows the relationship between the HC emission SD and the HC max emission with the Peak in-cylinder pressure over 200 cycles; Figure 12.11 (a) is the HC max emission at 10 bar IMEP and 2000 rpm at lambda 1.5, while Figure 12.11 (b) represents the maximum HC at the same load and speed with lambda of 2.75. The main observation is that in both cases, the higher the HC max emission happened, the higher the standard deviation over the cycles, which supports that the appearance of the spike is per cycle, leading to the huge variation between the HC max emission vs the averaged emission. Also, it's noted that the higher HC max values cause higher standard deviation due to the higher difference.
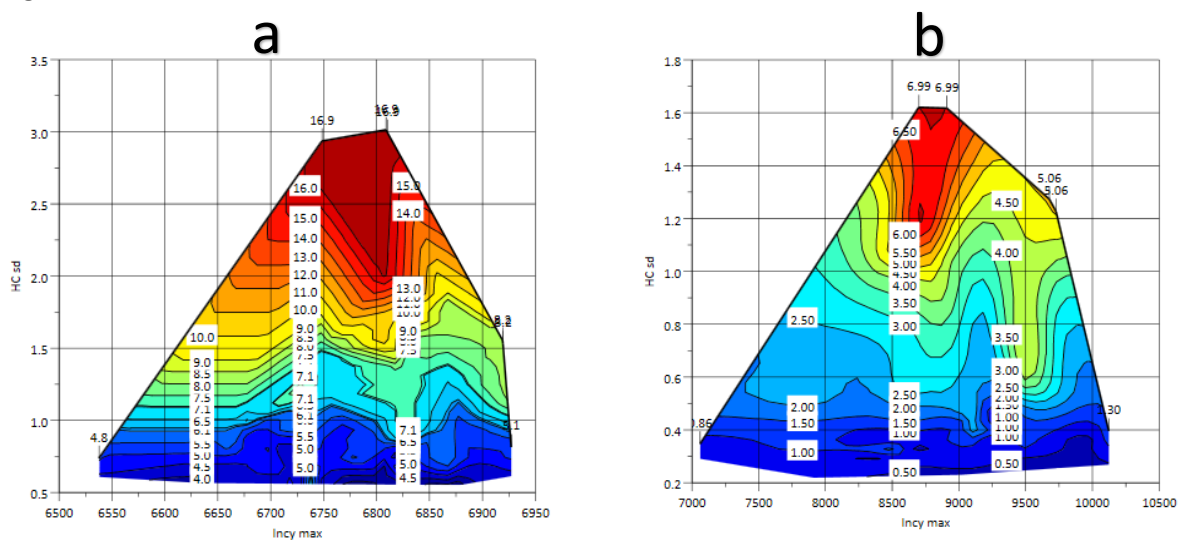
Figure 12. 11: the peak in-cylinder pressure on the x-axis, the HC SD on the y-axis, and the HC max on the z-axis.

12.4 Conclusion

This study aims to comprehensively evaluate the HC and CO_2 emissions of SI engines running on 100% hydrogen, utilising direct injection technology and an ultra-fast FID Cambustion analyser. The research involved conducting two sets of experiments: the load sweep and the lambda sweeps. Two analysis models were employed, with the first method entailing the collection of 300 cycles on average to evaluate engine performance and combustion characteristics, followed by an observation of instantaneous HC and CO_2 values in the crank domain.

The study's main findings can be summarised as follows. The ultra-fast FID Cambustion analyser provided accurate indications and captured the CO_2 and HC per 0.25 crack degrees. The averaged data shows an average of less than 10 ppm CO_2 and HC over lambda and load sweeps, which was at the limit of the instrument. The load sweep tests show no load dependency on the lubricant has averaged HC and CO_2 emissions. Thirdly, the performance and combustion characteristics show that hydrogen can operate with higher ITE over a wide range of loads with less than 100 PPM NO_x emissions.

Fourthly, the lambda sweep test shows the high advantage of using DI technology to mitigate intake backfire, the ability to operate on stoichiometric combustion, and the trade-off of HC emission vs CO_2 emissions. Fifthly, the cycle analysis shows the characteristics of the HC and CO_2 over the cycles and provides a better representation of the HC spikes over the steady state. The in-cylinder Peak pressure variation does not affect the HC spikes' values or frequency, representing the lubricant oil.

Finally, the study addressed the main question of whether lubricant oil significantly impacts CO_2 and HC emissions. In the last decade, H_2 ICE technologies have been introduced as a zero-carbon green technology. Furthermore, an interesting phenomenon was observed as the crank ventilation system uses a forced entire system to avoid the H_2 accumulation in the crank, which might have been dependent on lowering the lubricant oil emission. However, a full maintenance service was conducted after the test, and no visual damage was observed. In conclusion, the study provides valuable insights into the impact of lubricant oil on CO_2 and HC emissions. Future research could examine the impact of different oil properties on engine performance and emissions.

Chapter 13. Thesis Summary and Future Work

The thesis focused on investigating two sustainable fuels to mitigate CO_2 emission, whether by using second-generation Biogasoline as a drop-in fuel or by adopting hydrogen.

13.1 The Main Summary

To achieve net-zero aims, the current study conducts an examination that is confident in its analysis of two essential solutions. The first thing it does is investigate whether or not it is possible to use second-generation biofuels with different amounts of ethanol and Research Octan as direct drop-in replacements for fossil fuels.

Second, the research concentrates on hydrogen as the principal power source for internal combustion engine platforms. This study demonstrates the potential of hydrogen as a substitute for fossil fuels.

13.1.1 Summary of The Works Done on Biogasoline and Main Conclusions

The studies conducted on Bigosoline explored the effects of ethanol blend percentages on biofuels, including their impact on performance and emissions compared to fossil fuels. The research revealed that higher ethanol percentages resulted in greater knocking resistance, indicating significant potential for future applications. Furthermore, the findings showed that, except for slightly higher hydrocarbon levels, all biofuel samples exhibited similar trends in performance and emissions.

Another study focused on the impact of increased octane numbers on the second generation of biofuels. The results revealed that higher octane numbers offered increased thermal efficiency and engine stability compared to fossil fuels.

Finally, the researchers explored different injection strategies to combat PM emissions, a significant challenge for biofuels. The outcome was a remarkable reduction in low-load emissions by adapting 80% PFi to 20% DI.

The findings of the biogasoline study suggest promising potential for adopting second-generation biogasoline, with a range of ethanol production options suitable for diverse applications and a significant reduction in CO_2 life cycle emissions.

13.1.2 Summary of Design and Successful Implementation of The Hydrogen Fuel Supply System and H_2 Engine Testbed Facility

To ensure maximum safety, construct fire-resistant brick walls on three sides to effectively isolate the hydrogen operation bottles. Next, use a U-shaped metal structure to isolate the 6 mm hydrogen line, ensuring the building surface remains free from fire jets. Adjust the line height to eliminate potential risks from ground interactions and isolate the exhaust line for added safety. Adjust the shutdown system to thoroughly purge the entire line to maintain an empty outside line.

Inside the building, adopt a double piping system to guarantee complete isolation. Utilize a vacuum system to enhance system sensitivity and promptly respond to pressure loss, ensuring that the double piping remains isolated in the test cell environment. Design an automatic shutdown system that can activate in case of emergency or system failure, preventing any possibility of hydrogen gas leakage without the need for nitrogen purging.

This automatic shutdown system will run in case of double pipe leakage or system failure. Lastly, install extra sensors with high-speed valves to detect and isolate any potential hydrogen leakage within the engine and connect them to the automatic shutdown system. By implementing these measures, The operator and everyone on site can be confident in the safety and reliability of the hydrogen operation.

13.1.3 Main Findings of The H$_2$ Engine Works

The first study assessed the potential of DI H$_2$ in comparison to gasoline DI. The main findings showed higher thermal efficiency and near-zero carbon emissions. Also, the results showed the hydrogen's great ability to operate in a much wider AFR compared to gasoline with much higher engine stability. When comparing the DI hydrogen engine to the SI gasoline engine under the WOT condition (10bar IMEP), it was observed that the former's performance and emissions are less impacted by fuel injection pressure and timings. Moreover, during the early intake process, the injection of gaseous hydrogen successfully displaced more air, leading to a significantly higher boost pressure than the gasoline engine. Additionally, increasing the in-cylinder hydrogen injection pressure from 10-40 bar resulted in a noticeable boost in pressure.

In the forthcoming era, hydrogen has the potential to emerge as a zero-carbon alternative fuel for medium-duty spark ignition DI engines. With minor modifications to the existing infrastructure, this goal could be achieved. This is a significant step towards advancing the use of alternative fuels in the transportation sector.

Then, comparing the H$_2$ PFI vs. DI technologies shows the advantages of the DI, which has fewer PMEP losses and high thermal efficiency. Also, taking advantage of higher pressure and late injection allows more valve overlaps and eliminates the backfire phenomenon that allows running hydrogen at the stochiomtric combustion.

Converting smaller SI gasoline engines to run on hydrogen using a PFI or DI fuel system is highly feasible. Compared to gasoline engines, PFI and DI hydrogen engines operate with superior lean burn efficiency within a broad lambda range of 2.5 to 3.7. The PFI H$_2$ engine performs exceptionally well within a lambda range of about 1.5 to 3.7. In contrast, the DI H$_2$ engine can operate within a broader range, including stoichiometric mixture, without encountering backfire problems. The DI H$_2$ system could be employed with positive valve overlap to enhance scavenging effects while keeping hydrogen slip to a minimum. Moreover, a higher injection pressure of 40 bar can improve combustion under high-load conditions. This approach may be considered to optimise the system's performance in relevant applications.

A study has been conducted on the impact of H$_2$ DI position by comparing the central to the side DI. The main outcome is that the central DI has outperformed the side DI.

The CDI injection system exhibited longer combustion durations than its SDI counterpart, resulting in a slight increase of 0.2-0.5% in combustion efficiency and lower hydrogen slip in the exhaust.

Both injection systems showed similar emission characteristics, with NO$_x$ emissions rising with engine speed and load. NO$_x$ levels remained below 100 ppm in the low load range of 400 to 800 kPa IMEP, but increased rapidly beyond 1200 kPa IMEP.

Operating the hydrogen engine with a constant lambda of 2.75, CDI operations produced 50% less NO_x emissions and significantly less H2 slip than SDI operations.

The study highlights the significant impact of hydrogen injector location on the engine's performance and emissions, with in-cylinder mixing processes being the primary cause of differences observed in both systems.

A single-cylinder optical engine with either a centrally-mounted or a side-mounted hydrogen injector is being subjected to CFD studies and high-speed optical measurements to further understand the hydrogen injection process.

Investigating the main emission concerns of the H2ICE was a high priority in the thesis. An ultrafast NO_x emission was used to investigate NO_x in the crank domain. The study outcomes show that the NO_x characteristics are similar to gasoline with a slightly shifted pattern, and the NO_x can be almost zero by operating at lambda 3 or higher.

After conducting a thorough analysis of NO_x emissions across the crank-angle domain, it has been determined that the PFI system emits slightly less NO_x than the hydrogen DI system. This makes the PFI system a preferred option for SI engines that run on gasoline PFI and are interested in transitioning to hydrogen fuel. However, it should be noted that the PFI hydrogen system may experience backfiring when operated with near stoichiometric mixtures.

Further examination of NO_x emissions characteristics over time indicates that DI hydrogen engine operation is more stable and produces less NO_x variations than gasoline. Even when gasoline engines operate at their optimum point, hydrogen engines are more stable, resulting in lower NO_x emissions and less fluctuation between cycles.

Finally, the study of the CO_2 and HC spikes was analysed to address the main question of how much the lubricant emission in the H2ICE engines and the outcomes show nearly zero in the averaged domain. The cycle analysis shows nearly 18 ppm as a maximum spike per cycle, while HC spikes every 50 cycles with less than 20 ppm.

The overall outcome of the hydrogen study shows massive potential for directly adopting H2ICE on existing fossil fuel-based platforms, with higher efficiency gains and nearly zero carbon emissions as an engine-out.

13.2 Recommendations for Future Works

The present study has focused on examining the performance of a downsized SI engine, specifically in terms of thermal efficiency and NO_x emissions. However, there is potential for further exploration into achieving even higher thermal efficiency by incorporating a longer stroke and implementing an EGR system to reduce NO_x emissions significantly. Additionally, with hydrogen's high flame speed and advancements in direct injection technologies that mitigate the risk of backfire, it would be intriguing to investigate using water injection to slow the burn rate. This approach opens up the possibility of near stoichiometric combustion with pure hydrogen, which has significant implications for the industry.The hydrogen's great stability over lean combustion on the SI configurations opens the door to investigating the active and passive prechamber technologies.

References

[1]   Richard Stone, "Introduction to Internal Combustion Engines 4th Edition," *Palgrave Macmillan, Richard Stone*. 2012.

[2]   R. Diesel, "Einleitende Bemerkungen," in *Theorie und Konstruktion eines rationellen Wärmemotors*, Springer, 1893, p. 1.

[3]   P. Breeze, *An Introduction to Piston Engine Power Plants*. 2018. doi: 10.1016/b978-0-12-812904-3.00001-x.

[4]   K. Hoag and B. Dondlinger, "The Internal Combustion Engine—An Introduction," pp. 1–16, 2016, doi: 10.1007/978-3-7091-1859-7_1.

[5]   D. Bandyopadhyay *et al.*, "Challenges Overwhelmed to Meet BSVI Emissions with SPFI Fuel System for Heavy-Duty CNG Engine Application," *SAE Int J Adv Curr Pract Mobil*, vol. 4, no. 3, pp. 768–773, Sep. 2021, doi: 10.4271/2021-26-0102.

[6]   John Heywood, "John Heywood - Internal Combustion Engine Fundamentals-McGraw-Hill Education (2018)," 2018, [Online]. Available: https://www.accessengineeringlibrary.com/content/book/9781260116106

[7]   A. E. Alali, A. Al Tubeshat, and K. Al Khasawneh, "Performance analysis of stirling engine double-effect absorption chiller hybrid system for waste heat utilization from gas turbine modular helium reactor," *Energy Convers Manag*, vol. 251, p. 114976, Jan. 2022, doi: 10.1016/J.ENCONMAN.2021.114976.

[8]   Z. Meng, S. Ahling, and T. Tian, "Study of the Effects of Oil Supply and Piston Skirt Profile on Lubrication Performance in Power Cylinder Systems," *SAE Technical Papers*, no. December, Dec. 2019, doi: 10.4271/2019-01-2364.

[9]   Z. Liu *et al.*, "Hierarchical frequency control strategy of doubly-fed induction diesel generator under emergency condition," *Energy Reports*, vol. 8, pp. 657–667, Aug. 2022, doi: 10.1016/J.EGYR.2022.02.257.

[10]   "Air-fuel ratio, lambda and engine performance – x-engineer.org." Accessed: Jun. 27, 2021. [Online]. Available: https://x-engineer.org/automotive-engineering/internal-combustion-engines/performance/air-fuel-ratio-lambda-engine-performance/

[11]   K. D. Zschorsch, "Catalytic combustion," *The John Zink Hamworthy Combustion Handbook, Second Edition: Volume 1 - Fundamentals*, pp. 137–157, 2012, doi: 10.1201/b11619.

[12]   M. Hori, H. Nakamura, T. Tezuka, S. Hasegawa, and K. Maruta, "Characteristics of n-heptane and toluene weak flames in a micro flow reactor with a controlled temperature profile," *Proceedings of the Combustion Institute*, vol. 34, no. 2, pp. 3419–3426, Jan. 2013, doi: 10.1016/J.PROCI.2012.06.099.

[13]   K. C. Taylor, "Automobile catalytic converters," in *Catalysis*, Springer, 1984, pp. 119–170.

[14]   V. Ngu, J. Morchain, and A. Cockx, "In-depth analysis of reactive bubbly flow using two-way coupled spatio-temporal 1D model," *Chem Eng Sci*, vol. 261, p. 117963, Nov. 2022, doi: 10.1016/J.CES.2022.117963.

[15] "4 Charts Explain Greenhouse Gas Emissions by Countries and Sectors | World Resources Institute." Accessed: Jun. 28, 2021. [Online]. Available: https://www.wri.org/insights/4-charts-explain-greenhouse-gas-emissions-countries-and-sectors

[16] H. Ritchie and M. Roser, "Sector by sector: where do global greenhouse gas emissions come from?," *Our World in Data*, Mar. 2024, Accessed: May 20, 2024. [Online]. Available: https://ourworldindata.org/ghg-emissions-by-sector

[17] I. Renewable and E. Agency, "SUSTAINABLE INTENSIFICATION MAKING ROOM FOR ENERGY CROPS WITHOUT HARMING BIODIVERSITY".

[18] Y. Xie, T. Dallmann, and R. Muncrief, "Heavy-duty zero-emission vehicles Pace and opportunities for a rapid global transition," no. May, 2022.

[19] T. Earl *et al.*, "&Transport Environment Further information".

[20] The Royal Society, *Sustainable synthetic carbon based fuels for transport*. 2019. [Online]. Available: https://phys.org/news/2019-09-synthetic-fuels-carbon-footprint.html

[21] "A hydrogen vision for the UK," no. April, 2023.

[22] G. Cooper, "THE RENEWABLE FUEL STANDARD : AN ENDURING POLICY FOUNDATION".

[23] J. H. Stock, "THE R E N E WA BL E F UE L STANDARD : A PATH F ORWARD".

[24] BPC, "Options for Reforming the Renewable Fuel Standard," no. December, 2014.

[25] S. C. de Vries, G. W. J. van de Ven, M. K. van Ittersum, and K. E. Giller, "Resource use efficiency and environmental performance of nine major biofuel crops, processed by first-generation conversion techniques," *Biomass Bioenergy*, vol. 34, no. 5, pp. 588–601, 2010, doi: 10.1016/j.biombioe.2010.01.001.

[26] E. Sadeghinezhad *et al.*, "A comprehensive literature review of bio-fuel performance in internal combustion engine and relevant costs involvement," *Renewable and Sustainable Energy Reviews*, vol. 30. pp. 29–44, 2014. doi: 10.1016/j.rser.2013.09.022.

[27] A. Alaswad, M. Dassisti, T. Prescott, and A. G. Olabi, "Technologies and developments of third generation biofuel production," *Renewable and Sustainable Energy Reviews*, vol. 51, pp. 1446–1460, 2015, doi: 10.1016/j.rser.2015.07.058.

[28] M. Guo, W. Song, and J. Buhain, "Bioenergy and biofuels: History, status, and perspective," *Renewable and Sustainable Energy Reviews*, vol. 42, pp. 712–725, 2015, doi: 10.1016/j.rser.2014.10.013.

[29] "Global trends The biofuels debate Governmental energy Global production Global production Production targets Meeting these goals Proportion of global production of liquid biofuels in 2007," 1960.

[30] S. Jaichandar and K. Annamalai, "The Status of Biodiesel as an Alternative Fuel for Diesel Engine-An Overview," 2011.

[31] M. Junginger, "KEY MESSAGES BIOENERGY-A SUSTAINABLE AND RELIABLE ENERGY SOURCE A review of status and prospects."

[32]   M. V. Rodionova *et al.*, "Biofuel production: Challenges and opportunities," *International Journal of Hydrogen Energy*, vol. 42, no. 12. Elsevier Ltd, pp. 8450–8461, Mar. 23, 2017. doi: 10.1016/j.ijhydene.2016.11.125.

[33]   G. Joshi, J. K. Pandey, S. Rana, and D. S. Rawat, "Challenges and opportunities for the application of biofuel," *Renewable and Sustainable Energy Reviews*, vol. 79. Elsevier Ltd, pp. 850–866, 2017. doi: 10.1016/j.rser.2017.05.185.

[34]   H. Scharf, F. Arnold, and D. Lencz, "Future natural gas consumption in the context of decarbonization - A meta-analysis of scenarios modeling the German energy system," *Energy Strategy Reviews*, vol. 33, Jan. 2021, doi: 10.1016/j.esr.2020.100591.

[35]   J. Scheelhaase, S. Maertens, and W. Grimme, "Synthetic fuels in aviation - Current barriers and potential political measures," in *Transportation Research Procedia*, Elsevier B.V., 2019, pp. 21–30. doi: 10.1016/j.trpro.2019.12.015.

[36]   I. Ghiat and T. Al-Ansari, "A review of carbon capture and utilisation as a CO2abatement opportunity within the EWF nexus," *Journal of CO2 Utilization*, vol. 45, no. January, p. 101432, 2021, doi: 10.1016/j.jcou.2020.101432.

[37]   A. Bhavsar, D. Hingar, S. Ostwal, I. Thakkar, S. Jadeja, and M. Shah, "The current scope and stand of carbon capture storage and utilization ~ A comprehensive review," *Case Studies in Chemical and Environmental Engineering*, vol. 8, p. 100368, Dec. 2023, doi: 10.1016/J.CSCEE.2023.100368.

[38]   C. Wulf, J. Linßen, and P. Zapp, "Review of power-to-gas projects in Europe," *Energy Procedia*, vol. 155, pp. 367–378, 2018, doi: 10.1016/j.egypro.2018.11.041.

[39]   W. Liu, F. Wen, and Y. Xue, "Power-to-gas technology in energy systems: current status and prospects of potential operation strategies," *Journal of Modern Power Systems and Clean Energy*, vol. 5, no. 3, pp. 439–450, 2017, doi: 10.1007/s40565-017-0285-0.

[40]   C. Duncan, R. Roche, S. Jemei, and M. C. Pera, "Techno-economical modelling of a power-to-gas system for plant configuration evaluation in a local context," *Appl Energy*, vol. 315, p. 118930, Jun. 2022, doi: 10.1016/J.APENERGY.2022.118930.

[41]   A. Varone and M. Ferrari, "Power to liquid and power to gas: An option for the German Energiewende," 2015, doi: 10.1016/j.rser.2015.01.049.

[42]   C. Panzone, R. Philippe, A. Chappaz, P. Fongarland, and A. Bengaouer, "Power-to-Liquid catalytic CO 2 valorization into fuels and chemicals: focus on the Fischer-Tropsch route," 2020, doi: 10.1016/j.jcou.2020.02.009.

[43]   S. Singh *et al.*, "Hydrogen: A sustainable fuel for future of the transport sector", doi: 10.1016/j.rser.2015.06.040.

[44]   B. L. Salvi and K. A. Subramanian, "Sustainable development of road transportation sector using hydrogen energy system," 2015, doi: 10.1016/j.rser.2015.07.030.

[45]   J. A. Turner, "Sustainable Hydrogen Production," *Science (1979)*, vol. 305, no. 5686, pp. 972–974, Aug. 2004, doi: 10.1126/SCIENCE.1103197.

[46]   A. Ahmed, Q. Al-Amin, A. F. Ambrose, and R. Saidur, "Hydrogen fuel and transport system: A sustainable and environmental future," 2015, doi: 10.1016/j.ijhydene.2015.11.084.

[47]   "UK first major economy to halve emissions - GOV.UK." Accessed: May 23, 2024. [Online]. Available: https://www.gov.uk/government/news/uk-first-major-economy-to-halve-emissions

[48]   G. Conway, A. Joshi, F. Leach, A. García, and P. K. Senecal, "A review of current and future powertrain technologies and trends in 2020," *Transportation Engineering*, vol. 5, p. 100080, Sep. 2021, doi: 10.1016/J.TRENG.2021.100080.

[49]   T. M. (Trevor M.) Letcher, "Future energy : improved, sustainable and clean options for our planet," p. 792.

[50]   K. Y. Bjerkan, T. E. Nørbech, and M. E. Nordtømme, "Incentives for promoting Battery Electric Vehicle (BEV) adoption in Norway," *Transp Res D Transp Environ*, vol. 43, pp. 169–180, Mar. 2016, doi: 10.1016/J.TRD.2015.12.002.

[51]   E. Fantin, I. Raj, and M. Appadurai, "The Hybrid Electric Vehicle (HEV)—An Overview," pp. 25–36, 2021, doi: 10.1007/978-981-16-0719-6_3.

[52]   Y. Chen, "New Energy Vehicle Powertrain Technologies and Applications," 2023, doi: 10.1007/978-981-19-9566-8.

[53]   W. Schöffmann, H. Sorger, A. Fürhapter, P. Kapus, G. Teuschl, and C. Sams, "The ICE in the electrified powertrain – modular approach within a common platform between cost and CO2 optimization," pp. 75–101, 2019, doi: 10.1007/978-3-658-26528-1_5.

[54]   "Future Light and Heavy Duty ICE Powertrain Technologies", Accessed: Mar. 07, 2024. [Online]. Available: www.ertrac.org

[55]   V. S. Yaliwal, N. R. Banapurmath, N. M. Gireesh, and P. G. Tewari, "Production and utilization of renewable and sustainable gaseous fuel for power generation applications: A review of literature," *Renewable and Sustainable Energy Reviews*, vol. 34, pp. 608–627, Jun. 2014, doi: 10.1016/J.RSER.2014.03.043.

[56]   S. Pandey, "A critical review: Application of methanol as a fuel for internal combustion engines and effects of blending methanol with diesel/biodiesel/ethanol on performance, emission, and combustion characteristics of engines," *Heat Transfer*, vol. 51, no. 4, pp. 3334–3352, Jun. 2022, doi: 10.1002/HTJ.22453.

[57]   M. Sens and E. Binder, "Pre-Chamber Ignition as a Key Technology for Future Powertrain Fleets," *MTZ worldwide 2019 80:2*, vol. 80, no. 2, pp. 44–51, Jan. 2019, doi: 10.1007/S38313-018-0150-1.

[58]   N. Duarte *et al.*, "Internal combustion engines and biofuels: Examining why this robust combination should not be ignored for future sustainable transportation," 2021, doi: 10.1016/j.rser.2021.111292.

[59]   V. Mittal, R. Shah, N. Aragon, and N. Douglas, "A Perspective on the Challenges and Future of Hydrogen Fuel," *SAE International Journal of Sustainable Transportation, Energy, Environment, & Policy*, vol. 3, no. 1, pp. 31–39, Oct. 2021, doi: 10.4271/13-03-01-0003.

[60]   H. Eichlseder, T. Wallner, R. Freymann, and J. Ringler, "The potential of hydrogen internal combustion engines in a future mobility scenario," *SAE Technical Papers*, 2003, doi: 10.4271/2003-01-2267.

[61]   P. Nikolaidis and A. Poullikkas, "A comparative overview of hydrogen production processes," 2016, doi: 10.1016/j.rser.2016.09.044.

[62]   A. I. Osman *et al.*, "Hydrogen production, storage, utilisation and environmental impacts: a review," *Environ Chem Lett*, vol. 20, pp. 153–188, 2022, doi: 10.1007/s10311-021-01322-8.

[63]   "Safety and efficiency in your hydrogen production projects | TÜV SÜD Malaysia." Accessed: Jun. 06, 2023. [Online]. Available: https://www.tuvsud.com/en-my/themes/hydrogen/explore-the-hydrogen-value-chain/hydrogen-production

[64]   I. Dincer, "Green methods for hydrogen production," 2011, doi: 10.1016/j.ijhydene.2011.03.173.

[65]   C. Bauer *et al.*, "On the climate impacts of blue hydrogen production," 2022, doi: 10.1039/d1se01508g.

[66]   J. Yu, F.-J. Tian, M. C. Chow, L. J. Mckenzie, and C.-Z. Li, "Effect of iron on the gasification of Victorian brown coal with steam:enhancement of hydrogen production," 2005, doi: 10.1016/j.fuel.2005.05.026.

[67]   K. Kamonsuangkasem, S. Therdthianwong, A. Therdthianwong, N. / Cezro, and / Al, "Hydrogen production from yellow glycerol via catalytic oxidative steam reforming," 2012, doi: 10.1016/j.fuproc.2012.10.003.

[68]   J. Diab, L. Fulcheri, V. Hessel, V. Rohani, and M. Frenklach, "Why turquoise hydrogen will Be a game changer for the energy transition," 2022, doi: 10.1016/j.ijhydene.2022.05.299.

[69]   N. R. Neelameggham, G. Subramanian, and P. Kalamegham, "H2 Enriched Maroon Natural Gas and Pink Hydrogen".

[70]   A. M. Abdalla, S. Hossain, O. B. Nisfindy, A. T. Azad, M. Dawood, and A. K. Azad, "Hydrogen production, storage, transportation and key challenges with applications: A review," 2018, doi: 10.1016/j.enconman.2018.03.088.

[71]   E. Science, "Storage In The Form Of Pure H 2," vol. 6, no. 9, pp. 24–33, 2003.

[72]   "Ontario's Low-Carbon Hydrogen Strategy".

[73]   S. Mekhilef, R. Saidur, and A. Safari, "Comparative study of different fuel cell technologies," *Renewable and Sustainable Energy Reviews*, vol. 16, pp. 981–989, 2012, doi: 10.1016/j.rser.2011.09.020.

[74]   R. E. Izzaty, B. Astuti, and N. Cholimah, "Fuel cell book," *Angewandte Chemie International Edition, 6(11), 951–952.*, pp. 5–24, 1967.

[75]   K. Lim, N. Vaz, J. Lee, and H. Ju, "Advantages and disadvantages of various cathode flow field designs for a polymer electrolyte membrane fuel cell ☆," *Int J Heat Mass Transf*, vol. 163, p. 120497, 2020, doi: 10.1016/j.ijheatmasstransfer.2020.120497.

[76]   J. Larminie and A. Dicks, "Fuel Cell Systems Explained Second Edition", Accessed: Jun. 06, 2023. [Online]. Available: www.wiley.co.uk/fuelcellsystems.

[77]   Z. Stępień, "A comprehensive overview of hydrogen-fueled internal combustion engines: Achievements and future challenges," *Energies (Basel)*, vol. 14, no. 20, Oct. 2021, doi: 10.3390/EN14206504.

[78]   K. Wróbel, J. Wróbel, W. Tokarz, J. Lach, K. Podsadni, and A. Czerwiński, "Hydrogen Internal Combustion Engine Vehicles: A Review," *Energies 2022, Vol. 15, Page 8937*, vol. 15, no. 23, p. 8937, Nov. 2022, doi: 10.3390/EN15238937.

[79]   K. K. Rana, S. Natarajan, and S. Jilakara, "Potential of hydrogen fuelled IC engine to achieve the future performance and emission norms," *SAE Technical Papers*, Jan. 2015, doi: 10.4271/2015-26-0050.

[80]   R. J. Natkin, X. Tang, B. Boyer, B. Oltmans, A. Denlinger, and J. W. Heffel, "Hydrogen IC engine boosting performance and NOX study," *SAE Technical Papers*, 2003, doi: 10.4271/2003-01-0631.

[81]   M. Rajesh, K. Rana, M. Abraham, N. Saravanan, and G. P. Subash, "Development of hydrogen powered three wheeler engine," *SAE Technical Papers*, vol. 5, 2013, doi: 10.4271/2013-26-0002.

[82]   H. Eichlseder, T. Wallner, R. Freymann, and J. Ringler, "The potential of hydrogen internal combustion engines in a future mobility scenario," *SAE Technical Papers*, 2003, doi: 10.4271/2003-01-2267.

[83]   C. Lhuillier, P. Brequigny, F. Contino, and C. Mounaïm-Rousselle, "Experimental study on ammonia/hydrogen/air combustion in spark ignition engine conditions," *Fuel*, vol. 269, p. 117448, Jun. 2020, doi: 10.1016/J.FUEL.2020.117448.

[84]   A. Mohammadi, M. Shioji, Y. Nakai, W. Ishikura, and E. Tabo, "Performance and combustion characteristics of a direct injection SI hydrogen engine," *Int J Hydrogen Energy*, vol. 32, no. 2, pp. 296–304, Feb. 2007, doi: 10.1016/J.IJHYDENE.2006.06.005.

[85]   R. Zhang *et al.*, "Optical study on the effects of the hydrogen injection timing on lean combustion characteristics using a natural gas/hydrogen dual-fuel injected spark-ignition engine," *Int J Hydrogen Energy*, vol. 46, no. 39, pp. 20777–20789, Apr. 2021, doi: 10.1016/J.IJHYDENE.2021.03.171.

[86]   A. Kawamura, T. Yanai, Y. Sato, K. Naganuma, K. Yamane, and Y. Takagi, "Summary and Progress of the Hydrogen ICE Truck Development Project," *SAE Int J Commer Veh*, vol. 2, no. 1, pp. 110–117, Jun. 2009, doi: 10.4271/2009-01-1922.

[87]   Y. Karaya, S. K. Addepalli, and J. M. Mallikarjuna, "Effect of Fuel Injector Location and Nozzle-Hole Orientation on Mixture Formation in a GDI Engine: A CFD Analysis," *SAE Technical Papers*, vol. 2018-April, Apr. 2018, doi: 10.4271/2018-01-0201.

[88]   L. Rouleau, F. Duffour, B. Walter, R. Kumar, and L. Nowak, "Experimental and Numerical Investigation on Hydrogen Internal Combustion Engine," *SAE Technical Papers*, no. 2021, Sep. 2021, doi: 10.4271/2021-24-0060.

[89]   S. Wang, C. Ji, B. Zhang, and X. Liu, "Lean burn performance of a hydrogen-blended gasoline engine at the wide open throttle condition," *Appl Energy*, vol. 136, pp. 43–50, Dec. 2014, doi: 10.1016/j.apenergy.2014.09.042.

[90]   B. Zhang, C. Ji, S. Wang, and Y. Xiao, "Investigation on the cold start characteristics of a hydrogen-enriched methanol engine," in *International Journal of Hydrogen Energy*, Elsevier Ltd, Sep. 2014, pp. 14466–14471. doi: 10.1016/j.ijhydene.2014.04.012.

[91] P. V. Inbanaathan *et al.*, "Comprehensive study on using hydrogen-gasoline-ethanol blends as flexible fuels in an existing variable speed SI engine," *Int J Hydrogen Energy*, vol. 48, no. 99, pp. 39531–39552, Dec. 2023, doi: 10.1016/J.IJHYDENE.2023.03.107.

[92] J. Deng *et al.*, "Experimental study on combustion and emission characteristics of a hydrogen-enriched compressed natural gas engine under idling condition," *Int J Hydrogen Energy*, vol. 36, no. 20, pp. 13150–13157, Oct. 2011, doi: 10.1016/J.IJHYDENE.2011.07.036.

[93] J. Deng *et al.*, "Experimental study on combustion and emission characteristics of a hydrogen-enriched compressed natural gas engine under idling condition," *Int J Hydrogen Energy*, vol. 36, no. 20, pp. 13150–13157, Oct. 2011, doi: 10.1016/j.ijhydene.2011.07.036.

[94] V. Molkov, *Fundamentals of Hydrogen Safety Engineering I*. 2012.

[95] "fundamentals-of-hydrogen-safety-engineering-ii".

[96] S. Verhelst and T. Wallner, "Hydrogen-fueled internal combustion engines," *Prog Energy Combust Sci*, vol. 35, no. 6, pp. 490–527, 2009, doi: 10.1016/j.pecs.2009.08.001.

[97] H. Obermair, R. Scarcelli, and T. Wallner, "Efficiency improved combustion system for hydrogen direct injection operation," *SAE Technical Papers*, no. Equation 1, 2010, doi: 10.4271/2010-01-2170.

[98] Q. H. Luo, B. G. Sun, and H. Y. Tian, "The characteristic of polytropic coefficient of compression stroke in hydrogen internal combustion engine," *Int J Hydrogen Energy*, vol. 39, no. 25, pp. 13787–13792, Aug. 2014, doi: 10.1016/J.IJHYDENE.2014.04.035.

[99] S. Verhelst, P. Maesschalck, N. Rombaut, and R. Sierens, "Efficiency comparison between hydrogen and gasoline, on a bi-fuel hydrogen/gasoline engine," *Int J Hydrogen Energy*, vol. 34, no. 5, pp. 2504–2510, Mar. 2009, doi: 10.1016/J.IJHYDENE.2009.01.009.

[100] G. Arzamendi, P. M. Die, and L. M. Gandı, *Renewable hydrogen technologies: Renewable hydrogenenergy - An overview*. 2013.

[101] Y. Li, W. Gao, P. Zhang, Y. Ye, and Z. Wei, "Effects study of injection strategies on hydrogen-air formation and performance of hydrogen direct injection internal combustion engine," *Int J Hydrogen Energy*, vol. 44, no. 47, pp. 26000–26011, Oct. 2019, doi: 10.1016/j.ijhydene.2019.08.055.

[102] K. S. Chapman and A. Patil, "Performance, Efficiency, and Emissions Characterization of Reciprocating Internal Combustion Engines Fueled with Hydrogen/Natural Gas Blends ," 2008.

[103] J. Gao, X. Wang, P. Song, G. Tian, and C. Ma, "Review of the backfire occurrences and control strategies for port hydrogen injection internal combustion engines," *Fuel (Guildford)*, vol. 307, p. 121553, Jan. 2022, doi: 10.1016/J.FUEL.2021.121553.

[104] R. Zhang *et al.*, "Optical study on the effects of the hydrogen injection timing on lean combustion characteristics using a natural gas/hydrogen dual-fuel injected spark-ignition engine," *Int J Hydrogen Energy*, vol. 46, no. 39, pp. 20777–20789, Apr. 2021, doi: 10.1016/J.IJHYDENE.2021.03.171.

[105]   C. Lhuillier, P. Brequigny, F. Contino, and C. Mounaïm-Rousselle, "Experimental study on ammonia/hydrogen/air combustion in spark ignition engine conditions," *Fuel*, vol. 269, p. 117448, Jun. 2020, doi: 10.1016/J.FUEL.2020.117448.

[106]   S. Lee, G. Kim, and C. Bae, "Effect of injection and ignition timing on a hydrogen-lean stratified charge combustion engine," *International Journal of Engine Research*, vol. 23, no. 5, pp. 816–829, May 2022, doi: 10.1177/14680874211034682.

[107]   Y. Takagi, M. Oikawa, R. Sato, Y. Kojiya, and Y. Mihara, "Near-zero emissions with high thermal efficiency realized by optimizing jet plume location relative to combustion chamber wall, jet geometry and injection timing in a direct-injection hydrogen engine," *Int J Hydrogen Energy*, vol. 44, no. 18, pp. 9456–9465, Apr. 2019, doi: 10.1016/J.IJHYDENE.2019.02.058.

[108]   L. zhi Bao, B. gang Sun, and Q. he Luo, "Experimental investigation of the achieving methods and the working characteristics of a near-zero NOx emission turbocharged direct-injection hydrogen engine," *Fuel*, vol. 319, p. 123746, Jul. 2022, doi: 10.1016/J.FUEL.2022.123746.

[109]   "Coregas backs Hydrogen Mobility." Accessed: Jun. 07, 2023. [Online]. Available: https://www.coregas.co.nz/news/2018/hydrogen-mobility

[110]   E. Furimsky, "Hydroprocessing challenges in biofuels production," *Catal Today*, vol. 217, pp. 13–56, 2013, doi: 10.1016/j.cattod.2012.11.008.

[111]   A. Ajanovic, "Biofuels versus food production: Does biofuels production increase food prices?," 2010, doi: 10.1016/j.energy.2010.05.019.

[112]   S. Al-Zuhair, "Biochemical catalytic production of biodiesel," *Handbook of Biofuels Production: Processes and Technologies*, pp. 134–159, 2011, doi: 10.1533/9780857090492.2.134.

[113]   S. Karatzos, J. D. Mcmillan, and J. N. Saddler, "The Potential and Challenges of Drop-in Biofuels A Report by IEA Bioenergy Task 39 AUTHORS," 2014.

[114]   S. van Dyk, J. Su, J. D. Mcmillan, and J. (John) Saddler, "Potential synergies of drop-in biofuel production with further co-processing at oil refineries," *Biofuels, Bioproducts and Biorefining*, vol. 13, no. 3, pp. 760–775, May 2019, doi: 10.1002/BBB.1974.

[115]   P. K. Senecal and F. Leach, "Diversity in transportation: Why a mix of propulsion technologies is the way forward for the future fleet," *Results in Engineering*, vol. 4, p. 100060, Dec. 2019, doi: 10.1016/J.RINENG.2019.100060.

[116]   M. Thewes, M. Müther, A. Brassat, S. Pischinger, and A. Sehr, "Analysis of the effect of bio-fuels on the combustion in a downsized DI SI engine," *SAE Int J Fuels Lubr*, vol. 5, no. 1, pp. 274–288, Jan. 2012, doi: 10.4271/2011-01-1991.

[117]   T. L. Alleman, "Analysis of Ethanol Fuel Blends," *SAE Int J Fuels Lubr*, vol. 6, no. 3, pp. 870–876, Feb. 2013, [Online]. Available: http://www.jstor.org/stable/26273279

[118]   B. M. Masum, H. H. Masjuki, M. A. Kalam, I. M. Rizwanul Fattah, S. M Palash, and M. J. Abedin, "Effect of ethanol–gasoline blend on NOx emission in SI engine," *Renewable and Sustainable Energy Reviews*, vol. 24, pp. 209–222, Aug. 2013, doi: 10.1016/J.RSER.2013.03.046.

[119] P. Iodice, A. Amoresano, and G. Langella, "A review on the effects of ethanol/gasoline fuel blends on NOX emissions in spark-ignition engines A review on the effects of ethanol/gasoline fuel blends on NOX emissions in spark-ignition engines A review on the effects of ethanol/gasoline fuel blends on NOX emissions in spark-ignition engines," *Biofuel Research Journal*, vol. 32, pp. 1465–1480, 2021, doi: 10.18331/BRJ2021.8.4.2.

[120] A. Harrington, J. Hall, M. Bassett, E. Lu, and H. Zhao, "Combustion Characteristics and Exhaust Emissions of a Direct Injection SI Engine with Pure Ethanol and Methanol in Comparison to Gasoline," *SAE Technical Papers*, Aug. 2022, doi: 10.4271/2022-01-1089.

[121] H. Spiertz, "Challenges for Crop Production Research in Improving Land Use, Productivity and Sustainability," *Sustainability 2013, Vol. 5, Pages 1632-1644*, vol. 5, no. 4, pp. 1632–1644, Apr. 2013, doi: 10.3390/SU5041632.

[122] S. K. Bhatia, S. H. Kim, J. J. Yoon, and Y. H. Yang, "Current status and strategies for second generation biofuel production using microbial systems," *Energy Convers Manag*, vol. 148, pp. 1142–1156, 2017, doi: 10.1016/J.ENCONMAN.2017.06.073.

[123] Y. Li *et al.*, "Combustion, performance and emissions characteristics of a spark-ignition engine fueled with isopropanol-n-butanol-ethanol and gasoline blends," *Fuel*, vol. 184, pp. 864–872, Nov. 2016, doi: 10.1016/J.FUEL.2016.07.063.

[124] K. Nithyanandan, H. Wu, M. Huo, and C. F. Lee, "A Preliminary Investigation of the Performance and Emissions of a Port-Fuel Injected SI Engine Fueled with Acetone-Butanol-Ethanol (ABE) and Gasoline," *SAE Technical Papers*, vol. 1, Apr. 2014, doi: 10.4271/2014-01-1459.

[125] P. P. Peralta-Yahya and J. D. Keasling, "Advanced biofuel production in microbes," *Biotechnol J*, vol. 5, no. 2, pp. 147–162, Feb. 2010, doi: 10.1002/BIOT.200900220.

[126] M. Giampietro, S. Ulgiati, and D. Pimentel, "Feasibility of large-scale biofuel production," *Bioscience*, vol. 47, no. 9, pp. 587–600, 1997, doi: 10.2307/1313165.

[127] F. Contino, F. Foucher, F. Halter, G. Dayma, P. Dagaut, and C. Mounaïm-Rousselle, "Engine Performances and Emissions of Second-Generation Biofuels in Spark Ignition Engines: The Case of Methyl and Ethyl Valerates," *SAE Technical Papers*, vol. 6, Sep. 2013, doi: 10.4271/2013-24-0098.

[128] A. Hoth, C. P. Kolodziej, T. Rockstroh, and T. Wallner, "Combustion Characteristics of PRF and TSF Ethanol Blends with RON 98 in an Instrumented CFR Engine," *SAE Technical Papers*, vol. 2018-September, Sep. 2018, doi: 10.4271/2018-01-1672.

[129] Y. H. Teoh, H. G. How, K. H. Yu, H. G. Chuah, and W. L. Yin, "Influence of Octane Number Rating on Performance, Emission and Combustion Characteristics in Spark Ignition Engine," *Journal of Advanced Research in Fluid Mechanics and Thermal Sciences*, vol. 45, no. 1, pp. 22–34, 2018, Accessed: Aug. 28, 2023. [Online]. Available: https://www.akademiabaru.com/submit/index.php/arfmts/article/view/2178

[130] M. Shearian, B. Ghobadian, and S. Gorjian, "A critical review on life-cycle assessment and exergy analysis of Enomoto bio-gasoline production," *J Clean Prod*, vol. 379, no. P1, p. 134387, 2022, doi: 10.1016/j.jclepro.2022.134387.

[131]   A. M. Liaquat, M. A. Kalam, H. H. Masjuki, and M. H. Jayed, "Potential emissions reduction in road transport sector using biofuel in developing countries," *Atmos Environ*, vol. 44, no. 32, pp. 3869–3877, 2010, doi: 10.1016/j.atmosenv.2010.07.003.

[132]   J. Szyszlak-Bargłowicz, J. Wasilewski, G. Zając, A. Kuranc, A. Koniuszy, and M. Hawrot-Paw, "Evaluation of Particulate Matter (PM) Emissions from Combustion of Selected Types of Rapeseed Biofuels," *Energies (Basel)*, vol. 16, no. 1, 2023, doi: 10.3390/en16010239.

[133]   L. Chen, Z. Liang, X. Zhang, and S. Shuai, "Characterizing particulate matter emissions from GDI and PFI vehicles under transient and cold start conditions," *Fuel*, vol. 189, pp. 131–140, 2017, doi: 10.1016/j.fuel.2016.10.055.

[134]   C. Shi, C. Ji, Y. Ge, S. Wang, J. Yang, and H. Wang, "Effects of split direct-injected hydrogen strategies on combustion and emissions performance of a small-scale rotary engine," *Energy*, vol. 215, Jan. 2021, doi: 10.1016/j.energy.2020.119124.

[135]   R. Bahreini *et al.*, "Characterizing emissions and optical properties of particulate matter from PFI and GDI light-duty gasoline vehicles," *J Aerosol Sci*, 2015, doi: 10.1016/j.jaerosci.2015.08.011.

[136]   G. Karavalakis, D. Short, D. Vu, R. Russell, A. Asa-Awuku, and T. Durbin, "A Complete Assessment of the Emissions Performance of Ethanol Blends and Iso-Butanol Blends from a Fleet of Nine PFI and GDI Vehicles," *SAE Int J Fuels Lubr*, vol. 8, no. 2, pp. 374–395, 2015, doi: https://doi.org/10.4271/2015-01-0957 UI - 2015-01-0957.

[137]   B. Johansson *et al.*, "Exhaust PM Emissions Analysis of Alcohol Fueled Heavy-Duty Engine Utilizing PPC," *SAE Int J Engines*, vol. 9, no. 4, pp. 2142–2152, 2016, doi: https://doi.org/10.4271/2016-01-2288 UI - 2016-01-2288.

[138]   A. Harrington *et al.*, "Technical Assessment of the Feasibility of the use of Bio-Gasoline as a Drop-In Gasoline Fossil Fuel Replacement," *SAE Technical Paper Series*, vol. 1, pp. 1–12, 2022, doi: 10.4271/2022-01-1087.

[139]   "The Opportunity For Sustainable Fuels In High-Performance Engines - Coryton." Accessed: Sep. 30, 2022. [Online]. Available: https://coryton.com/latest/the-opportunity-for-sustainable-fuels-in-high-performance-engines/

[140]   M. J. Atkins and C. R. Koch, "A Well-to-Wheel Comparison of Several Powertrain Technologies," vol. 2003, no. 724, 2022.

[141]   C. E. Vehicles, "Life Cycle Analysis Comparison J A N U A R Y 2 0 22 ELECTRIC AND INTERNAL COMBUSTION ENGINE VEHICLES".

[142]   I. M. P. Machado and S. Atsumi, "Cyanobacterial biofuel production," *J Biotechnol*, vol. 162, pp. 50–56, 2012, doi: 10.1016/j.jbiotec.2012.03.005.

[143]   † X I A O Z H A N G , † A N D D I N G B A O W A N G, "Land Availability for Biofuel Production X I M I N G C A I", doi: 10.1021/es103338e.

[144]   "Are biofuels and e-fuels the only sustainable solution to power our existing fleet of internal combustion engines? - Coryton." Accessed: Sep. 30, 2022. [Online]. Available: https://coryton.com/latest/are-biofuels-and-e-fuels-the-only-sustainable-solution-to-power-our-existing-fleet-of-internal-combustion-engines/

[145] "Automotive fuels-Unleaded petrol-Requirements and test methods," 2008.

[146] R. Golzari, Y. Li, and H. Zhao, "Impact of Port Fuel Injection and In-Cylinder Fuel Injection Strategies on Gasoline Engine Emissions and Fuel Economy," no. Di, 2016, doi: 10.4271/2016-01-2174.Copyright.

[147] M. Mohamed, H. Zhao, A. Harrington, and J. Hall, "Experimental Investigation of Combustion Characteristics, Performance, and Emissions of a Spark Ignition Engine with 2ndGeneration Bio-Gasoline and Ethanol Fuels," *SAE Technical Papers*, Apr. 2023, doi: 10.4271/2023-01-0339.

[148] P. Price, B. Twiney, R. Stone, K. Kar, and H. Walmsley, "Particulate and Hydrocarbon Emissions from a Spray Guided Direct Injection Spark Ignition Engine with Oxygenate Fuel Blends," *SAE Technical Papers*, Apr. 2007, doi: 10.4271/2007-01-0472.

[149] J. Symonds, "Measurement of particle number emissions from engines with DMS Series," 2009.

[150] M. J. M. G. Ramos and J. S. Wallace, "Fuel Effects on Particulate Matter Emissions Variability from a Gasoline Direct Injection Engine," *SAE Technical Papers*, vol. 2018-April, 2018, doi: 10.4271/2018-01-0355.

[151] A. L. Sánchez and F. A. Williams, "Recent advances in understanding of flammability characteristics of hydrogen," *Prog Energy Combust Sci*, vol. 41, no. 1, pp. 1–55, Apr. 2014, doi: 10.1016/J.PECS.2013.10.002.

[152] P. C. Souers, "Hydrogen properties for fusion energy," p. 391, 1986.

[153] G. Alefeld and J. Voelkl, "Hydrogen in metals I - Basic properties," *tap*, vol. 28, 1978, Accessed: Jun. 08, 2023. [Online]. Available: https://ui.adsabs.harvard.edu/abs/1978tap....28.....A/abstract

[154] "FID50 | Flame Ionisation Detector | Cambustion." Accessed: Dec. 29, 2023. [Online]. Available: https://www.cambustion.com/products/engine-exhaust-emissions/hc-analyzers/fid50-flame-ionisation-detector

[155] "DMS500 Mk2 | Particulate Analyzer | Cambustion." Accessed: Sep. 30, 2022. [Online]. Available: https://www.cambustion.com/products/engine-exhaust-emissions/dms500-particulate-analyzer

[156] "Vieletech - Vieletech Combustion Analysis Toolkit." Accessed: Mar. 03, 2024. [Online]. Available: https://www.vieletech.com/productdetails/VCAT

[157] N. Peters and M. Bunce, "Lambda Determination Challenges for Ultra-Lean Hydrogen-Fueled Engines and the Impact on Engine Calibration," *SAE Technical Papers*, Apr. 2023, doi: 10.4271/2023-01-0286.

[158] M. Usman, M. W. Saleem, S. Saqib, J. Umer, A. Naveed, and Z. U. Hassan, "SI engine performance, lubricant oil deterioration, and emission: A comparison of liquid and gaseous fuel," *Advances in Mechanical Engineering*, vol. 12, no. 6, Jun. 2020, doi: 10.1177/1687814020930451/ASSET/IMAGES/LARGE/10.1177_1687814020930451-FIG7.JPEG.

[159] R. Amirante *et al.*, "Effects of lubricant oil on particulate emissions from port-fuel and direct-injection spark-ignition engines," *International Journal of Engine Research*, vol. 18, no. 5–6, pp. 606–620, Aug. 2017, doi: 10.1177/1468087417706602/ASSET/IMAGES/LARGE/10.1177_1468087417706602-FIG12.JPEG.